

Active Control of Loudspeakers:
An Investigation of Practical Applications

Andrew Bright

Ørsted·DTU – Acoustic Technology
Technical University of Denmark

Published by: Ørsted·DTU, Acoustic Technology, Technical University of Denmark, Building 352, DK-2800 Kgs. Lyngby, Denmark, 2002

This work is dedicated to the memory of

Betty Taliaferro Lawton Paddock Hunt (1916-1999)

and to

Samuel Raymond Bright, Jr. (1936-2001)

Table of Contents

Preface	9
Summary	11
Resumé	13
Conventions, notation, and abbreviations	15
Conventions	15
Notation	16
Abbreviations	20
1. Introduction	23
1.1. Active control of loudspeakers	28
1.2. Organisation of thesis	29
1.3. References	31
2. Loudspeaker models	33
2.1. Linear models of loudspeakers	33
2.1.1. Electrical dynamics	35
2.1.2. Mechanical dynamics	38
2.1.3. Electro-mechanical transduction	40
2.1.4. Acoustical components	40
2.1.5. Acoustic radiation	43
2.1.6. Linear frequency response	44
2.1.7. Response prediction of loudspeaker mounted in a sealed cabinet	44
2.1.8. Response prediction of a loudspeaker mounted in a vented-box enclosure	47
2.2. Nonlinear models of loudspeakers	48
2.2.1. Parametric nonuniformity and causes of nonlinearity	48
2.2.2. Nonlinear simulation	54
2.3. Discrete-time physical modelling	56
2.3.1. FIR filter for electrical admittance	58
2.3.2. IIR filter for receptance of an SDOF system	60
2.3.3. IIR filter for mobility of an SDOF system	62
2.3.4. Nonlinear discrete-time loudspeaker model	64
2.4. Parametric uncertainty	68
2.5. References	69
3. Theory of active control of loudspeakers	71
3.1. Feedback control for loudspeakers	72
3.1.1. Constant-current output amplifiers	72
3.1.2. Negative amplifier output impedance	72
3.1.3. Feedback processing using vibration measurement	74
3.2. Feedforward controllers	76
3.2.1. Linear feedforward processing	76

3.2.2.	Nonlinear feedforward processing	76
3.3.	Feedback linearisation.....	77
3.3.1.	Feedback linearisation of continuous-time systems.....	77
3.3.2.	Example: simplified closed box loudspeaker in continuous-time.....	80
3.3.3.	State observer and partial state measurement	82
3.3.4.	Feedforward formulation using a ‘simulation’ state observer	83
3.3.5.	Feedforward formulation assuming ideal alignment.....	84
3.3.6.	Feedback linearisation of discrete-time systems.....	86
3.3.7.	Feedback linearisation with a discrete-time loudspeaker model.....	87
3.4.	Adaptive feedforward controllers	88
3.5.	System identification by adaptive filtering	90
3.5.1.	General adaptive algorithms	90
3.5.2.	Adaptive IIR filters	92
3.6.	References.....	94
4.	Loudspeaker system identification	99
4.1.	Overview of approach, implementation, and evaluation	99
4.1.1.	Forms for developing an error equation.....	100
4.1.2.	Hardware implementation and system-under-test.....	101
4.1.3.	Software implementation	104
4.1.4.	Stability triangle.....	106
4.1.5.	Tolerance quadrilateral	106
4.1.6.	Frame-based updating	110
4.2.	Electrical current output-error form.....	112
4.2.1.	Updating R_{eb}	113
4.2.2.	Updating a_k	114
4.2.3.	Updating of σ_u as a feedforward coefficient	115
4.2.4.	Updating of σ_u as a dependent variable, defined by a_2	115
4.2.5.	Partial derivative of $\varepsilon_{oci}[n]$ with respect to ϕ_0	116
4.2.6.	Convergence performance	117
4.2.7.	Accuracy of the converged parameters for the current output-error form	124
4.2.8.	Updating ϕ_k	126
4.3.	Voltage output-error form.....	129
4.3.1.	Parameter updating	130
4.3.2.	Convergence performance	131
4.4.	Displacement equation-error form	138
4.4.1.	Displacement from the voltage equation.....	138
4.4.2.	Displacement from the force equation	138
4.4.3.	Error definition.....	138
4.4.4.	Parameter updating – linear case	139
4.5.	Conclusions regarding system identification	143
4.6.	References.....	144
5.	Applications of active control of a loudspeaker	145
5.1.	Linear equalisation.....	146
5.1.1.	Acoustic response with equalisation	146
5.1.2.	Displacement response with equalisation	148
5.2.	Compensation of nonlinear distortion.....	149
5.2.1.	Simulations of effective sensitivity increase vs. coil height	150
5.2.2.	Simulation results.....	155

5.2.3. Distortion compensation on shortened- height voice-coil loudspeakers.....	159
5.3. References.....	166
6. Conclusions	167
Appendix A. Experimental set-up and tuning	169
A.1. Hardware implementation of algorithms	169
A.2. Electrical impedance measurement	169
A.2.1. Differential vs. single-ended considerations.....	169
A.2.2. Extraneous resistances	170
A.2.3. Determination of extraneous resistances with single-ended I/O.....	172
A.3. Experimental set-up for diaphragm for vibration measurement.....	173
A.4. Experimental set-up for acoustic measurement	177
Appendix B. Experimental determination loudspeaker parameters	179
B.1. Parameters to be determined.....	179
B.2. Electrical parameter determination (R_{eb} , L_{eb} , and ϕ_0)	179
B.3. Mechanical parameter determination (m_d , c_d , and k_d)	182
B.4. References.....	186
Appendix C. Modal analysis of loudspeaker diaphragms	187
C.1. Introduction.....	187
C.2. Modal analysis of structural vibration	188
C.3. Experimental modal analysis	189
C.4. Interpretation of modal analysis on loudspeakers.....	190
C.4.1. Measuring structural FRF's on loudspeakers.....	190
C.4.2. Interpretation of curve-fit parameters	191
C.4.3. Differential vs. single-ended considerations.....	193
C.5. Summary	194
C.6. References.....	194
Appendix D. Rocking modes in single-suspension loudspeakers	197
D.1. Introduction	197
D.2. Low frequency modes of vibration of a single suspension loudspeaker	197
D.2.1. Translational vs. rotational modes of vibration	198
D.2.2. ‘Rocking’ modes of diaphragm vibration	198
D.3. Eigenvalue analysis	202
D.4. Problems with rocking modes	202
D.4.1. Mechanical tolerances.....	202
D.4.2. Acoustic radiation	202
D.5. References	203

Preface

This thesis is the result of a cooperative project between Nokia Research Center of Finland and The Section of Acoustic Technology at the Ørsted-DTU, Technical University of Denmark, funded by Nokia Mobile Phones, as a basic study of the electrodynamic loudspeaker. Theoretical work and academic study was performed at the Section of Acoustic Technology in Lyngby, Denmark. Experimental work was performed at the Acoustics Laboratories of Nokia Research Center in Tampere, Finland.

I am grateful to Kaarina Melkas of Nokia Research Center for her support and for her suggestion that I undertake this project. I am also grateful to Matti Hämäläinen and Leo Kärkkäinen of Nokia Research Center for their patient acceptance of my sometimes erratic project schedules. I would like to acknowledge Petri Haavisto and Jukka Saarinen of Nokia Research Center and Nick Courtis and Juha Backman of Nokia Mobile Phones for supporting this project (or at least not cancelling it – even when they perhaps should have).

I would like to thank my supervisors at the DTU, Karsten Bo Rasmussen, Jean-Dominique Polack, and Finn Jacobsen for the guidance, enthusiasm, and direction contributed by them to this project. I am also grateful to all of the support staff at the Department of Acoustics, for making a friendly atmosphere that was conducive to research.

I would like to acknowledge the many persons in Nokia Research Center and Nokia Mobile Phones who together form the 'Nokia Audio Community.' I would particularly like to thank John Cozens for his assistance in preparing experimental hardware, Leo Kärkkäinen again for his explanations of mathematical concepts, Kaarina Melkas again for providing magnetic field FEM simulation data, and Matti Kajala for his assistance in C-programming and using sound card drivers. More broadly, this project has benefited from the wide and varied discussions I have had with a great many persons within the Nokia Audio Community on aspects of audio, acoustics, and loudspeakers. It is my hope that this thesis may make some contribution to their work.

The final stages of research and writing of this project were made possible by grants from Nordisk Forskerutdanningsakademi (NorFA) and from The Nokia Foundation.

I would also like to acknowledge the direct and indirect support from my family, particularly CB and Mickey, given to me during this project, over distances short and long.

I am grateful to Philips Speaker Solutions for preparing the modified coil-height loudspeaker samples investigated in this project.

I would like to thank Wolfgang Klippel for technical suggestions to this project, and all those at Klippel GmbH for their assistance in fine-tuning their measurement system to the small loudspeakers studied in this project.

Significant indirect support for this project came from Suvi Takkinen and her expanding family.

I am personally indebted to Pontus Veneskoski and Ritva Jääskeläinen for their hospitality during the final experimental trials of this project.

Finally, love and thanks to Anu, Dori, Katja, Maxi, Paul, Sipe, Sophie & Thierry, and Ulriikka – for keeping me sane.

Summary

This thesis investigates applications of active control for loudspeakers. Active control is considered in this thesis as a tool to simplify the design or increase the performance of an audio reproduction system. This view has been made possible by recent reductions in the cost of hardware for digital signal processing. This thesis presents simple processing techniques for active control of loudspeakers, and shows how they can be used to increase the net sensitivity of electroacoustic systems.

Authors and inventors have previously promoted active control primarily as a means to improve the quality of an existing loudspeaker. A somewhat different view is taken in this thesis. Specifically, it is considered how introducing active control permits an audio reproduction system to more efficiently or more simply achieve its specified design target.

Practical considerations require active control to be implemented by digital processing. It is assumed in this thesis that, for active control to reduce cost, its processing algorithms should be no more complicated than common audio DSP algorithms already in use in a wide array of products. It is shown in this thesis that suitably simple algorithms for active control are made possible by using discrete-time models of loudspeaker dynamics. Additionally, the digital filters describing the loudspeaker dynamics are kept to the same order as common continuous-time models of loudspeaker dynamics. This achieves simplifications over previously published techniques for digital loudspeaker processing, which have modelled loudspeaker dynamics by numerical integration of continuous-time models, or by high-order non-recursive filters.

It is concluded after a review of literature that adaptive feedforward control is the most practical architecture for active control of loudspeakers. Its key advantages are its ability to tune itself to changes in a loudspeaker, and to do this without the need for a direct feedback signal, which is generally expensive and impractical to obtain. A simple feedforward nonlinear controller is developed by applying the theory of feedback linearisation to the discrete-time loudspeaker model developed.

Simple adaptive algorithms, using the discrete-time loudspeaker model mentioned above, are presented. These algorithms are used to determine parametric changes in a loudspeaker, known to occur due to thermal fluctuations, ageing, and other factors. The convergence properties of the adaptive algorithms are assessed with signals measured on actual loudspeakers.

Two applications of active control are presented. Linear active control, or equalisation as per classical loudspeaker theory, is discussed for a simple loudspeaker. The benefit of making such equalisation adaptive, and a simple manner in which this can be done with digital processing, is presented. A second, nonlinear application of active control is also considered. It is found that nonlinear active control permits a reduction in the height of a loudspeaker's voice-coil. A loudspeaker's sensitivity is inversely proportional to its moving mass, and as this moving mass is dominated by the voice coil in some loudspeakers, reduction of its height permits significant increase in sensitivity. Active control permits compensation of the nonlinear distortion created by the increase in transduction coefficient nonuniformity caused by this shortening of the voice coil height. Furthermore, it is shown that the sensitivity increase provided by shortening the voice-coil height is significantly greater than the additional amplifier output required for compensating the resulting increase in nonlinear distortion. Measurements of the nonlinear compensation performance with actual loudspeakers are presented.

Conclusions on optimal design of loudspeakers for use with active control are drawn, and suggestions for further research are given.

Resumé

Denne afhandling undersøger aktiv kontrol af højttalere. Aktiv kontrol betragtes som et værktøj der kan forenkle højttalerkonstruktioner eller forbedre højttaleres egenskaber i lydgengivelsessystemer. Dette er muliggjort af de senere års faldende priser på digitale signalbehandlingssystemer. Afhandlingen præsenterer forskellige forholdsvis enkle metoder til aktiv kontrol af højttalere, og viser hvordan de kan bruges til at forøge elektroakustiske systemers følsomhed.

Forskere og opfindere har hidtil primært interesseret sig for aktive metoder som et middel til forbedre eksisterende højttalertyper egenskaber. Denne afhandling har et lidt andet sigte. Det undersøges hvordan en højttalerkonstruktion kan modificeres således at der opnås en forbedring af egenskaberne ved hjælp af et aktivt system.

Aktive kontrollsystemer kan kun realiseres økonomisk ved hjælp af digital signalbehandling. Hvis aktive metoder skal reducere omkostningerne må det forudsættes at algoritmerne er så enkle som muligt - og ikke mere komplicerede end de algoritmer til audioformål som allerede anvendes i en lang række produkter. Det vises at rimeligt enkle signalbehandlingsalgoritmer kan udvikles ved hjælp af tids-diskrete højttalermodeller. De digitale filtre som beskriver højttalernes dynamiske egenskaber er begrænset til samme orden som almindelige tids-kontinuerte højttalermodeller. Herved er der opnået en forenkling sammenlignet med metoder til kontrol af højttalere beskrevet i litteraturen, idet disse metoder i almindelighed har modelleret højttalernes egenskaber ved hjælp af numerisk integration af tids-kontinuerte modeller eller med ikke-rekursive filtre af høj orden.

Efter en gennemgang af litteraturen konkluderes det at adaptiv feedforward-kontrol vil være særlig hensigtsmæssig i forbindelse med aktiv styring af højttalere. Dette hænger sammen med denne metodes evne til at justere sig ind efter de ændringer der kan forekomme i en højttaler uden brug af et direkte feedback-signal, som i almindelighed er dyrt og vanskeligt at opnå. Et ret enkelt, ikke-lineært feedforward-kontrollsysten er udviklet ved at anvende teorien for feedback-linearisering på den tids-diskrete højttalermodel.

En række adaptive algoritmer, baseret på den tids-diskrete højttalermodel, præsenteres. Disse algoritmer bruges til at bestemme de parametriske ændringer i en højttaler som vides at forekomme, bl.a. på grund af termiske fluktuationer og ældningsprocesser. Konvergensegenskaberne er bestemt med signaler som er målt på forskellige virkelige højttalere.

Afhandlingen undersøger to anvendelser af aktiv kontrol. Lineær aktiv styring af en højttaler (equalisation) diskutes. Fordelen ved adaptiv equalisation demonstreres. Ikke-lineær adaptiv styring bliver også undersøgt, og det konkluderes at en sådan styring gør det muligt at reducere svingspolens længde. Da højttaleres følsomhed er omvendt proportional med massen af det svingende system, som domineres af svingspolens masse, følger det at man kan opnå en forøgelse af højttalerens følsomhed. Dette resulterer imidlertid i øget ikke-lineær forvrængning. Det vises i afhandlingen at denne forvrængning kan ud kompenseres med aktiv kontrol. Endvidere viser det sig at forøgelsen af følsomheden er større end det ekstra forstærker-output som kræves til signalbehandlingen. Signalbehandlingssystemets gunstige virkning dokumenteres med målinger på virkelige højttalere.

Afslutningsvis præsenteres konklusioner vedrørende optimal design af højttalere med aktive kontrollsystemer, ligesom der gives en række forslag til yderligere forskning.

Conventions, notation, and abbreviations

Conventions

$x(t)$	A real-valued function of continuous-time
$x(s)$	The Laplace transform of $x(t)$
$X(s)$	A complex-valued transfer function
$x[n]$	A real-valued function of discrete-time
\mathbf{x}	A vector
$\mathbf{x} \in \Re^N$	A real-valued vector with N elements
\mathbf{X}	A matrix
$\dot{x}(t)$	The derivative of $x(t)$ with respect to time.
$\ddot{x}(t)$	The second derivative of $x(t)$ with respect to time.
$x^{(n)}(t)$	The n^{th} derivative of $x(t)$ with respect to time.
$\hat{x}(t)$	An estimate of $x(t)$

The Laplace transform of time-dependent quantities is used in this thesis, as given by

$$x(s) = \int_0^\infty x(t)e^{-st} dt$$

The resulting Laplace transform $x(s)$ is occasionally used in this thesis in the same equation as single-frequency (harmonic) exponential notation. In this case, we consider the Laplace transform evaluated at a single frequency. Note that if only a single frequency is considered, the time domain representation may be recovered using the complex exponential as follows:

$$x(t) = \operatorname{Re} \left\{ x(s) e^{-i2\pi f t} \right\}_{s=-i2\pi f}$$

This is equivalent to stating $s = -i\omega$. Readers accustomed to the convention $s = j\omega$ may consider: $i = -j$.

The following sign notation is used for discrete-time difference equations, and their use in discussing digital filters along with their z -transform:

$$\begin{aligned} y[n] &= b_0 x[n] + b_1 x[n-1] + \dots + b_M x[n-M] - a_1 y[n-1] - \dots - a_N y[n-N] \\ &\Rightarrow H(z) = \frac{\sum_{n=0}^M b_n z^{-n}}{1 + \sum_{n=1}^N a_n z^{-n}} \end{aligned}$$

where $y[n]$ is the output, $x[n]$ is the input, b_k are the feedforward coefficients, and a_k are the feedback coefficients. This is in contrast to some presentations wherein a_k are the feedforward coefficients, and b_k are the feedback coefficients. Also, in some presentations, the a_k (feedback) coefficients have the opposite sign.

Notation

In the case of overloaded (multiple use) symbols, definitions of their different uses are separated by a semicolon (;), and are listed in the order in which they appear in the text.

Some notation used in Appendices C and D is not listed here. All notation appearing in those appendices and not listed here is defined explicitly in those appendices.

a	vector of feedback coefficients of a digital filter
a_k	k^{th} feedback coefficient of a difference equation, or digital filter
$A_e(s)$	electrical admittance (multiplicative inverse of the electrical impedance)
A_n	n^{th} numerator coefficient of a partial-fraction-expansion
b	vector of feedforward coefficients of a digital filter
b_k	k^{th} feedforward coefficient of a difference equation, or digital filter
$B, B(x)$	magnetic flux density (average) in the coil gap created by the magnet in a loudspeaker, as a function of axial distance along the coil gap
c	vector of feedback coefficients of a differential equation
c_0	speed of sound in air under adiabatic conditions (approx. 343 m/s at 20 °C)
c_d	mechanical damping of the loudspeaker diaphragm
c_n	n^{th} feedback coefficient of generalised differential equation
c_p	effective resistance upon the fluid flow in a port
c_t	total mechanical damping of a loudspeaker diaphragm
$C_{\text{disp},n}$	specified displacement
d_n	n^{th} feedforward coefficient of a generalised differential equation
$d_{w_k}[n]$	gradient of the error surface $\xi(\mathbf{w})$ along the parameter w_k
$\hat{d}_{\phi_0}[n]$	estimate of the gradient of the error surface along the parameter ϕ_0
d	vector of feedforward coefficients of a differential equation; vector of gradient values of the error surface $\xi(\mathbf{w})$ with respect to its weighting parameter vector \mathbf{w}
e	transcendental number $= \sum_{n=0}^{\infty} 1/n!$
f	frequency
$f(s)$	force, in frequency (Laplace) domain, generic
$f_c(t), f_c(s), f_c[n]$	mechanical force on the diaphragm, in time (continuous), frequency, and discrete-time
$f_{cp}[n]$	force on the voice-coil, predicted from the force equation
f_0	the vacuum (acoustically unloaded), open-circuit resonance frequency
f_s	free-air resonance frequency of a loudspeaker
$\mathbf{f}(\mathbf{x}(t))$	feedback (system) vector field of a system represented in state-space form
F_{ma}	force due to magnetic attraction (solenoid effect), caused by nonuniform blocked electrical inductance
F_s	sampling rate (frequency) of a discrete-time system ($= 1/T_s$)
$\mathbf{g}(\mathbf{x}(t))$	input vector field of a system represented in state-space form
$h(t), h[n]$	impulse response, generic
$h_{dt}[n]$	impulse response of a discrete-time approximation to an differentiator
$h_{A_e}(t)$	impulse response of the electrical admittance
$h_{\int_{dt}}[n]$	impulse response of a discrete-time approximation to an integrator
$\mathbf{h}(\mathbf{x}(t))$	output vector field of a system expressed in state-space form
$H(s)$	transfer function, generic, in continuous-time (Laplace domain)

$H_{X_m}(z)$	mechanical mobility, in z -domain (discrete-time)
i	imaginary number, $= \sqrt{-1}$
$i(t), i(s)$	current, generic
$i_c(t), i_c(s), i_c[n]$	electrical current through the voice-coil in time (continuous), frequency, and discrete-time
$i_{c,m}[n]$	measured electrical current
$i_{c,p}[n]$	predicted electrical current
k	integer, generic
$k_1(x)$	deviation from the small-signal stiffness as a function of displacement
k_a	stiffness due to acoustic loading on the diaphragm of a loudspeaker
$k_d, k_d(x)$	effective stiffness of the diaphragm's suspension; as a function of displacement
k_t	total mechanical stiffness of a loudspeaker diaphragm
l	effective length of the voice-coil; integer, generic
l_{eff}	effective length of the voice-coil
L_{eb}	blocked electrical inductance (the effective inductance of the voice-coil when the voice-coil sees an infinite mechanical impedance)
$L_f^{(n)}\mathbf{h}(\mathbf{x}(t))$	n^{th} -order Lie derivative of the vector field $\mathbf{h}(\mathbf{x}(t))$ along the vector field $\mathbf{f}(\mathbf{x}(t))$
m_a	effective mass of acoustic loading on a loudspeaker diaphragm
m_d	effective moving mass of a loudspeaker diaphragm
m_t	total moving mass of a loudspeaker diaphragm
m_p	effective mass of fluid in a port, of a vented (ported) loudspeaker enclosure
n	integer, generic
N_ϕ	order of polynomial fit to the transduction coefficient
N_k	order of polynomial fit to the suspension stiffness
$p(t), p(s)$	acoustic pressure, generic
$p_{1m}(s)$	acoustic pressure at one (1) meter from a compact acoustic source
$p_b(s)$	pressure at back of diaphragm
$p_c(t)$	cavity acoustic pressure
$p_f(s)$	pressure at front of diaphragm
$p_r(s)$	far-field acoustic pressure
$p_{\sigma_u \cdot n}$	n^{th} coefficient of a polynomial approximation of the determination of σ_u in terms of a_2 (§2.3.3)
\mathbf{p}	new-signal-input-signal cross-correlation vector
\mathbf{P}	matrix for continuous-to-discrete-time feedback coefficient conversion according to the bilinear transform
Q	'quality-factor' of a system's resonance ($= \sqrt{km}/c$)
Q_{es}	electrical Q of a loudspeaker
Q_{ms}	mechanical Q of a loudspeaker
Q_{tc}	total Q of a loudspeaker mounted in a closed box
\mathbf{Q}	matrix for continuous-to-discrete-time feedforward coefficient conversion according to the bilinear transform
r	distance from acoustic source to acoustic receiver
r_d	effective radius of the loudspeaker diaphragm
R_{eb}	blocked electrical resistance (the effective resistance of the voice-coil when the voice-coil sees an infinite mechanical impedance, or DC electrical resistance)
\mathbf{R}	new-signal autocorrelation matrix

s	the ‘Laplace variable’: $s = -i\omega = -2\pi f\sqrt{-1}$
S_0	characteristic sensitivity of a filter
S_d	effective area of the loudspeaker diaphragm
S_p	effective area of a port
S_{eff}	effective sensitivity
t	time
T	temperature, in °C
T_s	sampling period (interval) of a discrete-time system ($=1/F_s$)
T_c	time constant of a filter $= 1/\omega_c$
$u(t), u(s)$	velocity, generic; control signal output from a controller; input to a system represented in state-space form
$u_d(t), u_d(s), u_d[n]$	diaphragm velocity
$u_p(t), u_p(s)$	port fluid velocity
$u_{df}[n]$	diaphragm velocity, simulated from the force equation
$u_{dv}[n]$	diaphragm velocity, simulated from the voltage equation
u	new-signal vector
$v(t), v(s)$	voltage, generic; generic input signal to a controller
$v_c(t), v_c(s), v_c[n]$	voltage drop across the terminals of the voice-coil
$v_{c,m}[n]$	measured voltage
$v_{c,p}[n]$	predicted voltage
$v_u(t)$	voltage generated by velocity of the voice-coil, or ‘back EMF’
V_0	volume of a cavity
V_{AS}	volume of air with equivalent loading stiffness to suspension stiffness
w	weight vector of a filter, generic
\mathbf{w}_{opt}	optimal weight vector (solution to the Wiener filtering problem)
$x_d(t), x_d(s)$	diaphragm displacement as a function of time t , as a function of s in frequency (Laplace) domain
$x_{df}[n]$	diaphragm displacement predicted from the force equation
$x_{dv}[n]$	diaphragm displacement predicted from the voltage equation
$X_m(s)$	mechanical mobility
$y(t), y[n]$	output, generic
$y_m(t), y_m[n]$	output, measured
$y_p(t), y_p[n]$	output, predicted
$Y_{mo}(s)$	open-circuit mechanical mobility
$Z_{eb}(s)$	blocked electrical impedance
$Z_e(s)$	total electrical impedance
$Z_{mo}(s)$	open-circuit mechanical impedance, i.e. the mechanical impedance (force/velocity ratio) of the diaphragm excluding electrical impedance and acoustical loading
$Z_m(s)$	general mechanical impedance
$Z_{rm}(s)$	mechanical-equivalent acoustic radiation impedance
$Z_{rmf}(s)$	mechanical-equivalent acoustic radiation impedance on the front of a diaphragm
$Z_{rmp}(s)$	mechanical-equivalent acoustic radiation impedance of a port radiating into free air
$Z_{rmr}(s)$	mechanical-equivalent acoustic radiation impedance on the rear of a diaphragm
$Z_{rad}(s)$	acoustic radiation impedance for lumped acoustic systems, i.e. the ratio of pressure to volume velocity of lumped acoustical radiator (note $Z_{rm}(s) = S_d^2 Z_{rad}(s)$, where S_d is the effective area)

α	temperature-resistance coefficient
$\alpha_k[n]$	derivative with respect to coefficient a_k
$\beta_k[n]$	derivative with respect to coefficient b_k
$\varepsilon[n]$	error
$\varepsilon_{oei}[n]$	error of the output-error electrical current algorithm
ζ	damping ratio
λ_n	n^{th} eigenvalue of a system, root of a denominator polynomial, pole in the s -plane
ξ	integrand stand-in variable for displacement (x)
ξ_n	n^{th} zero of a discrete-time system, in the z -plane
$\xi(\mathbf{w})$	error-surface function of the weight vector \mathbf{w}
μ	convergence parameter, generic
π	ratio of a circle's circumference to its diameter
π_n	n^{th} pole in the z -plane
ρ_0	density of air under adiabatic conditions ($\sim 1.21 \text{ kg/m}^3$)
σ_u	characteristic sensitivity of the discrete-time representation of the mechanical mobility of an SDOF system
σ_x	characteristic sensitivity of the discrete-time representation of the mechanical receptance of an SDOF system
ϕ_0	transduction coefficient, under small-signal conditions ($= B \cdot l$), also referred to as 'Bl-product,' or 'force-factor'
$\phi(x)$	transduction coefficient, displacement-dependent
ϕ_n	n^{th} -coefficient of a polynomial approximation to the variation of the transduction coefficient with respect to diaphragm displacement
χ^2	chi-squared error function
$\psi(x)$	inverse of the transduction coefficient ϕ as a function of displacement
ψ_n	n^{th} coefficient of a polynomial approximation to the inverse of the transduction coefficient
ω_0	undamped resonance frequency (in radians / sec.)
ω_z	undamped resonance frequency (in radians / sec.) of a system normalised to the sampling frequency of a digital system, $= 2\pi f_0 / F_s$
Ω	ohm
$\partial_{a_2} \sigma_u(a_2)$	derivative of σ_u (characteristic sensitivity of the discrete-time model of the mechanical mobility) with respect to a_2 , where σ_u is defined as a function of a_2
$\partial_{\phi u}[n]$	derivative of diaphragm velocity $u_d[n]$ with respect to ϕ_0 (small-signal transduction coefficient)
$\partial_{\phi_k u}[n]$	derivative of the diaphragm velocity $u_d[n]$ with respect to ϕ_k
$\partial_{\phi_k x_d}[n]$	derivative of ϕ_k with respect to $x_d[n]$
$\partial_{\phi_k \phi}[n]$	derivative of $\phi(x_d[n])$ with respect to ϕ_k
\S	section, e.g. §3.2.1 denotes sub-sub section 1 of sub-section 2 of Chapter 3.
$\S\S$	sections, e.g. §§3.1-3.3 denotes to sections 3.1 to 3.3.

Abbreviations

BEM	Boundary Element Method
DSP	Digital Signal Processor (Processing)
EMF	Electro-motive force (voltage); specifically as used in discussion of ‘Back-EMF,’ as created in electrodynamic electro-mechanical transducers.
FEM	Finite Element Method
FIR	Finite impulse response, in reference to digital (discrete-time) filters, also known as a transversal filter, or tapped delay line filter
FRF	Frequency response function
Hz	Hertz (cycles per second)
IIR	Infinite impulse response, in reference to digital (discrete-time) filters also known as a recursive digital filter, filter with feedback coefficients, or autoregressive moving-average (ARMA) model
LHS	Left-hand side
LMS	Least Mean Square (stochastic gradient) adaptive algorithm of Widrow and Hoff
RHS	Right-hand side
SDOF	Single-degree of freedom

1. Introduction

The loudspeaker is the basic device for generating sound with electronic systems. It is an old, well-known gadget, dating back to the invention of the telephone in 1875.¹ Its construction of magnets and coiled wire is familiar, sharing much with the rotating electric motor. The increases in inexpensive computing power in recent decades have spurred interest in the possibility that one might be able to do with a computer what cannot be done with the dead weight of magnets and wire-wound copper. This thesis is an investigation into details of several such possibilities.

Considerable research appeared on this subject in the 1990's. The declared purpose of most such research was to improve the quality of an existing loudspeaker by digital processing. Specifically, the most common target has been to reduce nonlinear distortion inherent to a loudspeaker's mechanical construction. A slightly different view is taken here. This thesis considers how simple electronic processing can improve the efficiency, or reduce the size or cost of a given loudspeaker design.

Such a custom designed processor-loudspeaker pair is practical only in the context of an *integrated audio system*, and is thus first briefly introduced. Its basic components are shown in Figure 1.1, comprising a signal processor, power amplifier, and loudspeaker, each of which may be briefly defined as follows:

Signal Processor: An electronic system for treating or modifying the audio signal in some way.

Power amplifier: A power-electronics system for converting the ‘information’ audio signal from the processor to a power-drive signal, with sufficient energy to drive the loudspeaker.

Loudspeaker: An electroacoustical transducer generating sound from the electrical power-drive signal produced by the power amplifier. It should generate sound linearly with respect to the electrical drive signal, i.e. it should reproduce sound with good ‘fidelity’, so that the information in the audio signal is reproduced in the sound made by the loudspeaker.

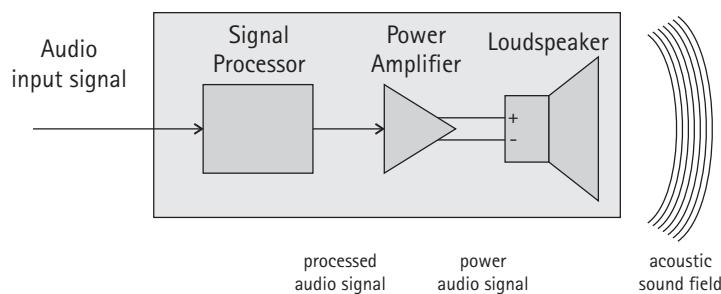


Figure 1.1: Integrated audio reproduction system.

This ‘integrated audio system’ is used in many different types of commercial products, e.g. telephones, hearing aids, television sets, integrated ‘hi-fi’ systems and ‘active monitors’ for speech or music reproduction. As mentioned above, such systems must reproduce the sound field with a certain fidelity to the audio input signal. Good fidelity reproduction is known to be necessary to maintain some desired degree of intelligibility of the speech, or quality of the music. Fidelity is not important

¹ The first moving-coil (electrodynamic) transducer for audio reproduction was described by Siemens (1874). However, Siemens’ device did not see widespread use as a loudspeaker as it is known today. It is generally acknowledged in the loudspeaker engineering community that the first appearance of what is now thought of as an electrodynamic loudspeaker was first developed by Rice & Kellogg in 1925 (see ref.).

in some types of audio reproductions systems, such as audio alert, warning, or alarm systems. These are not considered in this thesis.

The cost/benefit analysis of introducing loudspeaker-enhancing signal processing is different for some types of products using an integrated audio system. Mobile telephones, televisions, and modern integrated ‘hi-fi’ systems all employ fairly powerful digital computational systems for non-loudspeaker related processing. One example is the mobile telephone, which must employ significant digital signal processing for speech compression, i.e. coding and de-coding (codec processing). For such products, the cost of adding loudspeaker-specific processing is much less than other products without such processors, because the hardware and systems for performing such signal processing are already present in the product.

Most music signals, such as may be read from an audio compact disc (CD) or received with an FM radio, will have two or more separate audio signals (channels). Much research has been performed and continues on signal processing and loudspeaker design for proper reproduction of these ‘multi-channel’ audio signals. In this thesis, the focus is on details of the mechanical construction of the loudspeaker driver¹. As these details can be considered in isolation from multi-channel considerations, only single-channel audio systems (systems for reproducing a single audio input signal) are considered in this thesis.

Signal Processor

A signal processor may be used in an integrated audio system to treat or modify the audio signal in some way. As stated above, the purpose of the integrated audio system of Figure 1.1 is to acoustically reproduce some audio input signal. As the loudspeaker must reproduce this signal with fidelity, the signal processor may be employed as a *servo controller*.²

A servo system is considered in two blocks: a *controller*, and a *plant*. The controller sends a control signal $u(t)$ to the plant, based on some processing of the input signal $v(t)$, to ensure that the plant output $y(t)$ follows the input signal $v(t)$ as closely as possible. For the specific case of the integrated audio system of Figure 1.1, the servo controller should ensure that the sound field reproduced by the loudspeaker follows the audio input signal.

An intuitive feature to introduce to such a servo controller is to add closed-loop feedback. Closed-loop feedback systems feed the plant output back to the controller, as per the block diagram shown in Figure 1.2. For the case of the integrated audio system of Figure 1.1, this would mean giving the controller some feedback about how the loudspeaker is reproducing the audio input signal. Feeding the output $y(t)$ back to the controller theoretically permits the controller to compensate for problems or ‘errors’ in the plant (the loudspeaker), and thus maintain maximum fidelity between the input $v(t)$ and the output $y(t)$. If the signal processor can compensate for such problems, it will result in an overall higher fidelity of acoustic reproduction, improving the quality of the audio reproduction system.

¹ The term ‘loudspeaker driver’ is used here to denote a loudspeaker element in isolation from its enclosure.

² The term *servo controller* is used here as it is understood within the field of automatic control systems (e.g. Elgerd, 1967).

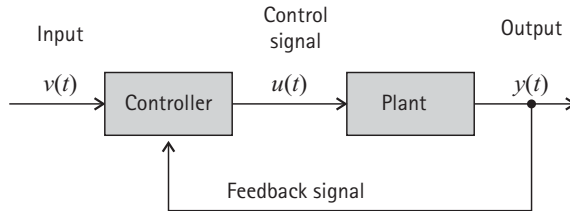


Figure 1.2: Structure of a feedback, or 'closed-loop', control system.

When considering the integrated audio system of Figure 1.1 as a servo system, the signal processor is part of the controller, and the loudspeaker is part of the plant. The power amplifier, however, may be either part of the controller, part of the plant, or part of both.¹

The advantage of a feedback controller is that it can automatically compensate for various problems in the loudspeaker. Typical ‘problems’ with loudspeakers are irregular frequency response² (causing ‘colouration,’ or ‘timbral imbalance’ in the sound), or nonlinear distortion (causing ‘muddiness’ or ‘fuzziness’ and other unpleasant characteristics in the sound). Loudspeaker designers and academics have studied and experimented with this kind of feedback system for nearly as long as there has been such a thing that one could call a ‘loudspeaker’ (Adams, 1979).

Feedback controllers for loudspeakers have a significant disadvantage: the output signal $y(t)$ of a loudspeaker is impractical to obtain. This disadvantage is explained as why no type of closed-loop controller for a loudspeaker has seen much commercial success, despite some 75 years of research and development in academia and industry on such controllers.³ The difficulty can be at least superficially understood by referring back to Figure 1.1. The ‘output’ of this system is the sound field radiated from the loudspeaker. One could ‘collect’ an output with a microphone at some point in the sound field, and employ this as a feedback signal. However, due to the nature of sound wave radiation this feedback signal will be different for different microphone positions. One solution to this problem could be to place the microphone at the listener’s ear. However, although such a system could theoretically serve as a good feedback signal, it would be good only for that one user, and only for one of the user’s ears. The sound field will be different between the user’s right and left ear, and as the user’s head moves relative to the loudspeaker. Thus correcting the sound for one ear would make it worse for the other ear, and even worse still for other listeners in the room.

An even more problematic aspect of such a feedback signal is that acoustic propagation from the loudspeaker to the microphone will introduce a delay, potentially causing the feedback system to fail basic Nyquist stability criteria, a fundamental measure of the stability of feedback systems. Other feedback signals have been tried such as measurement of the loudspeaker’s vibration or using a ‘back-EMF’ motional-induced signal. None of these systems have met with significant commercial success,

¹ Whether the power amplifier is part of the controller, plant, or both depends mainly on the design of the power amplifier, and whether the signal processor is designed with analogue or digital electronics. The different possibilities are discussed in detail in Chapter 3, ‘Theory of active control of loudspeakers.’

² Also referred to as ‘linear distortion.’

³ This problem of motional feedback for loudspeakers is discussed in many papers, e.g. Hanson (1973), Tillett (1975), Adams (1983), Greiner and Sims (1984), Mills and Hawksford (1989), and Klippel (1992), among others.

because of either excess cost or poor robustness, or both.¹ A more detailed review of these systems is in Chapter 3 of this thesis.

If the problematic dynamics of the loudspeaker could be known *a priori*, the controller could simulate them by an appropriate model, eliminating the need for measurement of an output signal. This type of processor is referred to as a *feedforward* or *open-loop* controller, a block diagram of which is shown in Figure 1.3. Dispensing the need to measure an output signal from the loudspeaker is a significant advantage of the feedforward controller. Its disadvantage, however, is that dynamics of the loudspeaker tend to drift with age, temperature, and other factors. Thus feedforward controllers are susceptible to parametric misalignment between the controller's model of the plant and the plant-under-control.

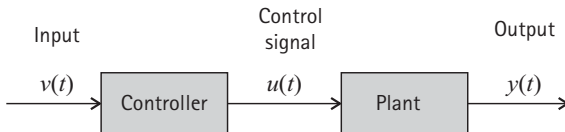


Figure 1.3: Structure of a feedforward, or 'open-loop', control system.

The problem of misalignment between the controller's a model of the plant and the actual plant can be solved by *system identification*. System identification uses the plant model to simulate, in real time, the plant's output. Using *adaptive filtering*, parameters of the model are tuned to minimise the difference between the output predicted by the model and that measured from the plant. The 'identified' parameters of the model can then be used by the feedforward processor, thereby ensuring it is properly tuned to the plant. Adding this feature to the feedforward controller results in a controller known as an *adaptive feedforward controller*, a block diagram of which is shown in Figure 1.4. The key advantage of the adaptive feedforward controller over the feedback controller is that it can use a more indirect output signal from the plant, which is more practical and thus less expensive to obtain. For this reason, it has been considered the most promising processor configuration for loudspeakers (Klippel, Nov. 1998), (Klippel, 1999).

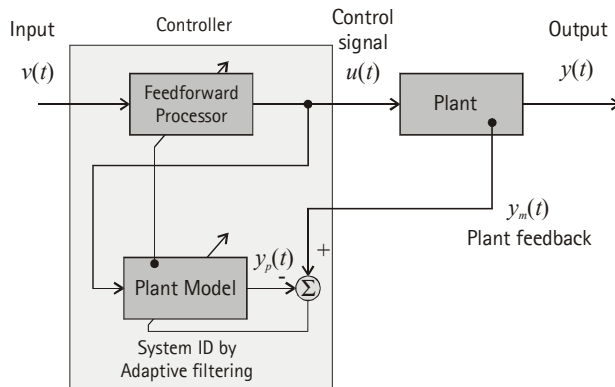


Figure 1.4: Structure of an adaptive feed-forward control system.

¹ This is in contrast to some other applications of motional feedback. One successful applications is for read/write head arms for disk drives, which use a drive mechanism very similar to that used in a loudspeaker (some disk drive terminology, such as 'voice-coil,' is even borrowed from the loudspeaker industry). The enabling factor for disk drives seems to come from the fact that position information for the read/write head arm can be determined directly from formatting information on the disk (Abramovitch and Franklin, 2002).

The basic theory of algorithms for updating the parameters of the plant model in the controller, using recursive adaptive filtering, is presented in Chapter 3.

Power Amplifier

Power amplifiers in modern systems are nearly invariably made from solid-state electronics. These designs produce amplifiers with low output impedance, otherwise known as constant output-voltage sources with fixed gain throughout the audio frequency range. Amplifiers employing vacuum-tubes, or ‘valves’ with considerable output impedance have not completely disappeared, though their manufacture and use has in the last few decades been relegated to a handful of historical enthusiasts and musical instrument amplifiers. To date, nearly all power amplifiers have operated on an analogue input signal. Newer amplifiers, variably referred to as ‘switching’ or ‘Class-D’ amplifiers, have shown the ability to operate on a digital audio input signal. As these amplifiers also produce a low impedance output, they may be treated conceptually in the same manner as traditional solid-state amplifiers.

Other, special types of amplifiers are discussed in the context of motional feedback in Chapter 3. However, these are included only for the historical background of the application of feedback to loudspeakers. In all other parts of this thesis, amplifiers are idealised as constant-gain, constant voltage sources.

Loudspeaker

The idea of a loudspeaker is likely to be familiar to anyone young enough to read this thesis. The original term comes from *loud speaker* (two words),¹ which was to be contrasted with a ‘regular’ speaker (a telephone receiver). It was ‘loud’ in that sound could be heard without it being held to the ear. Early loudspeakers (1900-1920) employed small reeds or diaphragms coupled to a horn. The horn acted as an impedance transformer, matching the high impedance of such mechanical diaphragms to the low impedance of air. The first widely successful loudspeaker not to use a horn was developed by Rice and Kellogg (1925). Their invention, known today as a ‘direct-radiator’² loudspeaker, is widely recognised as the first appearance of what is understood by a ‘loudspeaker’ today.

Loudspeakers have taken many different forms during their development, a good review of which was given already half-a-century ago by Beranek (1955).³ It is already clear in Beranek’s mid-century review that industry at large had settled on the *electrodynamic* loudspeaker type⁴. This type of loudspeaker uses the electrodynamic principle for electro-mechanical transduction, from which it derives its namesake. Other electro-mechanical transduction principles do exist, and have been used to construct other types of loudspeakers. A good contemporary review these different transduction principles is provided by Hixson and Busch-Vishniac (1997). As the electrodynamic transduction

¹ *Loud Speakers* was the title of the first textbook dedicated to loudspeakers. (McLachlan, 1934)

² Rice and Kellogg’s loudspeaker was a ‘direct’ radiator in the sense that sound was radiated directly from the diaphragm, without the acoustical aid of a horn. Although horn-loudspeakers remain in use for high-output loudspeaker systems for public address, nearly all loudspeakers for domestic, portable, and automotive audio systems use direct-radiator type loudspeakers.

³ It is a sad but generally acknowledged fact that precious little new has been done in loudspeaker design since the 1950’s. One manifestation of this appears in monthly patent reviews on loudspeakers by George L. Auspurger published in the *Journal of the Acoustical Society of America*, which all too often (accurately) read ‘Every few years someone patents the familiar invention from 195X...’

⁴ Electrodynamic-type loudspeakers are also referred to as *moving coil* loudspeakers.

principle remains the only one in widespread use in loudspeakers for audio-frequency reproduction, the electrodynamic loudspeaker is the only type considered in this thesis.¹

Audio systems which must reproduce the full audio frequency bandwidth typically use two or three loudspeakers, each for a separate frequency range. This due to the difficulty in reproducing the three-decade² wide bandwidth of the audio frequency range with a single transducer. This thesis is concerned with the effects of signal processing on mechanical construction of the loudspeaker, which can be considered in isolation from multi-transducer loudspeaker systems. Additionally, this thesis has focused particularly on the ‘microspeaker,’ intended for reproducing speech frequencies, which can be done effectively over a frequency bandwidth of only one decade. For these reasons, only single-loudspeaker systems are considered in this thesis.

1.1. Active control of loudspeakers

The goal of research reported in this thesis has been to find ways, if any, to simplify the mechanical construction or improve the efficiency of a loudspeaker by electronic signal processing. This is, broadly speaking, the same goal as other systems employing *active control*.

The idea of an ‘actively controlled’³ or ‘smart’ loudspeaker has been discussed by several authors. However, these previous discussions have referred to control of different aspects of the loudspeaker from those investigated in this thesis. Sophisticated digital systems for controlling high-count loudspeaker arrays, variably called ‘system controllers’ or ‘loudspeaker processors’ have been in commercial use for some years (Forsythe et al., 1994). In this thesis, the function of the processor is considered with regard to how it can simplify the mechanical construction of the loudspeaker.

Active control has shown the ability to produce a more economical solution than passive mechanical systems in various engineering problems. Two well-known examples are flight control of aerospace structures and the reduction of acoustic noise and vibration. Active control of aeroplanes, or ‘Fly-by-wire’ flight control provides two key advantages over passive-mechanical control systems: the ability to automatically stabilise an unstable system, and the reduction of weight of a mechanical hydraulic-assist system. These two features have seen Fly-by-wire flight control systems serve as a method for cost-reduction in commercial civilian aircraft (Collinson, 1999). Active control of acoustic noise has also proven more economical than passive techniques in some applications, such as hearing-protectors (ear defenders) and propeller-based passenger aircraft (Elliott, 1999). In both of these successful fields of active control, electronic processing offers a more economical solution than passive systems,

¹ It is generally considered within the Hi-Fi loudspeaker industry that the electrodynamic principle is used by at least 99% of all loudspeaker elements. One may arrive at a different percentage if one considers that telephones, personal stereo headphones, automotive audio systems, and portable consumer electronics have all exclusively used electrodynamic loudspeakers for several decades. As annual production of loudspeakers for these products runs into the hundreds of millions, the percentage figure is thought to be closer to 99.9999%.

One may wonder whether other known transduction principles have been neglected by force of habit over the decades. Perhaps the other principles could be used to great effect, but have been forgotten by the mainstream loudspeaker industry, be it by oversight, ‘technology momentum,’ or vested interest? The truth is that no small amount of effort has been spent trying to develop loudspeakers based on non-electrodynamic transduction principles. Any doubter of this fact is referred to Frederick Hunt’s 92-page historical review of electroacoustics in his 1954 text *Electroacoustics* (Hunt, 1954).

² The term ‘decade’ is used here to denote a range of frequencies wherein the highest frequency is 10 times the lowest frequency. One decade equals approximately 3.322 octaves.

³ The term *actively controlled loudspeaker* is intended to be different from an *active loudspeaker*; the latter term is commonly used to describe loudspeakers with built-in power amplifiers (i.e. in the same cabinet),

primarily through weight reduction, achieved by limiting some mechanical bulk needed for the equivalent passive solution, particularly for aerospace applications. To be sure, these applications of active control have a significant advantage over the loudspeaker: the cost of a civilian airplane is \$40-100 million, whereas a loudspeaker averages about \$1. This different cost basis for the addition of an active control system may explain why it has yet to be applied with commercial success to the loudspeaker.

Of particular interest in battery-powered audio reproductions systems is a loudspeaker's the pressure to voltage sensitivity in addition to its efficiency. This is due to the limited voltage output capability of amplifiers in battery-powered products. Due to the need to lower battery voltages in order to decrease the power consumption of logic circuits, the voltage available to power amplifiers is limited. Furthermore, no suitably compact and efficient voltage step-up converters are known to exist which could solve this problem. Thus in many cases, the acoustic output of audio systems in battery-powered products is limited by the voltage sensitivity of the loudspeaker, and not the power handling capabilities of the amplifier and loudspeaker.

It was suggested by Klippel (2000), that active control of nonlinear distortion in a loudspeaker be used to create the same displacement in an electrodynamic loudspeaker, but with a shorter voice-coil height. Furthermore, it was suggested that the additional output from the amplifier required for the shorter voice-coil would be modest. This shortening of the voice-coil height can result in a more efficient loudspeaker in two ways. Firstly, shortening the voice-coil height permits concentration of the coil wire into the strongest part of the magnetic field, resulting in a higher basic current-to-force electrodynamic transduction factor¹. Secondly, shortening the voice-coil height will reduce the moving mass of the loudspeaker; as the electrodynamic loudspeaker is a mass-controlled transducer, this will increase its basic sensitivity. The trade-off between a shorter coil height and the additional electrical output needed to compensate for the nonlinear distortion created by shortening the coil height is simulated in detail in Chapter 5.

The general result of these simulations shows that the highest overall-sensitivity is achieved for a coil-height approximately equal to the magnet gap height. This result has been confirmed with a series of measurements of specially-prepared shortened-coil-height loudspeakers, as reported in Chapter 5.

1.2. Organisation of thesis

Chapter 1. Introduction.

Chapter 2. Loudspeaker models: Classical linear and nonlinear models of the loudspeaker are reviewed. Application of these models to a miniature electrodynamic loudspeaker, defined as a microspeaker, is discussed. As active control systems use digital processing techniques that operate in discrete time, methods for representing the classical linear and nonlinear loudspeaker models in discrete time are reviewed. A simple discrete-time model of a loudspeaker including its dominant nonlinearities is developed from established theory. The chapter concludes with a presentation of causes of parametric variation in these models, leading to parameters which cannot be known *a priori*.

Chapter 3. Theory of active control of loudspeakers: This chapter presents the theory of signal processing for active control of loudspeakers. It presents classical and recently published theory in the context of loudspeakers. The discussion is divided into three categories: (i) feedback processing, (ii)

¹ Also known as a *transduction coefficient*, or *B-l-factor*; the latter term is most commonly used in the loudspeaker industry. This term is defined in the context of the general classical models of the loudspeaker in Chapter 2.

feedforward processing, and (iii) adaptive feedforward processing (as per Figures 1.2 – 1.4 above). The discussion concludes that the adaptive feedforward processing structure is the most practical for active control of loudspeakers.

This chapter includes a special section on the theory of feedback linearisation, which is included as an extended discussion on feedforward processing, i.e. (ii), above. The history of the application of feedback linearisation to the loudspeaker and how it is used to develop a nonlinear feedforward controller for active nonlinear control of loudspeakers is presented. In this section a new application of feedback linearisation to the loudspeaker – a discrete time form – is presented, using the discrete time loudspeaker model developed in chapter 2. This is used to develop a new, simple algorithm for nonlinear control of loudspeakers.

Following the conclusion that adaptive feedforward control is the most practical form for active loudspeaker control, a brief review of adaptive filtering theory is presented, with particular focus on the LMS algorithm for adaptive recursive (IIR) filters.

Chapter 4. Loudspeaker system identification: This chapter presents implementation of the system identification part of the adaptive feedforward controller of Figure 1.4. A direct-form LMS IIR output error algorithm is used to identify those parameters of the discrete-time loudspeaker model which cannot be known *a priori*, as discussed in chapter 2. Three different plant model structures are presented. Equations for iterative parameter identification are derived according to basic adaptive filtering theory. Convergence performance of the different plant model structures, using data measured on actual loudspeakers, are presented for different types of signals. Conclusions are drawn about the most efficient plant model structure for loudspeaker system identification.

Chapter 5. Applications of active control of a loudspeaker: Two applications of active control to a loudspeaker and their impact on loudspeaker design are considered. Linear control, or equalisation, is first considered briefly. Nonlinear control, or nonlinear distortion compensation, is considered in more detail.

The benefit of nonlinear distortion compensation is investigated by simulation. The trade-off between sensitivity increase from a reduced coil height versus the additional amplifier output required for compensation of nonlinear distortion caused by the reduced coil height is evaluated. From the simulation results, the overall sensitivity for different coil heights is considered as a function of coil displacement, for a range of frequencies.

Based on the simulation results, a special set of modified coil-height loudspeakers were prepared. Linear and nonlinear measurements on these samples are presented. The ability of the new algorithm for nonlinear control of loudspeakers, presented in chapter 3, to compensate harmonic distortion generated in these samples is assessed, and measurements of the reduction in harmonic distortion are presented. Conclusions are drawn about the optimal coil height of loudspeakers for use with active control.

Chapter 6. Conclusions: Conclusions are drawn on active control of loudspeakers using adaptive feedforward processing and how it can benefit loudspeaker design. Potential problems in commercial implementation are identified. Suggestions for further research are given.

Appendix A. Experimental set-up and tuning: Experimental set-ups used for measurements made in various parts of the thesis are presented. Diagrams and photographs of the experimental set-ups are shown. Some techniques used for equipment calibration and parameter tuning are presented.

Appendix B. Experimental determination loudspeaker parameters: A method for determining the linear parameters of a loudspeaker is presented. This provides accurate determination of parameters of the single-degree-of-freedom loudspeaker model, as well as methods for verification of the model by reference to measured frequency response functions. Results from this method are used to verify results from the adaptive algorithms presented in Chapter 4. As this method has not been previously published, it is included here.

Appendix C. Modal analysis of loudspeaker diaphragms: Techniques for developing multi-degree of freedom models for loudspeaker diaphragms based on traditional modal analysis for vibrating systems are presented. The techniques presented here could be used to develop higher-order models of loudspeaker diaphragm vibration for a feedforward processor, although such techniques are not presented in this thesis. The technique presented here do present a theoretical framework for understanding some discrepancies seen between models and measured results.

Appendix D. Rocking modes in single-suspension loudspeakers: Methods for modelling ‘rocking modes’ in single suspension loudspeakers are presented, based upon techniques for modal analysis of loudspeaker diaphragms presented in Appendix C. The models of rocking modes describe the discrepancy between measured and modelled results seen in other parts of the thesis.

1.3. References

- Abramovitch, Daniel, and Gene Franklin, “A Brief History of Disk Drive Control,” *IEEE Control Systems Magazine*, **22**, pp. 28-42. (June, 2002)
- Adams, G. J., *Optimisation and Motional Feedback Techniques in Loudspeaker System Design*, Ph.D. thesis, The University of Southampton. (Dec. 1979)
- Adams, G. J., “Adaptive control of loudspeaker frequency response at low frequencies,” presented at the 73rd convention of the AES. preprint no. 1983. *Journal of the Audio Eng. Soc. (Abstracts)* Vol. 31, p 361 (May 1983)
- Beranek, Leo L., “Loudspeakers and Microphones”, *J. Acoust. Soc. Amer.*, **26**, pp. 618-629. (Sept. 1955)
- Collinson, R. P. G., “Fly-by-wire flight control”, *Journal of Computing & Control Engineering*, **10**, pp. 141-152. (Aug., 1999)
- Elgerd, Olle I., *Control Systems Theory*, McGraw-Hill Kogakusha, Ltd., Tokyo, Japan. (1967)
- Elliott, Stephen J., “Down with Noise”, *IEEE Spectrum*, pp. 54-61. (June 1999)
- Forsythe, Kenton G., Gregory Burlingame, Andrew Rutkin, and Mark Lacas, “New Approaches to Loudspeaker System Control”, *proceedings of the 13th International Conference of the Audio Eng. Soc.*, pp. 58-63. (1994)
- Greiner, R. A., and T. M. Sims, Jr., “Loudspeaker Distortion reduction,” *Journal of the Audio Eng. Soc.*, **32**, pp. 956-963. (1984)
- Hanson, E. R., “A Motional Feedback Loudspeaker System,” *Presented at the 46th Convention of the AES*, preprint No. 924. (Sept. 1973)
- Hixson, Elmer L., and Ilene J. Busch-Vishniac, “Transducer Principles,” *Encyclopaedia of Acoustics, Chapter 159*, John Wiley & Sons, Inc., NY, NY; pp. 1889-1902. (1997)
- Hunt, Frederick V., *Electroacoustics*, Harvard University Press, Cambridge, Mass., USA. (1954)

- Klippel, Wolfgang, "The Mirror Filter-A New Basis for Reducing Nonlinear Distortion and Equalizing Response in Woofer Systems," *Journal of the Audio Eng. Soc.*, **40**, pp. 675-691. (Sept. 1992)
- Klippel, Wolfgang J., "Adaptive Nonlinear Control of Loudspeaker Systems," *Journal of the Audio Eng. Soc.* **26**, pp. 939-954. (Nov. 1998)
- Klippel, Wolfgang J., "Nonlinear Adaptive Controller for Loudspeakers with Current Sensor," presented at the 106th Convention of the AES (May 8-11, 1999), preprint no. 4864; *Journal of the Audio Eng. Soc.* (Abstracts), **47**, p. 512 (Jun. 1999)
- Klippel, Wolfgang J., Personal, unwritten correspondence, Paris, France. (February 22, 2000)
- McLachlan, N. W., *Loud Speakers*, Oxford University Press, London, England. (1934)
- Mills, P. G. L., and M. O. J. Hawksford "Distortion reduction in moving-coil loudspeaker systems using current-drive technology." *Journal of the Audio Eng. Soc.*, **37**, pp. 129-148. (Mar. 1989)
- Organ, Richard, *Avro Arrow*, Toronto, Stoddart Publishing Co. Limited, Toronto, Canada. (1992)
- Rice, Chester W., and Edward W. Kellogg, "Notes on the Development of a New Type of Hornless Loud Speaker," *Transactions of the American Institute of Electrical Engineers*, **44**, pp. 461-475. (April 1925)
- Siemens, Ernst Werner, U. S. Patent No. 149,797 (filed Jan. 20, 1874) issued Apr. 14, 1874.
- Tillett, G. W., "Motional Feedback in Loudspeakers," *Audio*, **59**, pp. 40-43. (Aug. 1975)
- Tomayko, James E., "Blind Faith: The United States Air Force and the Development of Fly-By-Wire Technology," *Technology and the Air Force*, U.S. Air Force, Washington, D.C., USA, p. 167. (1997)
- Tomayko, James E., *Computers Take Flight: A History of NASA's Pioneering Digital Fly-by-wire Project*, NASA Dryden Flight Research Center, Edwards, California, USA. (2000)

2. Loudspeaker models

This chapter reviews previously published linear and nonlinear models of loudspeakers. The classical linear models of the electrodynamic loudspeaker are developed here from first principles. Methods for introducing nonuniformity of the parameters of the classical linear models, leading to nonlinear models, are reviewed thereafter.

A study of methods for discrete-time representation of the classical linear models is given. Parametric variation in these models of the loudspeaker, due to thermal fluctuations and other factors, are discussed. At the end of the chapter, a nonlinear discrete-time model of the loudspeaker is developed by using simple continuous-to-discrete-time model conversion methods and the previously published nonlinear loudspeaker models, with special consideration for inherent discrete-time stability.

2.1. Linear models of loudspeakers

This research has focused specifically on ‘microspeakers;’¹ these are small, thin loudspeakers resembling earpieces or telephone receivers, used in hand-held telephones for generating alert tones and speech for hands-free telephony. The differences between the ‘microspeaker’ and traditional direct-radiator electrodynamic loudspeaker are explained in more detail below.

The basic elements of a thin electrodynamic loudspeaker, or ‘microspeaker,’ are shown in Figure 2.1. A coil of wire, called the ‘voice-coil’ (1), is attached to a diaphragm (2), that is mounted on a fixed frame (4) via a suspension (3). A magnetic field is generated by a permanent magnet (5) that is conducted to the region of the coil via a magnetic circuit (6). This generates a concentrated magnetic field in the region of the coil gap (7). Holes in the rear frame (8) provide ventilation to the rear enclosure.

According to laws of classical electrodynamics, due to the presence of the magnetic field, electrical current passing through the voice-coil will generate a force f_c in the direction shown in Figure 2.1 (assuming proper orientation of the coil current and magnetic field). This force f_c will generate a displacement x_d in the direction shown.

¹ The term ‘microspeaker’ is commonly used among producers and telephone manufacturers in North America, Japan, and the Pacific Rim. The term ‘telecom loudspeaker’ is more common in Europe. Although this thesis is published by a European institution, the term ‘microspeaker’ is used herein, for brevity, to distinguish this type of speaker from the traditional direct-radiator electrodynamic loudspeaker.

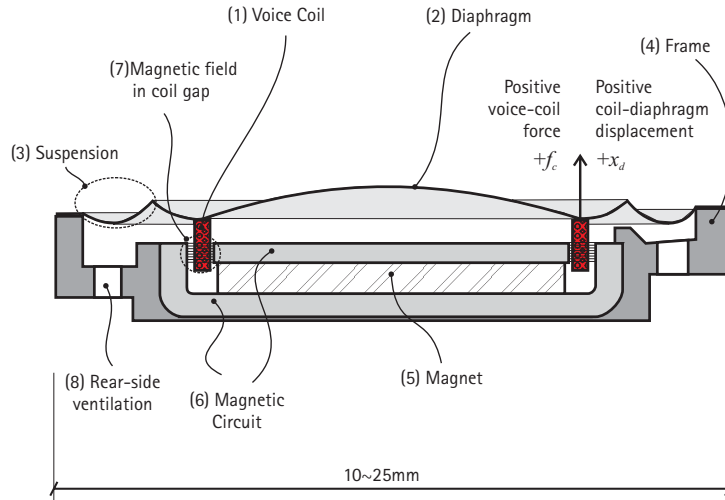


Figure 2.1: Cross-section of a thin electrodynamic loudspeaker ('microspeaker,') showing its basic components.

The microspeaker is made from the same basic elements as ordinary electrodynamic loudspeakers, differing primarily in scale and shape. There are some differences worth noting, which are pointed out here by comparison to a typical low-frequency electrodynamic loudspeaker, an example of which is shown in Figure 2.2. As shown in Figure 2.2, the voice-coil of a typical loudspeaker is placed on a former (1b), making a mechanical connection to the diaphragm (2a & 2b). The coil former is typically a hollow cylinder. This requires that the diaphragm be made in two parts, the outer diaphragm (2a) and a dust cap (2b), placed over the coil former. The dust cap increases the loudspeaker's overall effective radiating area and prevents foreign debris from entering the coil gap. The last difference that will be noted here is in the suspension; a typical loudspeaker employs two suspensions: an outer suspension (3a) connecting the diaphragm to the frame (often called the 'surround'), and an inner suspension (3b) connecting the coil former to the frame, often called the 'spider' due to its spoke construction in early generations of loudspeakers. The pair of suspensions create a strong stiffness against 'rocking' or 'wobbling' of the diaphragm-coil assembly. The absence of this second suspension in microspeakers makes the microspeaker particularly susceptible to this problem. This effect can be seen in several measurements presented in this thesis, and is discussed in detail in Appendix D.

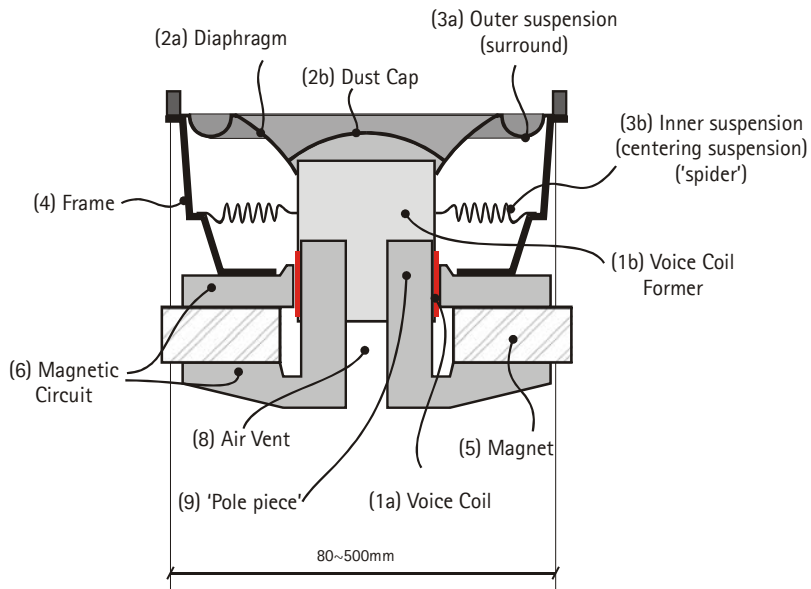


Figure 2.2: Cross section of a typical low-frequency electrodynamic loudspeaker.

At low displacements of the diaphragm-coil assembly, the electro-mechano-acoustic dynamics are linear, and thus linear models can be used to describe the relationship between the two.¹ At higher displacement, the relationship is not linear, as parameters of the model vary with displacement. Distinguishing between ‘high’ and ‘low’ displacement in this context depends on a specific loudspeaker’s construction. The dominant characteristics are the linearity of the restoring force provided by the suspension (3) and the uniformity of the force-factor created by the placement of the voice-coil (1) in the magnetic field (7). Linear models which form part of classical loudspeaker theory are presented below. The presentation is broken into the electrical (§2.1.1), mechanical (§2.1.2), and acoustical (§2.1.4) component, with a discussion of the application of these models to the microspeaker. Models of the parametric nonuniformity that result in nonlinear behaviour are presented in §2.2, along with measurements of this nonuniformity found in a typical sample of a microspeaker.

2.1.1. Electrical dynamics

A good, simple model for the electrical behaviour of a loudspeaker is shown in the current loop on the left-hand side of Figure 2.3.

¹ The terms ‘linear’ and ‘nonlinear’ are used here in the algebraic sense, i.e. wherein a linear system obeys the principles of scalability and superposition, and a nonlinear system does not.

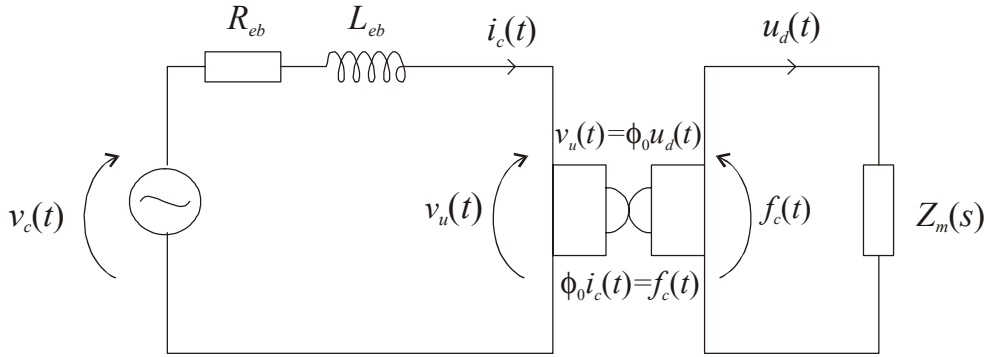


Figure 2.3: Simplified model of electrical elements in an electrodynamic loudspeaker.

The amplifier output is represented by the voltage source $v_c(t)$, as nearly all amplifiers used for loudspeakers are of low output-impedance, constant voltage type. The resistor R_{eb} represents the electrical resistance of the coil wire. Electrical inductance due to the voice-coil's shape and ferromagnetic material in its vicinity is modelled by the inductor L_{eb} . Electro-mechanical transduction is modelled by a *gyrator*, shown in the middle of Figure 2.3. This is similar to a transformer, except that voltage in the primary loop scales with the *current* in the secondary loop (as opposed to voltage in the secondary loop for a transformer.) The converse is true for current in the primary loop and voltage in the secondary loop. The current in the secondary loop, on the right-hand-side of Figure 2.3, is analogous to the voice-coil velocity $u_d(t)$, and therefore the voltage drop induced by the gyrator is the product $\phi_0 u_d(t)$, where ϕ_0 is the gyrator's constant. All of these effects may be combined into this single frequency (Laplace) domain equation:

$$v_c(s) = (R_{eb} + sL_{eb})i_c(s) + \phi_0 u_d(s) \quad (2.1)$$

where the terms in (2.1) have the following names:

$v_c(s)$	Voltage drop across the terminals of the voice-coil.
R_{eb}	Blocked electrical resistance.
L_{eb}	Blocked electrical inductance.
ϕ_0	Transduction coefficient (same as ' <i>B-l</i> -factor,' or 'force-factor.')
$u_d(s)$	Velocity of the diaphragm and coil assembly.
s	The 'Laplace variable,' $= -i\omega$, where $i = \sqrt{-1}$, and $\omega = 2\pi f$, where f is the frequency in Hz.

The terms R_{eb} and L_{eb} are the most common description of a loudspeaker's internal electrical impedance. Together they describe the electrical impedance when the coil may not move (is mechanically blocked.) It is thus called the *blocked electrical impedance*, and represented by the symbol $Z_{eb}(s)$. One may, therefore, generalise (2.1) to

$$v_c(s) = Z_{eb}(s)i_c(s) + \phi_0 u_d(s) \quad (2.2)$$

A phenomenon called *eddy currents* results in a reactive blocked electrical impedance that differs significantly from that of a simple inductor. A good model of this phenomenon was developed by Vanderkooy (1989), wherein the effect was described as an inductance varying with the square-root of frequency, i.e.:

$$\text{Im}\{Z_{eb}\} \propto \sqrt{f} \quad (2.3)$$

Typical examples of the blocked electrical impedance measured from actual loudspeakers are shown in Figure 2.4 and Figure 2.5. The measurement shown in Figure 2.4 is from a full-range loudspeaker, and that shown in Figure 2.5 is from a microspeaker. The ‘blocked’ condition (no mechanical movement) for the full-range loudspeaker has been ensured by placing cyanoacrylate adhesive (“super-glue”) in the coil gap. The measurement for the microspeaker has been synthesised by the difference between the total electrical impedance and the velocity-induced EMF by a measurement of the velocity, using a method described in detail in Appendix B.

The reactive (imaginary) part of the impedance of the full-range loudspeaker decreases linearly with frequency, as it would for a pure inductance, down only to about 200Hz. From 200 to 2000Hz it varies with $f^{1/2}$, as per the model developed by Vanderkooy, and above 2000Hz it is more or less invariant with frequency up to the end of the audio frequency range. This strong eddy-current effect has been intentionally introduced by the designer by attaching a hollow cylinder mounted on the pole piece (part (9) in Figure 2.2). This has the benefit of reducing the overall blocked electrical impedance at higher frequencies, thereby increasing the sensitivity at these frequencies (Rausch et al., 1999)¹. By contrast, no such effect is seen in the microspeaker. Its reactive impedance decreases linearly with frequency, and is thus well-modelled by a simple inductor over the audio frequency range.

It is also noted that, for the microspeaker, the overall level of the reactive impedance is low relative to the resistive part over the telephone-band frequency range (up to 4000Hz). This makes it possible, in some cases, to ignore the effect of the inductance, thereby significantly simplifying some aspects of modelling the loudspeaker’s dynamics.

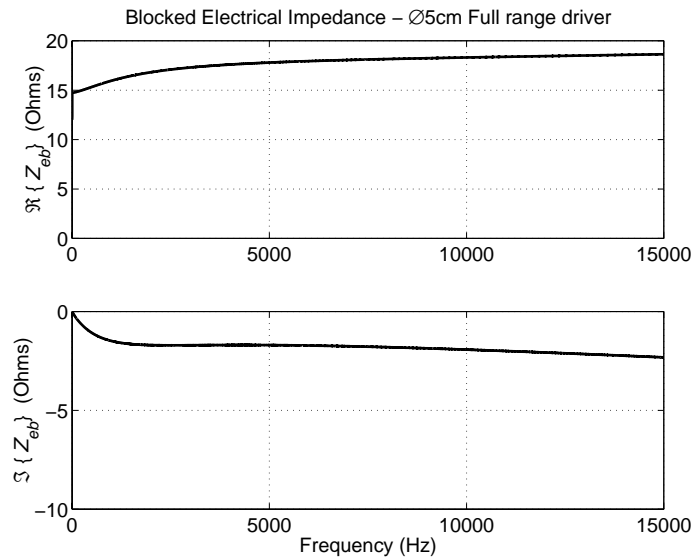


Figure 2.4: Typical blocked electrical impedance of a full-range loudspeaker. Upper: Real part; Lower: Imaginary part. This loudspeaker employs a hollow copper cylinder on the pole-piece to reduce the electrical inductance at high frequency [see Rausch et al. (1999), p. 417, Fig. 8, for a discussion of this effect].

¹ see Figures 8 and 10 of Rausch et al. (1999).

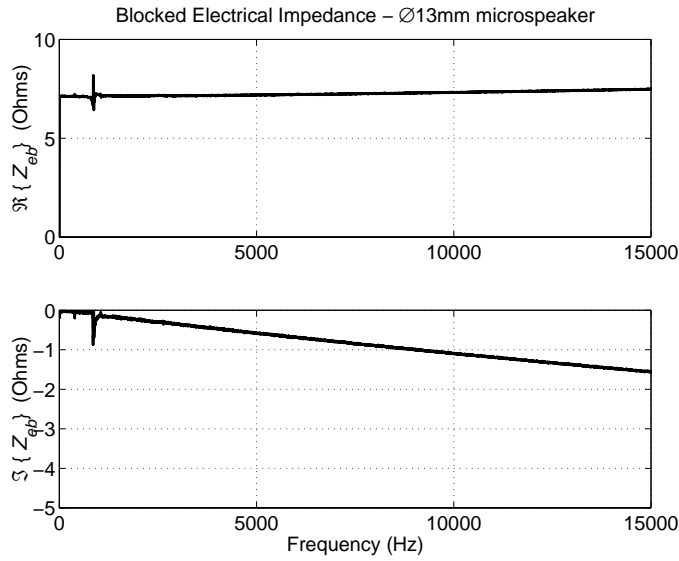


Figure 2.5: Typical blocked electrical impedance for a microspeaker. Upper: Real part; Lower: Imaginary part. The real part is synthesised using the RHS of (B.9), and the imaginary part is synthesised using the RHS of (B.10), both presented in Appendix B. The aberration appearing at approximately 900Hz is an error caused by large variations of with respect to frequency in the originally measured frequency response functions from which these were synthesised.

2.1.2. Mechanical dynamics

A good model of the mechanical dynamics of the electrodynamic loudspeaker is a single-degree-of-freedom (SDOF) mechanical oscillator.¹ A diagram showing an analogous mechanical system is shown in Figure 2.6.

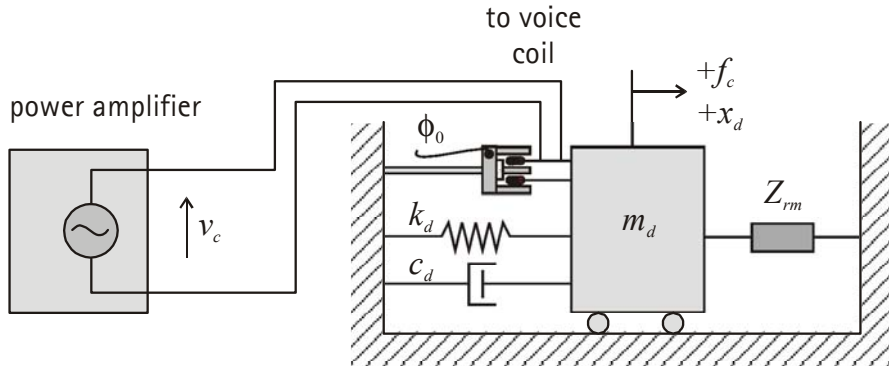


Figure 2.6: Single-degree-of-freedom (SDOF) mechanical representation of dynamics of an electrodynamic loudspeaker. The element Z_{rm} is a generalised mechanical impedance, representing the acoustic loading.

From classical mechanics, the SDOF system is described by this second-order linear inhomogeneous differential equation:

¹ Higher-order models of mechanical dynamics, or multi-degree of freedom (MDOF) models, have also been studied as part of the research for this thesis. They are not central to the theory of active control as developed in this thesis, though they are used to explain some differences between modelling and measurement in various parts of this thesis. For this reason, MDOF models of mechanical dynamics of loudspeakers are discussed in Appendix C and Appendix D.

$$m_d \ddot{x}_d(t) + c_d \dot{x}_d(t) + k_d x_d(t) = f_c(t) \quad (2.4)$$

where the terms in (2.4) have the following names:

m_d	Diaphragm mass
$x_d(t)$	Displacement of the diaphragm.
c_d	Damping due to the suspension.
k_d	Stiffness (restoring force) due to the suspension.
$f_c(t)$	Force on the voice-coil.

A generalised mechanical impedance $Z_{mo}(s)$ is defined by the Laplace transform of (2.4)

$$Z_{mo}(s) = \frac{f_c(s)}{u_d(s)} \Big|_{\substack{i_c(s)=0 \\ p_s(s)=0}} = sm_d + c_d + k_d / s \quad (2.5)$$

where $u_d(s)$ is the diaphragm velocity (i.e. the time derivative of $x_d(s)$, the diaphragm displacement). The term $Z_{mo}(s)$ is the *in-vacuo open-circuit mechanical impedance*. It describes the diaphragm's force to velocity ratio under these two conditions:

- The voice-coil is open-circuit ($i_c(s)=0$.)
- The loudspeaker is in a vacuum, removing acoustical loading ($p_s(s)=0$.)

The term $Z_{mo}(s)$ is also referred to as the ‘internal mechanical impedance.’

The *mobility* is another important transfer function of an SDOF system, as it more directly characterises its resonance. It is given by the multiplicative inverse of the impedance as so:

$$Y_{mo}(s) = \frac{u_d(s)}{f_c(s)} = \frac{1}{Z_{mo}(s)} = \frac{1}{sm_d + c_d + k_d / s} = \frac{s}{s^2 m_d + s c_d + k_d} \quad (2.6)$$

The denominator of this function may be factored as so:

$$Y_{mo}(s) = \frac{1}{m_d} \frac{s}{(s - \lambda_1)(s - \lambda_2)} \quad (2.7)$$

where λ_1 and λ_2 are the roots of the denominator polynomial of (2.6). These define the eigenvalues of the mechanical system, giving the location of the transfer function’s poles in the s -plane. They are calculated from the system’s physical parameters according to

$$\lambda_1, \lambda_2 = -\omega_0 \zeta \pm i \omega_0 \sqrt{1 - \zeta^2} \quad (2.8)$$

where ω_0 , the undamped natural frequency, is given by

$$\omega_0 = \sqrt{\frac{k_d}{m_d}} \quad (2.9)$$

and where ζ , the damping ratio, is given by:

$$\zeta = \frac{1}{2} \frac{c_d}{\sqrt{k_d m_d}} \quad (2.10)$$

The mobility transfer function of (2.7) may be further separated into first-order terms by partial fraction expansion, as so:

$$Y_{mo}(s) = \frac{1}{m_t} \frac{1}{\lambda_1 - \lambda_2} \left(\frac{\lambda_1}{s - \lambda_1} - \frac{\lambda_2}{s - \lambda_2} \right) \quad (2.11)$$

This form is particularly convenient for developing an expression for the impulse-response in continuous-time by inverse Laplace transform, as will be used later in this chapter.

2.1.3. Electro-mechanical transduction

Interaction between the electrical and mechanical components is caused by the classical electrodynamic interaction of line currents and static magnetic fields. As described in §2.1.1 above, the forcing term $f_c(t)$ on the right-hand-side of (2.4) is produced by a current flowing through a coil in the magnetic field, which may be modelled by

$$\begin{aligned} f_c(t) &= Bl i_c(t) \\ &= \phi_0 i_c(t) \end{aligned} \quad (2.12)$$

where $i_c(t)$ is the voice-coil current and l is the effective length of the voice-coil wire in a magnetic field of flux density B . These two quantities are often referred to together as the *B·l product*. As both l and B are constants, it is convenient to define their product as the single scalar ϕ_0 called the *transduction coefficient* on the urging of Birt (1991). The transduction coefficient ϕ_0 gives a ratio of force to current, and is therefore also referred to as the *force factor*.

2.1.4. Acoustical components

The acoustic fluid affects the mechanical behaviour of the loudspeaker. These effects can be modelled by linear components, assuming the acoustic pressures generated by the diaphragm are accurately described by the linear acoustic equations. These have the effect of adding terms on the left-hand-side of the basic diaphragm equation of motions, (2.4). As they are linear operators on $x_d(t)$, they may be separately lumped together, and defined as a single distinct impedance. For this reason, the acoustic effects on the mechanical behaviour are called the *acoustic radiation impedance*. Therefore the total mechanical impedance $Z_m(s)$ is defined by

$$Z_m(s) = \frac{f_c(s)}{u_d(s)} = Z_{mo}(s) + Z_{rm}(s) \quad (2.13)$$

where $Z_{rm}(s)$ is the *mechanical-equivalent acoustic radiation impedance*. It is related the traditional lumped-parameter acoustic impedance $Z_{rad}(s)$ by $Z_{rm}(s) = S_d^2 Z_{rad}(s)$ where S_d is the effective radiating area of the loudspeaker's diaphragm.

In most applications the loudspeaker is mounted in a cabinet or baffle that prevents acoustic interaction between the front and rear sides of the diaphragm. This permits the radiation impedance on the front and rear sides to be treated independently. From the 'point of view' of the loudspeaker, the front and rear loading may be summed together with the internal mechanical impedance as so:

$$Z_m(s) = Z_{mo}(s) + Z_{rmf}(s) + Z_{rmr}(s), \quad (2.14)$$

where $Z_{rmf}(s)$ is the front-side acoustic impedance, and $Z_{rmr}(s)$ is that on the rear-side. Parametric models of the radiation impedance are developed below.

Closed box enclosure

The simplest rear-acoustic loading commonly used for loudspeakers is a closed-box enclosure. Mounting a in such an enclosure, as per Figure 2.7, prevents front-to-back sound pressure cancellation,

resulting in monopole radiation (instead of dipole radiation, which would be the case without the enclosure).

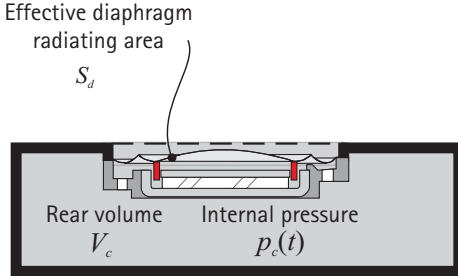


Figure 2.7: Loudspeaker mounted in a closed-box enclosure

If all dimensions of the cabinet are small compared to the largest wavelength considered, the pressure is constant throughout the cavity. In this case acoustic pressure $p(t)$ in the cavity is determined by the changes in the cabinet's volume caused by movement of the diaphragm. Consider the cavity of volume V_0 shown in Figure 2.8, wherein a pulsating sphere, the volume of which changes according to $V(t)$.

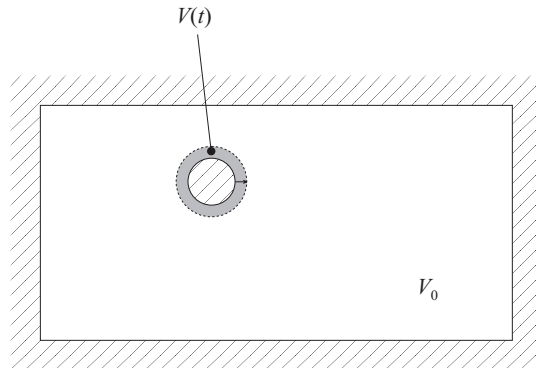


Figure 2.8: Cavity of volume V_0 containing a sphere with oscillating volume $V(t)$.

Assuming adiabatic temperature fluctuations, the acoustic pressure in the cavity will be

$$p(t) = \frac{V(t)}{V_0} \rho_0 c_0^2 \quad (2.15)$$

The added volume in the cavity $V(t)$ is equal to the product of the effective area S_d and average displacement $-x_d(t)$, where a positive displacement is directed outward from the cavity. Taking the time derivative of (2.15) and replacing $V(t)$ with $-S_d u_d(t)$ produces:

$$\frac{dp(t)}{dt} = -\frac{S_d u_d(t)}{V_0} \rho_0 c_0^2 \quad (2.16)$$

Rearranging these terms and converting to the Laplace domain gives

$$\frac{p_c(s)}{u_d(s)} = -\frac{S_d}{s} \frac{\rho_0 c_0^2}{V_c} \quad (2.17)$$

To convert this to a mechanical-equivalent impedance, one should multiply by S_d . Note that a positive pressure inside the cabinet, on the rear diaphragm, results in a force in the same direction as the

velocity. A positive reactive force resulting from a positive causal velocity denotes a negative impedance, and thus the effective mechanical impedance produced by the cavity is equal to the negative of the right-hand-side of (2.17), i.e.

$$Z_{rmr}(s) = \frac{S_d^2}{s} \frac{\rho_0 c_0^2}{V_c} \quad (2.18)$$

Vented-box enclosure

The addition of a second component to the closed-box enclosure, a lumped mass of air in a small duct as per Figure 2.9, creates an additional degree of freedom in the system. This system is characterised by the ratio of port fluid velocity to diaphragm velocity, and the resulting acoustic radiation impedance presented to the rear side of the driver. This benefits the system response by permitting a reduction in the cut-off frequency, as well as a reduction in the pressure/displacement ratio. The latter permits higher acoustic output for the same range of linear displacement.

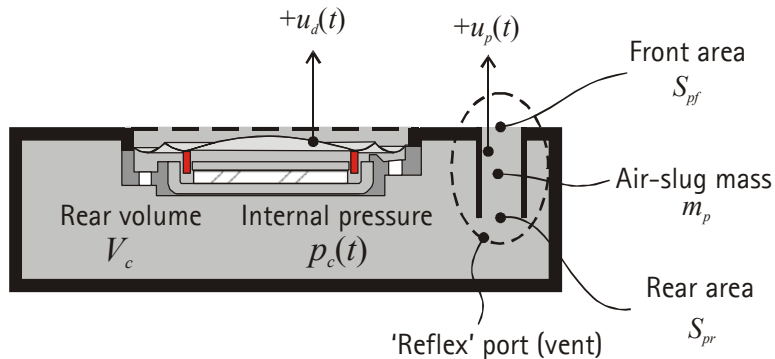


Figure 2.9: Definition of parameters used to for a single-degree-of-freedom model of ported cavity dynamics

The ratio of port fluid velocity to diaphragm velocity may be determined by first establishing an equation of motion for the port fluid velocity. From conservation of momentum, or forces, a linear equation may be derived as so:

$$(sm_p + c_p + Z_{rmp}(s))u_p(s) = p_c(s)S_p \quad (2.19)$$

The terms in (2.19) have the following names:

m_p	Mass of the air in the port
c_p	Flow resistance of the port
$Z_{rmp}(s)$	Acoustical impedance seen by the port on the cabinet exterior
$u_p(s)$	Port fluid velocity; positive velocity indicates flow out of the cabinet
$p_c(s)$	acoustic pressure inside the cabinet
S_p	Area of the port.

An analytical solution was developed for the radiation impedance of two pistons mounted in an infinite baffle (Klapman, 1940). As the result does not differ by more than 10% at low $k'a$ from the single-piston case, and as the impedance contributes less than 10% to the total lumped mass, this effect is considered negligible in most studies. Therefore the acoustical impedance seen by the port on the cabinet's exterior $Z_{rmp}(s)$ may, therefore, be incorporated into proper definition of m_p and c_p , i.e. by applying the appropriate 'end correction.' It is assumed in the following that this is the case, and thus the $Z_{rmp}(s)$ term is not used explicitly.

The acoustic pressure inside of the cavity is determined by motion of the diaphragm and fluid flow in the port according to

$$p_c(s) = \frac{\rho_0 c_0^2}{sV_c} [-S_d u_d(s) - S_p u_p(s)]. \quad (2.20)$$

The ratio of vent fluid velocity to diaphragm velocity is found by combining Eqs. (2.19) and (2.20), .

which, after some rearrangement, may be expressed as so:

$$\frac{u_p(s)}{u_d(s)} = \frac{-S_p S_d \frac{\rho_0 c_0^2}{sV_c}}{sm_p + c_p + S_p^2 \frac{\rho_0 c_0^2}{sV_c}} \quad (2.21)$$

The mechanical equivalent radiation impedance on the rear side of the diaphragm is defined as

$$Z_{rmr}(s) = -\frac{S_d p_c(s)}{u_d(s)}. \quad (2.22)$$

This can be expressed in terms of the physical constants of the system by replacing $p_c(s)$ with the RHS of Eq. (2.20) and then using (2.21) to express $u_p(s)$ in terms of $u_d(s)$. Doing this and rearranging terms produces:

$$Z_{rmr}(s) = S_d^2 \frac{\rho c^2}{sV_c} \left(1 - \frac{S_p^2 \frac{\rho_0 c_0^2}{sV_c}}{sm_p + c_p + S_p^2 \frac{\rho_0 c_0^2}{sV_c}} \right) \quad (2.23)$$

2.1.5. Acoustic radiation

The simplest model for acoustic radiation is

$$p_r(s) = s\rho_0 S_d u_d(s) \frac{e^{ikr}}{4\pi r} \quad (2.24)$$

This model is valid if the shortest wavelength of sound considered is longer than any dimension of the loudspeaker. The expression in (2.24) is simply the radiation from a point monopole source in free space, as discussed in elementary acoustics (Pierce, 1994). A feature of monopole radiation important to loudspeaker design is that the acoustic pressure is directly proportional without frequency dependence to the volume acceleration of the source. Consequently, in order to produce a frequency-independent acoustic pressure field, the loudspeaker should produce a constant volume acceleration with respect to input voltage.

If the loudspeaker is placed in a baffle, in the low $k \cdot a$ region the following will apply:

$$p_r(s) = s\rho_0 S_d u_d(s) \frac{e^{ikr}}{2\pi r} \quad (2.25)$$

This radiation conditions is the most commonly used in the loudspeaker industry. However, for small products using loudspeakers, e.g. a mobile phone, the 4π (full space) condition is more accurate.

More general models of radiation can be obtained using simulations from boundary element models. This permits calculation of the radiated pressure from an arbitrarily shaped object, with an arbitrary vibration distribution. As the focus of this thesis is on details of the mechanical construction of the loudspeaker, such methods are not considered in this thesis.

2.1.6. Linear frequency response

It is possible to predict the linear frequency response by combining Laplace domain representations of the voltage equation, (2.1), and the force equation, (2.4). As most loudspeaker systems are driven by low-output impedance, constant output voltage amplifiers, the loudspeaker's response is defined by the frequency response function referenced to the voice-coil voltage, $v_c(s)$. The first step in developing this transfer function is to combine the transduction equation, (2.12), with the general force equation, (2.13). This provides this expression for the current in terms of the velocity:

$$i_c(s) = \frac{1}{\phi_0} u_d(s) Z_m(s) \quad (2.26)$$

Substituting this into the voltage equation (2.1) and solving for the ratio $u_d(s)/v_c(s)$ provides:

$$\frac{u_d(s)}{v_c(s)} = \frac{\phi_0}{Z_{eb}(s)Z_m(s) + \phi_0^2} \quad (2.27)$$

Recall that $Z_m(s)$ is the sum of the internal mechanical and acoustical load impedances. Thus (2.27) describes the velocity to voltage ratio including the effects of acoustical loading.

From (2.24), the monopole free-field acoustic radiation depends directly on the diaphragm velocity. Therefore for the case of a loudspeaker mounted in a closed box, at low $k \cdot a$ numbers, the acoustic pressure may be determined by combining Eqs. (2.27) and (2.24) to give the ratio of pressure to input voltage

$$\frac{p_{r_p}(s)}{v_c(s)} = s \rho_0 S_d \frac{\phi_0}{Z_{eb}(s)Z_m(s) + \phi_0^2} \frac{e^{ikr_p}}{4\pi r_p} \quad (2.28)$$

Further characterisation of this formula is given in §2.1.7 below.

The total electrical impedance is a function that will be referred to many times in this thesis. Its Laplace-domain transfer function may be determined in a similar manner to the pressure response, above. By first combining the basic definition of mechanical impedance and the relationship between current and force given in (2.12), the velocity may be written in terms of the current according to

$$u_d(s) = \frac{\phi_0 i_c(s)}{Z_m(s)} \quad (2.29)$$

Substituting this into the voltage equation and solving for the ratio $v_c(s)/i_c(s)$ provides

$$Z_e(s) = \frac{v_c(s)}{i_c(s)} = Z_{eb}(s) + \frac{\phi_0^2}{Z_m(s)} \quad (2.30)$$

2.1.7. Response prediction of loudspeaker mounted in a sealed cabinet

Equation (2.28) describes the frequency response function of pressure / voltage in terms of the general electrical, mechanical, and acoustic radiation impedances of a given loudspeaker and the enclosure in which it is mounted. It does not, however, directly answer the question of how a loudspeaker and its cabinet should be designed in order to provide a certain desired response. General answers to the question of 'how to design a loudspeaker to achieve some desired response' were the subject a paper

by Thiele (1961) for vented-box loudspeakers,¹ along with a different presentation and extension of Thiele's work in a series of papers by Small (1971, 1972, Jan. 1973, Jun. 1973, Jul. 1973, Sep. 1973, and Oct. 1973).

It may be shown that if the loudspeaker is mounted in a sealed enclosure as per Figure 2.7, given certain assumptions, the transfer function has the form of a second-order high-pass filter. There are many theorems and laws for filter design that can be used to analyse the loudspeaker's response. First, however, it is necessary to re-write the expression of (2.28) into the same form as general high-pass filters are expressed. The papers by Thiele and Small mentioned above give connections between physical parameters of a loudspeaker (with its enclosure) and the parameters of high-pass filters. With this connection, the parameters of the high pass filter (defining the shape of the frequency response) can be directly known from the physical dimensions and manufacturing specifications of the loudspeaker.²

Following a method used by Thiele (1961) for vented-box loudspeakers, it was shown by Small (1971) that the response of a loudspeaker mounted in a closed-box, can be represented by this second-order high-pass filter:

$$H_{hp}(s) = S_0 \frac{s^2 T_c^2}{1 + sT_c/Q + s^2 T_c^2} \quad (2.31)$$

where

s = Laplace variable

S_0 = system gain

Q = Q-factor

T_c = System time constant = $1/\omega_c = 1/2\pi f_c$, where f_c is the system cut-off frequency.

The first step to write the voltage to pressure transfer function of (2.28) into this form is to parameterise the general electrical, mechanical, and acoustic radiation impedances (Z_{eb} , Z_{mo} , and Z_{rm} respectively), as so:

$$\begin{aligned} Z_{eb} &= R_{eb} + sL_{eb} \\ Z_{mo} &= sm_d + c_d + k_d/s \\ Z_{rm} &= sm_a + \rho c^2 S_d^2 / V_c s \end{aligned} \quad (2.32)$$

It is helpful to define a single expression for the total mechanical impedance, equal to the sum of the diaphragm and mechanical-equivalent acoustical impedance:

$$Z_m = Z_{mo} + Z_{rm} = sm_t + c_t + k_t/s \quad (2.33)$$

Here, a total mass and stiffness have been defined as

$$\begin{aligned} k_t &= k_d + S_d^2 \rho c_0^2 / V_c \\ m_t &= m_d + m_a \end{aligned} \quad (2.34)$$

¹ The description of the acoustic response of a vented-box loudspeaker as a fourth-order high-pass filter was first given by Novak (1959). However, Thiele's 1961 paper was the first to fully apply existing tools for active analogue filter design to vented box design.

² Although such a connection may not seem novel from a scientific point of view, Thiele and Small's work proved significantly useful to the loudspeaker engineering community. One indication of this is that the basic set of performance parameters for an electrodynamic loudspeaker, in isolation from its enclosure, are commonly referred to as the 'Thiele-Small parameters.'

In addition to the parameterisations of (2.32), it is necessary to assume that the effect of internal electrical inductance is insignificant, i.e. $L_{eb} = 0$, so that $Z_{eb} \approx R_{eb}$. Notice that, as per the measurement of the microspeaker shown in Figure 2.5, the net contribution of the electrical inductance to the total blocked electrical impedance is less than 10% below 5000Hz, and thus this assumption is reasonably justified, particularly at frequencies below 5000Hz.

If the acoustic pressure is considered at one (1) metre from the loudspeaker in a fully free (4π steradian) acoustic field, ignoring the phase lag caused by the wave propagation over the one meter distance, the acoustic propagation term can be simplified from $e^{ikr}/4\pi r$ to $1/4\pi$.

Acoustic response

With the above simplifications and by substituting Eqs. (2.32) and (2.33) into (2.28), it is possible to express the voltage to pressure transfer function in the second-order low-pass filter form of (2.31) as so:

$$\frac{p_{1m}(s)}{v_c(s)} = \frac{\rho_0 \phi_0 S_d}{4\pi R_{eb}} \frac{s^2}{m_t s^2 + s(c_t + \phi_0^2/R_{eb}) + k_t} \quad (2.35)$$

This may be described by a gain factor and a generic second-order high-pass filter as so:

$$\begin{aligned} H_{pv}(s) &= \frac{p_{1m}(s)}{v(s)} \\ &= S_0 H_{cb}(s) \\ &= S_0 \frac{s^2/\omega_0^2}{s^2/\omega_0^2 + s/\omega_0 Q_{tc} + 1} \end{aligned} \quad (2.36)$$

where

$$\omega_0 = \sqrt{\frac{k_t}{m_t}} \quad (\text{undamped resonance frequency})$$

$$Q_{tc} = \frac{\sqrt{k_t m_t}}{c_t + \phi_0^2/R_{eb}} \quad (\text{total } Q \text{ value})$$

$$S_0 = \frac{\rho_0 \phi_0 S_d}{4\pi m_t R_{eb}} \quad (\text{characteristic sensitivity})$$

Electrical impedance

The electrical impedance can be represented in a similarly compact form. For this purpose, it is necessary to define two different Q values. Using notation from Small (1972), these are:

Q_{es} : Electrical Q -factor; this is the Q -factor due to the effective damping provided by a constant output-voltage amplifier.

$$Q_{es} = \frac{\sqrt{k_t m_t}}{\phi_0^2/R_{eb}} \quad (2.37)$$

Q_{ms} : The mechanical Q -factor; this is the Q -factor due to the damping provided by mechanical resistance and resistive acoustic radiation impedance.

$$Q_{ms} = \frac{\sqrt{k_t m_t}}{c_t} \quad (2.38)$$

where c_t is the total damping as defined in (2.33).

With these definitions, the general electrical impedance of (2.30) may be expressed as this second-order narrow-bandpass filter:

$$Z_e(s) = R_{eb} \frac{\frac{s^2}{\omega_0^2} + \frac{s}{\omega_0 Q_{tc}} + 1}{\frac{s^2}{\omega_0^2} + \frac{s}{\omega_0 Q_{ms}} + 1} \quad (2.39)$$

The magnitude of the frequency response of the total electrical impedance as represented by the transfer function of (2.39) is plotted in Figure 2.10 for a typical set of values of ω_0 , R_{eb} , Q_{tc} , and Q_{ms} .

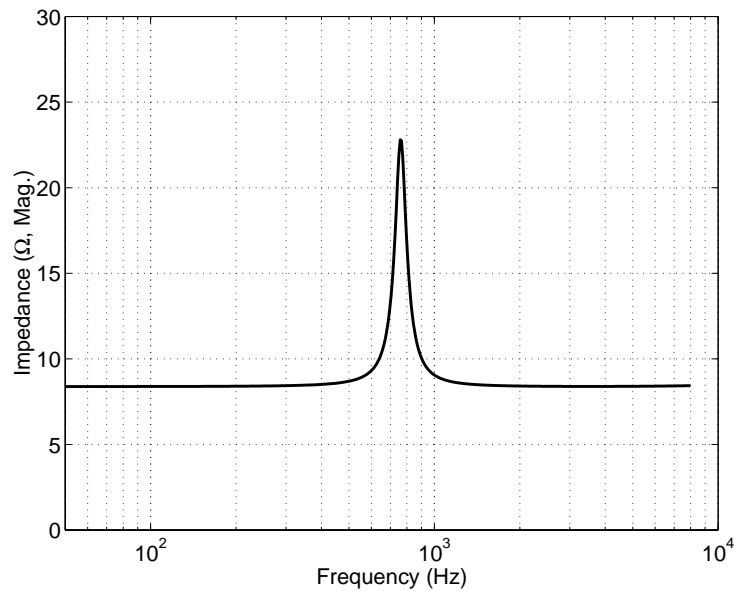


Figure 2.10: Plot of parameterised total electrical impedance, for a typical set of values of a microspeaker.

2.1.8. Response prediction of a loudspeaker mounted in a vented-box enclosure

The far-field acoustic pressure generated by a loudspeaker in a vented-box enclosure is caused by the sum of the volume velocity from the diaphragm and the port. If monopole radiation in a fully free field is considered, the acoustic pressure at one (1) metre, ignoring propagation delay, will be given by the diaphragm and port velocities according to

$$p_{1m}(s) = \frac{s\rho_0}{4\pi} (S_d u_d(s) + S_p u_p(s)) \quad (2.40)$$

Using the relation between port and diaphragm velocity given in (2.21), this may be re-written in terms of the diaphragm velocity alone as so

$$p_{1m}(s) = \frac{s\rho_0}{4\pi} \left(S_d - \frac{S_p^2 S_d \frac{\rho_0 c_0^2}{sV_c}}{sm_p + c_p + S_p^2 \frac{\rho_0 c_0^2}{sV_c}} \right) u_d(s) \quad (2.41)$$

This expression may be written in terms of the input voltage $v_c(s)$ using the general impedance form of the relationship between diaphragm velocity $u_d(s)$ and input voltage of (2.27). Separating out the

internal mechanical, front, and rear acoustical parts as per (2.14), the acoustic pressure may be written in terms of the input voltage as so

$$\frac{p_{1m}(s)}{v_c(s)} = \frac{s\rho_0}{4\pi} \left(S_d - \frac{S_p^2 S_d \frac{\rho_0 c_0^2}{sV_c}}{sm_p + c_p + S_p^2 \frac{\rho_0 c_0^2}{sV_c}} \right) \frac{\phi_0}{Z_{eb}(s)(Z_{mo}(s) + Z_{rmr}(s) + Z_{rmf}(s)) + \phi_0^2} \quad (2.42)$$

By using the same simplifications as for the closed box analysis presented in §2.1.7, it was shown by Novak (1959) that the above transfer function can be written as a fourth-order high pass filter. This description was used to interesting effect by Thiele (1961), who brought the full weight of tools for active analogue filter design to the problem of design & analysis of loudspeakers in a ported cabinet. Thiele wrote a table of different response types based upon the different standard alignments for a fourth-order high pass filter, which gave a compact description of the possible frequency response of a ported loudspeaker in terms of its physical dimensions and manufacturing specifications.

Specifically, to apply the theory presented by Thiele (1961), these simplifications are made:

$$\begin{aligned} Z_{eb}(s) &\equiv R_{eb} \\ Z_{mo}(s) + Z_{rmf}(s) &\equiv sm_t + c_t + k_d / s \end{aligned} \quad (2.43)$$

Using these simplifications and substituting the expression for the rear radiation impedance presented in the LHS of (2.23) for $Z_{rmr}(s)$ produces:

$$\frac{p_{1m}(s)}{v(s)} = \frac{s\rho_0}{4\pi} \left(S_d - \frac{S_p^2 S_d \frac{\rho_0 c_0^2}{sV_c}}{sm_p + c_p + S_p^2 \frac{\rho_0 c_0^2}{sV_c}} \right) \frac{\phi_0}{R_{eb}(Z_{rmr}(s) + sm_t + c_t + k_d / s) + \phi_0^2} \quad (2.44)$$

2.2. Nonlinear models of loudspeakers

Linear models are conceptual simplifications. They are valid for a limited range of operation. For the electrodynamic loudspeaker, the scope of range is mostly defined by the diaphragm-coil displacement. The range of applicability of the same model structure as that developed in §2.1 above may be extended by introducing displacement-dependence on several parameters of the model.

2.2.1. Parametric nonuniformity and causes of nonlinearity

Parametric nonuniformity and other causes of nonlinearity result in nonlinear distortion in the acoustic signal reproduced by a loudspeaker. Nonlinear distortion reduces the quality of the sound reproduced by the loudspeaker. This thesis does not aim to determine what degree of nonlinear distortion is acceptable. Instead, it is assumed that present levels of nonlinear distortion, in existing products, are proper compromises between construction expense and sufficiently low distortion for market acceptability.

Causes of nonlinearity in loudspeakers have been thoroughly researched, and are generally thought to be well-understood.

Identification and modelling of nonlinear mechanisms has been an active academic subject for most of the last century. The dominant mechanisms may be described as parametric nonuniformity, i.e. the variation of some linear parameter with excursion by some analytic description. The most common form for description of parameter non-uniformity is a polynomial power-series expansion in x_d , which

is used for most models of parameter non-uniformity in this thesis. This description is particularly convenient for real-time computation, as it requires simple polynomial evaluations in an otherwise linear model.

Different types of parametric nonuniformity and causes of nonlinearity are discussed in the following sub-sections.

A. Magnetic field nonuniformity

The magnetic field generated by the loudspeaker's magnet system, i.e. part (7) shown in Figure 2.1 and in Figure 2.2, will not be completely uniform over the region through which the coil will move. One may consider a displacement-dependent magnetic field $B(x_d)$, which describes the variation of the magnetic field along the axial direction of the coil's movement. From this, an effective transduction coefficient $\phi(x)$ may be calculated as so

$$\phi(x_d) = \int_{-\frac{h}{2}}^{\frac{h}{2}} B(\xi - x_d) d\xi \quad (2.45)$$

where h is the height of the voice-coil.

The transduction coefficient may be approximated a power series expansion of order N_ϕ

$$\hat{\phi}(x_d) \approx \phi(x) = \sum_{k=0}^{N_\phi} \phi_k x_d^k. \quad (2.46)$$

A plot of a typical measurement of the nonuniformity in the transduction coefficient is shown in Figure 2.11. The data shown in Figure 2.11 is for a 16mm diameter microspeaker of the basic type shown in Figure 2.1. This data was obtained with a commercial instrument for determining the coefficients of the polynomial approximation to $\phi(x_d)$, i.e. ϕ_k in (2.46). A description of this commercial instrument is provided by Klippel GmbH (2001).

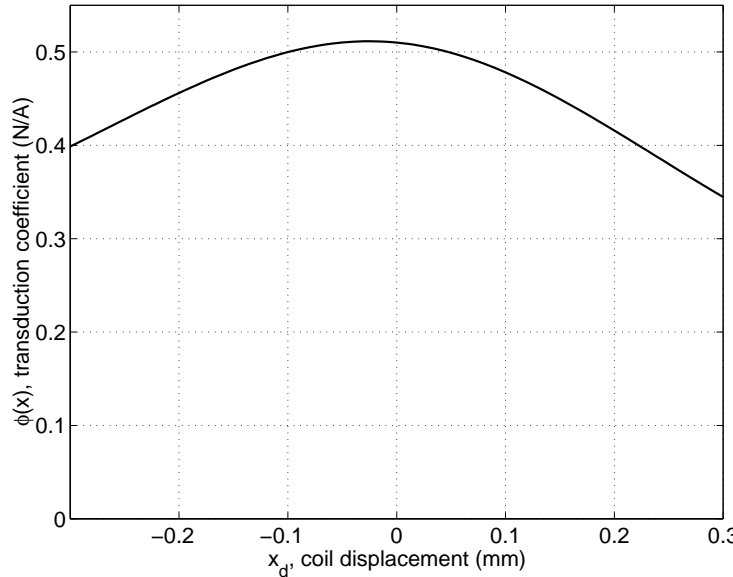


Figure 2.11: Measured nonuniformity in the transduction coefficient versus diaphragm-coil displacement, i.e. $\phi(x_d)$, for loudspeaker type shown in Figure 2.1.

The transduction coefficient $\phi(x_d)$ is not well-represented by a finite Taylor series if it is evaluated outside of the range of x -values on which the coefficients were determined. This can be seen in the top frame of Figure 2.12. This is particularly problematic during simulation of nonlinear behaviour, where it is interesting to simulate high diaphragm-coil displacement. If the transduction coefficient is negative, it can result in unstable simulation results.

A solution to this problem is to invert the transduction coefficient variation, and perform a polynomial fit on this. Representing this as $\psi(x_d)$, i.e.

$$\psi(x_d) = \sum_{n=0}^{N_\psi} \psi_n x_d^n, \quad (2.47)$$

the actual transduction coefficient function can be recovered from $1/\psi(x_d)$. A plot of $1/\psi(x_d)$ is shown in the lower frame of Figure 2.12. This technique is used to ensure stable results in the simulations presented in §§5.2.1 - 5.2.2.

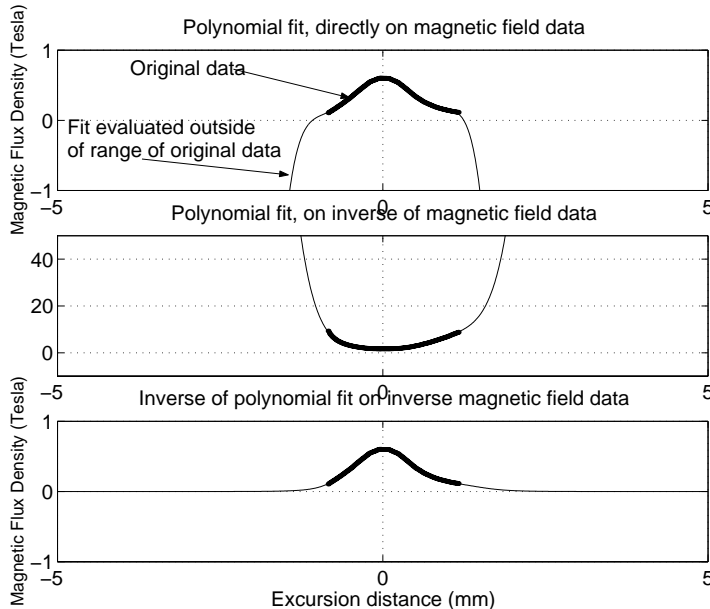


Figure 2.12: Polynomial fitting for force-factor (B.I factor) data; top frame shows how coefficients fit on direct data, when evaluated outside of range of direct data, can return a negative result. Bottom frame shows how fitting coefficients on inverse data, and evaluating as inverse function does not produce this problem.

B. Stiffness nonuniformity

Nonuniformity in the suspension exhibits itself either as a smooth, memory-less function of displacement, as a hysteretic function, or, when the diaphragm-coil assembly contacts other parts of the loudspeaker, as a discontinuous function. These three different types of stiffness nonuniformity are discussed separately below.

Gradual ('smooth') variation in the suspension

It is known that the stiffness presented by the suspension will not be uniform throughout the range of displacement. Typically, the stiffness will increase with higher displacements. This is known in mechanics as a 'hardening spring'.

This effect was analysed in some detail by Olson (1944), illustrating what is now referred to as the ‘jumping’ phenomenon. This refers to sudden changes in the response amplitude as the frequency of a sinusoidal excitation is swept upwards or downwards around the resonance frequency. Due to the fact that, with a hardening spring, the resonance frequency increases with increasing displacement, for a certain range of frequencies just above the small-signal resonance frequency, there will not be a unique response amplitude solution at higher levels. As the frequency is changed past a certain critical point, the response amplitude will ‘jump’ from the amplitude of one stable response to another.

The stiffness may be approximately described by a truncated power series, forming an order N_k -th order polynomial as so:

$$k_d(x_d) = \sum_{n=0}^{N_k} k_n x_d^n \quad (2.48)$$

A plot of the nonuniformity of the stiffness on a typical microspeaker is shown in Figure 2.13.

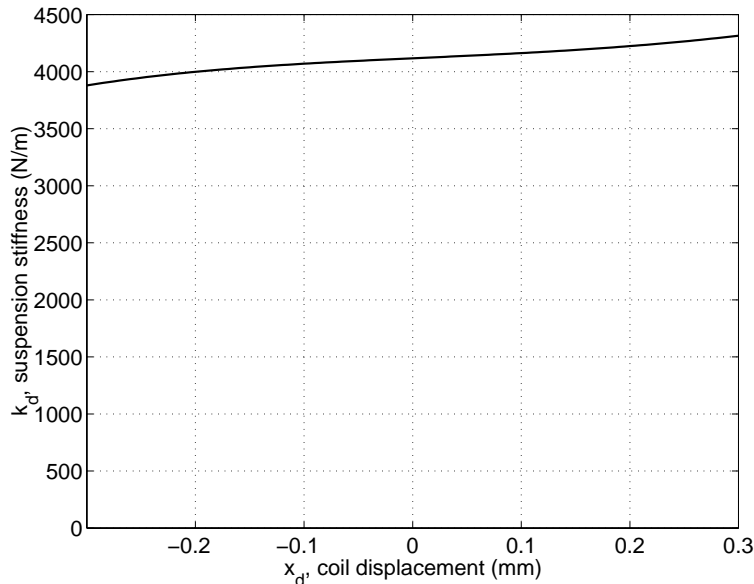


Figure 2.13: Measured nonuniformity in the suspension stiffness with respect to diaphragm-coil displacement, i.e. $k_d(x_d)$, on a sample of the loudspeaker type shown in Figure 2.1.

As can be seen in Figure 2.13, the stiffness variation does not appear as a ‘hardening spring,’ wherein the stiffness would increase with the absolute value of the displacement. This ‘hardening spring’ phenomenon is the most common form of stiffness nonuniformity seen in typical loudspeakers. Instead, it is clear from Figure 2.13 that the suspension of the microspeaker produces a stiffness that increases with forward displacement and decreases with rearward displacement. Stiffness nonuniformity of this shape is thought to be characteristic of the microspeaker with a suspension of the shape shown in Figure 2.1.

Buckling

Through various experiments and measurements made for this thesis, it was found that in some cases the suspension stiffness may exhibit some buckling, producing strong hysteresis (backlash). A measurement on a loudspeaker with such an effect is shown in Figure 2.14. This kind of stiffness nonuniformity cannot be modelled with a function of the type in (2.48). A more complicated, memory-dependent model would be needed. As this type of stiffness is a manufacturing defect to be avoided by proper mechanical design, a model of this effect is not considered in this thesis.

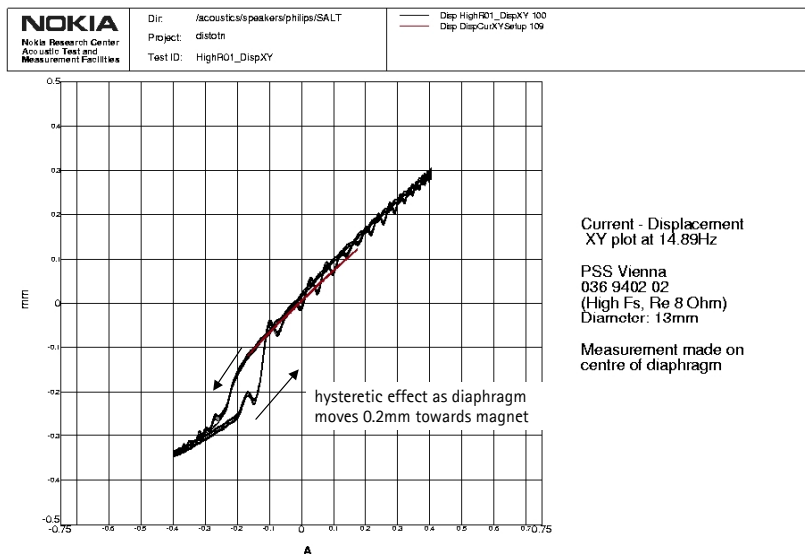


Figure 2.14: X-Y Voice-coil current-displacement plot for a microspeaker, showing effect of buckling in the suspension, at how it leads to 'backlash' in the displacement/current X-Y plot. Displacement is measured with a laser displacement interferometer (fringe counter), in an otherwise similar arrangement to that shown in Appendix A.

Suspension limit

There is a physical limit to the distance that the diaphragm-coil assembly may move. As the diaphragm moves forward, away from the magnet, the stiffness presented by the suspension will gradually increase, until the suspension is no longer flexing, but is instead under tension.

As the diaphragm moves rearward, the coil and/or the diaphragm will at some point contact the magnet and/or frame. At this point, the suspension stiffness k_d becomes ‘infinite,’ in the sense that no matter how much force is applied to the coil, the diaphragm-coil assembly will not move any further. This effect is referred to be some as ‘bottoming-out’ of the suspension, by analogy to a similar effect occurring in automobile suspensions.

The maximum displacement set by this suspension limit for the microspeakers investigated in this thesis is approximately 0.35mm peak.

This limit to the suspension can be modelled by setting the suspension to be infinite at the limiting value. The suspension is not modelled in this way in other parts of this thesis. Particularly, it is not modelled in the context of compensation of nonlinear distortion. Were this to be modelled, an attempt to compensate for the suspension limit would create an infinite gain in the compensator, which, to be sure, would be somewhat impractical.

C. Inductance nonuniformity

The electrical inductance L_{eb} will vary with coil position. As the coil moves forward, away from the magnet system, there will be less ferromagnetic material ‘seen’ by the magnetic field generated by the coil, producing a lower inductance. An example of this type of variation is shown in Figure 2.15. As can be seen in this figure, the inductance decreases with forward movement of the voice-coil, wherein there is less ferromagnetic material seen by the voice-coil.

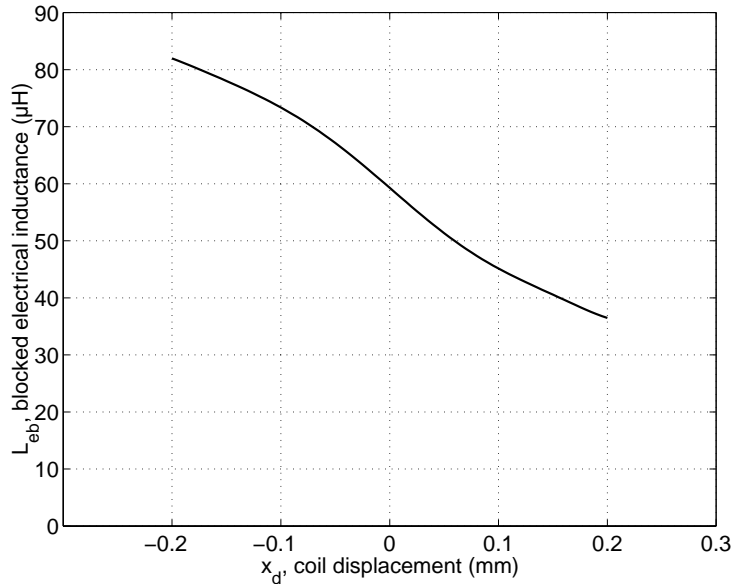


Figure 2.15: Measured nonuniformity in the blocked electrical inductance with respect to diaphragm-coil displacement, i.e. $L_{eb}(x_d)$, for the loudspeaker type shown in Figure 2.1.

As shown in Figure 2.5, the blocked electrical inductance makes a negligible contribution to the total electrical impedance in the speech-frequency range for the microspeaker. The variation of this inductance, though measurable, does not affect its overall performance at large signals. The nonlinearity produced by inductance nonuniformity is, therefore, only considered in the discussion on theory of nonlinear simulation presented in §2.2.2, and not in other parts of this thesis.

D. Mass nonuniformity

It was shown by Olsen and Thorborg (1995) that the effective mass of the loudspeaker diaphragm can change with position. It was found that the roll surround used in many loudspeakers produces a changing mass depending on whether the diaphragm is near its forward or rearward displacement extremity. This produced an effective moving mass which changed by some $\pm 20\%$ from its value at the equilibrium (rest) position. The variation of the mass with displacement was found to be well-modelled by a first order polynomial expansion in x_d .

Over the limited range of displacements of which the microspeaker considered in this thesis is capable, it is assumed that the mass is uniform.

E. Area nonuniformity

In the same study by Olsen and Thorborg (1995) that discovered mass-variation, it was also found that the effective area changes with displacement. This was found to be due to the same mechanism that caused the mass-variation, the changing behaviour of the surround. As the surround (outer suspension) is extended rearward from equilibrium, it contributes more to the effective radiation area. As it is extended forward from equilibrium, it contributes less. Over the range of possible excursions, variations in the effective area were found to be on the order of $\pm 12\%$. Similar to the mass variation, the area variation was found to be well-modelled by a first-order polynomial in x_d .

Over the limited range of displacements of which the microspeaker considered in this thesis is capable, it is assumed that the effective area is uniform.

F. Magnetic attraction force

The magnetic attraction force as it appears in electrodynamic loudspeakers was first discussed by Cunningham (1949). This effect is the result of the classical electrodynamic effect of the attractive force existing in a current-carrying wire for any ferromagnetic material in its vicinity. For the case of an electrodynamic loudspeaker, the coil will exhibit this force for the material in the magnet and magnetic circuit. It was noted by Cunningham that this force is related to the spatial derivative to the internal inductance of the coil, i.e.

$$F_{ma} = \frac{1}{2} i_c^2(t) \frac{dL_{eb}(x_d(t))}{dx_d(t)} \quad (2.49)$$

This ‘solenoid’ effect is problematic in largely-overhung voice-coils, which will produce significant gradients on the electrical inductance L_{eb} with respect to displacement of the coil. It was noted by Cunningham that this effect is reduced if the ferromagnetic material in the magnet system is near or at magnetic saturation.

This phenomenon introduces an additional forcing term to the force equation. As the force varies with the product of the square of the current $i_c(t)$ and derivative of the inductance, it will render the resulting differential equation nonlinear.

This effect is dependent upon nonuniformity in the electrical inductance. As explained in part C, above, nonuniformity in the electrical inductance is not considered for the speakers considered in this thesis. Thus the nonlinear mechanism of the magnetic attraction force is not considered in this thesis.

G. Frequency modulation distortion

Frequency modulation distortion results from the fact that the diaphragm will have a finite velocity as it vibrates. This effect has seen considerable academic interest (Klipsch, 1968), (Butterweck, 1989). Simulations of the magnitude of nonlinear distortion produced by this effect show that it is several orders of magnitude below that created by nonuniformity in the transduction coefficient and suspension stiffness (Zóltogórski, 1993).

2.2.2. Nonlinear simulation

From this point forward, only models of parametric nonuniformity which operate as *zero-memory* nonlinear systems will be considered. By ‘zero-memory,’ it is meant here that the model of nonlinearity depends only on instantaneous quantities of the system. This is a deliberate choice, as it makes analysis of the resulting nonlinear system significantly more simple than if the models were to conclude some ‘memory,’ i.e. to depend on past quantities of the system. Not all types of parametric nonuniformity can be modelled in this way. For example, the hysteretic stiffness shown in Figure 2.14 above does depend on past values of the displacement. This type of effect is not modelled in this thesis. This is because the end purpose of the nonlinear modelling that follows is to form the basis of an electronic processor for compensation of nonlinearity. It is judged that such memory-dependent parametric nonuniformity cannot be accurately modelled with practical controllers. It is furthermore judged that these types of problems must be solved by proper mechanical design, as they generally can not – in practice – be compensated for electronically.

Introducing the parametric nonuniformity discussed above into the voltage equation of (2.1) produces

$$v_c(t) = R_{eb}i_c(t) + L_{eb}(x_d(t)) \frac{di_c(t)}{dt} + \phi(x_d(t)) \frac{dx_d(t)}{dt} + i_c(t) \frac{dL_{eb}(x_d(t))}{dx} \frac{dx_d(t)}{dt} \quad (2.50)$$

The parametric nonuniformity may be introduced into the force equation in a similar manner. Using (2.12) to substitute the current for the force as the forcing term, and adding the magnetic attraction ('solenoid') force term to the RHS, the force equation becomes:

$$i_c(t)\phi(x_d(t)) = m_t(x_d(t)) \frac{d^2x_d(t)}{dt^2} + c_t \frac{dx_d(t)}{dt} + k_t(x_d(t))x_d(t) - \frac{1}{2}i_c^2(t) \frac{dL_{eb}(x_d(t))}{dx_d(t)} \quad (2.51)$$

Solution of these equations may be used to simulate the loudspeaker's behaviour given appropriate descriptions of the parameter nonuniformity. The equations are nonlinear in the displacement, $x_d(t)$, and therefore a general frequency-domain solution for the displacement in terms of the input voltage is not possible, as it is for the linear case presented in §2.1.6 above.

The Volterra series is a natural method for developing a general solution to the nonlinear equations. It theoretically permits precisely the same type of general solution for $x_d(s)$ in terms of the input $v_c(s)$ as is developed for the linear case above, in a quasi-frequency domain manner. Its application to the loudspeaker was first presented by Kaizer (1987). The Volterra series becomes highly complicated when higher than second-order nonlinearity (parameters which depend on a power of x_d greater than 2) are considered. Therefore although it has been demonstrated in literature that this method can be used to measure and compensate for loudspeaker nonlinearities with some success, it makes a poor general method for nonlinear analysis.

A more simple strategy for solving nonlinear differential equations than the Volterra series is Harmonic Balance. In this method, the system is analysed in the frequency domain, for a finite number of excitation frequencies. The frequency components generated in other terms in the system are iteratively calculated until the resulting error is reduced to some desired value. This method was proven effective by Klippel (June 1992) for single and multi-frequency excitation, for predicting harmonic and intermodulation distortion, as well as the 'jumping effects' found by Olson, described in §2.2.1, part B above. However, it is not suitable for computation on more complex waveforms or long arbitrary time series, whose frequency-domain description would require large numbers of frequency components in the input signal.

NARMAX modelling (Nonlinear auto-regressive moving-average with exogenous input) has been proposed as a method for identification of nonlinearities (Jang and Kim, 1994), and for nonlinear simulation (Potirakis et al., 1999). However, it is not suitable for developing an input-output characterisation from such nonlinear differential equations as Eqs. (2.50) and (2.51), without first deriving sample input-output time series by some other method. This is because there has yet to be any method established for determining coefficients of a NARMAX model from those of a nonlinear differential equation. All published work on NARMAX modelling to date is based on adaptation of the model to measured input-output time series data, and not determination from physical constants of a system. Thus NARMAX modelling does not permit simulation in the sense of the prediction of the performance of system based on its design characteristics without first building the system. Furthermore, it does not permit the development of a connection between the amount of nonlinearity of a loudspeaker to its design characteristics. The main utility in the NARMAX model is the ability to predict the nonlinear response of the loudspeaker for some arbitrary signal.

A common method for solving differential equations is numerical integration. Numerical integration was used for auralisation of nonlinearity by Christensen and Olsen (1996). It has also been used to predict harmonic and intermodulation distortion. This method is used in chapter 5, below, to analyse the changes in transduction coefficient nonuniformity, $\phi(x_d)$, caused by shortening of the voice-coil height.

2.3. Discrete-time physical modelling

In the loudspeaker models developed in §§2.1-2.2, all time-dependent quantities were defined with respect to continuous-time. In contrast, textbooks and other literature on modern digital signal processing theory and applications invariably consider controllers and processors operating in discrete-time. Practical implementation of active control can only be implemented by a digital processor.¹ The adaptive controller will need a model of the loudspeaker in order to perform system identification, for updating the feedforward part of the controller. This is not straightforward, as the basic parametric descriptions of systems in continuous-time is not the same as that in discrete-time. This is a basic problem for discrete-time control systems dealing with real-world plants, and will be considered at a fundamental level in this section.

This problem may be described succinctly as follows. Real, physical systems, are generally described by systems of differential equations, defined by two coefficient vectors **c** and **d**. These may be represented, along with the respective Laplace-domain transfer-function, as so:

$$\begin{aligned} c_N \frac{d^{(N)}y(t)}{dt^{(N)}} + \dots + c_1 \frac{dy(t)}{dt} + c_0 y(t) &= d_M \frac{d^{(M)}x(t)}{dt^{(M)}} + \dots + d_1 \frac{dx(t)}{dt} + d_0 x(t) \\ \Rightarrow H(s) = \frac{\sum_{n=0}^M d_n s^n}{\sum_{n=0}^N c_n s^n} \end{aligned} \quad (2.52)$$

Controllers handle systems with digital processing operating in discrete-time, defined by two coefficient vectors **a** and **b**. These generally describe systems in terms of difference equations, conveniently analysed by their *z*-domain transfer function:

$$\begin{aligned} a_N y[k-N] + \dots + a_1 y[k-1] + a_0 y[k] &= b_M x[k-M] + \dots + b_1 x[k-1] + b_0 x[k] \\ \Rightarrow H(z) = \frac{\sum_{n=0}^M b_n z^{-n}}{\sum_{n=0}^N a_n z^{-n}} \end{aligned} \quad (2.53)$$

Methods do exist for determining a set discrete-time coefficients **a** and **b**, directly from **c** and **d**, giving a discrete-time system with approximately the same frequency response as the continuous-time system described by **c** and **d**. However, these typically require detailed calculation, and suffer from numerical sensitivity complications, as is described below. From elementary discrete-time signal processing theory (e.g. Oppenheim and Schafer, 1989), there are two formal methods for determining the coefficient vectors **c** and **d** from **b** and **a**: the *bilinear transformation*, and *impulse invariance*.

¹ It is theoretically possible to implement such controllers with analogue processors. However, they are generally subject to drift, are difficult to program, and cannot be easily controlled by microcontroller (as would be needed for an actual commercial product). For these reasons, analogue implementation of an adaptive feedforward controller for a loudspeaker is considered impractical.

The bilinear transform determines a z -domain transfer function by the substitution

$$s = 2F_s \frac{1-z^{-1}}{1+z^{-1}} \quad (2.54)$$

It can be shown that the discrete-time coefficient vectors \mathbf{a} and \mathbf{b} resulting from the bilinear transformation are determined by matrix multiplication between the continuous-time coefficients \mathbf{c} and \mathbf{d} and matrices \mathbf{P} and \mathbf{Q} as so

$$\begin{aligned} \mathbf{a} &= \mathbf{P}\mathbf{c} \\ \mathbf{b} &= \mathbf{Q}\mathbf{d} \end{aligned} \quad (2.55)$$

where the columns of \mathbf{P} and \mathbf{Q} are polynomial coefficients resulting from, respectively, the M^{th} and N^{th} binomial expansion of the products between $(1-z^{-1})$ and $(1+z^{-1})$. The coefficient vectors \mathbf{c} and \mathbf{d} from the differential equation contain the physical information of the plant, and are thus those parameters of interest to the feedforward controller. They may be determined from the discrete-time coefficients \mathbf{a} and \mathbf{b} by multiplication by \mathbf{P}^{-1} and \mathbf{Q}^{-1} respectively. Although the matrices \mathbf{P} and \mathbf{Q} are generally invertible, they are fully populated, making this multiplication somewhat complicated – complicated to the extent that it would be unsuitable for real-time processing.

The method of *impulse invariance* performs a discrete-time sampling of the impulse response of the continuous-time system. The use of this method thus requires conversion of the polynomial ratio of (2.52) in s to a partial fraction expansion, from which the impulse response in continuous-time may be obtained by inverse Laplace transform. A discrete sampling of this continuous-time impulse response may be z -transformed, producing

$$H(z) = \frac{1}{F_s} \sum_{n=1}^N \frac{A_n}{1 - e^{\lambda_n T_s} z^{-1}} \quad (2.56)$$

where A_n are the numerator coefficients of the partial fraction expansion, and λ_n are the roots of the continuous-time denominator polynomial of (2.52). The expression in (2.56) may be expanded into the standard polynomial ratio in z^{-1} of (2.53), resulting in a set \mathbf{a} of coefficients suitable for a digital filter. The net effect of the impulse invariance method is to map the poles from the s -plane to the z -plane according to

$$\pi_n = e^{T_s \lambda_n} \quad (2.57)$$

where π_n is the n^{th} pole in the z -plane, and T_s is the sampling period. The sampling of this impulse response produces familiar aliasing effects. These aliasing effects can usually be compensated for by matching the overall-gain between the continuous- and discrete-time frequency response functions at some frequency for which the continuous-time frequency response function is simply defined. However, perhaps more problematic, is that this method requires that the roots of the continuous-time denominator polynomial be calculated. Such a calculation is difficult, and can fail due to finite-precision effects even for floating-point computation. Thus this method, in its formal form, is also considered unsuitable for development of a discrete-time model.

Due to these problems, specific discrete-time models of the loudspeaker are developed below. The exponential pole-mapping of (2.57) is used as a starting point, with slight modifications the ensure the frequency response of the discrete-time models matches that of the continuous-time. Particular effort has been made to ensure that the parameters of these models have direct physical interpretation.

2.3.1. FIR filter for electrical admittance

As discussed in the introduction, an adaptive feedforward controller requires an adaptive filter for system identification. The most well known and reliable methods for adaptive filtering use FIR filters for plant models. This is due to the fact that FIR filters are inherently stable, and that their error surfaces for any system are unimodal, without local minima. For this reason, an FIR filter describing the electrical admittance of the loudspeaker is investigated. The electrical admittance of the loudspeaker is considered because, as explained in the introduction, the electrical current is the only practical feedback signal available from the loudspeaker.

The suitability of an FIR filter for identifying a loudspeaker's parameters by its electrical impedance may be determined by analysis of the impulse response of the electrical admittance. As per the formal method of *impulse invariance* described above, an analytical expression for the impulse response may be obtained by inverse Laplace transform of the Laplace-domain expression for the transfer function. To consider how a digital FIR filter would react to the electrical admittance of a loudspeaker, distinct points of the resulting continuous-time impulse response are analysed. This is somewhat different to the formal *impulse invariance* method, wherein the individual terms of the analytical expression for the impulse response are converted to the z -domain (using special properties of the z -transform), and re-combined to the single ratio of powers in z^{-1} of (2.53). This method is not used here, as it would result in an IIR filter, whereas the original stated purpose here was to develop an FIR filter.

For the simplest case of a loudspeaker mounted in a closed box, this impulse response may be determined by inverse Laplace transform of the multiplicative inverse of the s -domain expression for the total electrical impedance given in (2.39). This may be expressed as so:

$$A_e(s) = \frac{1}{R_{eb}} - \frac{1}{\omega_0 Q_{es}} \frac{\omega_0^2}{R_{eb}} m_t Y_{m \cdot e}(s) \quad (2.58)$$

where $Y_{m \cdot e}(s)$ is the mechanical mobility as described by (2.6) in §2.1.2, with an important difference. The term $Y_{m \cdot e}(s)$ in (2.58) includes the effective damping produced by the 'back EMF.' In other words, the damping in $Y_{m \cdot e}(s)$ will be given by the sum of the mechanical damping c_t and the 'electrical damping,' ϕ_0^2/R_{eb} . A plot of the magnitude and phase of the frequency response of (2.58) is shown in Figure 2.16.

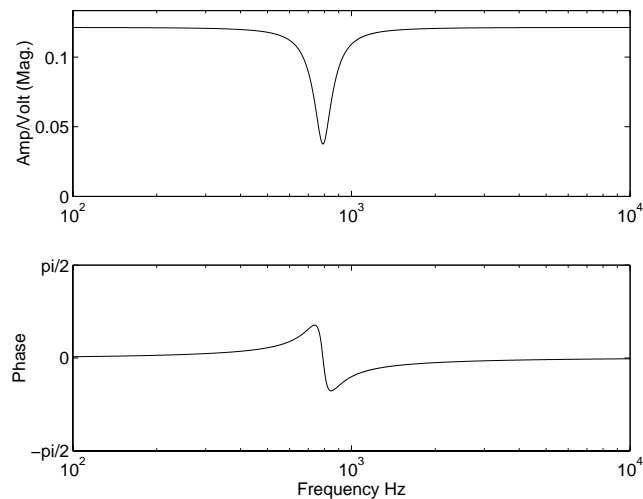


Figure 2.16: Magnitude and phase of the electrical admittance transfer function in (2.58) for a typical set of parameters.

It may be shown that the inverse Laplace transform of (2.58) is given by

$$h_{A_e}(t) = \frac{1}{R_{eb}} \delta(t) - \frac{1}{\omega_0 Q_{es} R_{eb}} \omega_0^2 e^{-\omega_0 \zeta t} \left(\cos \omega_d t - \frac{\omega_0 \zeta}{\omega_d} \sin \omega_d t \right) \quad (2.59)$$

The discrete-time representation of (2.59) is not given simply by the periodic sampling of the continuous-time time function as is done in the *impulse invariance* method described above, or for that matter in digital data acquisition. Instead, it is necessary to integrate over each sample period n , i.e.

$$h_{A_e}[n] = \int_{-T_s/2+nT_s}^{T_s/2+nT_s} h_{A_e}(t) dt \quad (2.60)$$

In this way the delta function in (2.59), $\delta(t) / R_{eb}$, becomes an impulse of height $1 / R_{eb}$. A plot of this discrete-time impulse response for a typical set of loudspeaker parameters is shown in Figure 2.17.

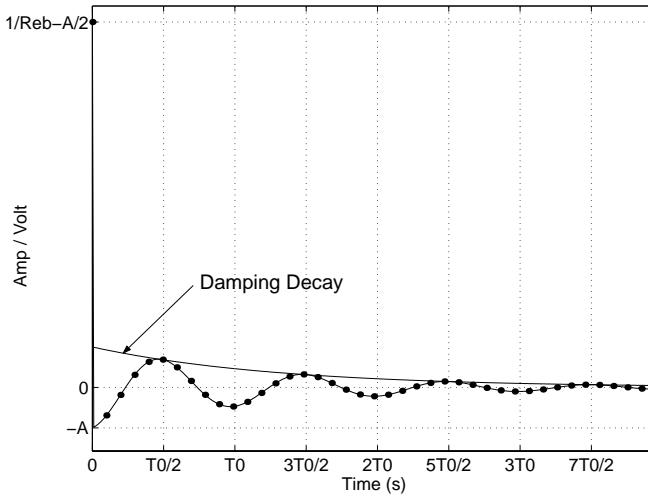


Figure 2.17: Impulse response of (2.59) for same set of parameters as Figure 2.16. Points on the impulse response denote locations of FIR filter taps as would occur given $F_s = 8\text{kHz}$. The x-axis tick marks are shown at intervals of T_0 , which is $1/f_0$, where f_0 is the resonance frequency.

An adaptive FIR filter operating on a loudspeaker's electrical admittance will identify discrete points of (2.59), as shown in Figure 2.17. From sufficient number of these points, the parameters may be identified by minimising the error between the values of these points and the formula of (2.59).

This method is considered too computationally expensive. This is because two computationally intense steps must be performed:

- Adaptation of sufficient length FIR filter
- Determination of parameters from identified FIR coefficients.

Figure 2.17 shows one of the best-case situations with respect to number of taps needed in the FIR filter. In this case, the ratio of the resonance frequency f_0 to the sampling frequency F_s is about 0.1. Here it is clear that at least 15 taps would be needed in order to make an accurate estimate of the resonance frequency and damping factor.

Perhaps even more difficult, however, is the final determination of the parameters ω_0 , ζ and ϕ_0 from the FIR filter coefficients. The error function resulting between these coefficients and (2.59) would be highly nonlinear in the parameters ω_0 , ζ and ϕ_0 , and would thus have to be determined by an iterative method (e.g. Newton's method). This type of meta-calculation is considered, for the present work, unsuitable for real-time processing.

2.3.2. IIR filter for receptance of an SDOF system

Knudsen et al. (1989) presented a formula for a second-order IIR filter giving the frequency response of a second-order mechanical system, and used this as a model of a loudspeaker's mechanical dynamics. In their paper, it is explained that the parameters of the IIR filter are related to the physical parameters of the mechanical system by simple expressions not presented in the paper. As these expressions will be used in several parts of this thesis in some detail, their derivation is presented here.

The s -domain transfer function for the mechanical receptance of a single mass-spring-damper (SDOF) system, according to elementary mechanical dynamics (e.g. Newland, 1989), is given by

$$X_m(s) = \frac{x_d(s)}{f_c(s)} = \frac{1}{m_t s^2 + c_t s + k_t} \quad (2.61)$$

In a method similar to that in §2.1.2, above, this may be written in factored, form,

$$X_m(s) = \frac{1}{m_t} \frac{1}{(s - \lambda_1)(s - \lambda_2)} \quad \lambda_1, \lambda_2 = -\omega_0 \zeta \pm i\omega_0 \sqrt{1 - \zeta^2} \quad (2.62)$$

The terms λ_1 and λ_2 are the poles of the transfer function, as they are the roots of the denominator polynomial in (2.61). As per impulse invariance described above, the basic form of a discrete-time transfer function may be obtained by mapping the poles of (2.62) to the z -plane, according to $\pi_n = e^{T_s \lambda_n}$. This provides

$$H_{X_m}(z) = \sigma_x \frac{z^{-1}}{1 + (-\pi_1 - \pi_2)z^{-1} + \pi_1 \pi_2 z^{-2}} \quad (2.63)$$

where σ_x is the characteristic sensitivity in z -domain, which shall be defined below. This z -domain representation may be written in standard form as

$$H_{X_m}(z) = \frac{b_1 z^{-1}}{1 + a_1 z^{-1} + a_2 z^{-2}}. \quad (2.64)$$

where

$$\begin{aligned} b_1 &= \sigma_x \\ a_1 &= -(\pi_1 + \pi_2) \\ a_2 &= \pi_1 \pi_2 \end{aligned} \quad (2.65)$$

In this way the coefficients of the discrete-time transfer function are determined from those of the continuous-time version according to:

$$\begin{aligned} a_1 &= -e^{-\omega_z \zeta + i\omega_z \sqrt{1 - \zeta^2}} - e^{-\omega_z \zeta - i\omega_z \sqrt{1 - \zeta^2}} \\ &= -2e^{-\omega_z \zeta} \cos(\omega_z \sqrt{1 - \zeta^2}) \\ a_2 &= e^{-2\omega_z \zeta} \end{aligned} \quad (2.66)$$

The z -domain characteristic sensitivity, σ_x , is determined by matching at a certain frequency the value of the z -domain frequency response in (2.63) to the s -domain frequency response in (2.61). The characteristic frequency is one for which the transfer function is most simply defined. For the mechanical receptance, this occurs at $f = 0$ (i.e. 0 Hz), where $X_m(s)$ in (2.61) is $1/k_t$. With the foregoing, σ_x is

$$\sigma_x = \frac{1 + a_1 + a_2}{k_t}. \quad (2.67)$$

The frequency response and pole-zero map of this discrete-time model of the receptance is shown in Figure 2.18, for three different resonance frequencies, and for three different damping values. The frequency response of the discrete-time model of receptance closely matches the continuous-time response in both magnitude and phase. The only difference occurs at high frequencies, close to the Nyquist frequency. At these high frequencies, the discrete-time model has a higher magnitude response than the continuous-time response. Due to the low-pass nature of the receptance function, it is assumed that the total percentage error of a broad-band signal filtered by this discrete-time model of the receptance would be minimal. If better accuracy were needed up the Nyquist frequency, this could be achieved by increasing the complexity of the filter, i.e. by increasing its order.

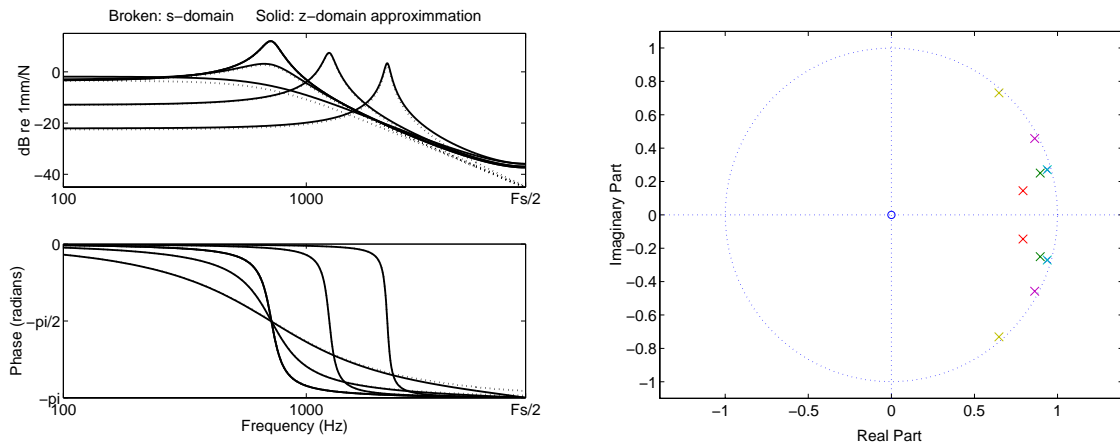


Figure 2.18, [left]: Frequency response comparison between continuous-time (broken) and discrete-time (solid) representation of the receptance; [right]: pole-zero map in z -plane of receptance model.

The continuous-time resonance frequency ω_0 and the damping ratio ζ can be determined from a_1 and a_2 , given certain limits on the range of values of a_1 and a_2 . In the s -plane, the damped natural frequency is the distance of the poles, λ_1 and λ_2 in (2.62), along the Imaginary axis. In other words, the damped natural frequency is given by the imaginary part of the poles, λ_1 and λ_2 . By the analogy that the imaginary axis of the s -plane is wrapped around the unit circle of the z -plane, the same damped natural frequency, normalised to the sampling frequency F_s , in z -domain will be given by the angle of the pole around the unit circle of the z -plane. Therefore the damped natural frequency is given by

$$\omega_0 T_s \sqrt{1 - \zeta^2} = \arctan\left(\frac{\text{Im}\{\pi_1\}}{\text{Re}\{\pi_1\}}\right) \quad (2.68)$$

where π_1 is the value of the pole in the z -plane. The real and imaginary parts of the pole π_1 are given by relating the factored form of (2.64) to its polar form in (2.63), resulting in

$$\begin{aligned}\text{Im}\{\pi_1\} &= \frac{1}{2}\sqrt{-a_1^2 + 4a_2} \quad \text{for } -a_1^2 < 4a_2 \\ \text{Re}\{\pi_1\} &= -\frac{1}{2}a_1\end{aligned}\tag{2.69}$$

A clue to finding the damping ratio ζ from a_1 and a_2 lies in recalling that it is related to the pole's distance to the imaginary axis in the s -plane, which in the z -plane translates to its distance to the unit circle. This distance is given by $(1 - \sqrt{a_2})$. Given the definitions of a_2 in (2.66), the square-root term is

$$\sqrt{a_2} = e^{-\omega_s \zeta}. \tag{2.70}$$

Therefore given the condition $a_2 > 0$ we have

$$-\omega_z \zeta = \ln(\sqrt{a_2}) \tag{2.71}$$

Inspection of Eqs. (2.68) and (2.71) shows the s -plane pole can be reconstructed from a_1 and a_2 as so

$$\lambda_1, \lambda_2 = F_s \left[\ln(\sqrt{a_2}) \pm i \arctan \left(\frac{\text{Im}\{\pi_1\}}{\text{Re}\{\pi_1\}} \right) \right] \tag{2.72}$$

Recalling that the undamped natural frequency can be determined from the magnitude of the continuous-time eigenvalue, i.e. $\omega_0 = |\lambda_1|$, the undamped natural frequency may be determined from a_1 and a_2 as so

$$\begin{aligned}\omega_z &= \sqrt{\ln^2(\sqrt{a_2}) + \arctan^2 \left(-\frac{\sqrt{-a_1^2 + 4a_2}}{a_1} \right)} \\ &= \omega_0 / F_s\end{aligned}\tag{2.73}$$

The damping ratio may be obtained from the above result and (2.71), giving:

$$\zeta = \frac{-\ln(\sqrt{a_2})}{\omega_0 T_s} \tag{2.74}$$

2.3.3. IIR filter for mobility of an SDOF system

As discussed in §2.1.2, the continuous-time transfer function of the mechanical mobility of an SDOF system is given in s -domain by

$$Y_m(s) = \frac{s}{s^2 m_t + s c_t + k_t} \tag{2.75}$$

A discrete-time approximation to the continuous-time description by using the same process as used for the mechanical receptance described in §2.3.2.

Thus we have

$$Y_m(z) = \frac{\sigma_u - \sigma_u z^{-2}}{1 + a_1 z^{-1} + a_2 z^{-2}} \tag{2.76}$$

where a_1 and a_2 are as defined in (2.65). The reference sensitivity σ_u is defined by matching the overall value of the discrete-time frequency response function to that of the continuous-time frequency response function. The continuous-time frequency response function for the mechanical mobility is most simply defined at $f = \omega_0$, where $Y_m(s) = 1/c_t$. Therefore the σ_0 is defined by matching the two frequency response functions at this frequency, providing

$$\sigma_u = \frac{1}{c_t} \frac{1 - (\pi_1 + \pi_2)e^{-i\omega_0 T_s} + \pi_1 \pi_2 e^{-2i\omega_0 T_s}}{1 - e^{-2i\omega_0 T_s}}. \quad (2.77)$$

The frequency response and pole-zero map of this discrete-time model of the mobility is shown in Figure 2.19. The response of the discrete-time model of mobility closely matches the continuous-time response in both magnitude and phase. Like the receptance function, the only difference occurs at high frequencies, close to the Nyquist frequency. Here, the discrete-time model has a lower magnitude response than the continuous-time response. The agreement between these two is considered acceptable for the present application.

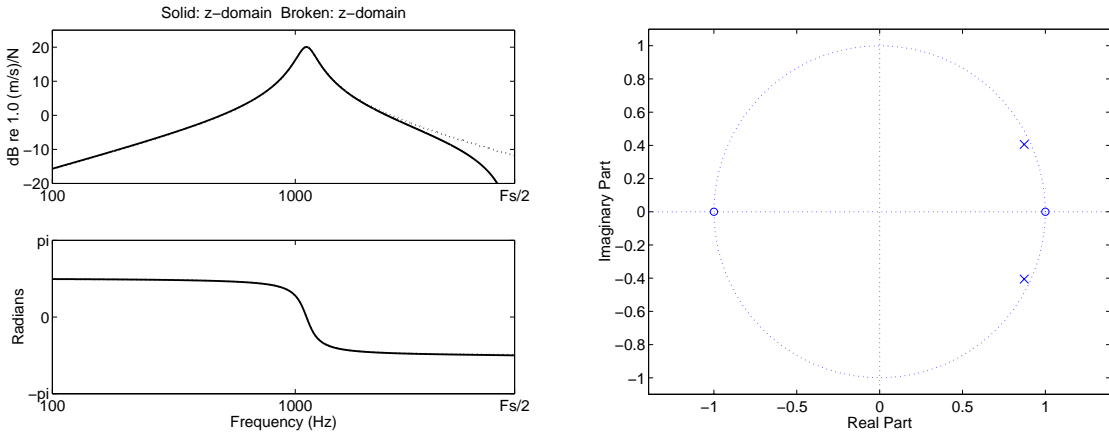


Figure 2.19 (a) – (c): Frequency response comparison between continuous-time (broken) and discrete-time (solid) representation of the mobility; [right]: pole-zero map in z -plane of mobility model.

The reference sensitivity σ_u can be defined in terms of a_1 and a_2 if the total mass m_t is fixed. By using the substitution $c_t = 2\zeta\omega_0 m_t$ we have

$$\sigma_u = \frac{1}{2\zeta\omega_0 F_s m_t} \frac{1 + a_1 e^{-i\omega_z} + a_2 e^{-2i\omega_z}}{1 - e^{-2i\omega_z}} \quad (2.78)$$

The terms ζ and ω_s may be determined from a_1 and a_2 as described in §2.3.2 above.

For real-time, real-valued processing, the definition of σ_u in (2.78) is too complicated. It has been found that σ_u depends only on the term a_2 . Furthermore, it has been found that, over the most interesting range of values of a_2 , σ_u may be determined approximately by a polynomial approximation as so

$$\sigma_u = \frac{1}{m_t F_s} \sum_{n=0}^N p_{\sigma_u \cdot n} a_2^n \quad (2.79)$$

where $p_{\sigma_u \cdot n}$ is the n^{th} coefficient of a polynomial approximation to the function of σ_0 in terms of a_2 . As shown in Figure 2.20, a third-order polynomial approximation ($N=3$) provides a good compromise between accuracy and complexity. An example of the accuracy of this polynomial fit is shown in Figure 2.20. Although there is significant deviation for a_2 below 0.4, only the range of a_2 from 0.6 to 1.0 is of interest for the type of loudspeaker of interest in this thesis. This can be seen clearly in Figure 4.9, in the discussion on the ‘tolerance quadrilateral,’ in §4.1.5.

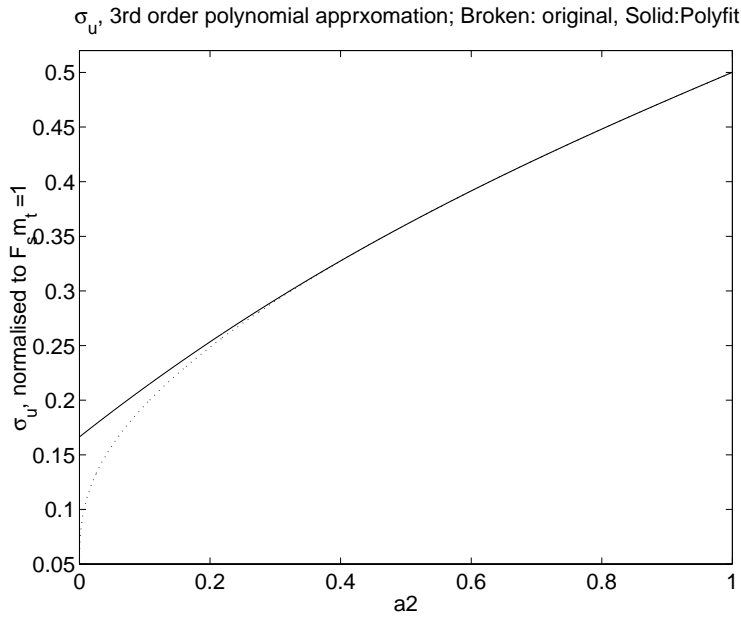


Figure 2.20: Reference sensitivity, σ_u vs. a_2 ; actual value (broken) vs. 3rd-order polynomial approximation (solid). Only the range of a_2 from 0.6 to 1.0 is of interest, and thus the deviation below 0.4 is not of concern.

2.3.4. Nonlinear discrete-time loudspeaker model

A linear model for the loudspeaker can be developed in discrete-time in the same manner as it is for the mechanical receptance and mobility in the preceding two sections. This is possible because, for the case of the loudspeaker mounted in a closed box, the mechanical dynamics of the system have a single degree of freedom. Accurate representation of the frequency response of single-degree-of-freedom mechanical dynamics is possible in discrete-time using the IIR filters for receptance and mobility described in §2.3.2 and 2.3.3, respectively, above. As mentioned above, Knudsen et al. (1989) used this discrete-time representation for parameter determination by digital system identification. This linear representation is used here. The linear representation is combined with nonlinear components, to produce a discrete-time nonlinear model. Using a technique developed by Klippel (1992), all nonlinear components are described by zero-memory systems. The key advantage of this method developed by Klippel is that the linear and nonlinear components are kept separate.

Only the dominant causes of nonlinearity are included in the nonlinear model presented here. Specifically, these are nonuniformity in the transduction coefficient $\phi(x_d)$ and suspension stiffness $k(x_d)$.

In §2.1.2, the mechanical dynamics of the loudspeaker are presented in terms of the mechanical mobility of an SDOF system. One can equally consider the mechanical receptance, wherein the displacement is considered as the output (instead of the velocity, for the mobility). Beginning with the linear discrete-time filter for the receptance derived in §2.3.2 above, the diaphragm displacement is given in terms of the force applied on the coil by the following difference equation:

$$x_d[n] = \sigma_x f_c[n-1] - a_1 x_d[n-1] - a_2 x_d[n-2] \quad (2.80)$$

The force on the voice-coil $f_c[n]$ may be calculated from the voice-coil current by

$$f_c[n] = \phi(x_d[n]) i_c[n] - k_l(x_d[n]) x_d[n] \quad (2.81)$$

where $k_l(x_d[n])$ is the variation of the suspension stiffness with displacement, excluding its value at equilibrium (k_d). Thus, if we consider the stiffness represented by the polynomial expansion of (2.48) in §2.2.1 part B, $k_l(x_d[n])$ is given by

$$k_l(x_d[n]) = \sum_{l=1}^{N_k} k_l x_d^l[n] \quad (2.82)$$

By dropping the electrical inductance term, the voice-coil current may be determined using the voltage equation of (2.50) as so¹

$$i_c[n] = \frac{1}{R_{eb}} [v_c[n] - \phi(x_d[n]) u_d[n]] \quad (2.83)$$

The velocity $u_d[n]$ appearing in (2.83) may be determined by differentiating the displacement signal. This differentiation may be represented by the following difference equation

$$\begin{aligned} u_d[n] &= h_{dt}[n] * x_d[n] \\ &= b_{dt,0} x_d[n] + b_{dt,1} x_d[n-1] - a_{dt,1} u_d[n-1] \end{aligned} \quad (2.84)$$

In principle values of the filter coefficients in (2.84) may be taken from the bilinear transform, discussed in the introduction to this sub-section, above. This will, however, lead to an unstable filter, and thus it is necessary to use a slightly modified value of $a_{dt,1}$. This is discussed in more detail below.

An explicit difference equation for calculating the displacement from the input voltage may be derived by combining (2.80) - (2.84), as so:

$$\begin{aligned} x_d[n] &= \sigma_x \left\{ \phi(x_d[n-1]) \left(\frac{1}{R_{eb}} \{v_c[n-1] - \phi(x_d[n-1]) h_{dt}[n] * x_d[n-1]\} \right) - k_l(x_d[n-1]) x_d[n-1] \right\} \\ &\quad - a_1 x_d[n-1] - a_2 x_d[n-2] \end{aligned} \quad (2.85)$$

A diagram showing the flow of processing of (2.85) is shown in Figure 2.21. An extremely important feature of (2.85) is that it is an *explicit* equation for predicting the displacement $x_d[n]$ from the input voltage $v_c[n]$, incorporating nonlinear models of the transduction coefficient and suspension stiffness. This is to say that only delayed samples of $x_d[n]$ appear in the RHS of this difference equation. Furthermore, the input signal, the voltage $v_c[n]$ also appears only as a delayed sample in the RHS. Equation (2.85) may, therefore, be seen as a one-step predictor for the diaphragm displacement from the input voltage. This important feature will be exploited for the development of a method for compensating nonlinear distortion produced by nonuniformity of the transduction coefficient and suspension stiffness, presented in §3.3.7.

¹ Although (2.50) is expressed in continuous-time, it contains no differential or other time-dependent operators, and may, therefore, be directly converted to discrete-time.

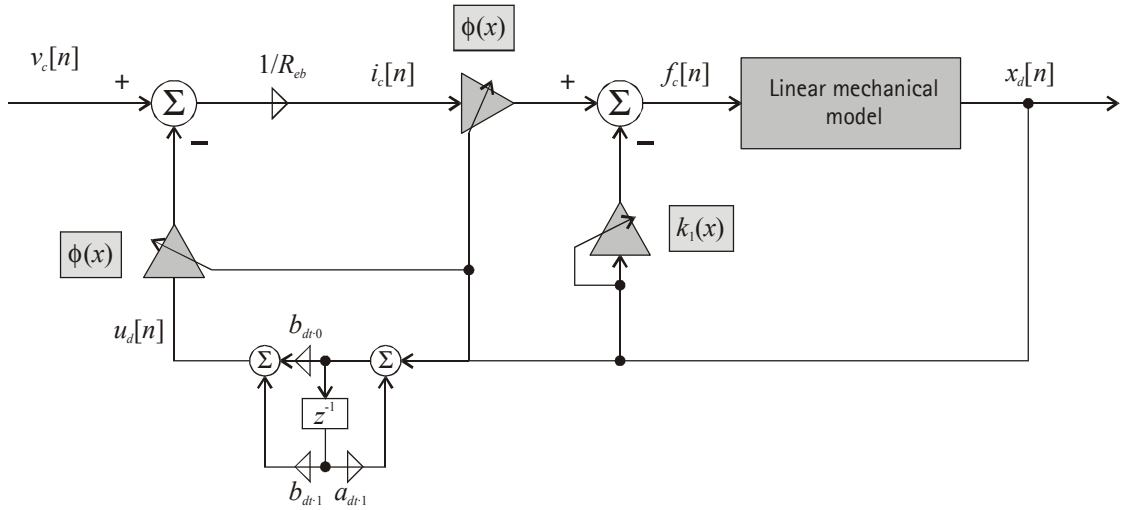


Figure 2.21: Flow diagram for the nonlinear prediction of displacement according to (2.85).

One problem with (2.85) is that it is inherently unstable, due to the nature of the approximation of differentiation made by the bilinear transformation used to derive the velocity signal by $h_{dt}[n]*x_d[n]$. This velocity signal, when fed back to the input, leads to an instability. This can be seen in the z -domain transfer function of (2.85) valid for the small-signal (linear) case. This z -domain transfer function is given by

$$H_{X_m}(z) = \frac{(\sigma_x \phi_0 / R_{eb}) z^{-1} + (\sigma_x \phi_0 / R_{eb}) z^{-2}}{1 + (2F_s \sigma_x \phi_0^2 / R_{eb} + a_{dt} + a_1) z^{-1} + (-2F_s \sigma_x \phi_0^2 / R_{eb} + a_2 + a_{dt} + a_1) z^{-2} + a_{dt} a_2 z^{-3}}$$

(2.86)

and a pole-zero plot for a typical set of parameters and for $a_{dt} = 1$ is shown in Figure 2.22. As can be seen on the left-hand side of the pole-zero plot in Figure 2.22, there is a pole (indicated by an ‘x’) outside of the unit circle – the basic characteristic for instability in an IIR filter. This problem will lead to high-frequency oscillation, rendering the filter useless. The problem can be corrected by reducing the value of a_{dt} to less than unity (<1). The pole-zero and frequency response of the same formula but with $a_{dt} = 0.85$ are shown in Figure 2.23. Here, it is shown that reducing a_{dt} in this way moves the pole inside the unit circle, thereby insuring stability, without significantly affecting the magnitude or phase response of the filter in the pass-band.

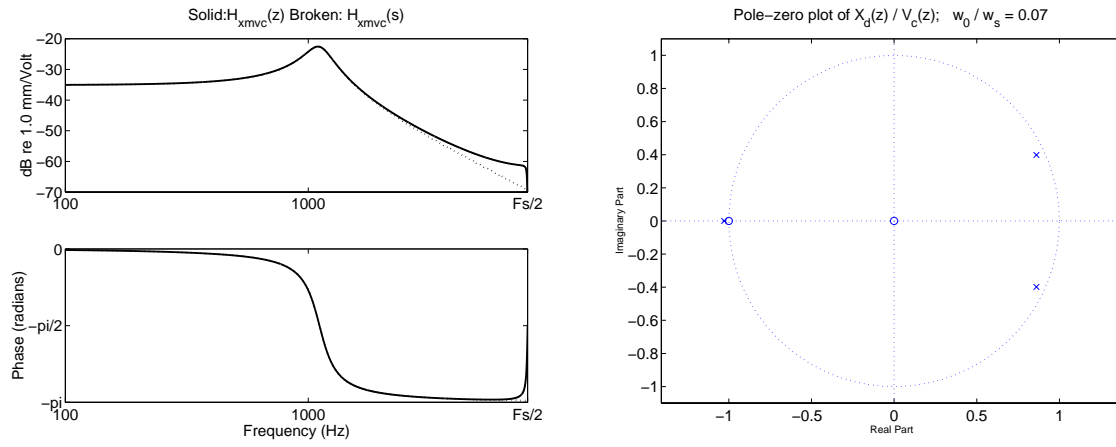


Figure 2.22: Linear analysis of Eq. (2.85), for $a_{dr,1}=1$; left: frequency response, magnitude (upper) and phase (lower); right: poles and zeros in z -plane. Notice pole (indicated by an 'x') just outside of the unit circle on the left-side of the plane.

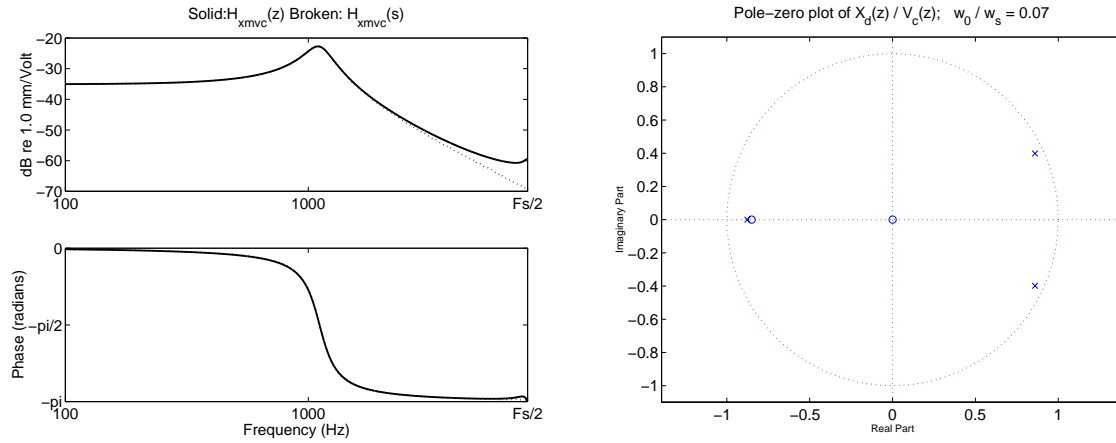


Figure 2.23: Linear analysis of Eq. (2.85), for $a_{dr,1}=0.85$; left: frequency response, magnitude (upper) and phase (lower); right: poles and zeros in z -plane.

2.4. Parametric uncertainty

The parameters of a loudspeaker cannot be known *a priori* from its design and manufacturing specifications. Parameters of any given loudspeaker will vary from one unit to another from the same production line due to manufacturing tolerances. Furthermore, the parameters will vary with time due to ageing, and with temperature variations.

Studies on the parametric variations of loudspeakers due to ambient temperature variations have been made by Krump (1997) and Hutt (May 2002). Both found the temperature variation to induce significant changes in the loudspeaker, with the strongest variations found in the suspension stiffness (k_d) and damping (c_d). A small variation in the transduction coefficient (ϕ_0) is also found. Significant variation on the mass m_d was found by Krump, though not by Hutt. It was suggested by Hutt (June, 2002) that variation in the mass m_d found by Krump was the result of temperature-induced variations in the suspension, leading to mass non-uniformity with excursion, as discussed in §2.2.1, part D, above. It is thus presumed that the variations in mass found by Krump were a ‘large-signal’ (nonlinear) effect, and not due to temperature-variation-induced changes in the small-signal moving mass. The results of these studies are summarised in Table 2.1, with a key difference for the suspension stiffness of the microspeaker, discussed below.

Parameter	Symbol	Temperature Variation coefficient	Manufacturing tolerance
DC-resistance	R_{eb}	$0.004 \cdot R_{eb} \cdot 0^{\circ}\text{C}$ ^(a)	$\pm 10\%$ ^(b)
Suspension damping	c_d	-0.05 ^(c)	$\pm 10\%$ ^(b)
Suspension stiffness	k_d	(none) ^(d)	$\pm 30\%$ ^(b)
Transduction coefficient	ϕ_0	-0.005 ^(e)	n/a

Table 2.1: Known parametric uncertainties due to temperature variation and manufacturing tolerances.

The studies by Krump and Hutt were made on more traditional low-frequency loudspeakers, more broadly akin to that shown in Figure 2.2 than the microspeaker. With respect to temperature-dependence of the stiffness, the microspeaker has an important difference to the typical loudspeaker. Specifically, the materials which make up the outer surround and inner spider suspensions are typically made of soft rubber and woven fabric, respectively. These are materials whose bulk modulii are known to have strong temperature-dependence. The microspeaker, by contrast nearly universally uses polycarbonate plastic for its suspension (part (3) of Figure 2.1.) There is no dependence of the Young’s modulus (and thus suspension stiffness) below 120 °C for polycarbonate plastic, as per Fig. 41 of Nashif and Lewis (1991). Above 120°C, various materials in the microspeaker, such as glues, insulators, and adhesives, begin to break down, causing irreparable damage. It is, therefore, considered that this microspeaker will not be used above 120°C. For this reason the temperature dependence of the suspension stiffness above this temperature is not considered.

^(a) *Handbook of Chemistry and Physics*, 36th Edition, Chemical Rubber Publishing Co.

^(b) Philips Loudspeaker Systems Telecom Vienna, datasheets 590-N for WD 005XX-series microspeakers.

^(c) Krump (1997)

^(d) For polycarbonate plastic suspension material.

^(e) Krump (1997)

2.5. References

- Beers, G. L. , and H. Beloar, "Frequency-Modulation Distortion in Loudspeakers," *Proc. IRE* **31**, 132. (Apr. 1943)
- Birt, David R., "Nonlinearities in Moving-Coil loudspeakers with Overhung voice-coils," *Journal of the Audio Eng. Soc.*, **39**, pp. 219-231. (April 1991)
- Butterweck, H. J., "About Doppler nonlinearities in loudspeakers," *Proceedings of the International Conference on Acoustics, Speech, and Signal Processing 1989*, pp. 2061-2063. (23-26 May, 1989)
- Christensen, Knud Bank, and Erling Sandermann Olsen, "Nonlinear Modelling of Low Frequency Loudspeakers – A More Complete Model," *presented at the 100th Convention of the Audio Eng. Soc.*, preprint 4205. (May 11-14, 1996)
- Cunningham, W. J., "Non-Linear Distortion in Dynamic Loudspeakers due to Magnetic Effects," *J. Acoustical Society of America*, **21**, pp. 202-207. (May, 1949)
- Hutt, Steve, "Ambient Temperature Variations on OEM Automotive Loudspeakers", *presented at the 112th Convention of the Audio Eng. Soc., Munich, Germany* Convention Paper 5507. (10-13 May, 2002)
- Hutt, Steve, personal correspondence. (7 June, 2002)
- Jang, Han-Kee, and Kwang-Joon Kim, "Identification of Loudspeaker Nonlinearities Using the NARMAX Modelling Technique," *Journal of the Audio Eng. Soc.* **42**, pp. 50-59. (Jan./Feb. 1994)
- Kaizer, A. J. M., "Modeling of the Nonlinear Response of an Electrodynamic Loudspeaker by a Volterra Series Expansion," *Journal of the Audio Eng. Soc.*, **35**, pp. 421-433. (June 1987)
- Klapman, S. J., "Interaction Impedance of a System of Circular Pistons", *J. of the Acoust. Soc. Amer.*, **11**, pp.289-295. (Jan. 1940)
- Klippel, Wolfgang, "Nonlinear Large-Signal Behaviour of Electrodynamic Loudspeakers at Low Frequencies," *Journal of the Audio Eng. Soc.* Vol. 40, No. 6 pp. 483-496 (June 1992)
- Klippel GmbH, "Large Signal Identification," Klippel GmbH, Aussiger Str. 3, 01277, Dresden, Germany. Available online at: <http://www.klippel.de/> (Aug. 22, 2001).
- Klipsch, Paul W., "Modulation Distortion in Loudspeakers," *J. Audio Eng. Soc.* pp. 194-206. (Presented at the April 29, 1968 34th Convention of the AES) (1968)
- Knudsen, M. H., J. Grue Jensen, V. Julskjær, and Per Rubak "Determination of Loudspeaker Driver Parameters Using a System Identification Technique," *Journal of the Audio Eng. Soc.*, **37**, pp. 700-708. (Sept. 1989)
- Krump, Gerhard, "Zur Temperaturabhängigkeit von Lautsprecherparametern," ("The Temperature Dependence of Loudspeaker Parameters") (in German), *presented at DAGA-97* (The Acoustical Society of Germany), (March 3-6, 1997), ISBN 3-9804568-2-X.
- Nashif, Ahid D., and Tom M. Lewis, "Data Base of the Dynamic Properties of Materials", *Sound and Vibration*, pp. 14-25. (July 1991)
- Newland, D. E., *Mechanical vibration analysis and computation*, Longman Scientific and Technical, Burnt Mill, Harlow, England. (1989)
- Novak, James F., "Performance of Enclosures for Low-Resonance, High-Compliance Loudspeakers," *IRE Transactions on Audio*, **AU-7**, pp. 5-13. (Jan.-Feb. 1959)
- Olsen, Erling Sandermann and Knud Thorborg, "Diaphragm Area and Mass Nonlinearities of Cone Loudspeakers," presented at the 99th Convention of the Audio Eng. Soc., preprint no. 4082. (1995)

- Olson, Harry F., *Elements of Acoustical Engineering*, Second Edition, D. Van Nostrand Co., Inc., New York, New York. (Sept. 1947)
- Olson, Harry F., *Acoustical Engineering*, D. Van Nostrand Co., Inc., New York, New York. (1957)
- Olson, Harry F., "Action of a direct radiator loudspeaker with non-linear cone suspension," *J. Acoust. Soc. Amer.*, **16** (1) pp.1-4. (July, 1944)
- Oppenheim, Alan V., and Ronald W. Schafer, *Discrete-time Signal Processing*, Prentice Hall, Englewood Cliffs, New Jersey, USA. (1989)
- Pierce, Allan D., *Acoustics: An Introduction to Its Physical Principles and Applications*, (1994 Ed.), Chapter 4, The Acoustical Society of America, Woodbury, New York, U.S.A.. (1994).
- Potirakis, S. M. , G. E. Alexakis, M. C. Tsilis, and P. J. Xenitides, "Time-domain nonlinear modelling of practical electroacoustic transducers." *Journal of the Audio Eng. Soc.* **47**, pp. 447-468. (June 1999)
- Rausch, R., R. Lerch, M. Kaltenbacher, H. Landes, G. Krump, and L. Kreitmeier, "Optimisation of Electrodynamic Loudspeaker-Design Parameters by Using a Numerical Calculation Scheme", *ACUSTICA-acta acustica*, **85**, pp. 412-419. (1999)
- Small, Richard H., "Direct-Radiator Loudspeaker System Analysis," *IEEE Transactions on Audio and Electroacoustics*, Vol. AU-19, pp. 269-281 (Dec. 1971)
- Small, Richard H., "Closed-Box Loudspeaker Systems, Part I: Analysis," *Journal of the Audio Eng. Soc.*, **20**, pp. 798-808. (Dec. 1972)
- Small, Richard H., "Closed-Box Loudspeaker Systems, Part II: Synthesis," *Journal of the Audio Eng. Soc.*, **21**, pp. 11-18. (Jan-Feb. 1973)
- Small, Richard H., "Vented-Box Loudspeaker Systems – Part 1: Small-Signal Analysis," *Journal of the Audio Eng. Soc.*, **21**, pp. 363-372. (Jun. 1973)
- Small, Richard H., "Vented-Box Loudspeaker Systems – Part 2: Large-Signal Analysis," *Journal of the Audio Eng. Soc.*, **21**, pp. 483-444. (Jul. 1973)
- Small, Richard H., "Vented-Box Loudspeaker Systems – Part 3: Synthesis," *Journal of the Audio Eng. Soc.*, **21**, pp. 549-554. (Sep. 1973)
- Small, Richard H., "Vented-Box Loudspeaker Systems – Part 4: Appendices," *Journal of the Audio Eng. Soc.* **21**, pp. 635-639. (Oct. 1973)
- Small, Richard H., "Loudspeaker Large-Signal Limitations," *presented at the 1st Australian Regional Convention of the Audio Eng. Soc.*, preprint no. 2102. (Sept 25-27, 1984)
- Thiele, A. N, "Loudspeakers in Vented Boxes," *Proceedings of the IRE Australia*, **22**, pp. 487-508 (Aug. 1961); reprinted in *Journal of the Audio Eng. Soc.*, **19**, pp. 382-392. (May 1971)
- Vanderkooy, John, "A Model of Loudspeaker Driver Impedance Incorporating Eddy Currents in the Pole Structure," *Journal of the Audio Eng. Soc.*, **37**, pp. 119-128. (Mar. 1989)
- Zóltogórski, Bonislaw, "Moving Boundary Condition and Non-Linear Propagation as the Sources of Non-Linear Distortions in Loudspeakers," *presented at the 94th Convention of the Audio Engineering Society*, preprint no. 3510. (16-19 Mar, 1993)

3. Theory of active control of loudspeakers

This chapter presents theory of systems for active control of loudspeakers. Active control is considered in the context of three possible architectures, *feedback*, *feedforward*, and *adaptive feedforward*, as they were presented in the introduction.

Several different feedback systems are discussed. Current feedback and negative output impedance amplifiers are first discussed, and a historical view of their development is given. ‘Motional feedback’ systems for active control, wherein a measured vibration signal is used for feedback, are then reviewed. Implementation problems of these feedback systems are discussed.

Feedforward processors are presented at a general level. Both linear and nonlinear feedforward processing is considered.

A special section on the theory of feedback linearisation is presented, along with a discussion on how this can be used to develop a nonlinear feedforward controller for a loudspeaker.

The theory of feedback linearisation is applied to the nonlinear discrete time model developed in §2.3.4, above. This leads to a simple algorithm for compensation of loudspeaker nonlinearities.

As discussed in §2.4, certain properties of the loudspeaker cannot be known *a priori*, as they are subject to drift due to various factors. It is for this reason necessary to make any feedforward controller *adaptive*, so as to be properly tuned to the loudspeaker. This leads to the *adaptive feedforward controller*, mentioned in the introduction, and shown in Figure 1.4. The adaptive part of this type of controller is performed using adaptive signal processing. A brief review of adaptive signal processing theory, and a special discussion on adaptive recursive (IIR) filters, is therefore presented at the end of this chapter.

3.1. Feedback control for loudspeakers

The improvement of loudspeakers by electrical means has been actively researched, more or less in parallel with research on the loudspeaker itself. The historical and technical context of feed-forward equalisation and nonlinear compensation lies in theory and design of *feedback* controllers. To this end, such well-known systems as *negative output impedance* amplifiers and *motional feedback* are reviewed.

3.1.1. Constant-current output amplifiers

A constant-current output amplifier offers a few advantages over the typical constant-voltage (low-impedance) power amplifiers. This can be seen, from a theoretical point of view, in a straightforward manner by inspection of the nonlinear differential equation pair of (2.50) and (2.51). If the coil-current $i_c(t)$ is held constant by the power amplifier, the nonlinear terms in the voltage equation (2.50) will not cause nonlinearity between the input and output (as they would for a constant-voltage amplifier). Only nonlinear terms in the force equation, (2.51) will generate nonlinear distortion. Perhaps more significantly, any changes in the DC resistance R_{eb} due to heating of the voice-coil (known as ‘power compression’) will not effect the resulting response. These benefits were used as arguments in favour of using constant-current output amplifiers by Mills and Hawksford (1989).

The primary complication in using a current-drive amplifier is that the electrical damping is lost, resulting in an excess Q_{tc} . Mills and Hawksford solved this problem by using some velocity feedback, wherein the velocity signal was obtained by a secondary winding on the voice-coil. Transformer-like coupling between the main drive coil and this sensing coil was compensated for by an appropriate network. The constant-current output amplifier does not seem to have received any interest since the work of Mills and Hawksford.

3.1.2. Negative amplifier output impedance

Before the negative feedback amplifier was formalised as a method for reduction of amplifier distortion, various feedback systems were proposed using some kind of interface to the loudspeaker. The first record of these is from Voigt (1925), whose patent describes the modified Wheatstone bridge shown in Figure 3.1. The bridge is connected between the amplifier and loudspeaker, producing a signal proportional to the diaphragm velocity. The velocity-analogous signal may be fed back into the input to the amplifier, thereby damping the loudspeaker’s resonance. This was seen as advantageous, as mechanical damping of this resonance would result in an efficiency loss, and additional passive electrical damping would require a larger magnet resulting in a higher cost and weight.

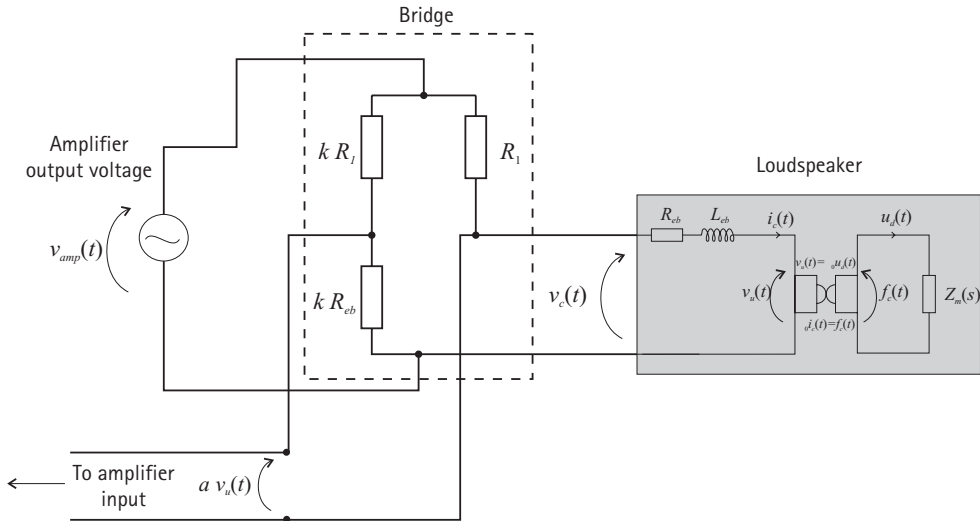


Figure 3.1: Basic diagram of the impedance bridge for generating velocity feedback signal to create a negative output impedance amplifier.

This principle has been written about by many authors over many years. It was described by Yorke and McLachlan (1951) who called it an ‘Amplifier of Variable Output Impedance’, Clements (1951, 1952) who called it ‘Positive Feedback’, Wentworth (1951) who called it ‘Inverse Feedback’, Childs (1952) who called it ‘Dynamic Negative Feedback’, and Wilkins (1956) who referred to it as ‘Control of Amplifier Source Resistance’. Agreement seemed to have come upon the term ‘Negative Output Impedance’, used by Werner (1957), Werner and Carrell (1958), Steiger (1960), Thiele (1961)¹, Ståhl (1981), and Normandin (1984). However, this system was simply referred to as the ‘bridge-version’ of motional feedback in papers by de Boer (1961), Klaassen and de Koning (1968), and Adams and Yorke (1976). Furthermore, on the commercial market it was referred to as ‘damping control’, a popular feature in the 1960’s, seen now only in the idiosyncratic electric-guitar amplifier market. Perennial terminology confusion was ensured in papers by Holdaway (1963), who referred to this as ‘Velocity Feedback,’ and Birt (1981), who demonstrated true creativity where one might have thought it exhausted with the name ‘Load-Adaptive Source Impedance.’ Little new was contributed to the subject by these latter authors, with the notable exception of Ståhl (1981) and Normandin (1984) who used it to interesting effect, which will be discussed below.

It is also possible to derive a velocity signal using the same principle as described above, but instead using active analogue electronics. Such a system was described by Bai and Wu (1999). This was used to generate a feedback signal for a digital feed-forward controller to provide linear adaptive equalisation. The work of Bai and Wu was developed in the context of control theory, wherein the analogue circuitry providing the velocity signal is referred to as an observer model.

The impedance bridge shown in Figure 3.1 can only provide a velocity-analogous signal to the controller under the following two conditions:

- The resistor in the lower-left leg maintains the value kR_{eb}
- The transduction coefficient ϕ_0 remains uniform with respect to diaphragm-coil displacement.

These two conditions are not always met. The actual DC resistance will change with coil temperature, which is affected by ambient temperature, and with heating due to thermal dissipation. At large

¹ This is mentioned in an off-hand manner in section 12 of Thiele’s famous 1961 paper (better known by its 1971 re-publication in the *J. of the Audio Eng Soc.*) the main subject of which was the application of analogue active-filter alignment tables to the design of vented (ported) enclosures.

displacements the transduction coefficient will not be uniform with respect to displacement, as discussed in §2.2.1, part A.

A further problem is that the velocity-analogous signal is proportional to the system output, the acoustic pressure, only if the loudspeaker is mounted in a closed box, wherein the acoustic pressure is given by the time-derivative of the diaphragm velocity as per (2.24). If the loudspeaker is mounted in a ported or horn-loaded enclosure, the relationship between velocity and pressure will be more complex. For this reason, the negative-output impedance amplifier is not a closed-loop control system in the strict sense of that shown in Figure 1.2.

Whether the system of Figure 3.1 may be described as ‘motional feedback’ also seems to be a matter of disagreement in literature. Adams (1979) firmly asserts “[this system] can rightly be considered as ... the use of motional feedback.”¹ The opposite is equally firmly asserted by Ståhl (1981) in his conclusions about a special application of a negative output impedance amplifier, wherein he states:

[The present system] is not a feedback system. In [a motional feedback] system, the output signal from the loudspeaker is sensed and in one way or another fed back to the amplifier. [The present system] instead uses an amplifier with a special output impedance to which the loudspeaker is connected.²

Confusing nomenclature aside, perhaps the most interesting use of the negative output impedance resulting from Figure 3.1 was the ‘*Amplifier Controlled Euphonic Bass*’ (ACE) amplifier described by Ståhl (1981). In addition to using this circuit to ‘cancel’ the effects of the DC-resistance, Ståhl described an amplifier wherein passive components are connected in parallel to the output of the amplifier’s terminals. This system removed the effect of the loudspeaker’s components, allowing the response to be controlled by selection of values of the passive components connected in parallel with the amplifier output. This technique found some commercial success in subwoofers which continues to this day.

Both the negative output-impedance amplifier and the ACE amplifier described above suffer from a tuning problem. Proper operation of both systems requires that the resistor kR_{eb} in the lower left leg of the bridge in Figure 3.1 be tuned to R_{eb} , the blocked electrical resistance of the loudspeaker. This is problematic, because the value of R_{eb} will change with coil temperature, which will change with ambient temperature and with heating due to resistive electrical power dissipation. The change in R_{eb} due to this temperature variation will be on the order of $-30 / + 60\%$. The effect of such changes in R_{eb} on the frequency response of an ACE amplifier-powered loudspeaker was found by Lechevalier (2000) to be between $\pm 2\text{dB}$ to $\pm 10\text{dB}$, dependent upon frequency.³

3.1.3. Feedback processing using vibration measurement

The first publication describing what is more commonly thought of as *motional feedback* appeared in Hanna (1927), wherein a secondary coil on a traditional loudspeaker served as an electrodynamic velocity sensor, the output of which was fed back into the input of an amplifier. An example of an electrodynamic loudspeaker with a suitable additional sensing coil is shown in Figure 3.2. The same

¹ p. 68, paragraph 5 of Adams (1979).

² p. 595, paragraph 3 of Ståhl (1981); it should be noted that Ståhl fails to point out that the negative impedance amplifier used in his system is equivalent to the ‘bridge-type MFB’ system Ståhl discusses subsequently on same page of his 1981 paper, in paragraph 5.

³ Figure 68, p. 60 of Lechevalier (2000).

system was described by Olson (1947),¹ Tanner (1951), and reviewed in a general discussion on motional feedback by Klaassen and de Koning (1968).

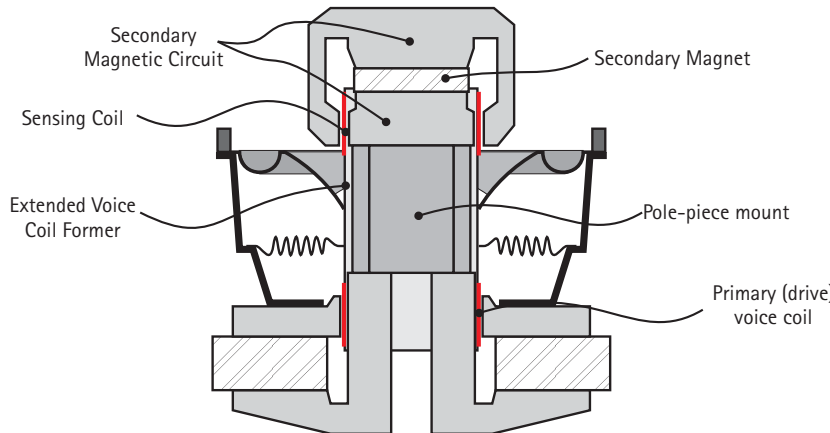


Figure 3.2: Example of an electrodynamic loudspeaker with a secondary magnet system and coil serving as an electrodynamic velocity sensor.

The obvious disadvantage of the system shown in Figure 3.2 is that it requires a secondary magnetic system, which will increase the cost and weight of the loudspeaker. A less expensive strategy is to add a secondary winding to the primary coil. This principle was first discussed in an application for microphones by de Boer and Schenkel (1948). This method has the problem that there will be transformer-coupling between the drive and sensor coils, as noted by Tanner (1951). This problem can be compensated for by additional coils, or electronically by an analogous model using active analogue electronics as was done by Mills and Hawksford (1989).

The first motional feedback system using the signal from an inertial accelerometer was described by Klaassen and de Koning (1968). These authors describe a system using an accelerometer mounted upon the dust cap (part 2b in Figure 2.2.) A distinct advantage of acceleration feedback is that, if the loudspeaker is mounted in a closed box, the shape of the frequency response of the acoustic pressure will be the same as the acceleration response. Thus the acceleration signal permits a more direct implementation of the closed-loop feedback system of Figure 1.2 than the velocity feedback systems. Unfortunately, due to the high cost of suitable accelerometers, commercial success of this technique has been limited, and now appears only in domestic ‘sub-woofers’ from a one manufacturer (Hall, 1989).

Other combinations of current, velocity, and acceleration feedback have been described in various papers. Greiner and Simms (1984) describe one such system, wherein a current and accelerometer are used to provide a fairly flat frequency response system, with moderate distortion reduction over the same unit driven by a constant-voltage output amplifier. Catrysse (1985) described a feedback system using a combination of current and velocity feedback, though in this case the velocity signal was obtained by differentiating a displacement signal obtained by a capacitive sensor. These systems have not received further interest since the publication of these papers, presumably due to the excess cost of the feedback sensors.

¹ pp. 158-159 of Olson (1947); also appears in the more widely available *Acoustical Engineering*, Olson (1957), pp. 168-169.

3.2. Feedforward controllers

3.2.1. Linear feedforward processing

Linear feedforward processing for loudspeakers has been in use for many years. Equalisation, by digital, and by passive and active analogue filters has been written on at length in literature, and widely successfully commercialised. Perhaps the most widespread application of linear feedforward equalisation of loudspeakers is the use of sixth-order vented box alignments described by Thiele (1961), among other authors.

Analogue passive and/or active components can be used to extend the low-frequency range of a loudspeaker, forming one of the simplest ‘feedforward processors’ for a loudspeaker. An informative review of these systems is given by von Recklinghausen (1985). Active analogue filters for equalising the low-frequency response of a loudspeaker has been shown as a simple method to control the overall-Q value and cut-off frequency of a loudspeaker mounted in a closed box (Leach, 1990). (This type of linear feedforward processing is studied further in Chapter 5.)

Frequency equalisation of the far-field response of a loudspeaker is a more sophisticated application of linear feedforward processing. The tactic has generally been to process the audio signal before sent to the loudspeaker with some filter having a response approximating the inverse of a measured response of the loudspeaker. Some research has focused on only low-frequency equalisation (Greenfield and Hawksford, 1991). Other research has been made on filter design for full-frequency equalisation (Karjalainen et al., 1999.) More research still has considered equalisation of the complete loudspeaker-room system (Kirkeby and Nelson, 1999.) Unfortunately, these latter projects and others similar to them apparently did not fully comprehend a statement in Greenfield and Hawksford’s 1991 paper, explaining:

The on axis measurement appears to be an obvious choice [for the response to be inverted]. But bearing in mind the requirement for [equalisation] over a listening space, the value of correcting small aberrations that occur in the on-axis response and do not occur [in] the off-axis response seems suspect. Indeed, this form of [equalisation] may prove detrimental to off-axis responses.

As mentioned in the introduction, the sound field produced by the loudspeaker will vary with different positions from the loudspeaker. For this and other reasons, detailed correction of the far-field response of a loudspeaker is not considered in this thesis.

3.2.2. Nonlinear feedforward processing

Perhaps the first discussion on feedforward compensation of loudspeaker nonlinearity appears in a paper by MacDonald (1959). This paper discusses how to compensate for simple distortion mechanisms such as squarers or cubers via pre- or post-distortion. Although the suggested application is for a loudspeaker, the paper does not consider specifics of applying this method to the loudspeaker, wherein the squarers and cubers would need to be made frequency dependent. The next step in such feedforward distortion compensation was not taken until over three decades later by Birt (1991), wherein nonuniformity of the transduction coefficient was compensated via a look-up table. The diaphragm displacement was measured by a capacitive sensor of the same type used by Catrysse (1985), described above. These methods for feedforward distortion compensation did not spur much commercial nor academic interest. This is presumably due to the complexity of the hardware, or processing, or both.

More recently, feedforward nonlinear processors for loudspeakers have been developed using the theory of feedback linearisation. Although, by its name, feedback linearisation was conceived as a method for designing feedback controllers, several successful adaptations have led to pure feedforward controllers. The theory of feedback linearisation and its application to loudspeakers is discussed in detail in the next section.

3.3. Feedback linearisation

Feedback linearisation, also called the *Differential Geometric Method for Nonlinear Control*, is a general, abstract, complete formal theory for the control of nonlinear dynamic systems. Although the word ‘feedback’ forms part of its name, it is not a pure closed-loop control system in the classical sense of a feedback servo controller. The method uses elements of feedforward control, in that it utilises a complete model of the system’s dynamics, and feedback control, as it uses a measurement (‘feedback’) of the system’s state. Together, these provide linear and nonlinear control of the plant’s dynamics.

Feedback linearisation was developed in the late 1980’s in the field of Automatic Control. Presentations of this theory have been published in textbooks by Isidori (1989), Nijmeijer and Schaft (1990), Slotine (1991), and Vidyasagar (1993). A concise review of the theory was presented in the introduction to a Ph.D. thesis by Vesterholm (1995). The presentation by Nijmeijer and Schaft is by far the most rigorous and pedantic, and thus unlikely to be understood by those without a thorough background in both control theory and differential geometry.

It is not clear who first applied feedback linearisation to loudspeakers. Beerling et al. (1994) cite a reference for application of feedback linearisation to a loudspeaker dated April 1992 (Suykens et al., 1992), wherein an inverse dynamics processor uses feedback signals from a model of the loudspeaker (observer model) to create a feed-forward distortion compensation processor. However, this reference gives no bibliographical information other than ‘*Leuven*.’ It is inferred by your author that this is an internal publication of Katholieke Universiteit Leuven, in Belgium, though this is not certain. Five months later in September of that year, Wolfgang Klippel published a now well-known paper describing a ‘Mirror Filter’ (Klippel, 1992). Klippel’s mirror filter operates in the same manner as the inverse-dynamic processor, with the exception that the loudspeaker’s behaviour is not modelled with a distinct observer model. Instead, the loudspeaker’s dynamics are simulated by direct processing of the audio input signal, leading to a controller which is overall more simple than that using an observer model (as in Berling et al.). Appropriately, the terms ‘inverse dynamics processor’ and ‘mirror filter’ can generally be understood to describe the same thing. Klippel did not, however, make reference to feedback linearisation theory, though this is not surprising, as at that time it was quite unknown in the audio and acoustics community wherein most studies on loudspeakers were made. All of this led to the similarity between the mirror filter and inverse dynamics processor to be missed, the clearest example of which appears in a paper by Schurer et al. (1998), a comparison study that considered the mirror filter to be in an entirely different category from methods based on feedback linearisation. It was finally recognised by Klippel (Nov., 1998) that the mirror filter is simply a feed-forward case of the integrator-decoupled form of feedback linearisation, wherein the system states are determined by processing of the input to the compensator, instead of by an observer model processing the output of the compensator. This difference is discussed in detail in §§3.3.4 and 3.3.5.

Feedback linearisation is based on a state-space description of the dynamics of the plant-to-be-controlled, which in this case is the loudspeaker. State-space descriptions are significantly different from the classical descriptions of loudspeaker dynamics. Thus the state-space representation and its role in DSP-based distortion compensation are first reviewed.

3.3.1. Feedback linearisation of continuous-time systems

Consider a general class of systems that may be described by this first-order differential equation:

$$\begin{aligned}\dot{\mathbf{x}}(t) &= \mathbf{f}(\mathbf{x}(t)) + \mathbf{g}(\mathbf{x}(t))u(t) \\ y(t) &= \mathbf{h}(\mathbf{x}(t))\end{aligned}\tag{3.1}$$

The system feedback function \mathbf{f} , the input function \mathbf{g} , and the output function \mathbf{h} are all considered to be nonlinear functions of the state vector $\mathbf{x}(t)$. A block diagram of such a system is shown in Figure 3.3.

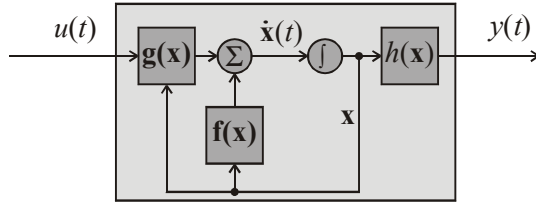


Figure 3.3: State-space representation of a nonlinear system.

The basic goal of linearisation is to create a linear relationship between some input signal and the output $y(t)$ in (3.1). In the formal theory of *Feedback Linearisation*, this is done by applying a *coordinate transformation* to the state vector $\mathbf{x}(t)$. The idea is to find a different state vector such that the operators \mathbf{f} , \mathbf{g} , and \mathbf{h} are not nonlinear. The formal theory of coordinate transformation of the state vector is not likely to be familiar to the audio, signal processing, or loudspeaker engineer. As it is not necessary for comprehension of how feedback linearisation is used for loudspeaker distortion compensation, it is thus not explained nor used in this thesis.

The essential feature of feedback linearisation is that by taking sufficient numbers of the total time derivative of the output $y(t)$, given certain conditions, one will eventually arrive at an expression that depends explicitly on the input. Such an expression can be inverted by simple algebraic manipulation. This inverted expression may then be used as a ‘control law,’ i.e. the basis for a controller (compensator), which will cancel-out (compensate) the nonlinearity in the system. As per §2.3 of Vesterholm (1995), the total time derivative of the output $y(t)$ of the system described by (3.1) may be represented as

$$\begin{aligned}\dot{y}(t) &= \frac{\partial \mathbf{h}(\mathbf{x}(t))}{\partial \mathbf{x}(t)} \dot{\mathbf{x}}(t) \\ &= \frac{\partial \mathbf{h}(\mathbf{x}(t))}{\partial \mathbf{x}(t)} (\mathbf{f}(\mathbf{x}(t)) + \mathbf{g}(\mathbf{x}(t))u(t))\end{aligned}\tag{3.2}$$

According to the theory of differential geometry, (3.2) may be re-written as the *Lie derivative* of $\mathbf{h}(\mathbf{x}(t))$ along the vector fields $\mathbf{f}(\mathbf{x}(t))$ and $\mathbf{g}(\mathbf{x}(t))$, using the notation

$$\dot{y}(t) = L_{\mathbf{f}} \mathbf{h}(\mathbf{x}(t)) + L_{\mathbf{g}} \mathbf{h}(\mathbf{x}(t))u(t)\tag{3.3}$$

The Lie derivatives are calculated from the dot-product (inner-, or scalar-product) between the vectors $\partial \mathbf{h}(\mathbf{x}(t))/\partial \mathbf{x}(t)$ and $\mathbf{f}(\mathbf{x}(t))$ and $\mathbf{g}(\mathbf{x}(t))$, i.e.

$$\begin{aligned}L_{\mathbf{f}} \mathbf{h}(\mathbf{x}(t)) &= \frac{\partial \mathbf{h}(\mathbf{x}(t))}{\partial \mathbf{x}(t)} \cdot \mathbf{f}(\mathbf{x}(t)) \\ L_{\mathbf{g}} \mathbf{h}(\mathbf{x}(t)) &= \frac{\partial \mathbf{h}(\mathbf{x}(t))}{\partial \mathbf{x}(t)} \cdot \mathbf{g}(\mathbf{x}(t))\end{aligned}\tag{3.4}$$

If $L_{\mathbf{g}} \mathbf{h}(\mathbf{x}(t)) \neq 0$, then the form of (3.3) will provide an explicit formula for the output $y(t)$ in terms of the input $u(t)$. If, instead, $L_{\mathbf{g}} \mathbf{h}(\mathbf{x}(t)) = 0$, then it will be necessary to take a higher-order time derivative of the output in order to obtain an explicit formula. Assuming this is so, the second derivative of the output is taken and represented as:

$$\ddot{y}(t) = L_{\mathbf{f}}^{(2)} \mathbf{h}(\mathbf{x}(t)) + L_{\mathbf{g}} L_{\mathbf{f}} \mathbf{h}(\mathbf{x}(t))u(t)\tag{3.5}$$

If the term $L_g L_f \mathbf{h}(\mathbf{x}(t))$ is zero, then it will again be necessary to obtain a still higher-order time derivative. Given certain conditions, one will eventually find a derivative of the output for which the term in which the input $u(t)$ appears will not be zero. By defining the order of the derivative at which this occurs as r , it may be said that the system concerned has a relative degree of r . The r^{th} -derivative of the output may be expressed as

$$y^{(r)}(t) = L_f^{(r)}(\mathbf{x}(t)) + L_g L_f^{(r-1)} \mathbf{h}(\mathbf{x}(t)) u(t) \quad (3.6)$$

As (3.6) *does* depend directly in the input $u(t)$, it can be used to form the basis of a nonlinear controller, or compensator. This controller will process the signal $v(t)$ according to the inverse of (3.6), and feed this to the input to the plant. Thus the output of the controller (fed to the input to the plant) is processed as so:

$$u(t) = \frac{v(t) - L_f^{(r)} \mathbf{h}(\mathbf{x}(t))}{L_g L_f^{(r-1)} \mathbf{h}(\mathbf{x}(t))} \quad (3.7)$$

the effect will be to create a linear relationship between the input $v(t)$ and the output $y(t)$ as so

$$y^{(r)}(t) = v(t) \quad \xrightarrow{L_f^{(r)}} \quad \frac{y(s)}{v(s)} = \frac{1}{s^r} \quad (3.8)$$

where r is the relative degree of the system, defined above.

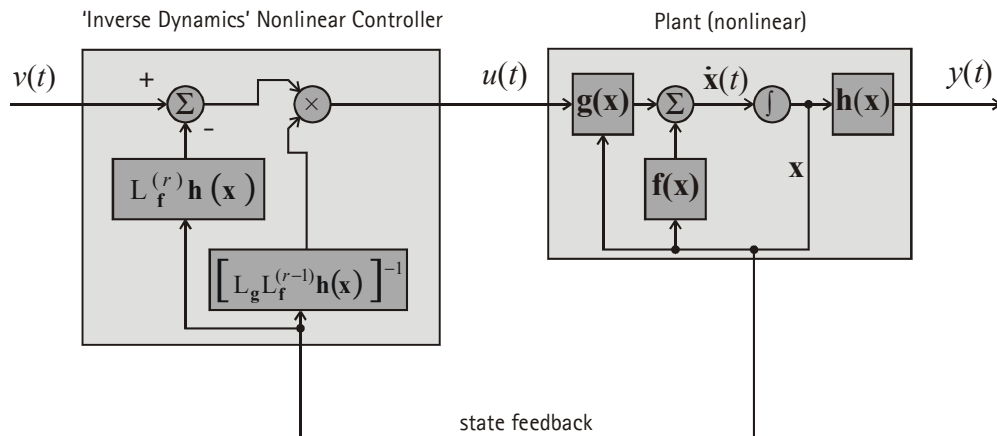


Figure 3.4: Block diagram of feedback linearisation control system.

The relationship in (3.8), between the system input and the output created by the inverse-dynamic controller, may not be desirable. The small-signal behaviour of the system, i.e. that which can be described by a linear model, may, in fact, be the desired input-output relationship. (This is particularly the case for the loudspeaker, as will be discussed below.) When this is the case, it is necessary to 're-introduce' the linear dynamics, by pre-filtering the signal $v(t)$.

It is assumed that for small-signals, nonlinearity in the plant may be neglected, and its input-output may be described by a linear transfer function as so:

$$H_{ld}(s) = \frac{y(s)}{u(s)} \quad (3.9)$$

The linear dynamics may be ‘re-introduced’ by pre-filtering the input to the inverse-dynamics controller $v(t)$ by a linear filter with the frequency response of the linear dynamics of the system, i.e. $H_{ld}(s)$ in (3.9). This is shown in block form in Figure 3.5. Note that with the linear dynamics ‘re-introduced’ in this way, the input to the controller is defined as $w(t)$, instead of $v(t)$.

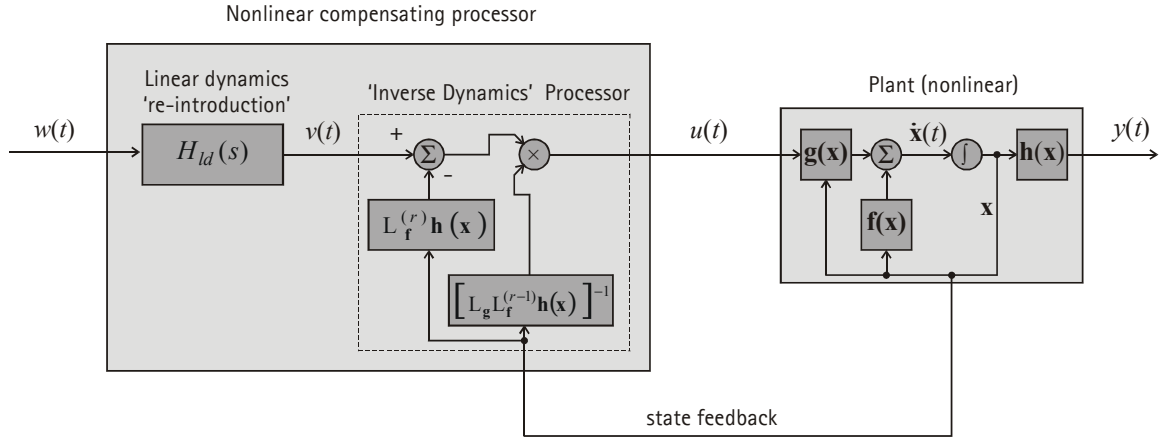


Figure 3.5: Feedback linearisation control system, with re-introduction of linear dynamics, providing compensation only of nonlinear dynamics.

3.3.2. Example: simplified closed box loudspeaker in continuous-time

We consider the state-space representation of the loudspeaker’s dynamics where the input $u(t)$ is defined as the voltage-drop across the loudspeaker’s terminals:

$$\begin{aligned}\dot{\mathbf{x}}(t) &= \mathbf{f}(\mathbf{x}(t)) + \mathbf{g}(\mathbf{x}(t))u(t) \\ y(t) &= \mathbf{h}(\mathbf{x}(t))\end{aligned}\tag{3.10}$$

As discussed above, the formal theory of feedback linearisation was first applied to a loudspeaker by Suykens et al. (1995,) in the paper mentioned in the introduction to this chapter. In Suykens’ 1995 paper, the details of applying the theory were worked out for a loudspeaker excluding any effects of acoustic loading. This was extended to the case of a loudspeaker in a vented cabinet (a single acoustic resonator) by Schurer (1997.) In the present example, we consider the case of a loudspeaker with simple acoustic loading, and with negligible electrical inductance. With these considerations, the system, input, and output vector fields are as follows:

$$\begin{aligned}\mathbf{f}(\mathbf{x}(t)) &= \begin{bmatrix} x_2(t) \\ -\frac{k_t(x_1(t))}{m_t}x_1 - \frac{1}{m_t}\left(c_t + \frac{\phi^2(x_1(t))}{R_{eb}}\right)x_2(t) \end{bmatrix} \\ \mathbf{g}(\mathbf{x}(t)) &= \begin{bmatrix} 0 \\ \frac{\phi(x_1(t))}{m_t R_{eb}} \end{bmatrix} \\ \mathbf{h}(\mathbf{x}(t)) &= \begin{bmatrix} x_1(t) \\ 0 \end{bmatrix}\end{aligned}\tag{3.11}$$

where the state vector $\mathbf{x}(t)$ is defined on \Re^2 as so

$$\mathbf{x}(t) = \begin{bmatrix} x_1(t) \\ x_2(t) \end{bmatrix} = \begin{bmatrix} x_d(t) \\ u_d(t) \end{bmatrix} = \begin{bmatrix} x_d(t) \\ \dot{x}_d(t) \end{bmatrix} \quad (3.12)$$

Other terms in (3.11) and (3.12) are as defined previously in §§2.1-2.2. Note that output $y(t)$ is defined as the diaphragm displacement $x_d(t)$. The diaphragm displacement is a suitable output, from the perspective of developing a feedback linearisation algorithm. However, from the perspective of evaluating the electro-acoustic performance of the loudspeaker, it is more interesting to analyse the acoustic pressure. The relationship between displacement and acoustic pressure is well-studied; see Small (1971).

The control law for a nonlinear compensator for the loudspeaker described by (3.10)-(3.12) is developed using the method described above to obtain an expression for the output $y(t)$ which depends explicitly on the input, which in this case is $u(t)$. The first time derivative of the output is given by

$$\begin{aligned} \dot{y}(t) &= L_f \mathbf{h}(\mathbf{x}(t)) + L_g \mathbf{h}(\mathbf{x}(t)) u(t) \\ &= [1 \ 0] \cdot \mathbf{f}(\mathbf{x}(t)) + [1 \ 0] \cdot \mathbf{g}(\mathbf{x}(t)) u(t) \\ &= x_2(t) \end{aligned} \quad (3.13)$$

The input $u(t)$ does not appear in the RHS of this expression. Thus it is necessary to take the next higher-order derivative of the output $y(t)$ with respect to time:

$$\begin{aligned} \ddot{y}(t) &= \frac{\partial \dot{y}(t)}{\partial \mathbf{x}(t)} \mathbf{f}(\mathbf{x}(t)) + \frac{\partial \dot{y}(t)}{\partial \mathbf{x}(t)} \mathbf{g}(\mathbf{x}(t)) u(t) \\ &= [0 \ 1] \mathbf{f}(\mathbf{x}(t)) + [0 \ 1] \mathbf{g}(\mathbf{x}(t)) u(t) \\ &= -\frac{k_t(x_1(t))}{m_t} x_1(t) - \frac{1}{m_t} \left(c_t + \frac{\phi^2(x_1(t))}{R_{eb}} \right) x_2(t) + u(t) \frac{\phi(x_1(t))}{m_t R_{eb}} \end{aligned} \quad (3.14)$$

As this expression *does* depend directly on the input $u(t)$ it can be used to derive a control law for linearisation (compensation of nonlinearity.) The control law for linearisation is simply the inverse of the relationship between $u(t)$ and $\ddot{y}(t)$ in (3.14). From the practical standpoint of implementing a controller with some input signal, we consider the input to this controller as $v(t)$. The controller operates on the input $v(t)$ according to:

$$u(t) = \frac{R_{eb}}{\phi(x_1(t))} \left[k_t(x_1(t)) x_1(t) + \left(c_t + \frac{\phi^2(x_1(t))}{R_{eb}} \right) x_2(t) + m_t v(t) \right] \quad (3.15)$$

The ‘control law’ for the controller, given in (3.15), creates the following relationship between $v(t)$ and $x_d(t)$:

$$\ddot{x}_d(t) = v(t) \quad \stackrel{L}{\Rightarrow} \quad \frac{x_d(s)}{v(s)} = \frac{1}{s^2} \quad (3.16)$$

Notice that (3.16) is equivalent to saying that the diaphragm acceleration will have a unity transfer function with respect to the input signal $v(t)$. Although this does have the advantage of eliminating nonlinear behaviour of the loudspeaker, it is not the desired *linear* input-output frequency response. At low frequencies, this response would generate very large displacement, thereby generating very large nonlinearities - beyond that which could be realistically controlled.

For a loudspeaker mounted in a closed-box, the desired linear acceleration frequency response is, as discussed in §2.1.7, a second-order high-pass filter. This desired response may be restored in the controller by pre-filtering the input to the nonlinear control law $v(t)$ by an appropriate low-pass filter. By defining the input to this filter as $w(t)$, such a filter should have the following transfer function:

$$\begin{aligned}
 H_{ld}(s) &= \frac{v(s)}{w(s)} \\
 &= \frac{1}{s^2/\omega_0^2 + s/\omega_0 Q_{tc} + 1}
 \end{aligned} \tag{3.17}$$

This filter ‘pre-emphasises’ $v(t)$, the input to the inverse dynamics processor. Given that the inverse dynamics processor eliminates all behaviour of the plant, i.e. both linear and nonlinear dynamics, the pre-emphasis the filter of (3.17) represents a re-introduction of the linear dynamics of the plant.

3.3.3. State observer and partial state measurement

The controller developed using the theory of feedback linearisation described in §3.3.1 above suffers from the same problem as traditional feedback processors described in §3.1 above. Namely, the controller developed according to feedback linearisation requires measurement of the state vector $\mathbf{x}(t)$. In the example of feedback linearisation applied to the loudspeaker mounted in a closed box described above, the state vector comprises the diaphragm displacement $x_d(t)$ and velocity $u_d(t)$. As per the discussion on traditional feedback systems, directly measuring the displacement and velocity is either impractical or expensive, or both.

One solution to this problem is to make a partial state measurement, i.e. to measure one state, and simulate the other states using a *state observer*. One example of how this can be done was presented by Beerling et al. (1994). In the system presented by Beerling et al., an inertial accelerometer is placed on the loudspeaker diaphragm. The state observer integrates and double integrates this signal from the accelerometer, and also calculates the voice-coil current $i_c(t)$ (needed in that case for compensation of nonlinearity caused by L_{eb} nonuniformity). The distinct disadvantage of this approach, for the microspeaker, is that no suitably inexpensive and lightweight accelerometer is available.

Another possibility would be to measure the voice-coil current, as per the arrangement shown in Figure 3.6. In this case, a state observer would simulate the state vector with an appropriate model of the loudspeaker. As it happens, there is problem rendering impractical any such approach wherein a state observer predicts the state vector from a measured signal.

There is a time-delay inherent to all sigma-delta A/D and D/A converters. Sigma-delta converters are used in all modern digital audio systems, due to their low cost relative to their frequency-resolution product. These converters use linear-phase interpolation and decimation filters for converting the high-frequency one-bit stream to the audio bandwidth full resolution (typically 16 bit) data stream. Such filters create a delay of some 20 or so samples (Zölzer, 1994), the exact number depending on the design of the interpolation filter. Thus the delay in the complete ‘round-trip’ caused by D/A and A/D conversion would be some 40 samples. This would make the state predicted by the state observer of Figure 3.6 some 40 samples ‘late’ for the input signal $v(t)$. For audio systems, this effect limits the bandwidth of this type of controller such that it is impractical.

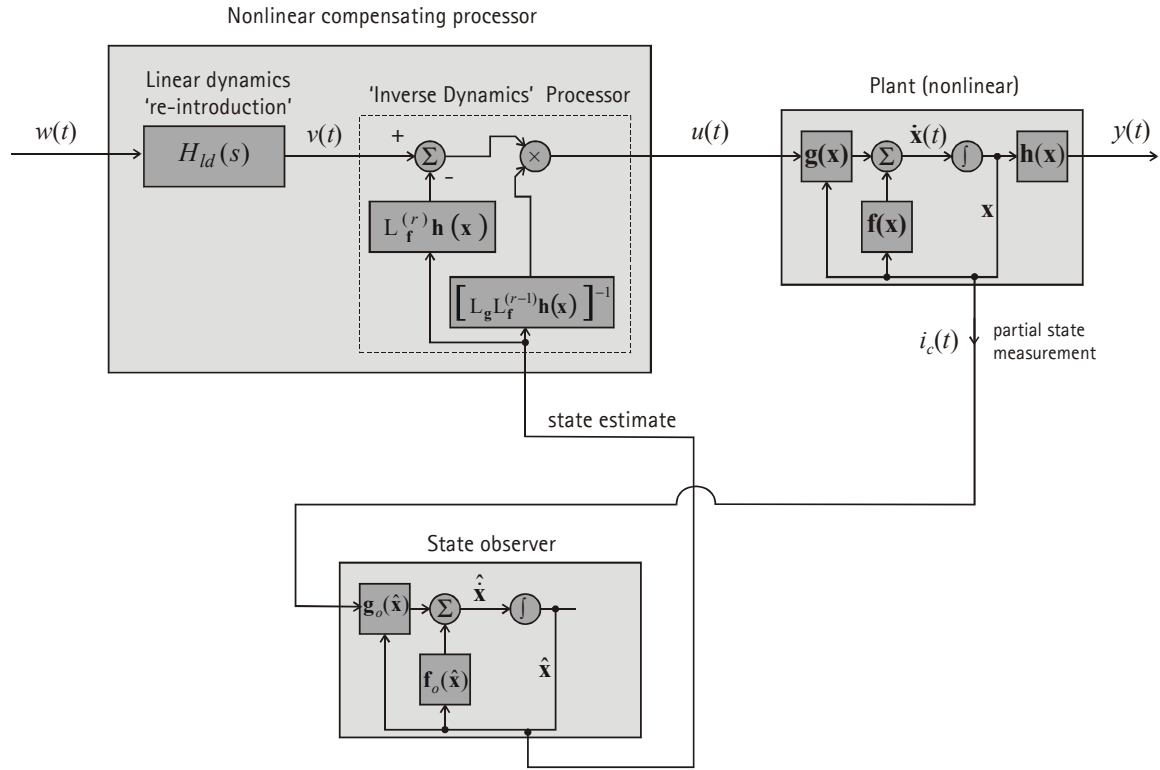


Figure 3.6: State vector estimation based on partial state measurement, e.g. $i_c(t)$, and a state observer.

3.3.4. Feedforward formulation using a ‘simulation’ state observer

A feedback linearisation-based controller presented by Schurer et al. (1997) employed a state observer which made no measurement on the plant whatsoever. In this system described by Schurer et al., the input to the state observer was the *output* from the controller $u(t)$, as per Figure 3.7. This is theoretically possible, as the to the system $v_c(t)$ – and with an appropriate and accurate model of the system, the state vector can be predicted from the output of the controller $u(t)$. In this case, the feedback linearisation controller uses no signal from the actual plant. This results in a controller of the pure (non-adaptive) feedforward type, as per Figure 1.3.

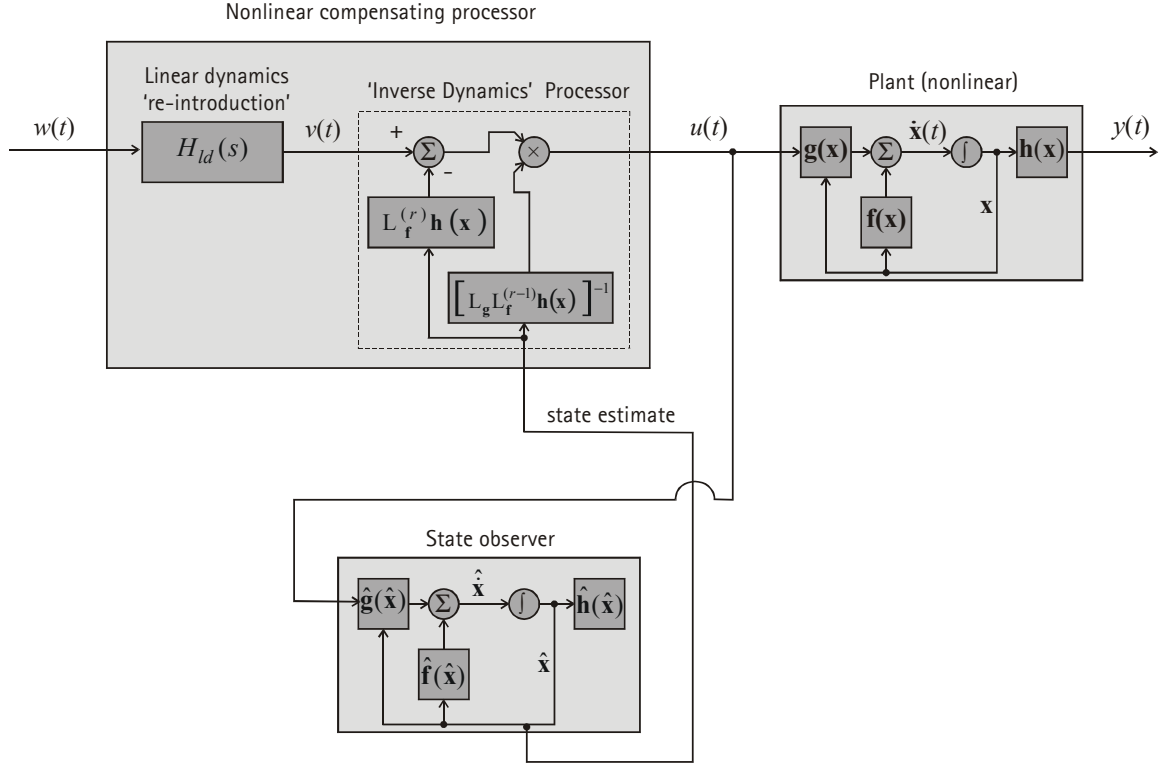


Figure 3.7: State observer used to determine \hat{x} , an estimate of the system's state vector.

Schurer implemented the complete controller with digital processing. The digital processor, operating in discrete time, cannot directly implement a model of the loudspeaker which is expressed in continuous time with differential operations.¹ Schurer's solution to this problem was to form his model of the loudspeaker in the state-space first-order differential equation of (3.2), and solve this equation by numerical integration. In this way, the new value of the state vector is predicted from the existing value of the state vector and its derivative as so

$$\mathbf{x}[n] = \sum_{j=1}^N \alpha_j \mathbf{x}[n-j] + \sum_{j=1}^M \beta_j \dot{\mathbf{x}}[n-j] \quad (3.18)$$

where α_j and β_j are coefficients defined by numerical integration rules .

One disadvantage to this approach is that, due to the feedback loop created between $u(t)$, the estimated state $\hat{\mathbf{x}}[n]$, and the use of this estimated state in the inverse dynamics processor, it can become unstable.

3.3.5. Feedforward formulation assuming ideal alignment

According to the theory of feedback linearisation, if the parameters of the inverse dynamics processor of Figure 3.4 are tuned to the actual plant with reasonable accuracy, the state vector can be simulated from the input to the nonlinear controller $v(t)$ in a more simple manner than using the state observer described in §3.3.4. This is a result of (3.8), stating that, if the Inverse Dynamics processor is accurately tuned to the plant, the r^{th} derivative of the output will be given by the input to the nonlinear controller, $v(t)$.

¹ This problem was discussed at a general level in §2.3, and is the motivation for developing the discrete-time models of the loudspeaker developed in that section.

The simplification provided by this method is easily demonstrated for the case of the closed-box loudspeaker, ignoring L_{eb} , described in §3.3.2. According to (3.16), the first system state $x_1(t) = x(t)$ will have its second time derivative directly equal to the modified control input $v(t)$. Therefore, assuming the feedback linearisation law in (3.15) operates properly, the system states can be determined by integration of the input to the Inverse Dynamics controller, $v(t)$.

As mentioned above, integration cannot be performed directly in a digital implementation. It is necessary to perform a numerical approximation to the integration. The system states are, therefore, approximated as so:

$$x_1[n] = \sum_{j=1}^N \alpha_j x_1[n-j] + \sum_{j=1}^M \beta_j x_2[n-j] \quad (3.19)$$

$$x_2[n] = \sum_{j=1}^N \alpha_j x_2[n-j] + \sum_{j=1}^M \beta_j v[n-j]. \quad (3.20)$$

A block diagram of the controller wherein the states are computed as above is shown in Figure 3.8.

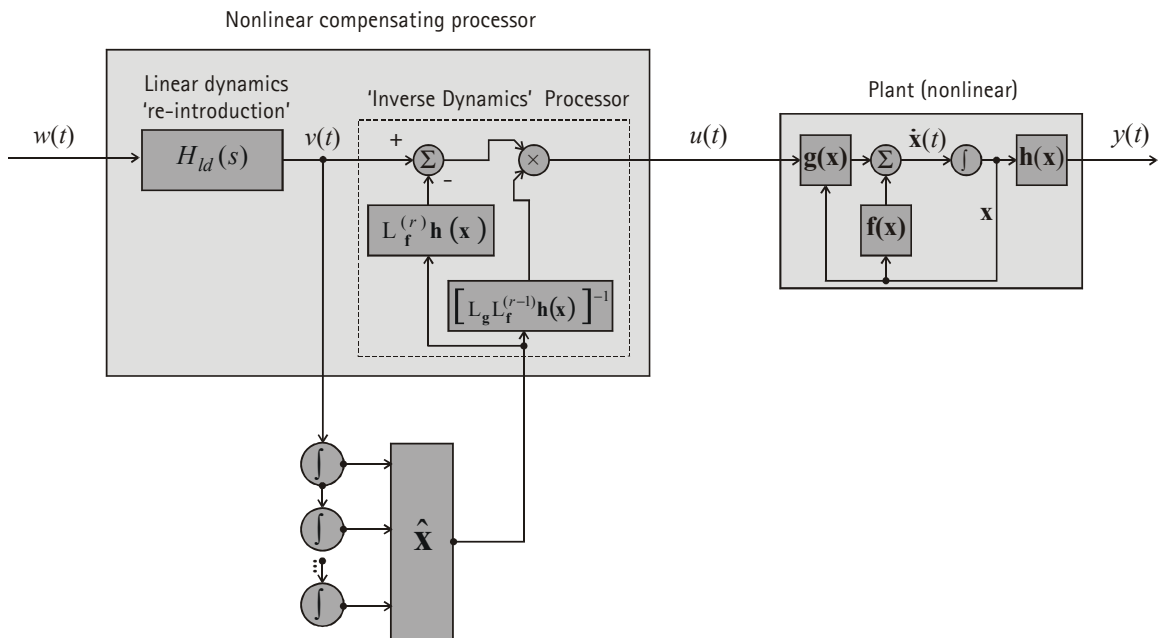


Figure 3.8: State calculation by direct integration of input to nonlinear controller.

Note that if L_{eb} is to be considered in the loudspeaker, the state vector will include the voice-coil-current $i_c(t)$. The voice-coil current cannot be determined from the input to the nonlinear controller $v(t)$ by simple integration. Instead, it is necessary to predict the current using the linear voltage equation of (2.1), as explained by Klippel (1992). Given that the state vector will invariably include the diaphragm velocity $u_d(t)$, that the voice-coil voltage will also generally be known, and that there are no memory-dependent terms in (2.1), calculating the current in this way is quite simple and straightforward – considerably more simple than using the state observer described in §3.3.4 above.

3.3.6. Feedback linearisation of discrete-time systems

A formulation of feedback linearisation also exists for discrete-time systems. Using this discrete-time formulation is attractive because it is more practical to implement the compensator with a digital processor. As explained above, previous applications of feedback linearisation to the loudspeaker have used continuous-time formulations, and then used discretisations of certain parts in order to implement the controller in a digital processor.

Using the discrete-time model of the loudspeaker developed in §2.3.4 above, it has been found that the discrete-time formulation of feedback linearisation can be directly applied to a controller for compensation of loudspeaker nonlinearity.

For the application of discrete-time feedback linearisation, it is necessary to consider the system in the following state-space form

$$\begin{aligned} \mathbf{x}[n+1] &= \mathbf{f}(\mathbf{x}[n]) + \mathbf{g}(\mathbf{x}[n])u[n] \\ y[n] &= \mathbf{h}(\mathbf{x}[n]) \end{aligned} \quad (3.21)$$

where all these terms have the same meaning as for the continuous-time form of (3.1) above.

Application of feedback linearisation to the system of (3.21) by considering the system output at time interval $n+1$:

$$\begin{aligned} y[n+1] &= \mathbf{h}(\mathbf{x}[n+1]) \\ &= \mathbf{h}(\mathbf{f}(\mathbf{x}[n]) + \mathbf{g}(\mathbf{x}[n])u[n]) \end{aligned} \quad (3.22)$$

If the derivative of the RHS of this with respect to the input $u[n]$ is not zero, i.e. if

$$\frac{\partial y[n+1]}{\partial u[n]} \neq 0 \quad (3.23)$$

then an input-output link is established, and the output can be solved in terms of the input. If this derivative is zero, then it will be necessary to take the next output sample, as so

$$\begin{aligned} y[n+2] &= \mathbf{h}(\mathbf{f}(\mathbf{x}[n+1]) + \mathbf{g}(\mathbf{x}[n+1])u[n+1]) \\ &= \mathbf{h}(\mathbf{f}(\mathbf{h}(\mathbf{f}(\mathbf{x}[n]) + \mathbf{g}(\mathbf{x}[n])u[n])) + \mathbf{g}(\mathbf{h}(\mathbf{f}(\mathbf{x}[n]) + \mathbf{g}(\mathbf{x}[n])u[n]))u[n+1]) \\ &= \mathbf{h} \circ (\mathbf{f}, \mathbf{g}u[n+1]) \circ (\mathbf{f}, \mathbf{g}u[n]) \end{aligned} \quad (3.24)$$

where \circ denotes ‘composition’. If the derivative of the RHS with respect to the input is again zero, it will be necessary to take again a higher-order composition. This procedure is repeated until one finds the derivative of the r^{th} composition with respect to the input to not be zero, represented as

$$y[n+r] = \mathbf{h}^r \circ (\mathbf{f}, \mathbf{g}u[n]) \quad (3.25)$$

There is not a general expression for the inverse of this expression for $u[n]$ as there is for the continuous-time case in (3.7). The form of the solution will depend on the specific nature of the system, input, and output vector fields, \mathbf{f} , \mathbf{g} , and \mathbf{h} , respectively.

In the next section, this discrete-time formulation of feedback linearisation is applied to the discrete-time model of a loudspeaker, developed in §2.3.4 above, to provide a simple algorithm for compensation of nonlinear distortion in a loudspeaker.

3.3.7. Feedback linearisation with a discrete-time loudspeaker model

This section presents a new discrete-time implementation of feedback linearisation for compensation of nonlinear distortion in a loudspeaker. This is done by applying the discrete-time formulation of feedback linearisation presented above to the discrete-time nonlinear loudspeaker model presented in §2.3.4

The motivation for developing a new algorithm for nonlinear distortion compensation is cost-reduction. In Chapter 5, discussions on the cost of nonlinear distortion compensation assume the only cost of the compensation is the additional amplifier output it requires. An important consequence of this is that the algorithm for performing the compensation must be as simple as existing algorithms running on DSP's in the target product – so as not to increase the cost of the hardware performing the compensation processing. A rough quantification of this limit is that the algorithm should not be more complicated than several second-order IIR filters. This limit precludes the use of more complex distortion-compensation algorithms such as Volterra series methods, Neural Networks, NARMAX models, or other ‘black-box’ methods. To this end, a new, simple, distortion compensation algorithm suitable for DSP implementation has been developed and is presented here. As stated above, simplicity has been maintained by using the nonlinear discrete-time model of the loudspeaker dynamics developed in §2.3.4, and applying the discrete-time formulation of feedback linearisation.

This is an alternative to previous digital implementations of feedback linearisation for compensation of nonlinear distortion. As discussed in §3.3.4, Schurer (1997) used numerical integration to simulate a continuous-time model of the loudspeaker. The method presented here, using a discrete-time model of the loudspeaker, avoids the need for this simulation.

Consider the displacement output from the voice-coil voltage by the nonlinear discrete-time model of (2.85),

$$x_d[n+1] = \sigma_x \left\{ \phi(x_d[n]) \left(\frac{1}{R_{eb}} \{v_c[n] - \phi(x_d[n])u_d[n]\} \right) - k_1(x_d[n])x_d[n] \right\} - a_1x_d[n] - a_2x_d[n-1] \quad (3.26)$$

where all the terms have the same definitions as in chapter 2. As per the theory of feedback linearisation for a discrete-time system one considers the derivative of the output with respect to the input. In (3.26), the output is $x_d[n]$, and the input is $v_c[n]$. It can be seen by inspection of the RHS of (3.26) that its derivative with respect to $x_d[n]$ will depend explicitly on the input $v_c[n]$.

According to the theory of feedback linearisation, the control law is obtained from (3.26) by inverting the relationship defined between $x_d[n]$ and $v_c[n]$. This inverted relationship, obtained by straightforward algebraic manipulation, is as so:

$$v_c[n] = R_{eb} \left(\frac{1}{\phi(x_d[n])} \left\{ \frac{1}{\sigma_x} (x_d[n+1] + a_1x_d[n] + a_2x_d[n-1]) + k_1(x_d[n])x_d[n] \right\} + \phi(x_d[n])u_d[n] \right) \quad (3.27)$$

This equation may be interpreted as specifying the voltage needed to produce a certain displacement. It may be used as a control law for nonlinear compensation, as it calculates the voice-coil voltage needed to achieve a certain displacement, as per the nonlinear loudspeaker model of (3.26). Interpreted in this way, it defines the input-output relationship of a controller, the input to which is the specified displacement $x_d[n]$, and the output from which is the necessary voltage $v_c[n]$ to produce this

displacement. By replacing $x_d[n]$ with $r_p[n]$ and $v_c[n]$ with $r_{lin}[n]$, this nonlinear control law may be defined as

$$r_{lin}[n-1] = \frac{R_{eb}}{\sigma_x \phi(r_d[n-1])} \left(r_p[n] + \left\{ \sigma_x k_1(r_p[n-1]) + a_1 \right\} r_p[n-1] + a_2 r_p[n-2] + \frac{\sigma_x \phi(r_d[n-1])}{R_{eb}} u_{d-e}[n-1] \right) \quad (3.28)$$

where $r_p[n]$ is the input to the nonlinear controller, $r_{lin}[n]$ is the output from the nonlinear controller, and $u_{d-e}[n]$ is an estimate of the diaphragm-coil velocity. The estimate of the diaphragm-coil velocity $u_{d-e}[n]$ is computed by differentiating the input to the nonlinear controller $r_p[n]$ as so:

$$\begin{aligned} u_{d-e}[n] &= h_{dt}[n] * r_p[n] \\ &= b_{dt,0} r_p[n] + b_{dt,1} r_p[n-1] - a_{dt,1} u_{d-e}[n-1] \end{aligned} \quad (3.29)$$

where the coefficients of this differentiation approximation are as discussed in §2.3.4.

An important feature of the nonlinear control law of (3.28) is its simplicity. It effectively consists of a second-order IIR filter, plus the addition of the polynomial evaluations for $\phi(r_d[n])$ and $k_1(r_d[n])$.

The studies presented in Chapter 5 consider that the nonuniformity in the suspension stiffness is negligible. As shown in an example measurement in Figure 2.13, the stiffness nonuniformity is minor.

A necessary addition to the control law of (3.28) is the ‘re-introduction of linear dynamics,’ as per the presentation of feedback linearisation of continuous-time systems presented in §3.3.1. For the case of (3.28), this is done by pre-filtering $r_{lin}[n]$ with a filter having the linear response of the displacement response. This can be done in a straightforward manner, with linear second-order IIR filter.

The effectiveness of a controller using the algorithm in (3.28) is evaluated by measurements presented in §5.2.3, below.

One interesting development in the application of feedback linearisation to loudspeakers came from Klippel (Jun. 1998). This paper showed that filtering for re-introduction of linear dynamics can be combined with the nonlinear control law. Klippel’s work was done for the continuous-time formulation of feedback linearisation. Attempts were made as part of research for this thesis to make the same simplification to this discrete-time formulation of feedback linearisation, but were unsuccessful. This may be a topic for further research.

3.4. Adaptive feedforward controllers

As discussed in the introduction, the general problem of a pure feedforward controller is its sensitivity to model uncertainties. As discussed in §2.4, various characteristics of the loudspeaker change with temperature and ageing. As the actual loudspeaker’s properties drift from those assumed by the feedforward controller, the performance of the feedforward controller will decrease. This sensitivity to model uncertainties was explained by Schurer (1997, p. 7) as the primary disadvantage of feedforward nonlinear compensation systems.

As discussed in the introduction, tuning the parameters used in the model of the loudspeaker used by the feedforward processor can be done by *system identification*.¹ System identification is the process of tuning the input-output characteristics of a model of a dynamic system to that of an actual dynamic system. A feedforward controller using this features is generally referred to as an *adaptive feedforward controller*.

Some literature has appeared on adaptive feedforward control for loudspeakers. Research on *linear* adaptive feedforward control, focusing on loudspeaker-room equalisation, has been published by Elliott and Nelson (1989), Kuriyama and Furukawa (1989), Radcliffe and Gogate (1992), Craven and Gerzon (1992), and Elliott et al. (1994). These methods attempted to achieve equalisation of the complete electroacoustic path, to the point of the listener, typically using high-order adaptive FIR digital filters.

Research on *nonlinear* adaptive feedforward control has also been published. Klippel (Nov. 1998) presented a method for parametric determination of the nonlinear characteristics of a loudspeaker by nonlinear adaptive filtering.

In this thesis, *linear* adaptive control is of primary interest. It is considered that only the linear properties of the loudspeaker are subject to drift.² Although the advantages of nonlinear control are the focus of the thesis, the nonlinear properties to be controlled are considered static – i.e. they can be known *a priori*. This is because they are defined by the geometry of the construction of the loudspeaker; it is assumed that this can be known for a given loudspeaker type.

Additionally, only *parametric*, or ‘grey box’ loudspeaker system identification is considered in this thesis. High-order FIR filters, Volterra filters, NARMAX models, Neural networks and other ‘black-box’ methods are not considered. This is a choice, driven by the need to keep the complete adaptive feedforward controller simple. The need for simplicity is driven by cost.

Restricting loudspeaker system identification to parametric methods precludes using the FIR model presented in §2.3.1, and requires the use of the IIR filter models §§2.3.2 and 2.3.3. The background theory on adaptation of an IIR filter model is presented in the next section (§3.5). Chapter 4 presents details of applying this theory to the loudspeaker, and measurements of its identification performance.

By a remarkable stroke of luck, the five parameters which vary with manufacturing tolerance, temperature, and age, and thus cannot be known *a priori*, can all be determined from the electrical impedance. Although six parameters define the complete lumped parameter model of the loudspeaker, one of these – the diaphragm-coil moving mass m_d – can be known *a priori*, as it will not change throughout the lifetime of the loudspeaker. This permits the feedforward processor to be fully tuned to a loudspeaker by analysis of only the electrical impedance (i.e. without direct vibration measurement). This is significant, as the electrical impedance can be analysed by a simple measurement of the electrical voice-coil current, and does not need vibration measurement which is impractical and expensive.

¹ System identification is a general field in applied electrical, signal processing, control engineering, and basic terms used for discussions on the subject are different in each of these three fields. The discussion used here most closely follows that used in the field of signal processing.

² As per the discussion in §2.4, the parameters known to drift with temperature and other considerations are summarised in Table 2.1.

3.5. System identification by adaptive filtering

As discussed in the introduction, an adaptive feedforward controller as shown in Figure 1.4 uses a plant model to tune the feedforward controller to the plant. The plant model is implemented as an adaptive filter performing system identification on the plant. This adaptive filter calculates a predicted output $y_p[n]$ from the input $u[n]$ using a weighting vector \mathbf{w} , according to a filter function $f(u[n], \mathbf{w})$. The weighting vector \mathbf{w} is tuned to minimise, in a mean-square sense, the error $\epsilon[n]$, calculated as the difference between the measurable plant output $y_m[n]$ and the predicted plant output $y_p[n]$. When the adaptive filter has reduced the error $\epsilon[n]$ below some threshold, it will begin to update the feedforward processor in Figure 1.4 accordingly.

In order to determine variation in those parameters given in Table 2.1, the filter function $f(u[n], \mathbf{w})$ must be designed along the specific dynamics of the plant. This is in contrast to many applications of adaptive filtering, wherein the plant is treated as a ‘black-box’, the dynamics of which cannot be known, and the purpose of the filter is simply to minimise the mean-square value of $\epsilon[n]$ in absolute terms. It is particularly important that the dynamics of $f(u[n], \mathbf{w})$ be analogous to those of the plant if an indirect output signal is measured such as the voice-coil-current. If in this case the dynamics of $f(u[n], \mathbf{w})$ are different from the plant, the updated weight vector will not be readily usable by the feedforward processor.

The difference between the measured plant output $y_m[n]$ and the predicted plant output provides an error signal $\epsilon[n]$, as shown in Figure 3.9. The parameter vector \mathbf{w} is determined by minimising the error $\epsilon[n]$ in a mean-square sense. This is the basic arrangement for using an adaptive filter for system identification, as described in standard textbooks by Widrow and Stearns (1985) and Haykin (1996).

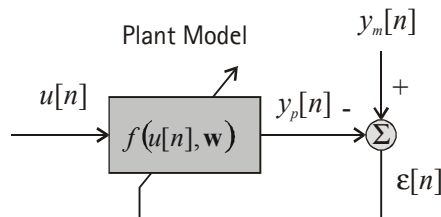


Figure 3.9: Basic arrangement of an adaptive filter performing system identification.

3.5.1. General adaptive algorithms

Several methods exist for tuning the weight vector \mathbf{w} such that it will minimise the error between the filter’s predicted output $y_p[n]$ and the measured output $y_m[n]$. Generally, such an optimally tuned filter is referred to as a Wiener Filter.¹

For audio systems considered in time-domain, the weighting vector is nearly invariably a real-valued vector of length N , i.e.:²

$$\mathbf{w} = [w_1 \quad w_2 \quad \dots \quad w_N] \quad \mathbf{w} \in \Re^N. \quad (3.30)$$

An error surface $\xi(\mathbf{w})$ is defined by the expectation value of the mean-square error, as so:

$$\xi(\mathbf{w}) = E[\epsilon^2[n]] = E[(y_m[n] - y_p[n])^2] = E[(y_m[n] - f(u[n], \mathbf{w}))^2] \quad (3.31)$$

¹ The name ‘Wiener Filter’ comes from a definition for an optimally tuned continuous-time filter, published by Wiener and Hopf (1931).

² The weight vector \mathbf{w} is defined here as a row-vector; in other presentations of adaptive filtering, it is typically defined as a column-vector.

This error surface is the expectation value of the error for different values of the weighting vector \mathbf{w} , for a given input signal $u[n]$ and a given measured signal $y_m[n]$. The purpose of the adaptive filter is to find the values of \mathbf{w} which give the minimum value of $\xi(\mathbf{w})$. This value of \mathbf{w} is called the *optimum value*, noted by \mathbf{w}_{opt} .

For an N^{th} -order linear FIR filter (also transversal, non-recursive, or purely feedforward filter), the filter function $f(u[n], \mathbf{w})$ is the scalar product between a vector \mathbf{u} , a delay-line of the input signal of the same length as \mathbf{w} , and \mathbf{w} as so:

$$f(u[n], \mathbf{w}) = \mathbf{u} \cdot \mathbf{w} = [u[n] \ u[n-1] \ \dots \ u[n-N-1]] \mathbf{w} \quad (3.32)$$

In this case the error surface of Figure 3.9 becomes:

$$\xi(\mathbf{w}) = E[y_m^2[n]] + \mathbf{w} \cdot \mathbf{R} \mathbf{w} - 2\mathbf{p} \cdot \mathbf{w} \quad (3.33)$$

where \mathbf{R} is the input-signal autocorrelation matrix, and \mathbf{p} is the input-signal-to-measured-signal cross-correlation vector.¹ It can be shown that if $y_m[n]$ is described by the signal $u[n]$ by a linear, time-invariant system, then the values of \mathbf{w} which will minimise the error $\varepsilon[n]$ in a mean-square sense are given by²

$$\mathbf{w}_{\text{opt}} = \mathbf{R}^{-1} \mathbf{p} \quad (3.34)$$

This result in (3.34) is independent of the choice of the filter function $f(u[n], \mathbf{w})$. However, it can only be used if the matrix \mathbf{R} can be inverted (is not singular). For the FIR filter, \mathbf{R} will generally be invertible, and thus (3.34) provides a general solution for finding \mathbf{w}_{opt} for this type of filter. However, this is not generally used in practical adaptive filters, because it is computationally expensive to calculate the matrix \mathbf{R} and vector \mathbf{p} and subsequently invert \mathbf{R} . Considerable research has gone into reducing the complexity of computing these values, leading to a body of algorithms referred to as *recursive least squares* (or *method of least squares*, or *sequential regression*)³. These methods are not presented nor is their application investigated in this thesis, as more simple algorithms have been found to work, which are explained hereafter.

Instead of determining \mathbf{w}_{opt} in one step as in (3.34), adaptive filters usually use an iterative method. If the error surface $\xi(\mathbf{w})$ is uni-modal, i.e. is convex with a single global minimum, \mathbf{w}_{opt} may be determined by updating \mathbf{w} along the gradient of $\xi(\mathbf{w})$. To this end, the gradient of $\xi(\mathbf{w})$ is defined as

$$\mathbf{d} = \nabla \xi(\mathbf{w}) = \begin{bmatrix} \frac{\partial \xi(\mathbf{w})}{w_0} & \frac{\partial \xi(\mathbf{w})}{w_1} & \dots & \frac{\partial \xi(\mathbf{w})}{w_N} \end{bmatrix} \quad \mathbf{d} \in \Re^{N+1} \quad (3.35)$$

Using the method of *steepest descent*, the weighting vector \mathbf{w} can be iteratively shifted to its optimum value. A new estimate of the weighting vector is obtained by subtracting from its previous estimate the gradient \mathbf{d} , as scaled by convergence parameter μ ⁴. In this way, one has $\mathbf{w}[n+1]$, an updated estimate of \mathbf{w} , obtained as so

¹ These are standard concepts in adaptive filtering (signal processing). A basic explanation may be found on p. 20 of Widrow and Stearns (1985). A more detailed description may be found in §2.3 of Haykin (1996).

² This represents the solution to the Wiener-Hopf equations for a linear, discrete-time system, where the weight vector \mathbf{w} describes the coefficients of an FIR filter; see p. 22 of Widrow and Stearns (1985) or p. 206 of Haykin (1996).

³ See pp. 147-153 of Widrow and Stearns (1985), or pp. 483-533 of Haykin (1996).

⁴ The convergence parameter μ may also be a vector, in such case each element of the gradient vector \mathbf{d} is weighted differently.

$$\mathbf{w}[n+1] = \mathbf{w}[n] - \frac{1}{2}\mu \mathbf{d}[n] \quad (3.36)$$

where μ is the convergence parameter, and $\mathbf{d}[n]$ is the error surface gradient for weighting vector $\mathbf{w}[n]$. The convergence parameter μ must be carefully chosen. If μ is too small, it will require large numbers of iterations to obtain \mathbf{w}_{opt} ; if μ is too large, the value $\mathbf{w}[n+1]$ will overshoot \mathbf{w}_{opt} , leading to erratic convergence or unstable calculation.

The method of steepest decent does not itself provide a sufficiently simple algorithm for real-time calculations. This is because the derivatives $\partial\xi(\mathbf{w})/\partial w_k$ are expensive to compute, particularly if they must be recalculated at each time interval n . Widrow and Hoff (1960) found that the gradient of the expectation value of the error, defined in (3.35), may be approximated by the gradient of the instantaneous value of the error, as so:

$$d_{w_k}[n] \approx \hat{d}_{w_k}[n] = 2\varepsilon[n] \frac{\partial \varepsilon[n]}{\partial w_k} = -2\varepsilon[n] \frac{\partial y_p[n]}{\partial w_k} \quad (3.37)$$

where $\hat{d}_{w_k}[n]$ is the instantaneous estimate of the gradient of the error surface along the parameter w_k at time interval n . With this simplification, the weighting vector may be updated in the same manner as (3.36) as so

$$\begin{aligned} \mathbf{w}[n+1] &= \mathbf{w}[n] - \frac{1}{2}\mu \hat{d}_{w_k}[n] \\ &= \mathbf{w}[n] + \mu \varepsilon[n] \nabla_{\mathbf{w}} y_p[n] \end{aligned} \quad (3.38)$$

where $\nabla_{\mathbf{w}} y_p[n]$ is a vector containing the instantaneous values of the derivatives of the output with respect to each element of the weighting vector \mathbf{w} at time index n . This method for updating \mathbf{w} was named by Widrow and Hoff as the *LMS algorithm*. It is referred to as a *stochastic gradient* method, due to its estimation of the true gradient, defined in (3.35), with only its instantaneous value. Additionally, one does not need to consider the derivative of the *square* of the error with respect to each weighting coefficient, but simply the derivative of the error signal itself. Experience has shown that this estimation leads only to a random error in the estimate of the gradient, which averages to zero over multiple iterations of updating, leading to an unbiased estimate of \mathbf{w}_{opt} . The remarkable combination of simplicity and effectiveness of this algorithm have led to its widespread commercial use in adaptive equalisation, control, array beam-forming, and echo cancellation, among other applications.

The most common filter structure used for adaptive filtering is the FIR filter, as it is inherently stable. For this type of filter, the LMS algorithm reduces to a form even simpler than (3.38). The derivative $\partial y_p / \partial w_k$ reduces to $u[n-k-1]$, producing

$$\mathbf{w}[n+1] = \mathbf{w}[n] + 2\mu \varepsilon[n] u[n] \quad (3.39)$$

3.5.2. Adaptive IIR filters

As explained in §2.3 above, a compact-discrete-time model of a loudspeaker requires an IIR filter. It is known that adaptive algorithms for IIR filters have several difficulties that those for FIR filters, described above, do not. Recent tutorials by Shynk (1989) and Netto et. al. (1995) describe these problems, and how different adaptive algorithms addressed them. Briefly, these problems are:

- Risk of instability
- Slow convergence rate
- Risk of convergence to local (non-global) error minima

These problems have been judged to be surmountable for the discrete-time loudspeaker model for two reasons:

- A great deal of *a priori* knowledge of the ‘system-to-be-identified,’ the electrical admittance of the loudspeaker, is available.
- Initial guess of the filter’s parameters can be made within a short range from their actual value.

The LMS IIR algorithm, is identical to the LMS algorithm for the FIR algorithm of (3.39), except for the expression for the derivatives of output error with respect to the weighting coefficients. For the IIR filter, the filter output is calculated recursively, complicating the definition of the derivative of the output with respect to the weighting coefficients w_k . Consider the basic definition of an IIR filter, wherein the filter output is calculated as:

$$y_p[n] = b_0 x[n] + b_1 x[n-1] + \dots + b_M x[n-M] - a_1 y_p[n-1] - a_2 y_p[n-2] - \dots - a_N y_p[n-N] \quad (3.40)$$

According to the ‘small step-size approximation’ developed by White (1975), the derivatives of the output $y_p[n]$ with respect to the feedback weighting coefficients a_k and feedforward coefficients b_k may be approximated by the following recursive calculation

$$\frac{\partial y_p[n]}{\partial a_k[n]} \approx y[n-k] + \sum_{n=1}^N a_k[n] \frac{\partial y_p[n-k]}{\partial a_k[n]} \doteq \alpha_k[n] \quad (3.41)$$

$$\frac{\partial y_p[n]}{\partial b_k[n]} \approx x[n-k] + \sum_{n=1}^M a_k[n] \frac{\partial y_p[n-k]}{\partial a_k[n]} \doteq \beta_k[n] \quad (3.42)$$

With this definition, the derivatives may be calculated recursively as so

$$\alpha_k[n] = y[n-k] + \sum_{k=1}^N a_k[n] \frac{\partial y_p[n-k]}{\partial a_k[n]} \quad (3.43)$$

$$\beta_k[n] = x[n-k] + \sum_{k=1}^M a_k[n] \frac{\partial y_p[n-k]}{\partial a_k[n]} \quad (3.44)$$

This is an important general feature of the LMS algorithm for IIR filters. It will be applied to various filter structures serving as discrete-time models of the loudspeaker. The details of this application is the subject of the next chapter.

It has been proposed by Feintuch (1976) that the latter sums in (3.41) and (3.42) can be discarded. However, it remains contentious discarding these sums does or does not lead to bias error in the converged values. For this reason, this simplification has not been used. It may be a suitable subject for further research.

Adaptive lattice-form IIR filters have received much interest in recent years (Parikh et al., 1980). The primary advantage of lattice-form IIR filters is the simplicity with which their stability may be assessed. However, it was found as part of background research for this thesis that the connection between physical parameters of a system and the parameters of a lattice filter are considerably more complicated than in the direct IIR form presented above. For this reason, lattice-form IIR filters are not investigated for the loudspeaker system identification.

3.6. References

- Adams, G. J., and R. Yorke, "Motional feedback in loudspeaker systems," *Monitor, Proceedings of the IREE*, pp. 85-93 (March 1976)
- Adams, G. J., *Optimisation and Motional Feedback Techniques in Loudspeaker System Design*, Ph.D. thesis, The University of Southampton. (Dec. 1979)
- Bai , Mingsian R., and Hsinping Wu, "Robust control of a sensorless bass-enhanced moving-coil loudspeaker system," *J. Acoust. Soc. Amer.*, **105**, pp. 3283-3289. (June 1999)
- Beerling, Marcel A. H., Cornelis H. Slump, and Otto E. Hermann, "Reduction of Nonlinear Distortion in Loudspeakers with Digital Motional Feedback," *presented at the 96th Convention of the Audio Eng. Soc.*, preprint 3820. (26 Feb. – 1 Mar., 1994)
- Beers, G. L. , and H. Beloar, "Frequency-Modulation Distortion in Loudspeakers," *Proc. IRE* **31**, 132. (Apr. 1943)
- Birt, David R., "Loudspeaker Power Amplifiers with Load-Adaptive Source Impedance," *Journal of the Audio Eng. Soc.*, **36**, pp. 552-561. (July/Aug. 1988)
- Birt, David R., "Nonlinearities in Moving-Coil loudspeakers with Overhung voice-coils," *Journal of the Audio Eng. Soc.*, **39**, pp. 219-231. (April 1991)
- de Boer, Egbert, "Theory of motional feedback," *IRE Transactions on Audio* pp. 15-21. (1961 Jan/Feb)
- de Boer, Jan, and Gerrit Schenkel, "Electromechanical Feedback", *J. Acoust. Soc. Amer.*, **20**, pp. 641-647. (Sept. 1948)
- Catrysse, J. A. M., "On the Design of Some Feedback Circuits for Loudspeakers," *Journal of the Audio Eng. Soc.*, **33**, pp. 430-435. (June 1985)
- Childs, U. J., "Loudspeaker Damping with Dynamic Negative Feedback," *Audio Engineering*, **36**, pp. 11-13, pp. 32-33. (Feb. 1952)
- Christensen, Knud Bank, and Erling Sandermann Olsen, "Nonlinear Modelling of Low Frequency Loudspeakers – A More Complete Model," *presented at the 100th Convention of the Audio Eng. Soc.*, preprint 4205. (May 11-14, 1996)
- Clements, W., "New Approach to Loudspeaker Damping," *Audio Engineering*, **35**, pp. 20-22, pp.54-55. (Aug. 1951)
- Clements, W. "It's Positive Feedback", *Audio Engineering*, p. 20, pp. 57-59. (May 1952)
- Craven, P. G., and M. A. Gerzon, "Practical Adaptive Room and Loudspeaker Equalization for Hi-Fi Use," *Proceedings Audio Eng. Soc. U. K. Conf. on DSP*, pp. 121-153. (1992)
- Elliott, Stephen J., and Phil A. Nelson, "Multiple-Point Equalization in a Room Using Adaptive Digital Filters," *J. Audio Eng. Soc.*, **37**, pp. 899-907. (Nov. 1989)
- Elliott, Stephen, Lev Bhatia, Shirin Dehghan, Adrian Fu, Magnus Stewart, and Dave Wilson, "Practical implementation of low-frequency equalisation using adaptive digital filters", *J. Audio Eng. Soc.*, **42**, pp. 988-998. (Dec. 1994)
- Feintuch, P. L., "An Adaptive Recursive LMS Filter," *Proceedings of the IEEE*, pp. 1622-4624. (Nov. 1976)
- Greiner, R. A., and Travis Sims, Jr., "Loudspeaker Distortion Reduction", *Journal of the Audio Eng. Soc.*, **32**, pp. 956-963. (Dec. 1984)
- Greenfield, R., and M. O Hawksford, "Efficient Filter Design for Loudspeaker Equalisation," *J. Audio Eng. Soc.*, **33**, pp. 436-443. (June 1985)

- Eng. Soc.*, **39**, pp. 127-139. (March 1991)
- Hall, David S., "Design Considerations for an Accelerometer-Based Dynamic Loudspeaker Motional Feedback System," *presented at the 87th Convention of the Audio Eng. Soc.*, preprint no. 2863. (Oct. 18-21, 1989)
- Hansen, Edward R., "A Motional Feedback Loudspeaker System," *presented at the 46th Convention of the Audio Eng. Soc.*, preprint no. 924. (1973)
- Haykin, Simon, *Adaptive Filter Theory*, Prentice Hall, New Jersey, USA, 3rd edition. (1996)
- Holdaway, H. W., "Controlling the Upper-Frequency Characteristics of Velocity-Feedback Loudspeaker Systems," *IEEE Transactions on Audio*, pp. 174-182 (Sept.-Oct. 1963)
- Hutt, Steve, "Ambient Temperature Variations on OEM Automotive Loudspeakers", *presented at the 112th Convention of the Audio Eng. Soc., Munich, Germany* Convention Paper 5507. (10-13 May, 2002)
- Hutt, Steve, personal correspondence. (7 June, 2002)
- Isidori, A., *Nonlinear Control Systems*, Springer Verlag (1989)
- Jang, Han-Kee, and Kwang-Joon Kim, "Identification of Loudspeaker Nonlinearities Using the NARMAX Modeling Technique," *Journal of the Audio Eng. Soc.*, **42**, pp. 50-59. (Jan./Feb. 1994)
- Karjalainen, Matti, Esa Piirilä, Antti Järvinen, and Jyri Huopaniemi, "Comparison of Loudspeaker Equalisation Methods Based on DSP Techniques," *Journal of the Audio Eng. Soc.*, **47**, pp. 14-31. (Jan. 1999)
- Kirkeby, Ole, and Philip A. Nelson, "Digital Filter Design for Inversion Problems in Sound Reproduction," *Journal of the Audio Eng. Soc.*, **47**, pp. 583-595. (Jul. 1999)
- Klaassen, J. A., and S. H. de Koning, "Motional feedback with loudspeakers," *Philips Technical Review*, **29**, pp. 148-157. (1968)
- Klippel, Wolfgang J., "The Mirror Filter – A New Basis for Reducing Nonlinear Distortion and Equalising Response in Woofer Systems," *Journal of the Audio Eng. Soc.*, **40**, pp. 675-691. (Sept. 1992)
- Klippel, Wolfgang J., "Direct Feedback Linearisation of Nonlinear Loudspeaker Systems," *Journal of the Audio Eng. Soc.*, **46**, pp. 499-507. (Jun. 1998)
- Klippel, Wolfgang J., "Adaptive Nonlinear Control of Loudspeaker Systems," *Journal of the Audio Eng. Soc.*, **46**, pp. 939-954. (Nov. 1998)
- Klippel, Wolfgang J., Personal, unwritten correspondence, Paris, France. (February 22, 2000)
- Krump, Gerhard, "Zur Temperaturabhängigkeit von Lautsprecherparametern," ("The Temperature Dependence of Loudspeaker Parameters") (in German), *presented at DAGA-97* (The Acoustical Society of Germany), (March 3-6, 1997), ISBN 3-9804568-2-X.
- Kuriyama, J.; Furukawa, Y, "Adaptive Loudspeaker System," *Journal of the Audio Engineering Society*, **37**, pp.919-26. (Nov. 1989)
- Lechevalier, Yohan, *Low frequency response of loudspeakers*, final report for diplom d'Ingenieur Electrique, Institut National des Sciences Appliquées de Lyon. (May 31, 2000)
- Leach, W. Marshall , Jr., "A Generalised Active Equaliser for Closed-Box Loudspeaker," *J. Audio Eng. Soc.*, **38**, pp. 142-146. (Mar. 1990)
- MacDonald, J. Ross, "Nonlinear Distortion Reduction by Complementary Distortion," *IRE Transactions on Audio*, pp. 128-133. (Sept.-Oct. 1959)

- Mills., P. G. L., and M. O. J. Hawksford, "Distortion reduction in moving-coil loudspeaker systems using current-drive technology", *Journal of the Audio Eng. Soc.*, **37**, pp. 129-148. (Mar. 1989)
- Nashif, Ahid D., and Tom M. Lewis, "Data Base of the Dynamic Properties of Materials", *Sound And Vibration*, pp. 14-25. (July 1991)
- Netto, Sergio L., Paulo S. R. Diniz., and Panajotis Agathoklis, "Adaptive IIR Filtering Algorithms for System Identification: A General Framework," *IEEE Transactions on Education*, **38**, pp. 54-66. (Feb. 1995)
- Nijmeijer, H., and A. J. van der Schaft, *Nonlinear Dynamical Control Systems*, Springer-Verlag. (1990)
- Normandin, Richard, "Extended Low Frequency Performance of Existing Loudspeaker Systems," *Journal of the Audio Eng. Soc.*, **32**, pp. 18-22. (Jan./Feb. 1984)
- Olson, Harry F., *Elements of Acoustical Engineering*, Second Edition, D. Van Nostrand Co., Inc., New York, New York. (Sept. 1947)
- Olson, Harry F., *Acoustical Engineering*, D. Van Nostrand Co., Inc., New York, New York. (1957)
- Parikh, D. , N. Ahmed, and S. D. Stearns, "An Adaptive Lattice Algorithm for Recursive Filters", *IEEE Transactions on Acoustics, Speech and Signal Processing*, **ASSP-25**, pp. 110-111. (Feb. 1980)
- Potirakis, S. M. , G. E. Alexakis, M. C. Tsilis, and P. J. Xenitides, "Time-domain nonlinear modelling of practical electroacoustic transducers." *Journal of the Audio Eng. Soc.* **47**, pp. 447-468. (June 1999)
- Radcliffe, J., and S. D. Gogate, "Identification and modeling of speaker dynamics for acoustic control application," *ASME J. Vib. Acoust.*, **38**, pp. 295-300. (1992)
- Rausch, R, R. Lerch, M. Kaltenbacher, H. Landes, G. Krump, and L. Kreitmeier, "Optimisation of Electrodynamic Loudspeaker-Design Parameters by Using a Numerical Calculation Scheme", *ACUSTICA-acta acustica*, **85**, pp. 412-419. (1999)
- von Recklinghausen, Daniel R., "Low-Frequency Range Extension of Loudspeakers," *Journal of the Audio Eng. Soc.*, **33**, pp. 440-446. (June 1985)
- Schurer, Hans , A. G. J. Nijmeijer, M. A. Boer, C. H. Slump, and O. E. Herrmann, "Identification and compensation of the electrodynamic transducer nonlinearities," *Proceedings of ICASSP-97*, **3**, pp. 2381-2384, ISBN: 0-8186-7919-0. (1997)
- Schurer, Hans, Cornelis H. Slump, and Otto E. Herrmann "Exact Input-Output Linearisation of an Electrodynamic Loudspeaker" presented at the 101st Convention of the Audio Eng. Soc., *Journal of the Audio Eng. Soc.* (Abstracts), Vol. 44, p. 1156, (Dec. 1995) pre-print 4334
- Schurer, Hans, *Linearisation of Electroacoustic Transducers*, Ph.D. Thesis, University of Twente Enschede, ISBN 90-365-1032-5. (1997)
- Schurer, Hans, Cornelis H. Slump, and Otto E. Herrmann, "Theoretical and Experimental Comparison of Three Methods for Compensation of Electrodynamic Transducer Nonlinearity," *Journal of the Audio Eng. Soc.*, **46**, pp. 723– 740. (Sept. 1998)
- Shynk, John J., "Adaptive IIR Filtering", *IEEE ASSP Magazine*, pp. 4-21. (April 1989)
- Slotine, J-J. E., *Applied Nonlinear Control*, Prentice Hall Inc., Edgewood Cliffs, N.J., USA. (1991)
- Small, Richard H., "Direct-Radiator Loudspeaker System Analysis," *IEEE Transactions on Audio and Electroacoustics*, Vol. AU-19, pp. 269-281 (Dec. 1971)

- Small, Richard H., "Loudspeaker Large-Signal Limitations," *presented at the 1st Australian Regional Convention of the Audio Eng. Soc.*, Sept 25-27, 1984. preprint no. 2102.
- Steiger, W. "Transistor Power Amplifiers with Negative Output Impedance," *IRE Transactions on Audio*, pp. 195-201. (Nov./Dec. 1960)
- Ståhl, K. E., "Synthesis of loudspeaker mechanical parameters by electrical means: a new method for controlling low-frequency loudspeaker behaviour," *Journal of the Audio Eng. Soc.*, **29**, pp587-696. (Sep. 1981)
- Suykens, Johan, Joos Vandewalle, and Johan van Ginderdeuren, "Control of distortion in an electrodynamic loudspeaker, Part I", Leuven. (April 22, 1992)
- Suykens, Johan, Joos Vandewalle, and Johan van Ginderdeuren, "Feedback linearisation of nonlinear distortion in electrodynamic loudspeakers," *Journal of the Audio Eng. Soc.*, **43** pp. 690-694. (Sept. 1995)
- Tanner, R. L., "Improving Loudspeaker Response with Motional Feedback", *Electronics*, p. 172, pp.228-240. (March 1951)
- Thiele, A. N, "Loudspeakers in Vented Boxes," *Proceedings of the IRE Australia*, **22**, pp. 487-508 (Aug. 1961)); reprinted in *Journal of the Audio Eng. Soc.*, **19**, pp. 382-392. (May 1971)
- Vesterholm, Thomas, *Applied Nonlinear Control – Possibilities and Limitations*, Ph.D. thesis, The Technical University of Denmark, Institute of Automation (1995). ISBN 87-87950-68-5
- Vidyasagar, M., *Nonlinear Systems Analysis*, Prentice Hall Inc., Edgewood Cliffs, N.J., USA (1993)
- Voigt, P. G. A. H., "Improvements in or Relating to Thermionic Amplifying Circuits for Telephony," *British Patent No. 231*, 972 filed Jan. 1924, issued April 1925.
- Wentworth, J. P., "Loudspeaker Damping by the use of Inverse Feedback," *Audio Engineering*, p. 21 (December 1951)
- Werner, R. W., "Effect of Negative Impedance Source on Loudspeaker Performance", *J. Acoust. Soc. Amer.*, **29**, pp. 335-340. (March 1957)
- Werner, R. E., and R. M. Carrell, "Application of negative output impedance amplifiers to loudspeaker systems," *Journal of the Audio Eng. Soc.* (Oct. 1958)
- Widrow, Bernard, and M. E. Hoff, Jr., "Adaptive switching circuits," *IRE WESCON Convention Record*, part 4, pp. 96-104. (1960)
- Widrow, Bernard, and Samuel D. Stearns, *Adaptive Signal Processing*, Prentice Hall, New Jersey, USA. (1985)
- Wiener, Norbert, and E. Hopf, "On a class of singular integral equations", *Proceedings of the Prussian Academy, Math-Physics Series*, p. 696. (1931)
- White, S. A., "An adaptive recursive digital filter", *Proceedings of the 9th Asilomar Conference on Circuits, Systems, and Computers*, pp. 21-25. (Nov. 1975)
- Wilkins, C. A., "Control of Amplifier Source Resistance," *Journal of the Audio Eng. Soc.*, **4**, pp. 9-13. (Jan. 1956)
- Yorke, R., and K. R. McLachlan, "Amplifier of Variable Output Impedance", *Wireless Engineer*, **28**, pp. 222-225. (July 1951)
- Zölzer, Udo, *Digital Audio Signal Processing*, John Wiley & Sons Ltd, Chichester, England. (1997)

4. Loudspeaker system identification

This chapter presents methods for loudspeaker system identification. The focus is specifically on those aspects of the loudspeaker which cannot be known outright from its design and manufacturing specifications. These are properties of the loudspeaker which vary due to manufacturing tolerances, temperature changes, and ageing, as discussed in §2.4.

In order to ensure that the algorithms for system identification meet the criterion for simplicity set out in the introduction, i.e. that the algorithms not be more complicated than existing audio DSP algorithms, an iterative system identification procedure must be used, using adaptive filtering, the basics of which were presented in §3.5, above.

Again, to simplify the system for active control, an adaptive filter structure is chosen which corresponds to the physical dynamics of the loudspeaker. As discussed in control systems theory, this is to say the system identification uses *grey-box* model structures as opposed to *black-box* model structure (Ljung, 1999, p.13). In this way, the parameters identified by the adaptive filter can be directly used by the feedforward processor, and do not require transformation (as would be necessary if a black-box model were used¹). It is for this reason that the discrete-time model for a loudspeaker is developed in §2.3, above.

An overview of the approach to system identification is given in §4.1. This section first describes the three different error signals used. A description of the hardware implementation and the loudspeaker-under-test is given in §4.1.2. A description of the software implementation of the algorithms is given in §4.1.3.

The approach to loudspeaker system identification is nearly identical to that described by Knudsen et al. (1989). The parameter updating algorithm used here, however, is the standard LMS IIR output-error algorithm (presented in §3.5.2). Knudsen et al. used techniques more common to off-line system identification, which can be roughly understood in the terms of adaptive signal processing as batch-processing equation-error or ARMAX techniques. These latter parameter updating methods are by far more stable and robust than the LMS IIR output-error algorithm. However, they were considered too computationally expensive for the present application. As part of research for this thesis, it was found that by using special *a priori* knowledge available for a given loudspeaker, convergence, stability and robustness of the IIR LMS algorithm could generally be guaranteed. Discussions on how this was done are presented in §§4.1.4 - 4.1.6.

4.1. Overview of approach, implementation, and evaluation

A brief overview of the three different forms for generating an error equation under study in this thesis are presented in §4.1.1. The hardware

The linear dynamics of the loudspeaker in all of these forms are based on second-order IIR filters. As the parameters of these IIR filters are adapted, the conditions for stability of an IIR filter are reviewed

¹ One example of a black-box model for the loudspeaker would be an FIR model of the electrical impedance. As discussed in §2.3.1, it would be necessary to identify the physical parameters of a loudspeaker from the coefficients of the adapted FIR filter before they could be used by a feedforward processor. This type of processing is considered too computationally expensive.

in §4.1.4. In early trials of the system identification algorithms, it was found that the convergence was either slow or erratic.

It was found that, by using tolerance information which can be known *a priori* about any loudspeaker, the parameters of the IIR filters could be kept within a minimum distance of their optimum values. This has been achieved by use of a ‘tolerance quadrilateral,’ presented in §4.1.5.

4.1.1. Forms for developing an error equation

As per the discussion on feedback processing for loudspeakers in §3.1, direct output signals from the loudspeaker such as a sound field measurement or vibration measurement are expensive and/or impractical to obtain. For this reason, plant models (loudspeaker models) defining the structure of the adaptive filter for system identification are considered only for the electrical characteristics of the loudspeaker. These consider (in discrete time) measurement of the voice-coil voltage $v_{c\cdot m}[n]$ and the voice-coil current $i_{c\cdot m}[n]$. Two obvious plant models suggested by Knudsen et al. (1989) with these two signals available are:

- Electrical admittance (prediction of current from the measured, or known, voltage)
- Electrical impedance (prediction of voltage from the measured current)

In the *electrical admittance output error* form, an adaptive filter makes an estimate (‘prediction’) of the voice coil current $i_{c\cdot p}[n]$. The input to this filter is the measured voice-coil voltage $v_{c\cdot m}[n]$ and measured voice-coil current $i_{c\cdot m}[n]$. In this form, the electrical inductance L_{eb} is assumed to be negligible. With this assumption, the basic voltage equation of (2.1) has no differential operators, and can thus be expressed directly in discrete time as so:

$$v_c[n] = R_{eb}i_c[n] + \phi(x_d[n])u_d[n] \quad (4.1)$$

Solving for current in this equation produces

$$i_c[n] = \frac{1}{R_{eb}}(v_c[n] - \phi(x_d[n])u_d[n]) \quad (4.2)$$

The strategy of this ‘admittance output error form’ is to predict the electrical current with this equation, using a measurement of the voice-coil voltage, and a prediction of the diaphragm-coil velocity. The classical adaptive filtering techniques described in §3.5 are used to adapt free parameters in order to minimise the difference between the measured and predicted current, in a mean-square sense. Investigations into the performance of this plant model structure for loudspeaker parameter identification are presented in §4.2, below.

In the *electrical impedance output error* plant model structure, the measured voice-coil current $i_{c\cdot m}[n]$ is used to calculate a predicted voice-coil voltage $v_{c\cdot p}[n]$. This is done directly as per the voltage equation of (4.1). This predicted voice-coil voltage is compared with the measured voice-coil voltage $v_{c\cdot m}[n]$, and as per the electrical admittance structure described above, parameters are tuned to minimise the error between the two. (Note that since solid-state power amplifiers provide constant-output voltage, the voice-coil voltage can be known from the output signal from the controller, and thus need not be measured separately.) It is shown that identification of the electrical inductance L_{eb} can also be performed with only a modest increase in complexity. Investigations into the performance of this plant model structure for loudspeaker parameter identification are presented in §4.3, below.

An alternative to these two plant model structures are motional-signal equation error techniques. Such a technique was presented by Klippel (1999), wherein the diaphragm-coil velocity $u_d(t)$ is predicted by the force equation and the voltage equation, both including parametric nonuniformity of the type described in §2.2.1. An error signal, to be minimised in a mean-square sense, is obtained from the difference between the velocity predicted by the force and voltage equation, as so:

$$\epsilon_{eeu}[n] = \frac{1}{\phi(x_d[n])} \left(v_{c\cdot m}[n] - R_{eb} i_{c\cdot m}[n] - L_{eb} h_{dt}[n] * i_{c\cdot m}[n] \right) - h_{Y_m}[n] * \left(\phi(x_d[n]) i_c[n] \right) \quad (4.3)$$

where $h_{dt}[n]$ is the impulse response of a differentiation approximation as discussed in §2.3.4, and $h_{Y_m}[n]$ is the impulse response of the mechanical mobility as discussed in §2.3.3.

Klippel showed how this method could be used to identify coefficients of truncated polynomial series approximations to the parametric nonuniformity in the transduction coefficient, suspension stiffness, and blocked electrical inductance.

One disadvantage in the development of this error equation in (4.3) is that it requires the displacement signal $x_d[n]$. This is needed for evaluation of the transduction coefficient nonlinearity, i.e. evaluation of $\phi(x_d[n])$. This can, of course, be obtained by integration of the displacement signal. However, it has been found to be simpler to base the error equation on the displacement, obviating the need to compute it as an extra step. This form is based on this error equation:

$$\epsilon_{eex}[n] = h_{dt}[n] * \left[\frac{1}{\phi(x_d[n])} \left(v_{c\cdot m}[n] - R_{eb} i_{c\cdot m}[n] - L_{eb} h_{dt}[n] * i_{c\cdot m}[n] \right) \right] - h_{X_m}[n] * \left(\phi(x_d[n]) i_c[n] \right) \quad (4.4)$$

where $h_{X_m}[n]$ is the impulse response of the mechanical receptance, as discussed in §2.3.2. This method is referred to here in as the *displacement equation error* plant model. Basics of its performance are presented in §4.4. It is found that this displacement equation error method is considerably more complicated than the current and voltage output error methods described above. For this reason, this method is not considered in complete detail.

The system identification techniques developed in this chapter are suitable only for a loudspeaker mounted in a closed box. Modelling more complex acoustic enclosures has not been considered.

4.1.2. Hardware implementation and system-under-test

The adaptive algorithms for system identification were investigated on actual loudspeakers. A block diagram of the hardware system used is shown in Figure 4.1. Note that Figure 4.1 shows a block for the feedforward processing systems as well, although these are not discussed in this chapter.

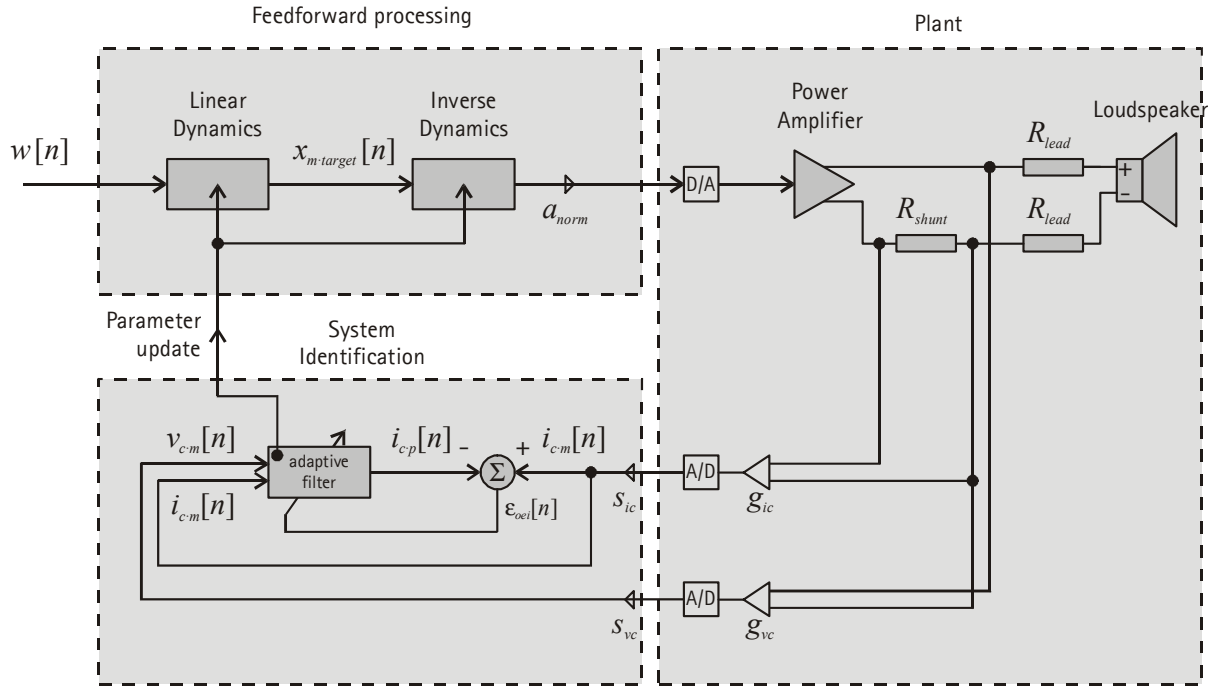


Figure 4.1: Block diagram of hardware used for investigation of the loudspeaker system identification algorithms presented in this chapter. Note this figure also shows the 'feedforward processing' blocks, presented in §3.3, and investigated experimentally in chapter 5. This chapter presents theory and experimental results of only the 'system identification' block.

A photograph of the mounting of the loudspeaker under-test for experimental trials of the system identification algorithms presented in this chapter is shown in Figure 4.2. A detail of this figure is shown in Figure 4.3. The loudspeaker used is a standard ø16mm microspeaker currently available on the market. This is a widely used microspeaker, for reproducing speech and alert-tones in hand-portable phones. Its general features and proportions are as shown in Figure 2.1.

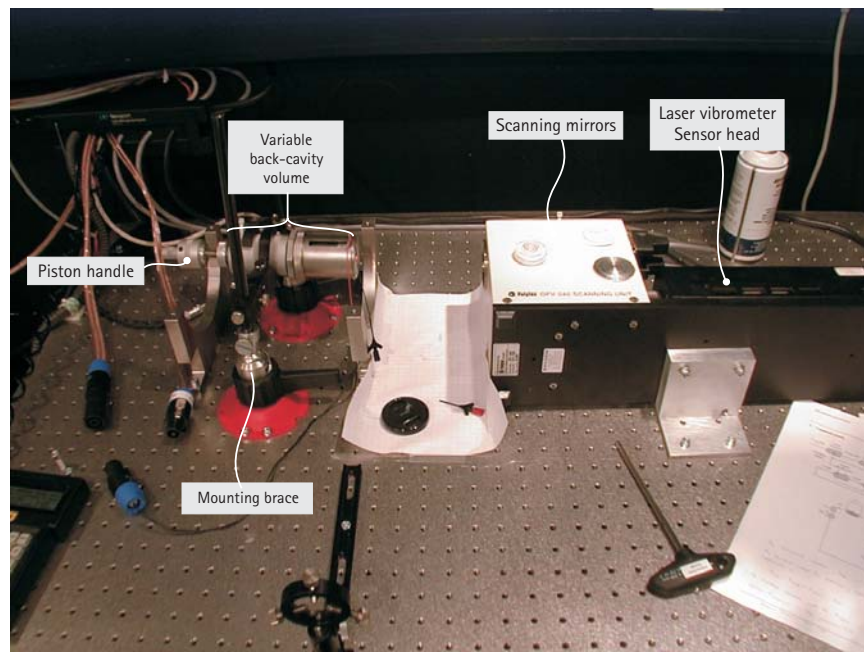


Figure 4.2: Photograph of mounting of loudspeaker under-test during experimental trials of the system-identification algorithms presented in this chapter.

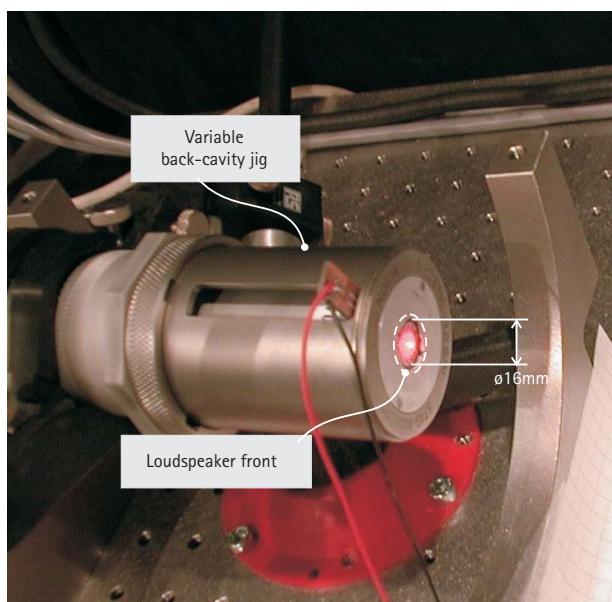


Figure 4.3: The loudspeaker is highlighted in the photograph by the broken white ellipse. The red dot at the centre of the speaker is reflected light from the laser vibrometer, used to verify results of the system identification.

The red¹ dot visible at the centre of the loudspeaker Figure 4.3 is reflected light from the laser vibrometer. The laser vibrometer was used to verify the values to which the system identification algorithms converged. Signals from the laser vibrometer were not used by the system identification algorithms directly. As per Figure 4.1, the algorithms used only electrical voltage and current signals.

¹ The dot will of course appear white if a black-and-white printing process was used.

The loudspeaker was mounted in a variable back-cavity jig, the stainless-steel and aluminium cylindrical structure shown in Figure 4.2. This provides an acoustically sealed back-cavity for the loudspeaker such that it may be modelled as described in §2.1.7. The total volume of the rear-cavity may be easily varied via a travelling piston. A threaded handle for the piston, as labelled in Figure 4.2, permits coarse and fine adjustment of the rear-cavity volume. This permits direct variation of the effective resonance frequency f_0 . This proved considerably useful for quick analysis of the tracking performance of the system identification algorithms.

Additional photographs of the experimental set-up for evaluation of the system identification algorithms are presented in Appendix A.

4.1.3. Software implementation

The system identification algorithms were implemented on a standard desktop PC, using an Intel Pentium II processor, with a clock speed of 266 MHz. The algorithm was written using standard ANSI C functions. Analogue input/output was facilitated with a standard sound card. A header file written by Antti Vähälä of Nokia Research Center was used to handle data transfer between the C-program and the sound card. No dedicated audio DSP processor was used. Despite not using any special, dedicated audio DSP processing hardware, no problems with real time performance were found, even at the highest sampling rate of 48 kHz.¹

No special programming tricks were used in the implementation of the algorithms presented herein. Programming was done more or less by direct implementation of the difference equations written in the thesis. For this reason, the C-code used for processing is not presented here, as it does not contain any new information from that which is already presented in the equations.

The operation of the algorithm was controlled by a simple graphical user interface. A snapshot of this graphical user interface is shown in Figure 4.4.

¹ Your author was surprised to not have a problem with real-time performance at this highest sampling rate of 48kHz. It had generally been assumed that PC's were not capable of running any type of audio DSP algorithms on their own, i.e. without using dedicated audio DSP processors. That these algorithms were able to run in real time without the use of dedicated DSP hardware served as a testament to your author to the advances made in the processing capabilities of ordinary desktop PC's in recent years.

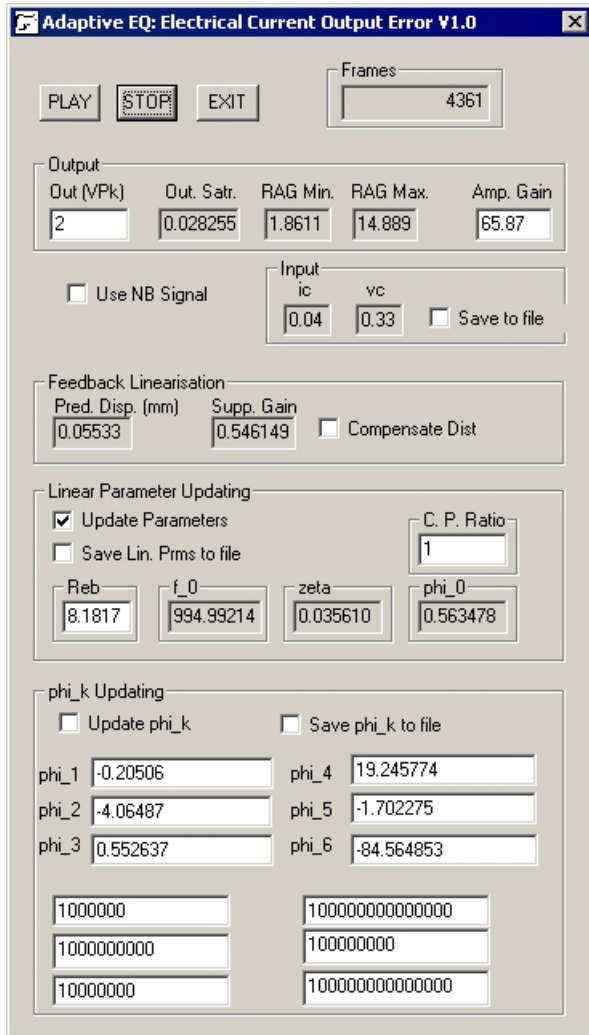


Figure 4.4: User interface for C-programs. This interface has controls for the system identification algorithm presented in this chapter, as well as for the nonlinear distortion compensation algorithm presented in §3.3.7 and investigated experimentally in §5.2. The version of the interface shown in this figure is for controlling the electrical-current output-error form of the system identification algorithm, presented in §4.2.

Data variables and computation used double floating point precision. Problems associated with fixed-point computation were not considered.

Sampling rates of 8 kHz, 16 kHz, and 48 kHz were investigated. Convergence time of the algorithm, as measured in seconds, is not appreciably different for the different sample rates. All of the convergence plots presented below were recorded from data processed at 16kHz.

4.1.4. Stability triangle

According to elementary theory of discrete-time signal processing (Oppenheim and Schafer, 1989), an IIR filter is inherently stable only if the poles of its z -domain transfer function all lie inside of the unit-circle of the z -plane. For a second-order IIR filter, this criteria may be expressed as three inequalities which must all be true:

$$\begin{aligned} a_2 &< 1 \\ a_2 &> (-a_1 - 1) \\ a_2 &> (a_1 - 1) \end{aligned} \tag{4.5}$$

These criteria are plotted graphically in Figure 4.5

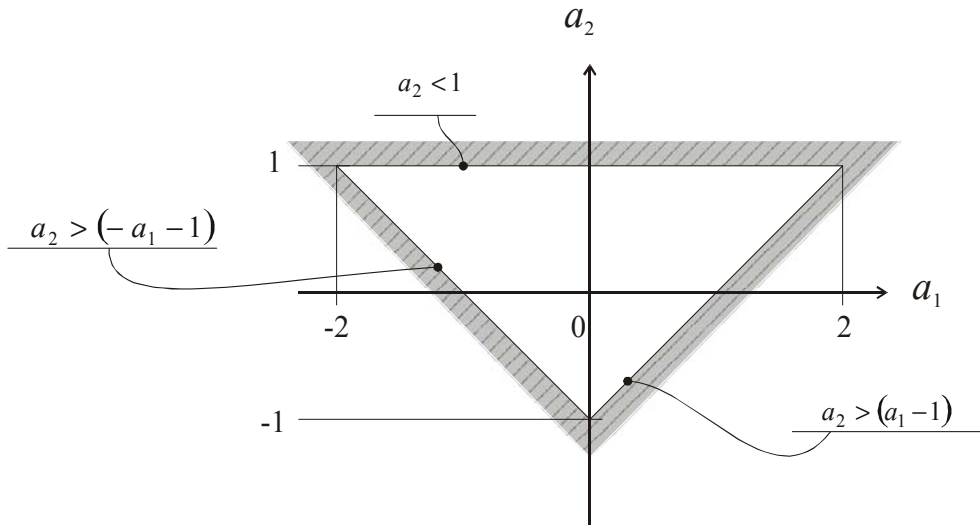


Figure 4.5: Geometric representation of the stability criteria described in (4.5)

The stability triangle was used in early trials of the adaptive IIR algorithm, by assessing the truthfulness of the inequalities in (4.5). If any of these inequalities were found to be untrue, the parameters were not updated by the instantaneous gradient estimate.

Although use of the stability triangle in this way did prevent unstable calculation, convergence was generally poor. As discussed below, this was found to be due to the nature of the error surface in a_k , and not due to instability.

4.1.5. Tolerance quadrilateral

In early trials of the electrical-current output-error algorithm, convergence of the a_k parameters was, erratic, slow, and/or unpredictable. For some initial values, the parameters would converge rapidly. Other initial values lead to erratic updating, eventually forcing the a_k values to the edge of the stability triangle. Still other trials showed initial convergence of the parameters toward their optimal values, resulting in unstable convergence as they approached the optimum values.

In order to better understand the convergence dynamics, a simulation was made of the a_1 , a_2 error surface. The error was calculated over a range of values of a_1 , a_2 for 4 seconds of measured data on an actual loudspeaker. The resulting error surface is shown in a contour plot in Figure 4.6, and in a 3-D surface mesh in Figure 4.7. Note that the parameter space region over $-1 < a_2 < 0$ is not analysed. Although this region is within the stability triangle, it does not correspond to physically realisable parameter values, as will be shown below.

It is particularly clear from Figure 4.7 that this error surface *does* have a single global minimum, occurring at around $a_1 = -1.8$, $a_2 = 0.97$. Thus it does not suffer from the problem of local minima of some adaptive IIR filtering cases as described by Johnson and Larimore (1977).

The problematic feature of this error surface is that its gradient is sharp only in the vicinity of the global minimum. As can be seen from the contour plot (Figure 4.6), for much of the a_1 , a_2 parameter space the error is around 26~27%, with a very small slope. As, for the LMS algorithm, the convergence rate is directly proportional to the slope, selecting initial values in this region will lead to very slow convergence. Although a higher convergence parameter could be used to increase the convergence rate, this would lead to large parameter spread and potentially unstable convergence as the parameters approach the global minimum, where the slope of the error surface is larger.

The solution to this problem has been to use *a priori* information available about the actual variation in a_1 and a_2 . It was explained in §2.4 above that the loudspeaker's parameters can be known within certain tolerances. By translating these known tolerances in the physical parameters into a_1 and a_2 , the region of the a_1 , a_2 parameter space which must be considered by the adaptive algorithm may be reduced to that region of the space wherein the slope of the error surface is not small.

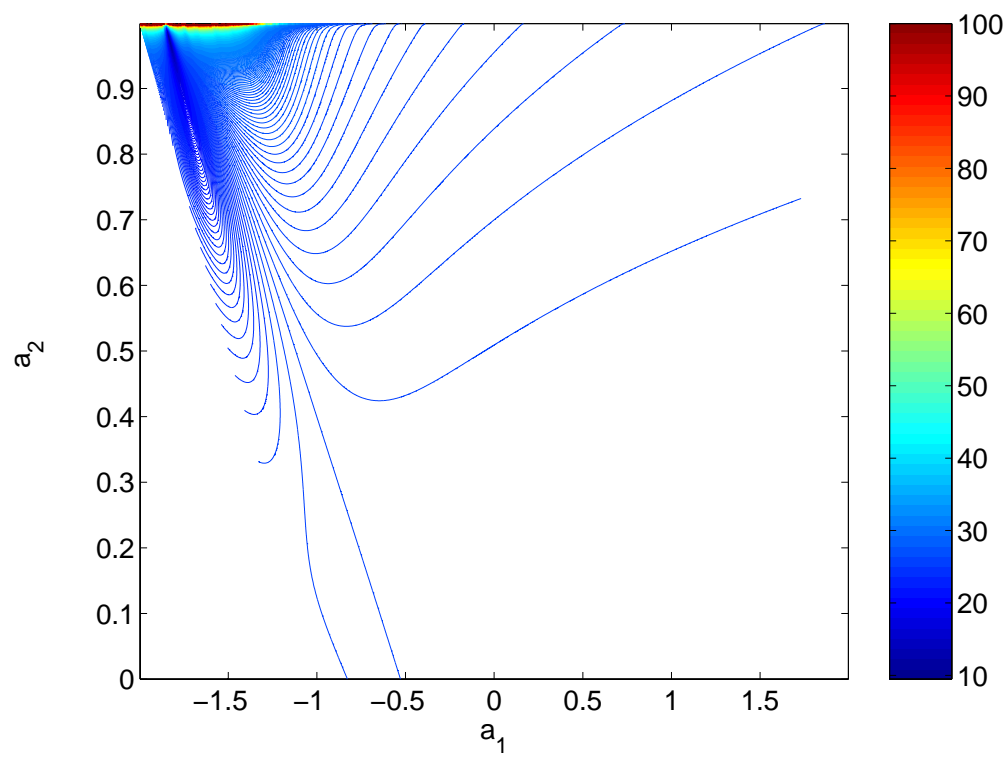


Figure 4.6: Contour lines of the error surface, in percent. The difference in error between each contour line is 0.1%.

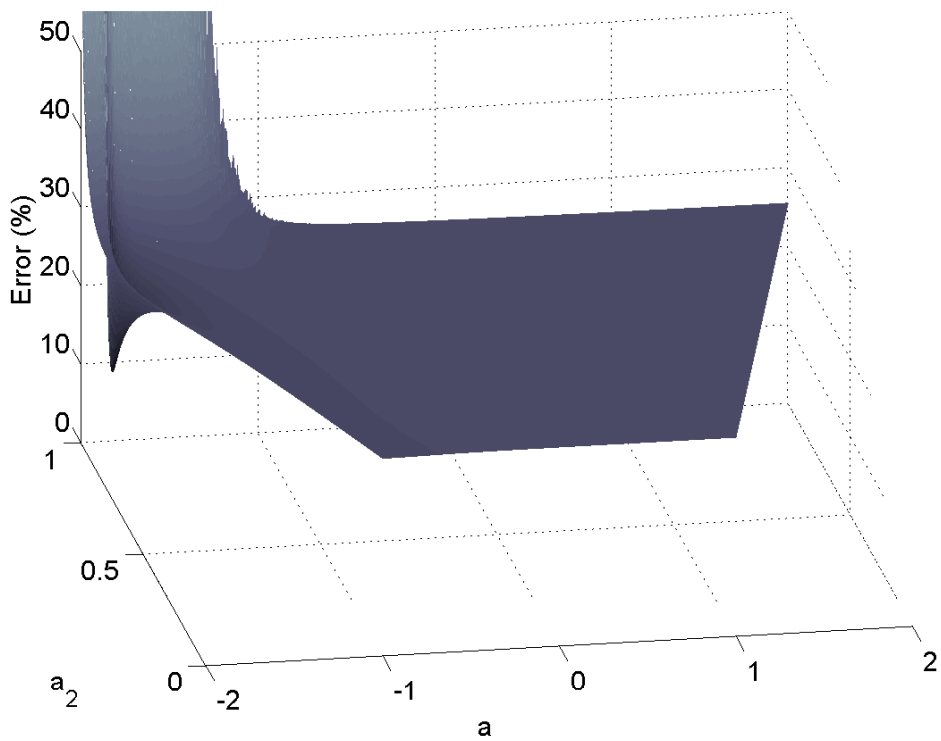


Figure 4.7: Plot of the error surface vs. a_1 and a_2 .

It is first necessary to consider how variations in the resonance frequency (normalised to F_s) and damping ratio ζ translate to changes in a_1 and a_2 . In Figure 4.8, lines of constant resonance frequency and damping ratio are shown in the a_1 , a_2 parameter space. As can be seen from this figure, in the upper left-hand corner, where the minimum in the error surface occurs, these lines are approximately straight. That these lines are straight permits imposition of frequency and damping tolerance criteria by simpler expressions in a_1 and a_2 than the direct formulae of (2.66).

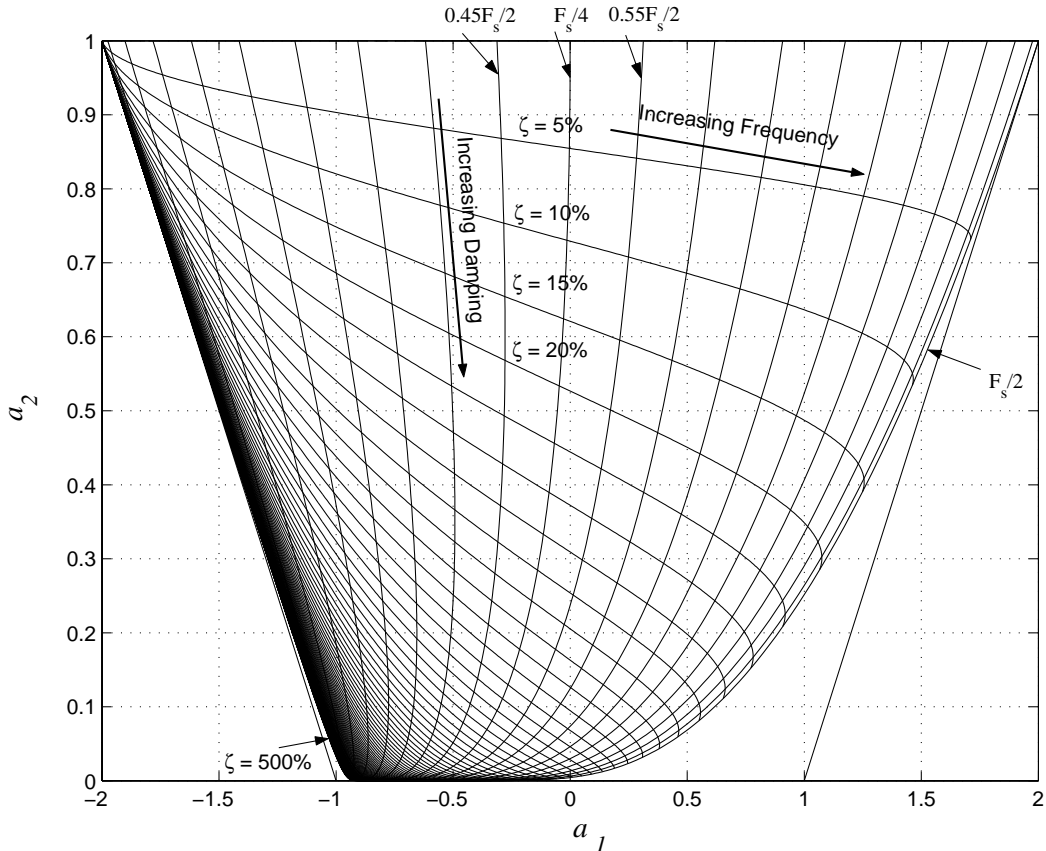


Figure 4.8: Lines of constant resonance frequency (normalised to F_s) and damping ratio ζ in the a_1 , a_2 parameter space. Notice no lines go below $a_2 = 0$, even though this would result in a stable filter.

Imposition of known limits in variations in the resonance frequency and damping ratio restricts the a_1 , a_2 parameters space which must be searched. By considering the following limits:

$$\begin{aligned} f_{act} &= f_0 \pm 25\% \\ \zeta_{act} &= \zeta_0 (-90\% + 360\%) \end{aligned} \tag{4.6}$$

the a_1 , a_2 space is reduced to the region shown in Figure 4.9.

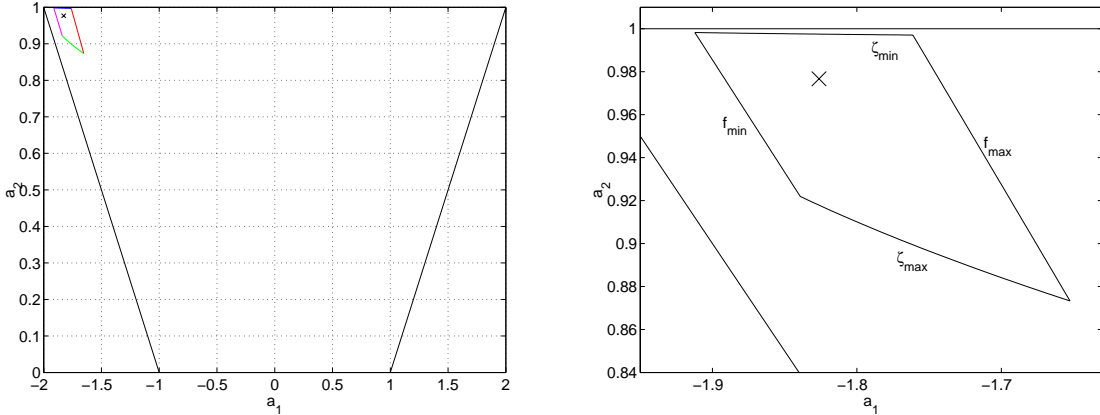


Figure 4.9: Normalised resonance frequency and damping ratio tolerances of (4.6) in the $[a_1, a_2]$ parameter space. [left] complete region of physically realisable $[a_1, a_2]$ values; [right] focused view around target values. The 'x' in both graphs indicates the target value.

As discussed above and can be seen from Figure 4.9, the limits form approximately straight lines in a_1 , a_2 . This permits maintaining updated values of a_1 and a_2 within these limits to be performed by this algorithm:

$$\begin{aligned} \text{if } (a_2 > \zeta_{\min,1}a_1 + \zeta_{\min,0}), \quad a_2 &= \zeta_{\min,1}a_1 + \zeta_{\min,0} \\ \text{if } (a_2 < \zeta_{\max,1}a_1 + \zeta_{\max,0}), \quad a_2 &= \zeta_{\max,1}a_1 + \zeta_{\max,0} \\ \text{if } (a_1 > f_{\max,1}a_2 + f_{\max,0}), \quad a_1 &= f_{\max,1}a_2 + f_{\max,0} \\ \text{if } (a_1 < f_{\min,1}a_2 + f_{\min,0}), \quad a_1 &= f_{\min,1}a_2 + f_{\min,0} \end{aligned} \quad (4.7)$$

where the terms $[\zeta_{\min,1}, \dots, \zeta_{\min,0}, f_{\max,1}, \dots, f_{\min,0}]$ are coefficients defining the four lines of a quadrilateral approximating the limits in Figure 4.9.

4.1.6. Frame-based updating

Most audio signal processing uses frame-based processing. The motivation behind this comes primarily from lossy-compression (coding) techniques, referred to as speech or audio coding. These algorithms operate in the frequency domain, and therefore must operate on one frequency-transformed frame of time data at a time. Typical frame lengths are on the order of 20ms, though this can vary significantly depending on the application.

Such frame-based processing has no direct theoretical impact on the adaptive algorithm developed here. However, it can be used to reduce the computational overhead required for assessment of the tolerance quadrilateral. It has been found that the estimate of the gradient can be ‘accumulated’ over one frame such that

$$\hat{d}_{a_k \cdot acc}[j] = \sum_{n=1}^{N_{frame}} \hat{d}_{a_k}[n] \quad (4.8)$$

where $\hat{d}_{a_k \cdot acc}[j]$ is the gradient estimate accumulated over the j^{th} -frame, and where the frame has N_{frame} samples. The adapted parameters are then updated according to this accumulated gradient according to

$$a_k[j+1] = a_k[j] - \mu_{a_k} \hat{d}_{a_k \cdot acc}[j] \quad (4.9)$$

The advantage of this technique is that the tolerance quadrilateral assessment of (4.7) need be made only once for each frame, instead of for each sample. Although the parameters are updated only once per frame (instead of for each sample), due to the stochastic nature of estimation of the gradient in the LMS algorithm, the accumulation of the instantaneous estimate of the gradient over the frame length results in a more accurate estimate of the gradient for the end-of-frame updating. The net results is that the convergence rate using only end-of-frame updating tends to be about the same as sample-by-sample updating.

4.2. Electrical current output-error form

The adaptive filter for the electrical current output error plant model structure is shown in Figure 4.10. The method for developing this model is the same as used to develop the discrete-time nonlinear loudspeaker model presented in §2.3.4.

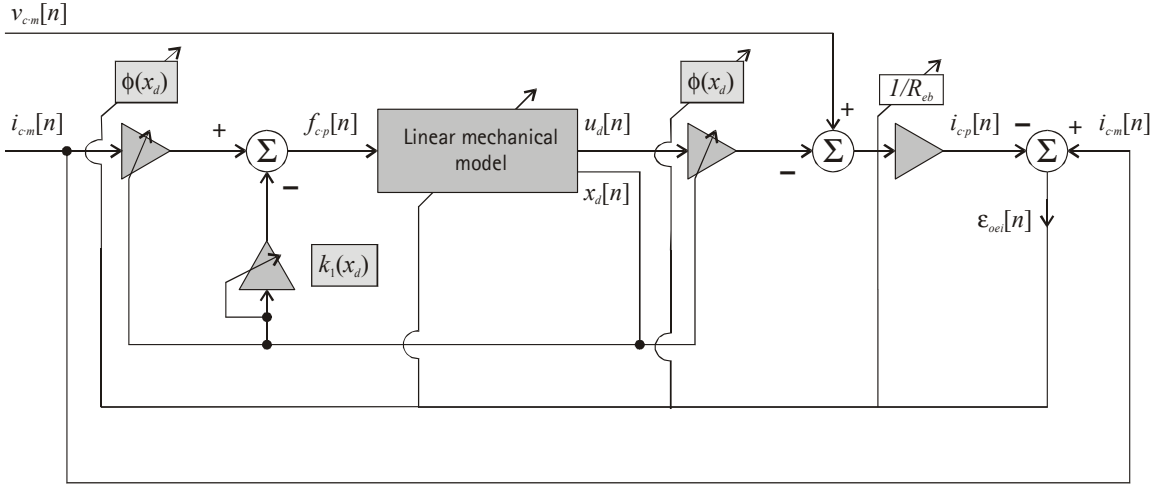


Figure 4.10: Block diagram of electrical current output error (ECOE) plant model structure. Notice that linear and nonlinear components are separated. This diagram shows the inclusion of nonuniform force factor and stiffness. Other parameter nonuniformity, as discussed in §2.2.1, may be included in a similar manner, though in some cases require more complicated linear dynamics models, e.g. calculation of acceleration.

This plant model calculates a predicted current signal $i_{cp}[n]$. An error signal $\epsilon_{oei}[n]$ is obtained by comparing the predicted current signal with a measured current signal $i_{cm}[n]$ as so:

$$\epsilon_{oei}[n] = i_{cm}[n] - i_{cp}[n] \quad (4.10)$$

The predicted current signal is calculated according to the voltage equation of (2.1). By ignoring the effects of the blocked electrical inductance L_{eb} (as discussed towards the end of §2.1.1), the predicted current is calculated as per:

$$i_{cp}[n] = \frac{1}{R_{eb}}(v_{cm}[n] - \phi(x_d[n]) u_d[n]) \quad (4.11)$$

where $v_{cm}[n]$ is the measured voltage, $u_d[n]$, is the diaphragm velocity predicted according to the force equation, and other terms are as previously presented. The diaphragm velocity $u_d[n]$ and displacement $x_d[n]$ are computed according to the ‘linear mechanical model’ in Figure 4.10, incorporating the linear second-order dynamics of the mechanical dynamics of a loudspeaker mounted in a closed box, as discussed in §2.1.7. These second-order dynamics are implemented in discrete time using the discrete-time models of mobility (presented in §2.3.3) and receptance (presented in §2.3.2) to calculate the velocity $u_d[n]$ and displacement $x_d[n]$, respectively, from the force on the voice-coil $f_{cp}[n]$. Explicitly, they are calculated as per this second-order IIR filter:

$$u_d[n] = \sigma_u f_{cp}[n] - \sigma_u f_{cp}[n-2] - a_1 u_d[n-1] - a_2 u_d[n-2] \quad (4.12)$$

where σ_u is the reference sensitivity for the discrete-time mobility z -domain transfer function defined in §2.3.3, a_1 and a_2 are the feedback coefficients defining the poles of the system as per §2.3.3,¹ and $f_{cp}[n]$ is the predicted force on the voice-coil predicted from the electrical current as per:

$$f_{cp}[n] = \phi(x_d[n])i_{cm}[n] - k_1(x_d[n])x_d[n] \quad (4.13)$$

The displacement signal is calculated iteratively from the force using

$$x_d[n] = \sigma_x f_{cp}[n-1] - a_1 x_d[n-1] - a_2 x_d[n-2] \quad (4.14)$$

as defined in §2.3.2, and $f_{cp}[n]$ is the predicted force as per (4.13).

Notice that the displacement signal $x_d[n]$ appears in the expression for the predicted force $f_{cp}[n]$ and vice-versa. Thus it would at first appear that this equation pair form only an *implicit* and not *explicit* method for calculating the displacement from the current. However, notice that the force $f_{cp}[n]$ appears as a *delayed* sample in the equation for $x_d[n]$. It is thus possible to ‘predict’ the displacement one-sample ahead. This can then be used in the calculation of the next sample of the predicted force $f_{cp}[n]$.

Linear case

The linear case, wherein parameter nonuniformity with respect to displacement is assumed to be negligible, is first considered. If models of the parameter nonuniformity are known, this linear case may be defined by the approximations

$$\begin{aligned} \phi(x_d[n]) &\approx \phi_0 \\ k_1(x_d[n]) &\approx 0 \end{aligned} \quad (4.15)$$

Given the above assumption, the formula for calculating predicted force $f_{cp}[n]$ in (4.13) simplifies to

$$f_{cp}[n] = \phi_0 i_{cm}[n] \quad (4.16)$$

Combining (4.11) and (4.12) and assuming the linear case described above, the error is calculated by

$$\varepsilon_{oei}[n] = i_{cm}[n] - \frac{1}{R_{eb}} \left[v_{cm}[n] - \phi_0 \left(\phi_0 \sigma_u \left(i_{cm}[n] - i_{cm}[n-2] \right) - a_1 u_d[n-1] - a_2 u_d[n-2] \right) \right] \quad (4.17)$$

where $u_d[n]$ is calculated iteratively as per (4.12), and where $f_{cp}[n]$ is calculated from the measured current $i_{cm}[n]$ as per (4.16).

The LMS algorithm is used to iteratively update the parameters R_{eb} , ϕ_0 , a_1 and a_2 such that the error signal $\varepsilon_{oei}[n]$ is minimised in a mean-square sense. As explained in §3.5.1, the LMS algorithm uses a simple stochastic gradient, determined from the product of the error signal and the derivative of the error signal of the parameter to be updated. As the error signal defined in (4.17) is not of standard FIR or IIR form, its derivatives for each of the parameters to be updated are derived for each parameter in a separate section below.

4.2.1. Updating R_{eb}

The derivative of the error, defined for the linear case in (4.17), with respect to the DC-resistance R_{eb} is given by

¹ Note that these feedback coefficients are the same as those for the mechanical displacement. This is because the mechanical mobility has the same pole locations as the mechanical receptance.

$$\frac{\partial}{\partial R_{eb}} \varepsilon_{oei}[n] = \frac{1}{R_{eb}^2} (v_{c\cdot m}[n] - \phi_0 u_d[n]) - \frac{1}{R_{eb}} \frac{\partial}{\partial R_{eb}} (v_{c\cdot m}[n] - \phi_0 u_d[n]) \quad (4.18)$$

Given that $v_{c\cdot m}[n]$ is a measured value, and that $u_d[n]$ is calculated from the measured value $i_{c\cdot m}[n]$ without use of R_{eb} , the derivative with respect to R_{eb} is zero. Therefore, the last term in this equation is zero, reducing the partial derivative of the error $\varepsilon_{oei}[n]$ with respect to the DC resistance R_{eb} to

$$\frac{\partial}{\partial R_{eb}} \varepsilon_{oei}[n] = \frac{1}{R_{eb}^2} (v_c[n] - \phi_0 u_d[n]) \quad (4.19)$$

Notice that the term in parentheses on the RHS of (4.19) is the same as that appearing in the definition of the predicted current $i_{c\cdot p}[n]$. Thus this derivative may be written more compactly as

$$\frac{\partial}{\partial R_{eb}} \varepsilon_{oei}[n] = \frac{i_{c\cdot p}[n]}{R_{eb}} \quad (4.20)$$

From this the instantaneous estimate of the gradient of the error surface along R_{eb} is given by

$$\begin{aligned} \hat{d}_{R_{eb}}[n] &= \varepsilon_{oei}[n] \frac{\partial \varepsilon_{oei}[n]}{\partial R_{eb}} \\ &= \varepsilon_{oei}[n] \frac{i_{c\cdot p}[n]}{R_{eb}} \end{aligned} \quad (4.21)$$

with which the estimate of the DC-resistance may be updated using the LMS algorithms as so

$$R_{eb}[n+1] = R_{eb}[n] - \mu_{R_{eb}} \varepsilon_{oei}[n] \frac{i_{c\cdot p}[n]}{R_{eb}} \quad (4.22)$$

4.2.2. Updating a_k

As noted above, neither the measured current $i_{c\cdot m}[n]$ nor the predicted force $f_{c\cdot p}[n]$ depend on the feedback coefficients a_k . Therefore the derivative of the error with respect to a_k is that of a standard output-error IIR algorithm where the IIR filter concerned is that for the mechanical mobility. Thus generally one has

$$\begin{aligned} \frac{\partial}{\partial a_k} \varepsilon_{oei}[n] &= \frac{\partial}{\partial a_k} (-i_{c\cdot p}[n]) \\ &= -\frac{\partial}{\partial a_k} \frac{1}{R_{eb}} [v_{c\cdot m}[n] - \phi_0 u_d[n]] \\ &= \frac{\phi_0}{R_{eb}} \frac{\partial}{\partial a_k} u_d[n] \end{aligned} \quad (4.23)$$

The derivative of the velocity predicted from the force equation $u_d[n]$ with respect to the feedback coefficients a_k is

$$\frac{\partial}{\partial a_k} u_d[n] = -u_d[n-k] - a_1 \frac{\partial u_d[n-1]}{\partial a_k} - a_2 \frac{\partial u_d[n-2]}{\partial a_k}. \quad (4.24)$$

By defining

$$\alpha_k[n] = \frac{\partial}{\partial a_k} u_d[n], \quad (4.25)$$

the derivative of $u_d[n]$ with respect to the feedback coefficients a_k may be calculated iteratively according to

$$\alpha_k[n] = -u_d[n-k] - a_1\alpha_k[n-1] - a_2\alpha_k[n-2]. \quad (4.26)$$

The instantaneous estimate of the gradient of the error surface along the parameter a_k is therefore given by

$$\begin{aligned} \hat{d}_{a_k}[n] &= \varepsilon[n] \frac{\partial \varepsilon_{eo}[n]}{\partial a_k} \\ &= \varepsilon[n] \frac{\phi_0}{R_{eb}} \alpha_k[n] \end{aligned} \quad (4.27)$$

where $\alpha_k[n]$ is calculated iteratively as per (4.26). The a_k parameters are updated according to the LMS algorithm as so:

$$a_k[n+1] = a_k[n] - \mu_{a_k} \hat{d}_{a_k}[n] \quad (4.28)$$

where μ_{a_k} is a convergence parameter specific to a_k . Summing up explicitly, this is

$$a_k[n+1] = a_k[n] - \mu_{a_k} \varepsilon[n] \frac{\phi_0}{R_{eb}} \alpha_k[n] \quad (4.29)$$

4.2.3. Updating of σ_u as a feedforward coefficient

The partial derivative of the error with respect to the overall gain of the mobility is given by

$$\frac{\partial}{\partial \sigma_u} \varepsilon_{eo}[n] = \frac{\partial}{\partial \sigma_u} (-i_{c,p}[n]) = \frac{\partial}{\partial \sigma_u} \left(- \left[\frac{1}{R_{eb}} v_c[n] - \frac{\phi_0}{R_{eb}} u_d[n] \right] \right) = \frac{\phi_0}{R_{eb}} \frac{\partial}{\partial \sigma_u} u_d[n] \quad (4.30)$$

The partial derivative of the velocity $u_d[n]$ with respect to the overall gain σ_0 is

$$\frac{\partial}{\partial \sigma_u} u_{d,f}[n] = f_{c,p}[n] - f_{c,p}[n-2] - a_1 \frac{\partial u_{d,f}[n-1]}{\partial \sigma_u} - a_2 \frac{\partial u_{d,f}[n-2]}{\partial \sigma_u} \quad (4.31)$$

The partial derivative of the velocity $u_d[n]$ with respect to σ_0 may be defined as $\beta_{\sigma_0}[n]$, and calculated recursively as so

$$\beta_{\sigma_u}[n] = f_{c,p}[n] - f_{c,p}[n-2] - a_1 \beta_{\sigma_u}[n-1] - a_2 \beta_{\sigma_u}[n-2] \quad (4.32)$$

The term σ_0 is then updated in the traditional manner as so

$$\sigma_u[n+1] = \sigma_u[n] - \mu_{\sigma_u} \varepsilon[n] \frac{\phi_0}{R_{eb}} \beta_{\sigma_u}[n] \quad (4.33)$$

Attempting to update σ_u in this manner leads to poor convergence of the parameters in general. This is understood to be a reflection of the fact that σ_u is not an independent parameter; it is determined directly by a_2 , as explained in §2.3.2, above. For this reason, a different approach to updating this parameter is taken, which is explained in the next section.

4.2.4. Updating of σ_u as a dependent variable, defined by a_2

It is shown in §2.3.2 that σ_u can be accurately approximated as a third-order polynomial function of a_2 as so

$$\sigma_u(a_2) = \frac{1}{m_t F_s} \sum_{n=0}^3 p_{\sigma_u \cdot n} a_2^n \quad (4.34)$$

Thus σ_u may be determined from updated values of a_2 , instead of being updated as an adaptive filter coefficient. Thus its derivative with respect to the error $\varepsilon_{oei}[n]$ is not considered.

However, it is important to note that calculating σ_u as per (4.34) changes the derivative of the error with respect to a_2 , because σ_u becomes a function of a_2 . To consider how to re-write the derivative of the error $\varepsilon_{oei}[n]$ with respect to a_2 , the derivative of σ_u is first considered. With σ_u defined as (4.34), its partial derivative w.r.t a_2 is defined as, and calculated by

$$\begin{aligned} \partial_{a_2} \sigma_u(a_2) &\doteq \frac{\partial \sigma_u}{\partial a_2} \\ &= \frac{1}{m_t F_s} \sum_{n=0}^{N-1} n p_{\sigma_u \cdot n+1} a_2^{n-1} \end{aligned} \quad (4.35)$$

With this definition and method for calculation of the derivative of σ_u with respect to a_2 , the derivative of the error $\varepsilon_{oei}[n]$ with respect to a_2 , originally given in (4.26), becomes

$$\frac{\partial}{\partial a_2} \varepsilon_{oei}[n] = \frac{\partial}{\partial a_2} u_d[n] = \partial_{a_2} \sigma_u(f_{c \cdot p}[n] - f_{c \cdot p}[n-2]) - u_d[n-2] - a_1 \frac{\partial u_d[n-1]}{\partial a_2} - a_2 \frac{\partial u_d[n-2]}{\partial a_2} \quad (4.36)$$

We again define $\alpha_2[n] = \partial/\partial a_2 u_{d,f}[n]$ and calculate it recursively as

$$\alpha_2[n] = \partial_{a_2} \sigma_u(f_{c \cdot p}[n] - f_{c \cdot p}[n-2]) - u_{d,f}[n-2] - a_1 \alpha_2[n-1] - a_2 \alpha_2[n-2] \quad (4.37)$$

This value of $\alpha_2[n]$ is therefore used in (4.29), instead of that given before in (4.26), for updating a_2 .

4.2.5. Partial derivative of $\varepsilon_{oei}[n]$ with respect to ϕ_0

The partial derivative of the error $\varepsilon_{oei}[n]$ with respect to the transduction coefficient ϕ_0 is given by

$$\begin{aligned} \frac{\partial}{\partial \phi_0} \varepsilon_{oei}[n] &= \frac{\partial}{\partial \phi_0} (-i_{c \cdot p}[n]) \\ &= \frac{\partial}{\partial \phi_0} \frac{\phi_0}{R_{eb}} u_d[n] \\ &= \frac{1}{R_{eb}} u_d[n] + \frac{\phi_0}{R_{eb}} \frac{\partial}{\partial \phi_0} u_d[n] \end{aligned} \quad (4.38)$$

Given the definition of $u_d[n]$ in (4.12), its derivative with respect to ϕ_0 is given by

$$\frac{\partial}{\partial \phi_0} u_d[n] = \sigma_u(i_{c \cdot m}[n] - i_{c \cdot m}[n-2]) - a_1 \frac{\partial}{\partial \phi_0} u_d[n-1] - a_2 \frac{\partial}{\partial \phi_0} u_d[n-2]. \quad (4.39)$$

This is defined as $\partial_{\phi u}[n]$ and calculated recursively as

$$\partial_{\phi u}[n] = \sigma_u(i_{c \cdot m}[n] - i_{c \cdot m}[n-2]) - a_1 \partial_{\phi u}[n-1] - a_2 \partial_{\phi u}[n-2]. \quad (4.40)$$

Therefore, explicitly, the partial derivative of the error $\varepsilon_{oei}[n]$ with respect to ϕ_0 is

$$\frac{\partial}{\partial \phi_0} \varepsilon_{oei}[n] = \frac{1}{R_{eb}} u_d[n] + \frac{\phi_0}{R_{eb}} \partial_{\phi u}[n] \quad (4.41)$$

where $\partial_{\phi_0}[n]$ is calculated recursively as per (4.40). Therefore the instantaneous estimate of the gradient of the error surface along the parameter ϕ_0 is

$$\hat{d}_{\phi_0}[n] = \varepsilon[n] \left(\frac{1}{R_{eb}} u_d[n] + \frac{\phi_0}{R_{eb}} \partial_{\phi_0}[n] \right) \quad (4.42)$$

and thus the update equation

$$\phi_0[n+1] = \phi_0[n] - \mu_{\phi_0} \hat{d}_{\phi_0}[n] \quad (4.43)$$

is given explicitly by

$$\phi_0[n+1] = \phi_0[n] - \mu_{\phi_0} \varepsilon[n] \left(\frac{1}{R_{eb}} u_d[n] + \frac{\phi_0}{R_{eb}} \partial_{\phi_0}[n] \right) \quad (4.44)$$

4.2.6. Convergence performance

The convergence performance of the electrical current output error adaptive algorithm has been investigated for a variety of signals and initial values. These are presented in Figure 4.11 - Figure 4.28, as per Table 4.1.

Input signal	Initial a_n val.	Time span of plots	(page)	a_n plots	$\zeta, \omega_0, R_{eb}, \phi_0$ plots	Q_{tc}, Q_{ms} , Err plots
Noise, 0-2kHz	Upper right	30s	p. 118	Figure 4.11	Figure 4.12	Figure 4.13
Noise, 0-2kHz	Upper left	30s	p. 119	Figure 4.14	Figure 4.15	Figure 4.16
Noise, 0-2kHz	Lower left	30s	p. 120	Figure 4.17	Figure 4.18	Figure 4.19
Noise, 0-2kHz	Lower right	46s	p. 121	Figure 4.20	Figure 4.21	Figure 4.22
Speech, Male	Lower left	80s	p. 122	Figure 4.23	Figure 4.24	Figure 4.25
Music	Lower left	160s	p. 123	Figure 4.26	Figure 4.27	Figure 4.28

Table 4.1: Figure numbers for different input signals and settings of initial values of a_n .

The convergence performance using white noise is relatively good. The resonance frequency f_0 is identified (from an initial guess of at least 20% away from its actual value) in as quickly as two seconds. Identification of the damping ratio ζ is slower, being identified in approximately 10 to 20 seconds, depending on whether the initial guess is above or below the actual value. The mechanical and total resonance quality values, Q_{ms} and Q_{tc} respectively, are determined from the damping ratio ζ , and thus also require 10 to 20 seconds to be identified. One exception to these convergence times is the case for which the initial guess of a_n is in the lower right corner of the tolerance quadrilateral, shown in Figure 4.20 - Figure 4.22, on p. 121.

Convergence for the speech and music signals is considerably slower than for the white noise signal. As per Figure 4.24, for the speech signal the resonance frequency is identified in about 10 seconds, and the damping ratio is identified after 70 seconds. Approximately the same performance is seen for the music signal. This may be a considerable problem for actual product implementation. Techniques for obtaining faster convergence performance without increasing variance in the converged parameters may be a subject of further research.

The accuracy of the values to which the parameters converged, by comparison to values measured using other laboratory techniques, is quite good. Further detail is presented in §4.2.7.

Convergence for initial values of a_1, a_2 in upper-right corner of tolerance quadrilateral

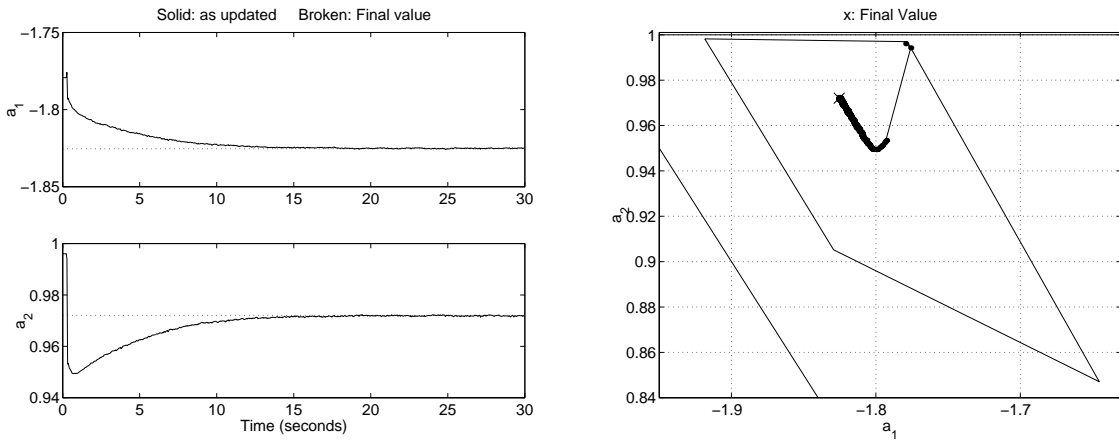


Figure 4.11: [left] a_1 and a_2 vs. time; [right] a_1 vs. a_2 .

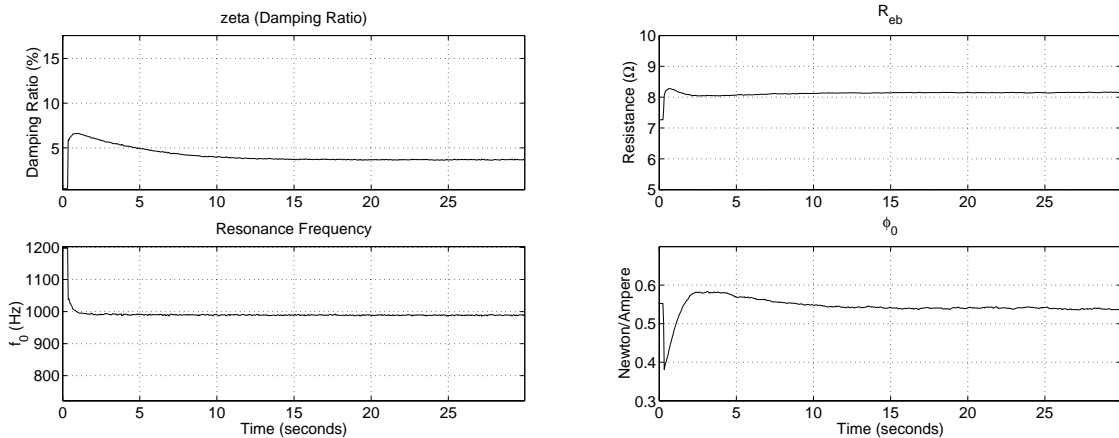


Figure 4.12: [left, upper]: Damping ratio (ζ); [left, lower]: Resonance Frequency; [right, upper] DC (blocked) electrical resistance (R_{eb}); [right, lower]: Transduction coefficient (ϕ_0).

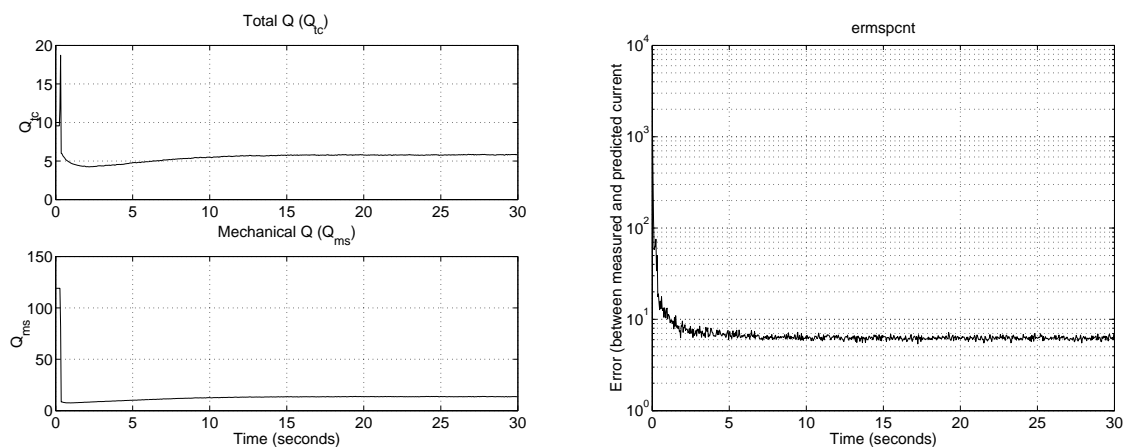
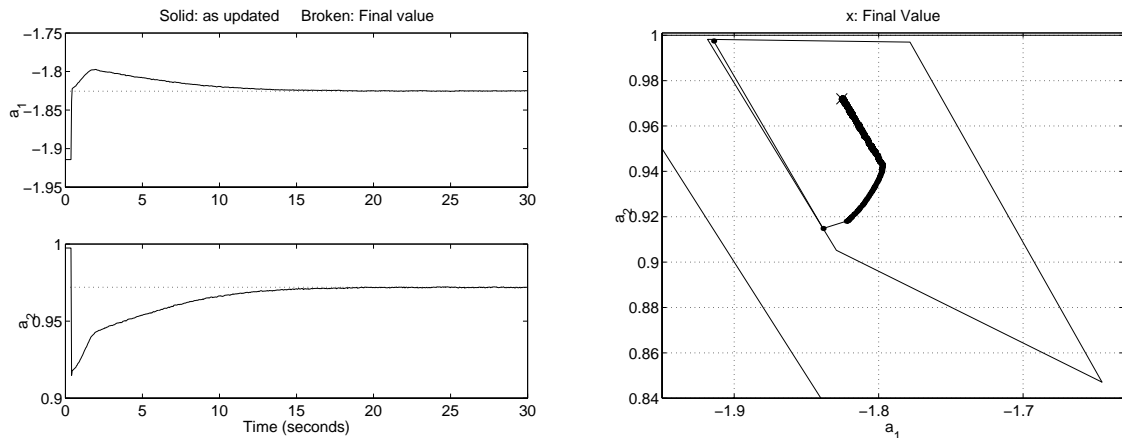
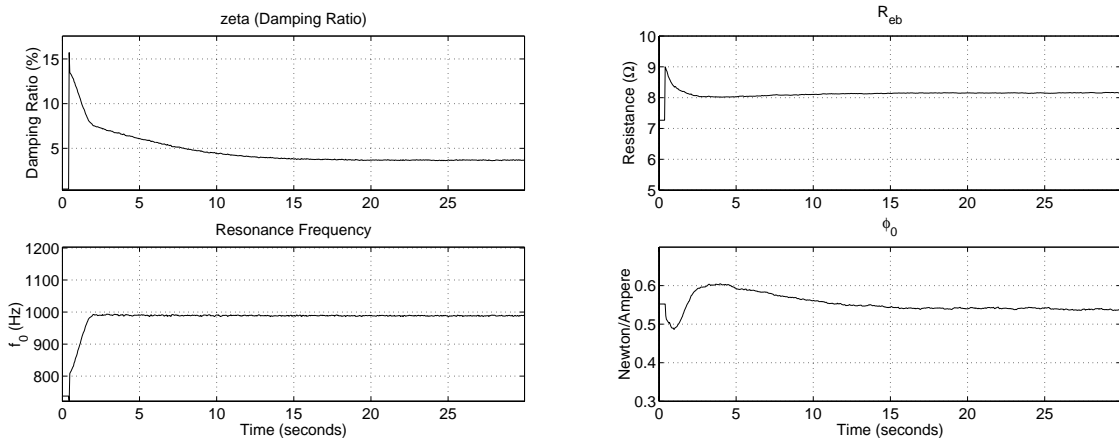
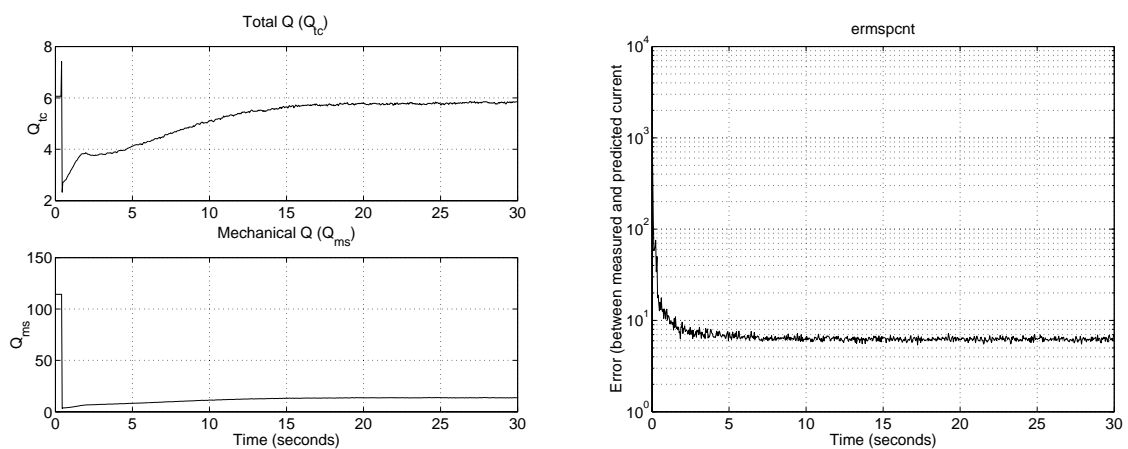


Figure 4.13: [left, upper]: Total Q -factor (Q_{tc}); [left, lower]: Mechanical Q -factor; [right]: Percentage error.

Convergence for initial values of a_1, a_2 in upper-left corner of tolerance quadrilateralFigure 4.14: [left] a_1 and a_2 vs. time; [right] a_1 vs. a_2 .Figure 4.15: [left, upper]: Damping ratio (ζ); [left, lower]: Resonance Frequency; [right, upper] DC (blocked) electrical resistance (R_{eb}); [right, lower]: Transduction coefficient (ϕ_0).Figure 4.16: [left, upper]: Total Q -factor (Q_{ic}); [left, lower]: Mechanical Q -factor; [right]: Percentage error.

Convergence for initial values of a_1, a_2 in lower-left corner of tolerance quadrilateral

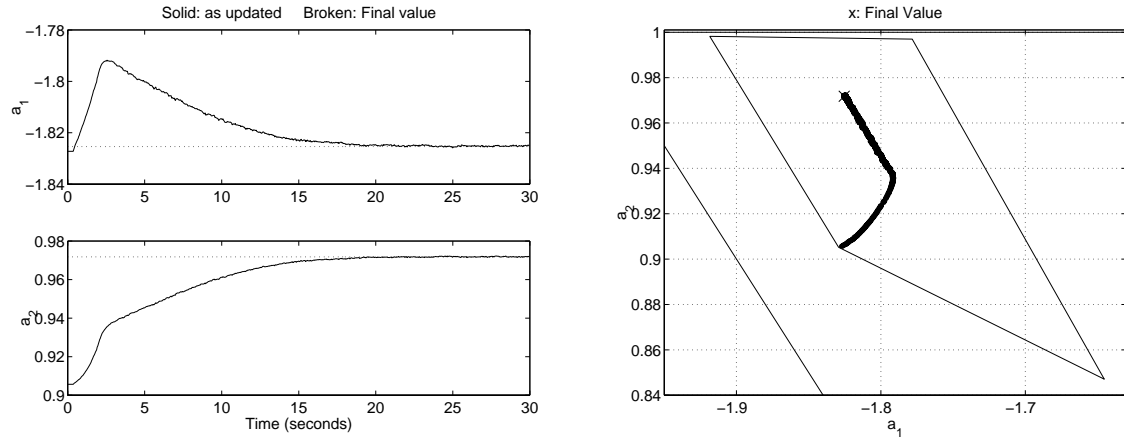


Figure 4.17: [left] a_1 and a_2 vs. time; [right] a_1 vs. a_2 .

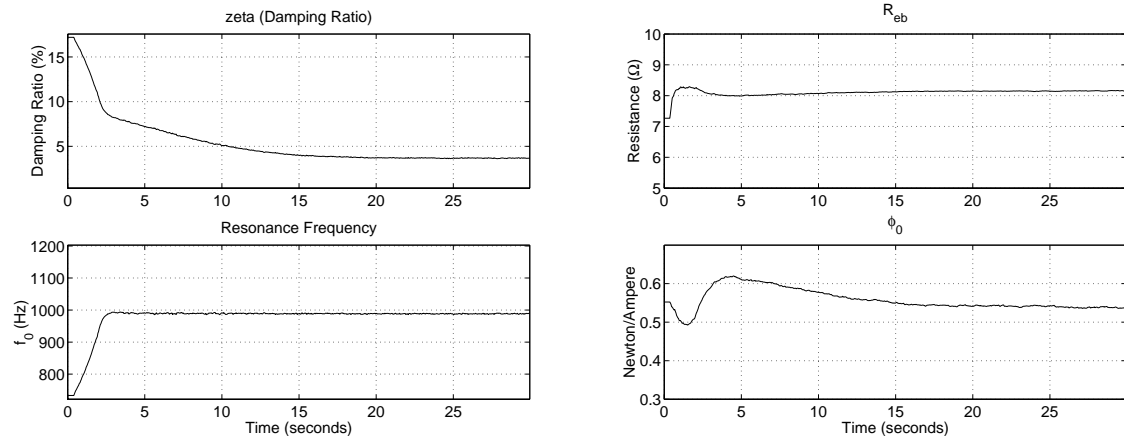


Figure 4.18: [left, upper]: Damping ratio (ζ); [left, lower]: Resonance Frequency; [right, upper] DC (blocked) electrical resistance (R_{eb}); [right, lower]: Transduction coefficient (ϕ_0).

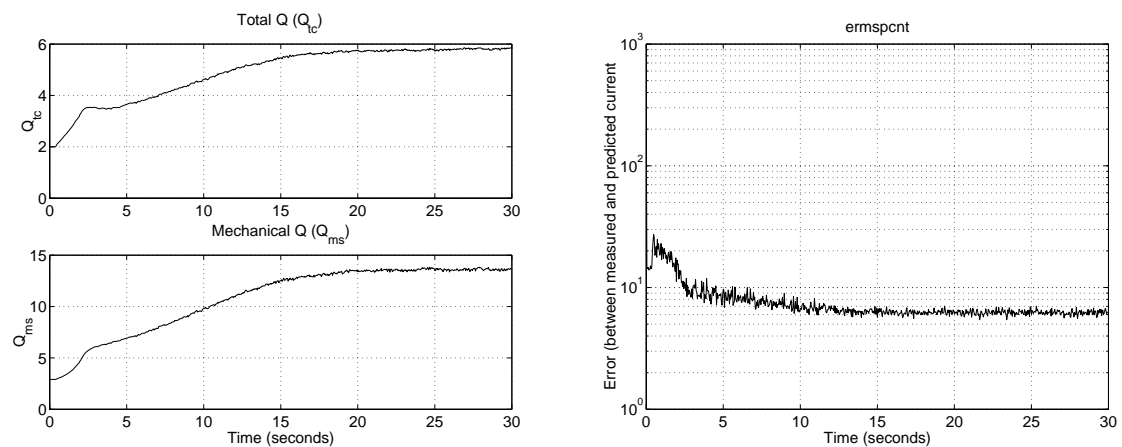


Figure 4.19: [left, upper]: Total Q -factor (Q_{tc}); [left, lower]: Mechanical Q -factor; [right]: Percentage error.

Convergence for initial values of a_1, a_2 in lower-right corner of tolerance quadrilateral

Note: time axis is from 0 to 46.5 secs.; previous graphs were from 0 to 30 secs.

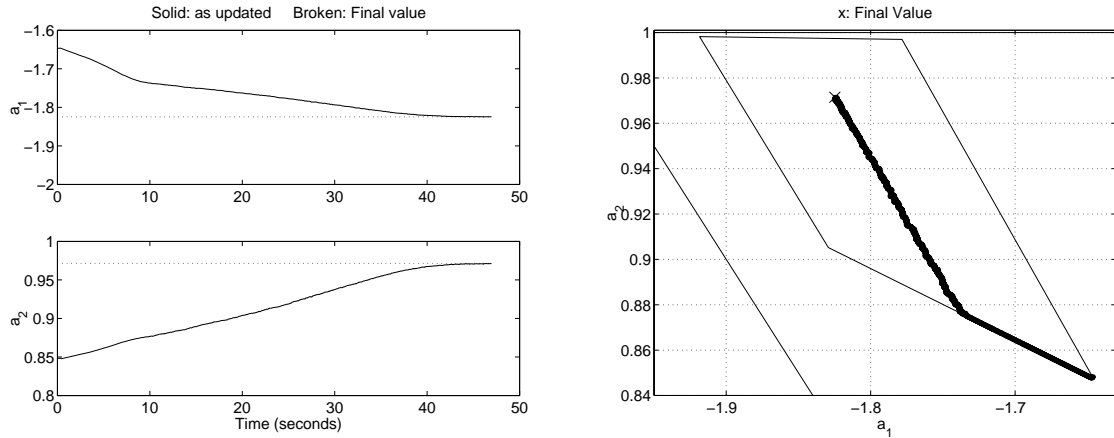


Figure 4.20: [left] a_1 and a_2 vs. time; [right] a_1 vs. a_2 .

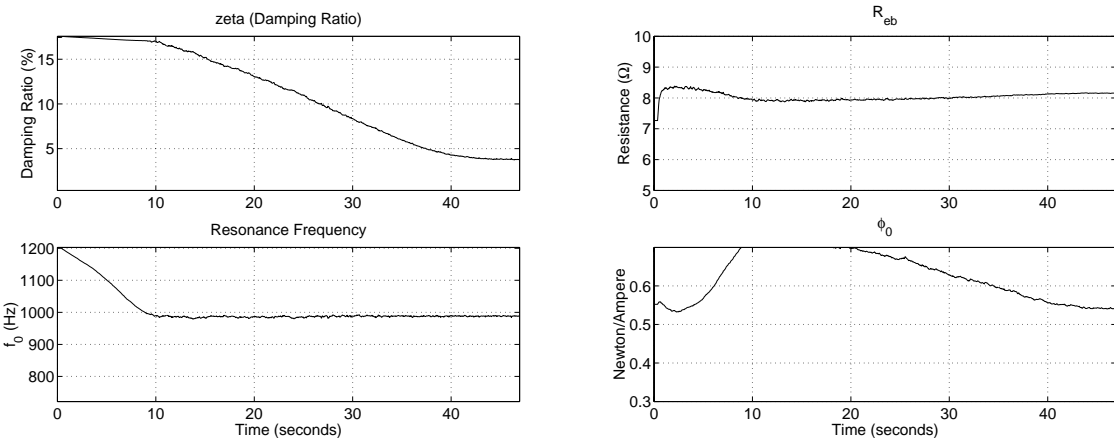


Figure 4.21: [left, upper]: Damping ratio (ζ); [left, lower]: Resonance Frequency; [right, upper] DC (blocked) electrical resistance (R_{eb}); [right, lower]: Transduction coefficient (ϕ_0).

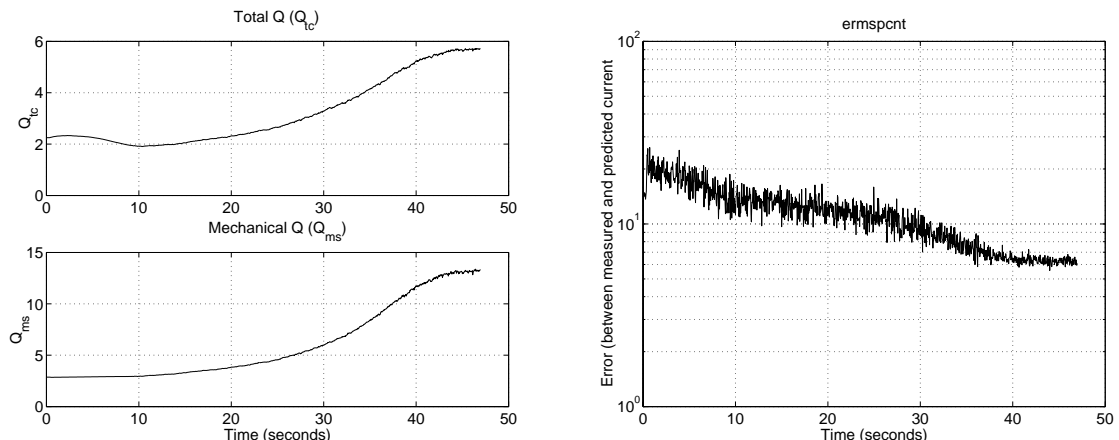


Figure 4.22: [left, upper]: Total Q -factor (Q_{tc}); [left, lower]: Mechanical Q -factor; [right]: Percentage error.

Convergence for initial values of a_1, a_2 in lower-left corner of tolerance quadrilateral
 Signal: Male speech; speech activity duty cycle: 50%.

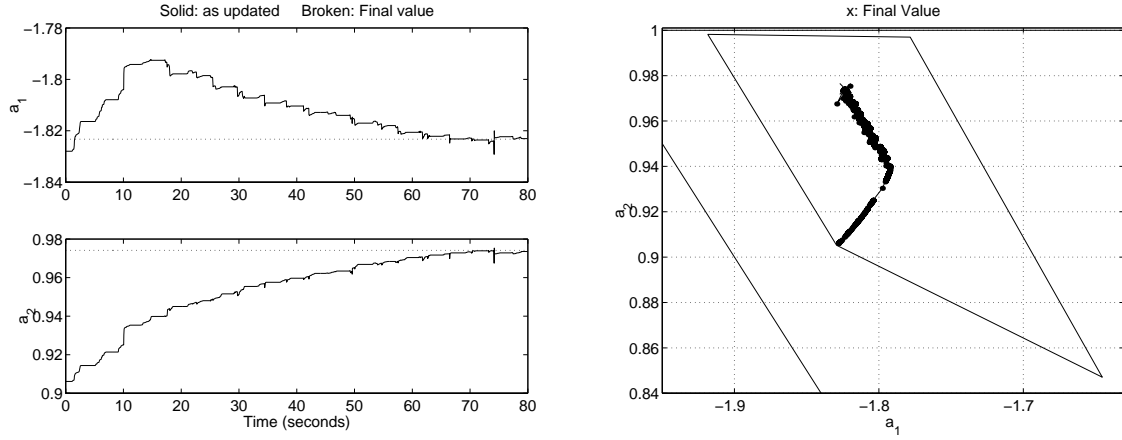


Figure 4.23: [left] a_1 and a_2 vs. time; [right] a_1 vs. a_2 .

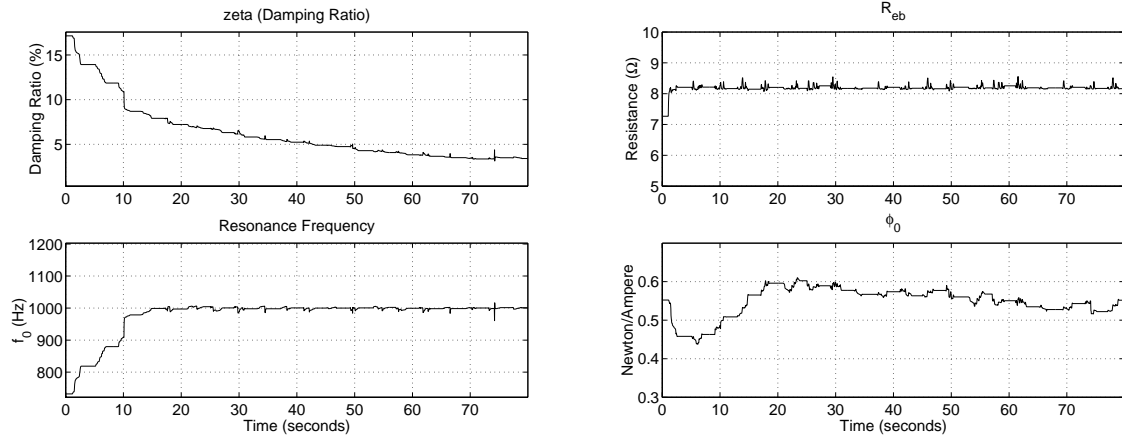


Figure 4.24: [left, upper]: Damping ratio (ζ); [left, lower]: Resonance Frequency; [right, upper]: DC (blocked) electrical resistance (R_{eb}); [right, lower]: Transduction coefficient (ϕ_0).

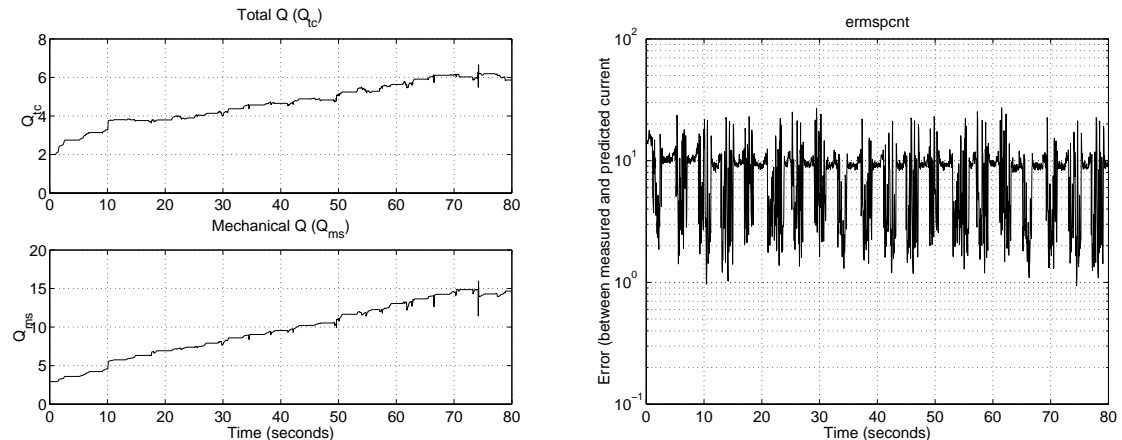


Figure 4.25: [left, upper]: Total Q -factor (Q_{tc}); [left, lower]: Mechanical Q -factor; [right]: Percentage error.

Convergence for initial values of a_1, a_2 in lower-left corner of tolerance quadrilateral
Signal: Music¹

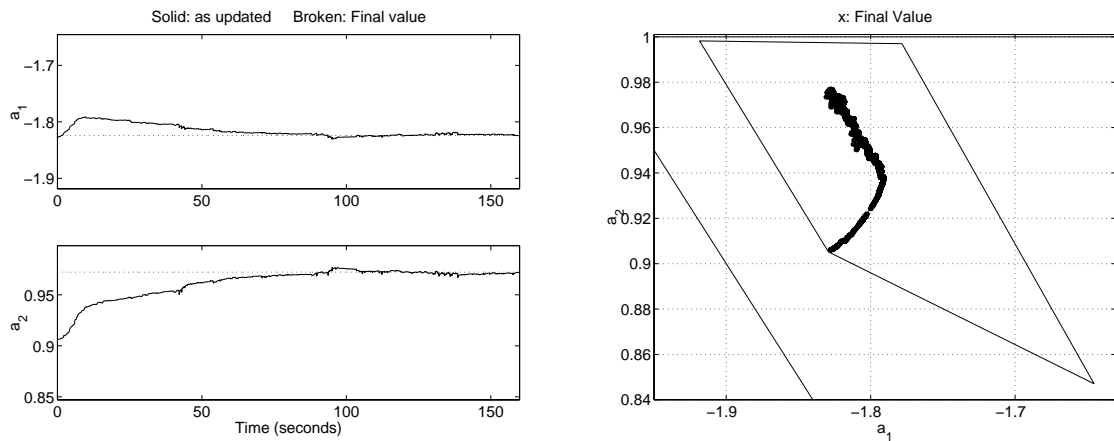


Figure 4.26: [left] a_1 and a_2 vs. time; [right] a_1 vs. a_2 .

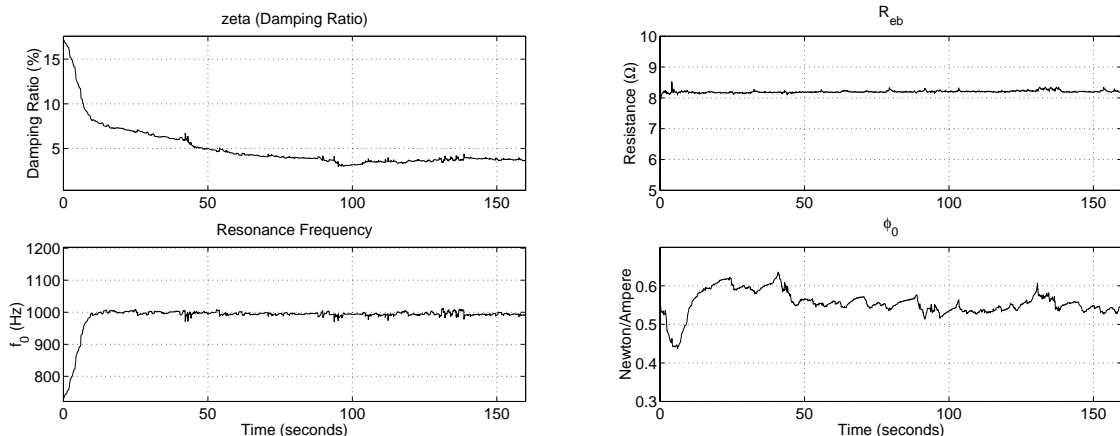


Figure 4.27: [left, upper]: Damping ratio (ζ); [left, lower]: Resonance Frequency; [right, upper]: DC (blocked) electrical resistance (R_{eb}); [right, lower]: Transduction coefficient (ϕ_0).

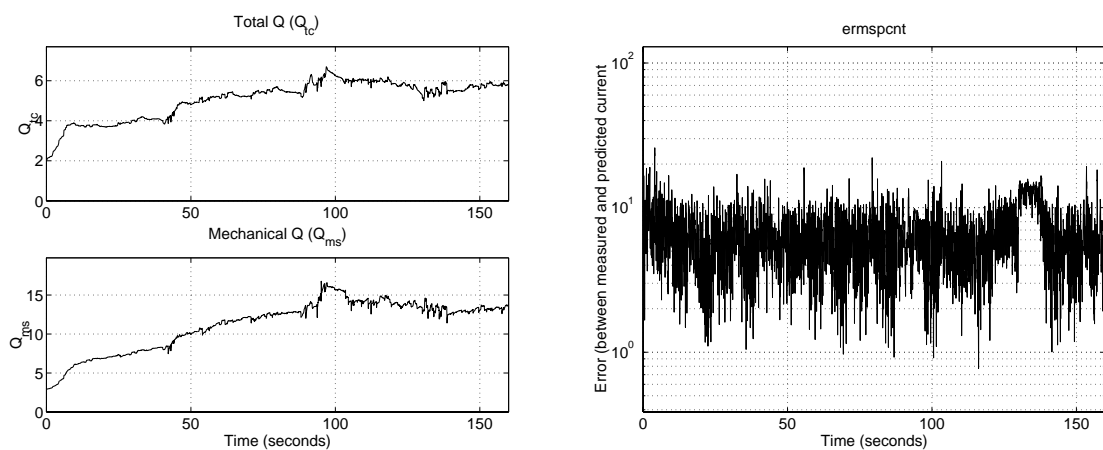


Figure 4.28: [left, upper]: Total Q -factor (Q_{tc}); [left, lower]: Mechanical Q -factor; [right]: Percentage error.

¹ The music used was a ‘popular music’ song, artist: DJ Spiller, title: *Groovejet*, © 2000 Positiva Records.

4.2.7. Accuracy of the converged parameters for the current output-error form

The accuracy of the values to which adaptive algorithm converged has been assessed by comparison between frequency response function (FRF) synthesised from the converged parameters, and actual measurement of the FRF.

The voltage-to-displacement FRF was measured using a laser displacement vibrometer based on a fringe-counter signal decoder. Further details of the experimental set-up are given in Appendix A. This measured FRF is the red curve plotted in Figure 4.29 (magnitude) and in Figure 4.30 (phase).

The same voltage-to-displacement FRF has been synthesised using with the z -transform of (2.86) (setting $z = e^{i\omega T_s}$), using the values of R_{eb} , ϕ_0 , a_1 , and a_2 to which the adaptive algorithm converged. This synthesised function is the blue curve plotted in Figure 4.29 (magnitude) and in Figure 4.30 (phase).

To ensure proper functioning of the prediction of the diaphragm-coil displacement $x_d[n]$, the predicted displacement was fed to the analogue output of one channel of the processing hardware. This ‘predicted’ displacement signal was measured with the same frequency response analyser, and is shown as the green curve in Figure 4.29 (magnitude) and in Figure 4.30 (phase). This predicted signal (in green) closely corresponds to the synthesised FRF (in blue), and it is thus concluded that the displacement is being predicted correctly.

As can be seen in Figure 4.29 and Figure 4.30, the measured value (in red) deviates from the value synthesised from the converged parameters (in blue) at frequencies below 180Hz and at around 1.7kHz. The deviation below 180Hz is explained by a small leak in the rear cavity in which the microspeaker was mounted. Below approximately 180Hz, the acoustic stiffness of the rear cavity is lost, resulting in a higher receptance sensitivity. Above 180Hz, acoustic resistance of air flow in the leak is high enough to render the leak negligible, and thus the effective acoustic stiffness of the cavity appears in the measured receptance functions.

The aberration 1.7kHz is due to a rocking mode present in the microspeaker’s vibration dynamics. This is due to the single-suspension construction of the microspeaker, as discussed in §2.1. This phenomenon is discussed in detail in Appendix D.

The signal used for the FRF measurement was white noise, with a bandwidth of 0 to 2 kHz. As there is no significant spectral content above 2.5kHz, the FRF measurements are very ‘noisy’ above this frequency.

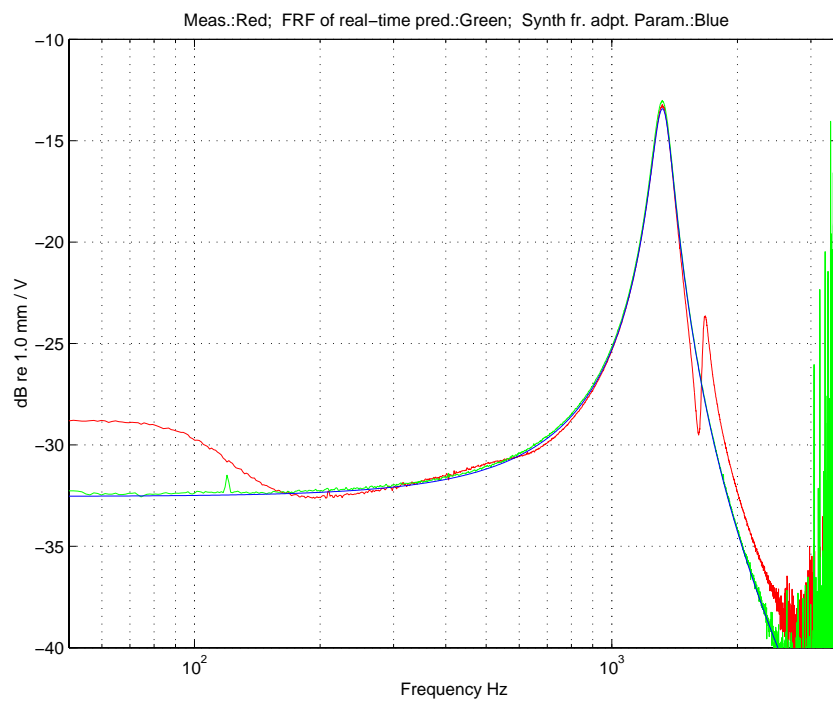


Figure 4.29: Magnitude of measured receptance (red) vs. synthesised receptance from converged parameter values (blue), and measurement of predicted displacement / voice-coil voltage, where the displacement is predicted by the algorithm (green).

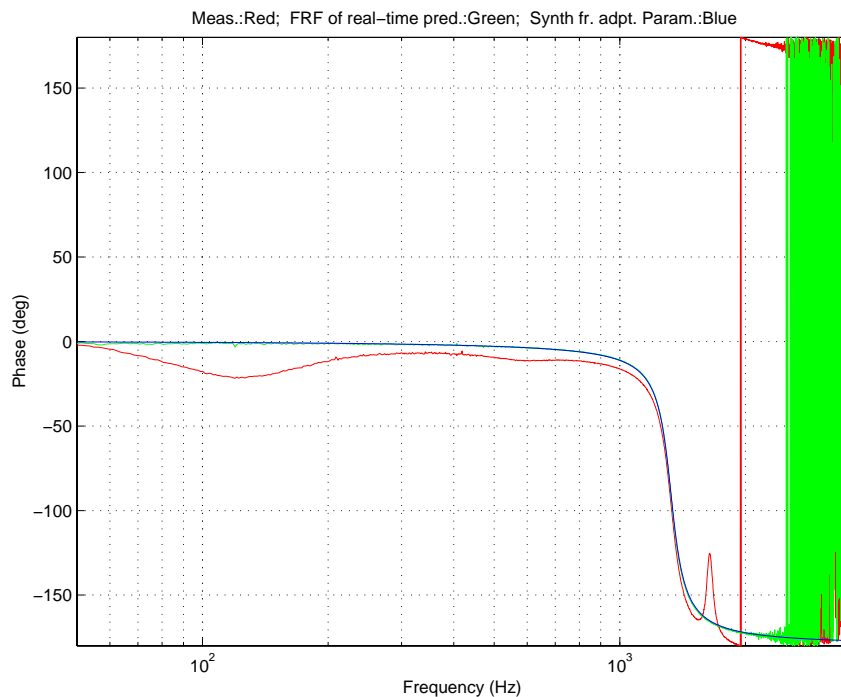


Figure 4.30: Phase of measured receptance (red) vs. synthesised receptance from converged parameter values (blue), and measurement of predicted displacement / voice-coil voltage, where the displacement is predicted by the algorithm (green).

4.2.8. Updating ϕ_k

In addition to the determination of parameters defining the linear properties of the loudspeaker, it may also be interesting to see whether the nonlinear characteristics of the loudspeaker can be identified. Here, the nonlinear property of the loudspeaker considered is the nonuniformity in the transduction coefficient, as discussed in §2.2.1 part A.

Following the general strategy presented by Klippel (1999), the approach presented here is to define nonuniformity of the transduction coefficient as a polynomial expansion in x_d (the diaphragm-coil displacement). The derivatives of the coefficients of this polynomial expansion are defined with respect to an error signal. The polynomial coefficients are then iteratively updated using these derivatives according to the standard LMS algorithm. The difference between the presentation here and that given by Klippel is that an electrical current output-error signal as per Figure 4.10 is considered here, instead of the velocity equation error signal used by Klippel.

An important initial problem to be considered is the derivative of $\phi(x_d[n])$ with respect to ϕ_k . Consider the description of $\phi(x)$ in §2.2.1, part A, above wherein it is described as an N_ϕ^{th} -order polynomial expansion in $x_d[n]$.

Given that $x_d[n]$ depends on ϕ_k , the derivative of $\phi(x_d[n])$ with respect to ϕ_k is given by

$$\frac{\partial}{\partial \phi_k} \phi(x_d[n]) = x_d^k[n] + \phi_1 \frac{\partial}{\partial \phi_k} x_d[n] + \phi_2 \frac{\partial}{\partial \phi_k} x_d^2[n] + \dots + \phi_{N_\phi} \frac{\partial}{\partial \phi_k} x_d^{N_\phi}[n]. \quad (4.45)$$

The displacement $x_d[n]$ is calculated from the measured current $i_{c,m}[n]$, as described in (4.14) and (4.13). This calculation involves the use of $\phi(x_d[n])$. Therefore we treat $x_d[n]$ as a function of ϕ_k . In this way, the derivative of the l^{th} -power of $x_d[n]$ with respect to ϕ_k is

$$\frac{\partial}{\partial \phi_k} x_d^l[n] = l x_d^{l-1}[n] \frac{\partial}{\partial \phi_k} x_d[n] \quad (4.46)$$

Given the formula for calculating the displacement $x_d[n]$ from the measured coil current $i_{c,m}[n]$ in (4.14) and (4.13), the derivative of the displacement $x_d[n]$ with respect to ϕ_k is

$$\frac{\partial}{\partial \phi_k} x_d[n] = \sigma_x \frac{\partial}{\partial \phi_k} \phi(x_d[n-1]) i_{c,m}[n] - a_1 \frac{\partial}{\partial \phi_k} x_d[n-1] - a_2 \frac{\partial}{\partial \phi_k} x_d[n-2]. \quad (4.47)$$

By defining this derivative as $\partial_{\phi_k x_d}[n]$, it may be calculated recursively as so:

$$\partial_{\phi_k x_d}[n] = \sigma_x \frac{\partial}{\partial \phi_k} \phi(x_d[n-1]) i_{c,m}[n-1] - a_1 \partial_{\phi_k x_d}[n-1] - a_2 \partial_{\phi_k x_d}[n-2]. \quad (4.48)$$

With this definition the derivative of the l^{th} -power of $x_d[n]$ with respect to ϕ_k in (4.46) may be expressed as

$$\frac{\partial}{\partial \phi_k} x_d^l[n] = l x_d^{l-1}[n] \partial_{\phi_k x_d}[n] \quad (4.49)$$

Substituting this expression into in the definition of the derivative of $\phi(x_d[n])$ with respect to ϕ_k in (4.45) gives:

$$\frac{\partial}{\partial \phi_k} \phi(x_d[n]) = x_d^k[n] + \partial_{\phi_k x_d}[n] \sum_{l=1}^{N_\phi} \phi_l l x_d^{l-1}[n] \quad (4.50)$$

The summation term in (4.50) is in fact $\partial\phi(x_d[n])/\partial x_d[n]$. An important feature of this summation is that it is not specific to k . Therefore it need be calculated only once, and the same value may be used for all of the ϕ_k derivatives. For this reason it is abbreviated as $\phi(\partial x_d[n])$ such that (4.50) may be expressed as

$$\frac{\partial}{\partial \phi_k} \phi(x_d[n]) = x_d^k[n] + \partial_{\phi_k x_d}[n] \phi(\partial x_d[n]) \quad (4.51)$$

This definition makes possible the following explicit recursive formula for $\partial_{\phi_k x_d}[n]$:

$$\partial_{\phi_k x_d}[n] = \sigma_x \left(x_d^k[n-1] + \partial_{\phi_k x_d}[n-1] \phi(\partial x_d[n-1]) \right) i_{c \cdot m}[n-1] - a_1 \partial_{\phi_k x_d}[n-1] - a_2 \partial_{\phi_k x_d}[n-2]. \quad (4.52)$$

The importance of the ‘predictive’ nature of the discrete-time representation of the mechanical mobility developed in §2.3.4 is revealed again in (4.52); were it not to be predictive, (4.52) would be an implicit, and not an explicit equation.

For convenience, the derivative of $\phi(x_d[n])$ with respect to ϕ_k is abbreviated as $\partial_{\phi_k \phi}[n]$.

With the above definitions, it is possible to consider the derivative the error $\varepsilon_{eo}[n]$ with respect to ϕ_k . The only term in the error which depends on ϕ_k is the velocity term $u_d[n]$, and thus:

$$\begin{aligned} \frac{\partial}{\partial \phi_k} \varepsilon_{eo}[n] &= \frac{\partial}{\partial \phi_k} \left(\frac{\phi(x_m[n])}{R_{eb}} u_{m \cdot d}[n] \right) \\ &= \frac{u_{m \cdot d}[n]}{R_{eb}} \partial_{\phi_k \phi}[n] + \frac{\phi(x_m[n])}{R_{eb}} \partial_{\phi_k u}[n] \end{aligned} \quad (4.53)$$

The term $\partial_{\phi_k u}[n]$ is the derivative of the velocity $u_d[n]$ with respect to ϕ_k . It is calculated recursively in a manner similar to parametric derivatives of u_d , e.g. a_n described in §4.2.2, as so:

$$\partial_{\phi_k u}[n] = \sigma_u \left(\partial_{\phi_k \phi}[n] i_{c \cdot m}[n] - \partial_{\phi_k \phi}[n-2] i_{c \cdot m}[n-2] \right) - a_1 \partial_{\phi_k u}[n-1] - a_2 \partial_{\phi_k u}[n-2] \quad (4.54)$$

Summarising concisely, one first calculates for all k

$$\phi(\partial x_d[n]) = \sum_{l=1}^{N_\phi} l \phi_l x_d^{l-1}[n]$$

Then for each k , one calculates

$$\partial_{\phi_k x_d}[n] = \sigma_x \partial_{\phi_k \phi}[n-1] i_{c \cdot m}[n-1] - a_1 \partial_{\phi_k x_d}[n-1] - a_2 \partial_{\phi_k x_d}[n-2]$$

From which is calculated

$$\partial_{\phi_k \phi}[n] = x_d^k[n] + \partial_{\phi_k x_d}[n] \phi(\partial x_d[n])$$

With which is calculated

$$\partial_{\phi_k u}[n] = \sigma_u \left(\partial_{\phi_k \phi}[n] i_{c \cdot m}[n] - \partial_{\phi_k \phi}[n-2] i_{c \cdot m}[n-2] \right) - a_1 \partial_{\phi_k u}[n-1] - a_2 \partial_{\phi_k u}[n-2]$$

With which one calculates

$$\frac{\partial}{\partial \phi_k} \varepsilon_{eo}[n] = \frac{u_d[n]}{R_{eb}} \partial_{\phi_k \phi}[n] + \frac{\phi(x_d[n])}{R_{eb}} \partial_{\phi_k u}[n]$$

The convergence of values of the coefficients ϕ_k using this algorithm was found to be poor. Convergence is either unstable or slow (depending on the convergence parameter values), and did not

consistently converge to the same values for the same loudspeaker & signal. At the time of writing it was not clear why good convergence could not be achieved. Further investigation of techniques for determining values of ϕ_k using this method is suggested as a topic for further research.

4.3. Voltage output-error form

We consider a traditional output error form where an error signal is derived from

$$\epsilon_{oev}[n] = v_{cm}[n] - v_{cp}[n] \quad (4.55)$$

where $v_{cm}[n]$ is the measured voltage signal, and $v_{cp}[n]$ is the predicted voltage signal. A block diagram of this form for system identification is shown in Figure 4.31.

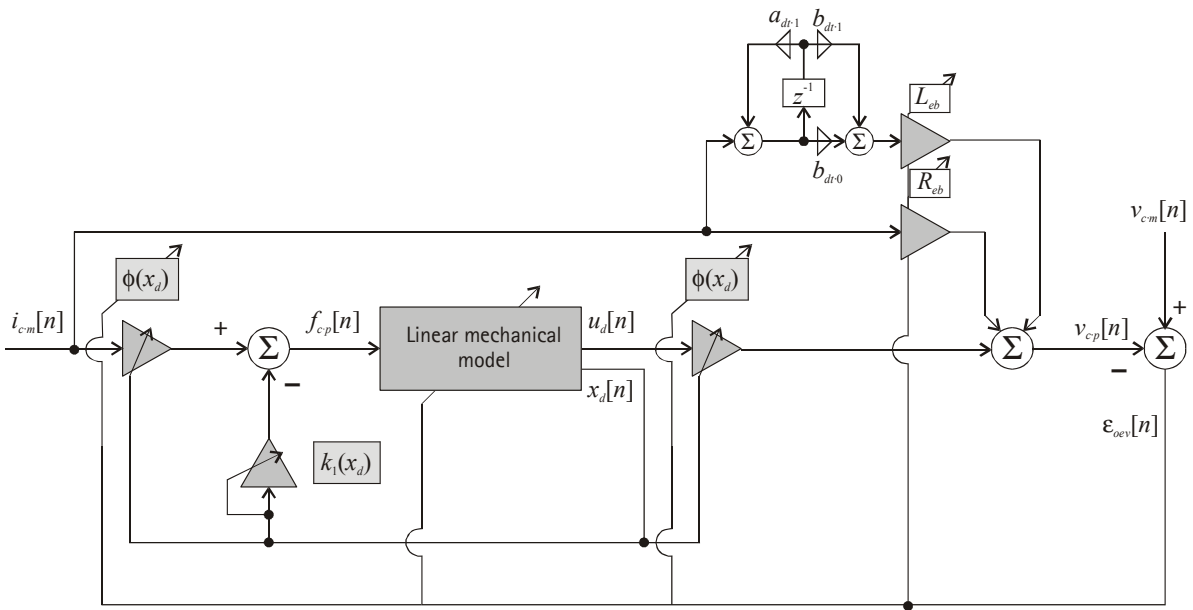


Figure 4.31: Block diagram of the voltage output error form for loudspeaker system identification. Notice that this form of the updating algorithm includes L_{eb} , as per (4.57), below.

The ‘measured’ voltage signal $v_{cm}[n]$ may be measured, i.e. sampled with an A/D converter. Alternatively, if the power amplifier is assumed to be linear and its gain is known, it may be calculated from the input signal.

The predicted voltage signal is calculated from

$$v_{cp}[n] = R_{eb}i_{cm}[n] + \phi(x_d[n])u_d[n] \quad (4.56)$$

where $i_{cm}[n]$ is the measured current signal, and $u_d[n]$ is the velocity predicted from the force equation. The velocity signal $u_d[n]$ is iteratively calculated in the same manner as for the current output error, defined in Eq. (4.12), above. As a result, the derivatives of ϕ_0 , ϕ_k , and a_1 and a_2 with respect to the error for this voltage output-error form are similar as they were for the current output-error form.

It is possible to include the effects of a blocked electrical inductance quite easily. By making an approximate differentiation of the electrical current, the effects of the electrical inductance may be included as follows:

$$v_{cp}[n] = R_{eb}i_{cm}[n] + L_{eb}h_{dt}[n]*i_{cm}[n] + \phi(x_d[n])u_d[n] \quad (4.57)$$

where $h_{dt}[n]$ is the impulse response of a differentiation approximation, as in (2.84) presented in §2.3.4.

4.3.1. Parameter updating

Updating R_{eb}

$$\frac{\partial}{\partial R_{eb}} \epsilon_{oev}[n] = -i_{c\cdot m}[n] \quad (4.58)$$

The R_{eb} estimate is therefore updated by

$$R_{eb}[n+1] = R_{eb}[n] + \mu_{R_{eb}} \epsilon[n] i_{c\cdot m}[n] \quad (4.59)$$

Updating L_{eb}

The derivative of the error is with respect to L_{eb} is given by

$$\frac{\partial}{\partial L_{eb}} \epsilon_{oev}[n] = -h_{dt}[n] * i_{c\cdot m}[n] \quad (4.60)$$

The L_{eb} estimate is therefore updated by

$$L_{eb}[n+1] = L_{eb}[n] + \mu_{L_{eb}} \epsilon_{oev}[n] h_{dt}[n] * i_{c\cdot m}[n] \quad (4.61)$$

Updating a_k

As noted above, neither the measured current $i_{c\cdot m}[n]$ nor the predicted force $f_{cp}[n]$ depend on the feedback coefficients a_k . Therefore the derivative of the error with respect to a_k is that of a standard output-error IIR algorithm where the IIR filter concerned is that for the mechanical mobility. Thus generally one has

$$\begin{aligned} \frac{\partial}{\partial a_k} \epsilon_{oev}[n] &= \frac{\partial}{\partial a_k} (-v_{c\cdot p}[n]) \\ &= -\phi_0 \frac{\partial}{\partial a_k} u_{d\cdot f}[n] \end{aligned} \quad (4.62)$$

The derivative of the $u_{d\cdot f}[n]$ with respect to the feedback coefficients a_k here is the same as for the electrical current output error form defined in §4.2. Thus the instantaneous estimate of the gradient of the error surface along the parameter a_k is therefore given by

$$\hat{d}_{a_k}[n] = -\epsilon[n] \frac{\partial \epsilon_{oev}[n]}{\partial a_k} = \epsilon[n] \phi_0 \alpha_k[n] \quad (4.63)$$

where $\alpha_k[n]$ is calculated iteratively as per (4.26). The a_k parameters are updated according to the LMS algorithm as so:

$$a_k[n+1] = a_k[n] - \mu_{a_k} \hat{d}_{a_k}[n] \quad (4.64)$$

where μ_{a_k} is a convergence parameter specific to a_k . Summing up explicitly, this is

$$a_k[n+1] = a_k[n] - \mu_{a_k} \epsilon[n] \phi_0 \alpha_k[n] \quad (4.65)$$

Updating ϕ_0

The partial derivative of the error $\epsilon_{oev}[n]$ with respect to the transduction coefficient ϕ_0 is given by

$$\begin{aligned}
\frac{\partial}{\partial \phi_0} \varepsilon_{oev}[n] &= \frac{\partial}{\partial \phi_0} (-v_{c,p}[n]) \\
&= -\frac{\partial}{\partial \phi_0} \phi_0 u_{d,f}[n] \\
&= -u_{d,f}[n] - \phi_0 \frac{\partial}{\partial \phi_0} u_{d,f}[n]
\end{aligned} \tag{4.66}$$

The derivative of $u_{d,f}[n]$ with respect to ϕ_0 is defined as $\partial_{\phi u}[n]$, and is calculated iteratively as per (4.40). Therefore, explicitly, the partial derivative of the error $\varepsilon_{oev}[n]$ with respect to ϕ_0 is

$$\frac{\partial}{\partial \phi_0} \varepsilon_{oev}[n] = -u_{d,f}[n] - \phi_0 \partial_{\phi u}[n] \tag{4.67}$$

Therefore the instantaneous estimate of the gradient of the error surface along the parameter ϕ_0 is

$$\hat{d}_{\phi_0}[n] = \varepsilon[n] (-u_{d,f}[n] - \phi_0 \partial_{\phi u}[n]) \tag{4.68}$$

and thus the update equation

$$\phi_0[n+1] = \phi_0[n] - \mu_{\phi_0} \hat{d}_{\phi_0}[n] \tag{4.69}$$

is given explicitly by

$$\phi_0[n+1] = \phi_0[n] - \mu_{\phi_0} \varepsilon[n] (u_{d,f}[n] + \phi_0 \partial_{\phi u}[n]) \tag{4.70}$$

Updating ϕ_k

The derivative of the k^{th} coefficient of $\phi(x)$ for the voltage output error form is

$$\begin{aligned}
\frac{\partial}{\partial \phi_k} \varepsilon_{eov}[n] &= \frac{\partial}{\partial \phi_k} (-\phi(x_d[n]) u_d[n]) \\
&= -u_d[n] \partial_{\phi_k \phi}[n] - \phi(x_d[n]) \partial_{\phi_k u}[n]
\end{aligned} \tag{4.71}$$

where $\partial_{\phi_k \phi}[n]$ and $\partial_{\phi_k u}[n]$ are as defined for the electrical current output error form in §4.2.8.

4.3.2. Convergence performance

The convergence performance of the electrical current output error adaptive algorithm has been investigated for a variety of signals and initial values. These are presented in Figure 4.32 -Figure 4.46, as per Table 4.2.

Input signal	Initial a_n val.	L_{eb} adaptation	Duration	(page)	a_n plots	$\zeta, \omega_0, R_{eb}, \phi_0$ plots	Q_{tc}, Q_{ms} , Err plots	L_{eb} plot
Noise, 0-2kHz	Upper left	No	30s	p. 133	Figure 4.32	Figure 4.33	Figure 4.34	-
Noise, 0-2kHz	Target	Yes	30s	p. 134	Figure 4.35	Figure 4.36	-	Figure 4.37
Noise, 0-2kHz	Lower left	Yes	30s	p. 135	Figure 4.38	Figure 4.39	Figure 4.40	Figure 4.38
Speech, Male	Lower left	Yes	142s	p. 136	Figure 4.41	Figure 4.42	Figure 4.43	Figure 4.41
Music	Lower left	Yes	145s	p. 137	Figure 4.44	Figure 4.45	Figure 4.46	Figure 4.44

Table 4.2: Figure numbers for different input signals and settings of initial values of a_n .

The convergence of the voltage output error algorithm is not appreciably different from the electrical current output error form. The resonance frequency tends to converge quickly, and whereas the

damping factor (and the Q -values derived from it) take longer to converge, up to 20 seconds with white noise, and up to 60 seconds with speech and music signals.

The additional parameter identified by this form of the algorithm, the blocked electrical inductance L_{eb} , converges quite quickly, as shown in Figure 4.37 (left side). Furthermore, the convergence of L_{eb} does not have a significant effect on the value of other converged parameters. This can be seen from the figures on page 134. At $t = 5.64$ seconds, the convergence of the L_{eb} is begun. Other parameters had been allowed to converge to their final values, before convergence of L_{eb} was begun. As can be seen in the figures on page 134, the convergence of L_{eb} does not significantly affect the converged values of the other parameters. This is important, as it indicates that the non-convergence of L_{eb} does not cause bias errors in the values to which other parameters converge.

The parameter spread in L_{eb} for the speech and music signals is very large, up to 50% for the music signal. This is considered unsatisfactory performance. Lower spread in the converged value of L_{eb} would be needed if speech or music signals are used during parameter determination. This is suggested as a possible subject for further research.

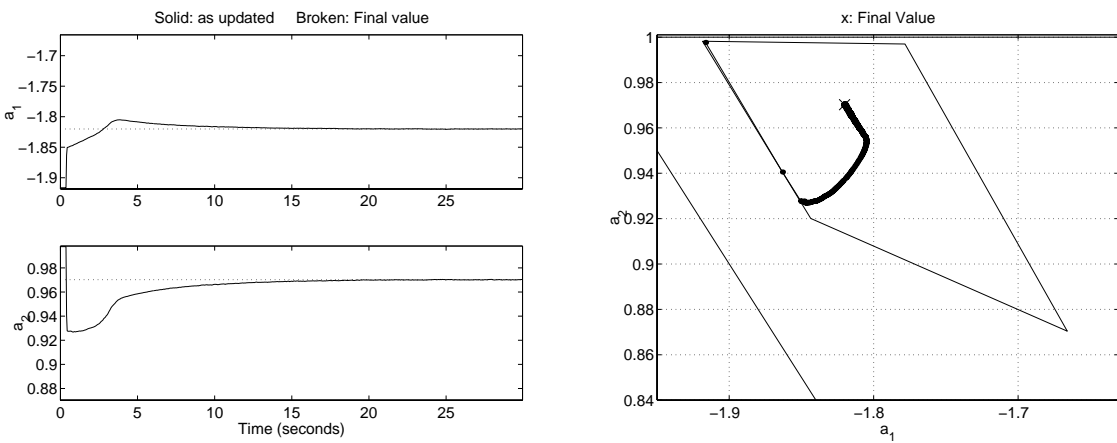


Figure 4.32: [left] a_1 and a_2 vs. time; [right] a_1 vs. a_2 .

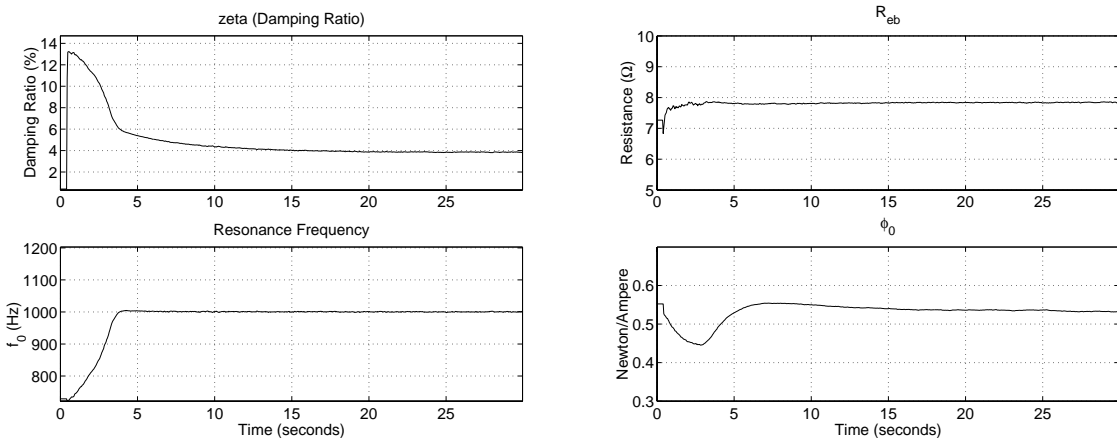


Figure 4.33: [left, upper]: Damping ratio (ζ); [left, lower]: Resonance Frequency; [right, upper] DC (blocked) electrical resistance (R_{eb}); [right, lower]: Transduction coefficient (ϕ_0).

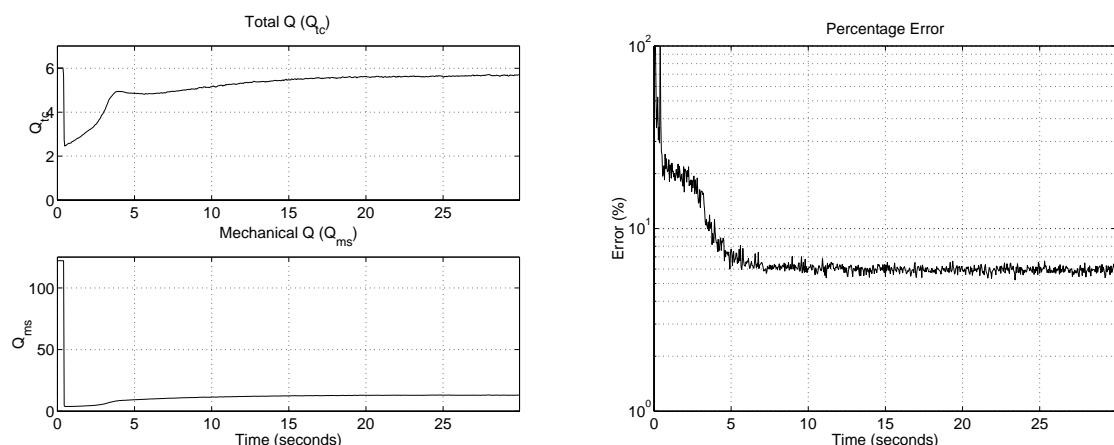


Figure 4.34: [left, upper]: Total Q -factor (Q_{tc}); [left, lower]: Mechanical Q -factor; [right]: Percentage error.

Effect of including adaptation of L_{eb} on other parameters. At $t = 5.64$ seconds, the convergence parameter for L_{eb} is set from zero to its regular value. There is a slight effect on the determined values of ζ and ϕ_0 . [Note that Figure 4.37 (bottom left) shows the adapted value of L_{eb} and not Q_{tc} and Q_{ms} as in previous figures.]

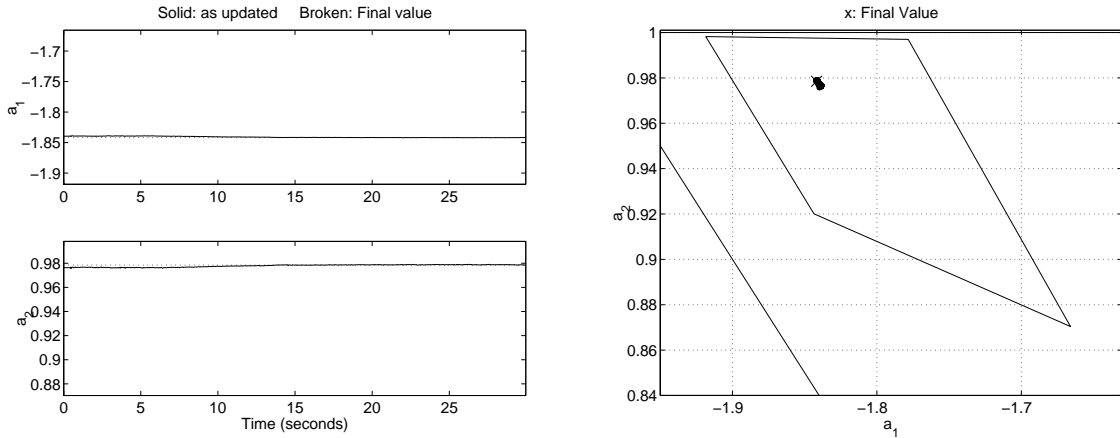


Figure 4.35: [left] a_1 and a_2 vs. time; [right] a_1 vs. a_2 .

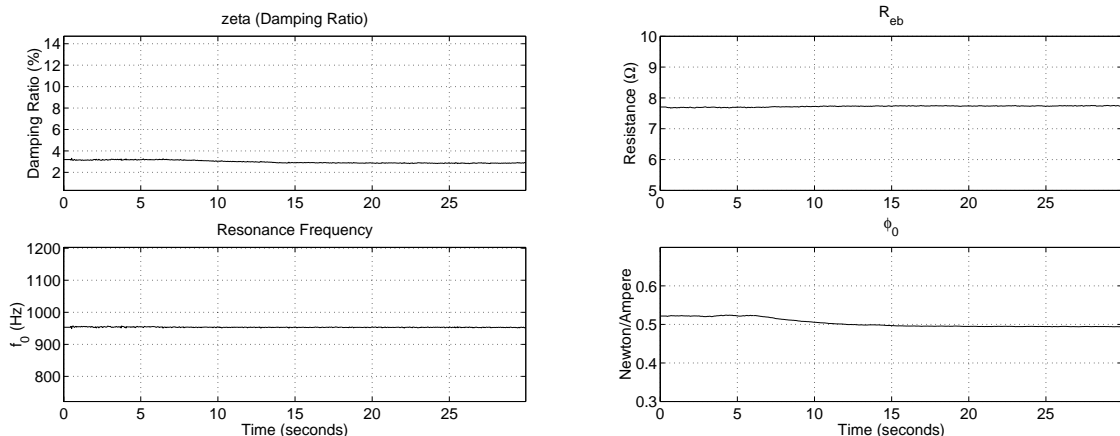


Figure 4.36: [left, upper]: Damping ratio (ζ); [left, lower]: Resonance Frequency; [right, upper] DC (blocked) electrical resistance (R_{eb}); [right, lower]: Transduction coefficient (ϕ_0).

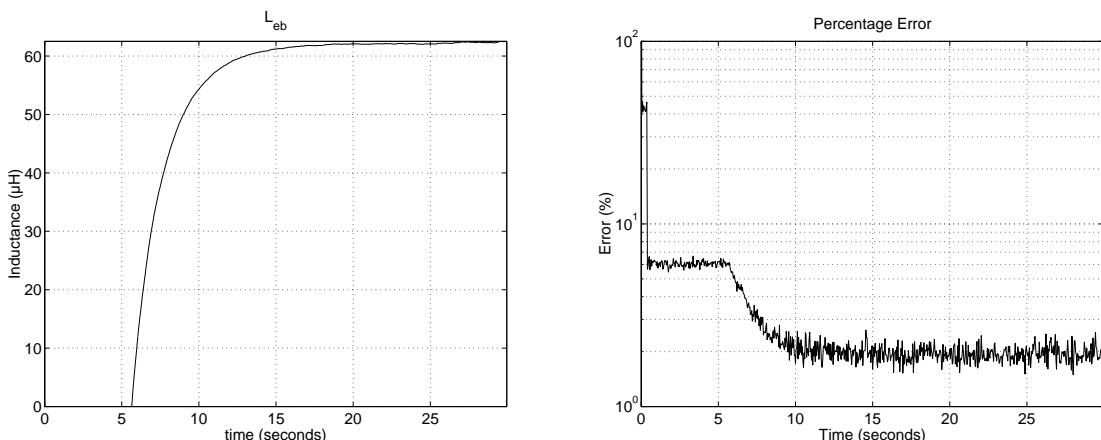


Figure 4.37: [left]: L_{eb} vs. time [right]: Percentage error.

Convergence for initial values of a_1 , a_2 in lower-left corner of tolerance quadrilateral.
Including adaptation of L_{eb} .

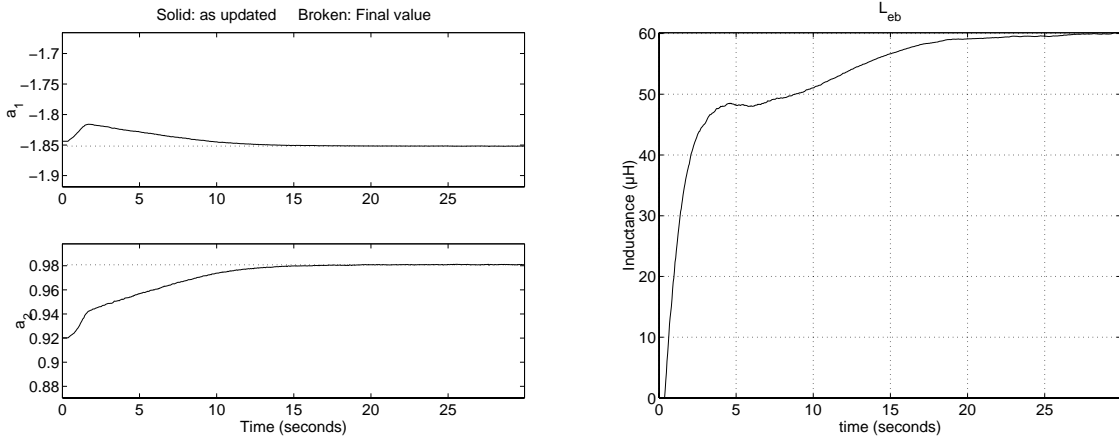


Figure 4.38: [left] a_1 and a_2 vs. time; [right] L_{eb} vs. time.

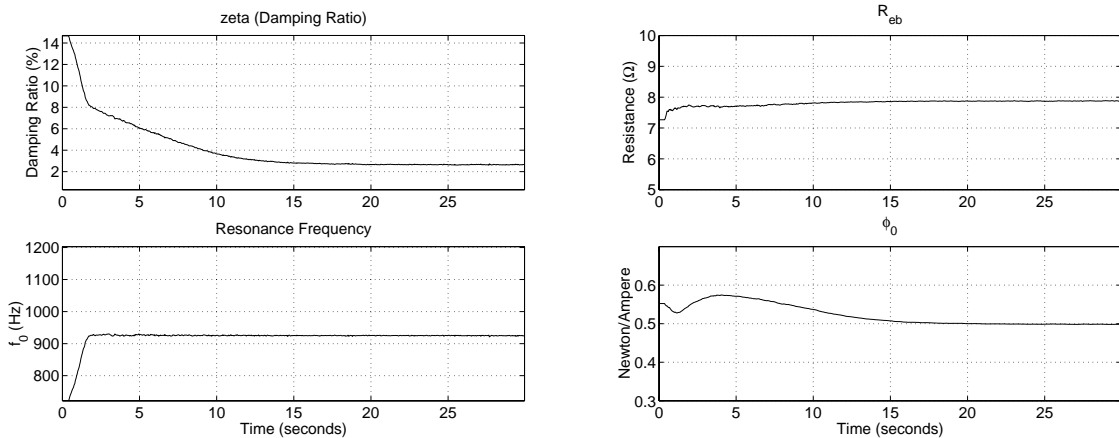


Figure 4.39: [left, upper]: Damping ratio (ζ); [left, lower]: Resonance Frequency; [right, upper] DC (blocked) electrical resistance (R_{eb}); [right, lower]: Transduction coefficient (ϕ_0).

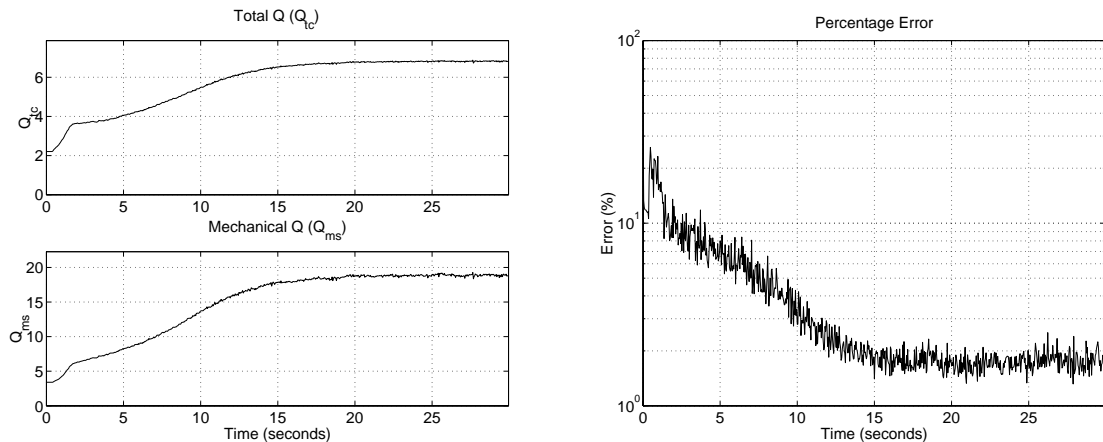


Figure 4.40: [left, upper]: Total Q -factor (Q_{tc}); [left, lower]: Mechanical Q -factor; [right]: Percentage error.

Convergence for initial values of a_1, a_2 in lower-left corner of tolerance quadrilateral
 Signal: Male speech; speech activity duty cycle: 50%.

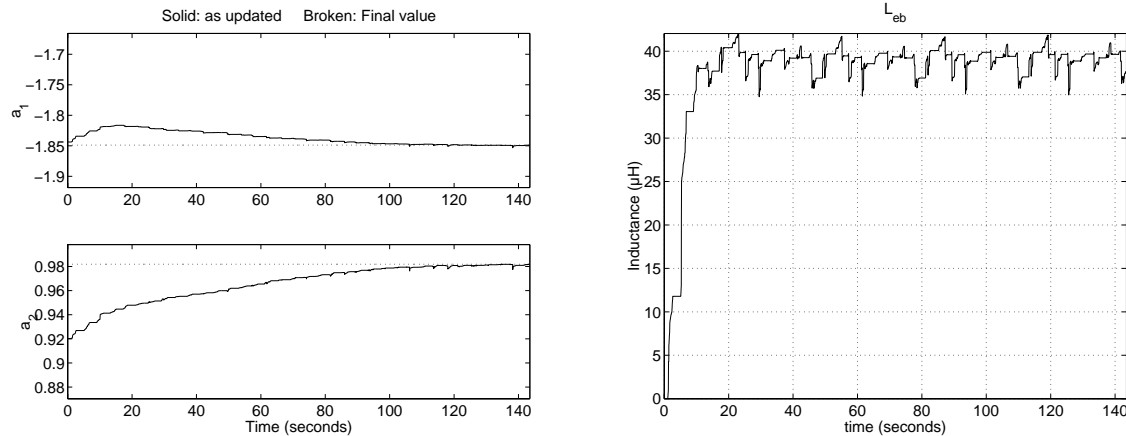


Figure 4.41: [left] a_1 and a_2 vs. time; [right] L_{eb} vs. time.

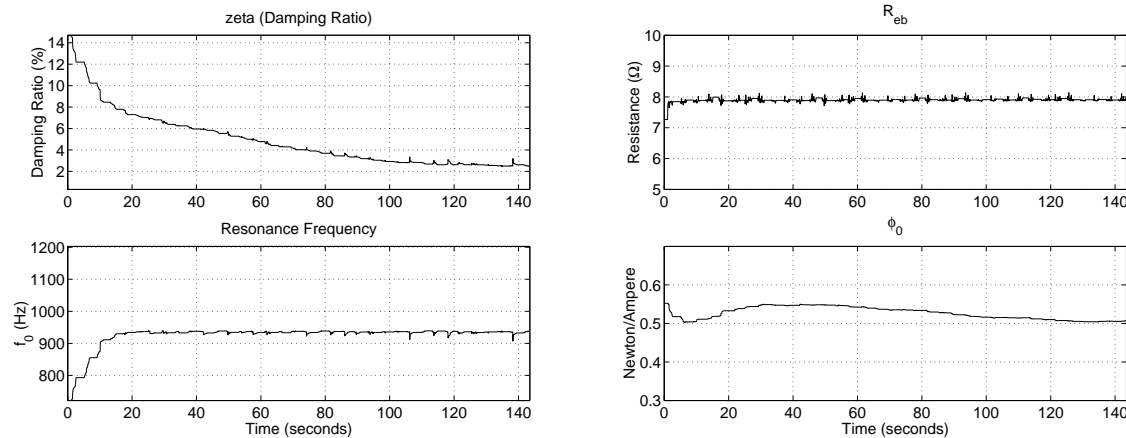


Figure 4.42: [left, upper]: Damping ratio (ζ); [left, lower]: Resonance Frequency; [right, upper] DC (blocked) electrical resistance (R_{eb}); [right, lower]: Transduction coefficient (ϕ_0).

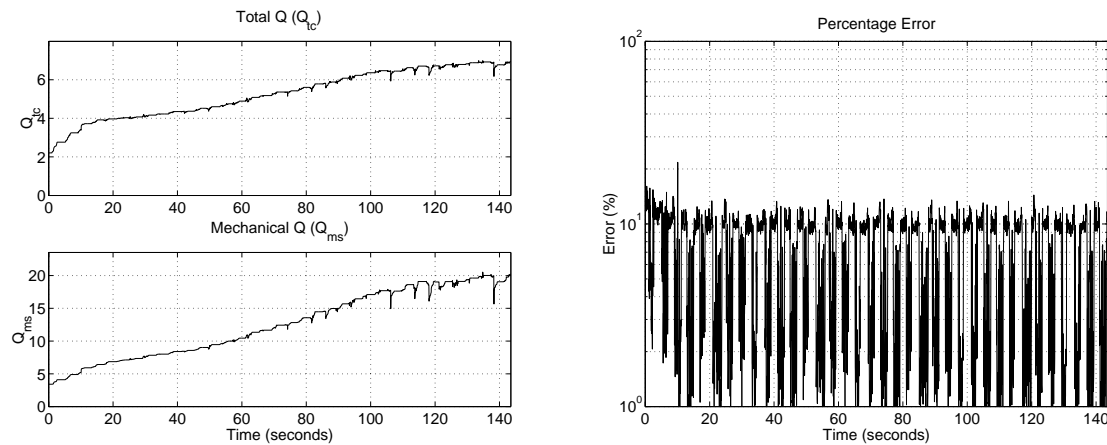


Figure 4.43: [left, upper]: Total Q -factor (Q_{tc}); [left, lower]: Mechanical Q -factor; [right]: Percentage error.

Convergence for initial values of a_1 , a_2 in lower-left corner of tolerance quadrilateral

Signal: Music¹

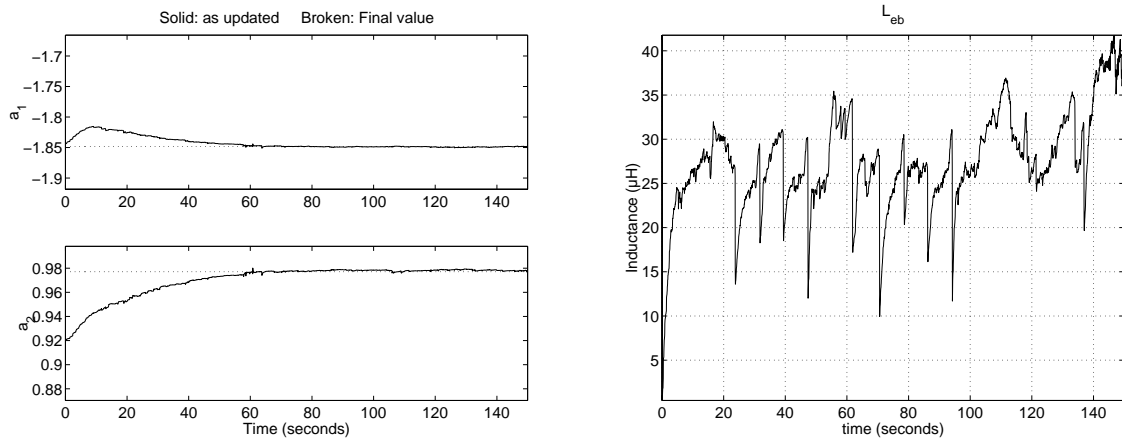


Figure 4.44: [left] a_1 and a_2 vs. time; [right] L_{eb} vs. time.

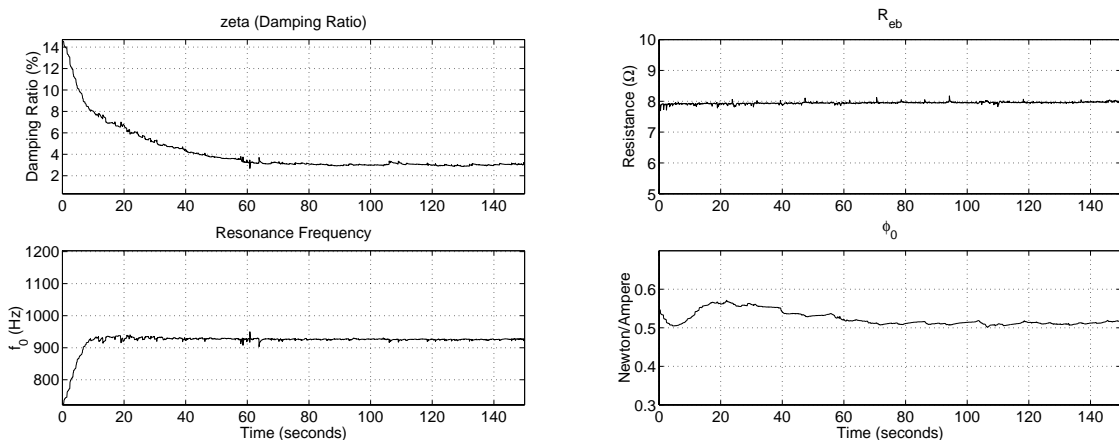


Figure 4.45: [left, upper]: Damping ratio (ζ); [left, lower]: Resonance Frequency; [right, upper] DC (blocked) electrical resistance (R_{eb}); [right, lower]: Transduction coefficient (ϕ_0).

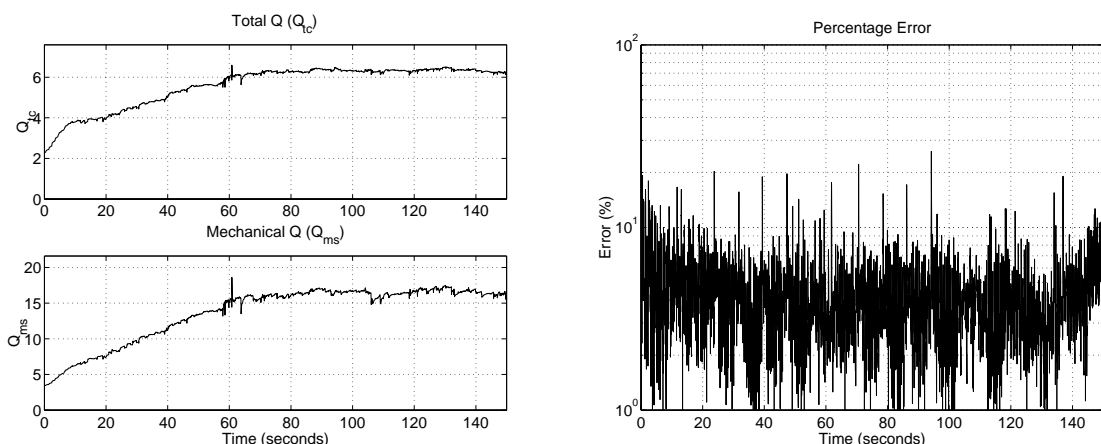


Figure 4.46: [left, upper]: Total Q -factor (Q_{tc}); [left, lower]: Mechanical Q -factor; [right]: Percentage error.

¹ The music used was a ‘popular music’ song, artist: DJ Spiller, title: *Groovejet*, © 2000 Positiva Records.

4.4. Displacement equation-error form

The displacement equation error form is considered as an alternative to the velocity equation error form presented by Klippel. The displacement must be calculated for nonlinear parameter updating in Klippel's form (1999). Thus it would be simpler to use the displacement signal as the basis of an error function outright.

4.4.1. Displacement from the voltage equation

The displacement is predicted by the voltage equation by isolating and integrating the velocity signal. The velocity signal may be predicted by the voltage equation according to:

$$u_{d\cdot v}[n] = \frac{1}{\phi(x)}(v_c[n] - R_{eb}i_c[n]) \quad (4.72)$$

This signal is integrated to provide a displacement signal.

$$x_{d\cdot v}[n] = h_{\int dt}[n] * u_{d\cdot v}[n] \quad (4.73)$$

The convolution in (4.73) will be implemented as a difference equation. Specific details of this difference equation directly impact convergence performance of the algorithm, and are thus addressed below.

4.4.2. Displacement from the force equation

The displacement may be calculated from the force according to the mechanical receptance defined in §2.3.2 as per:

$$\begin{aligned} x_{d\cdot f}[n] &= f_{c\cdot p}[n] * h_{X_m}[n] \\ &= \sigma_x f_{c\cdot p}[n-1] - a_1 x_{d\cdot f}[n-1] - a_2 x_{d\cdot f}[n-2] \end{aligned} \quad (4.74)$$

The force $f_{c\cdot p}[n]$ may be calculated from the measured electrical current as so

$$f_{c\cdot p}[n] = \phi(x_{d\cdot f}[n]) i_{c\cdot m}[n] - k_1(x_{d\cdot f}[n]) x_{d\cdot f}[n] \quad (4.75)$$

Again, the importance of the predictive nature of the displacement difference equation (4.74) appears. The present sample of the displacement $x_{d\cdot f}[n]$ is calculated from the previous samples of the ‘input’ (the force) $f_{c\cdot p}[n]$. If (4.74) were not ‘predictive,’ it would form with (4.75) an implicit, and not explicit, equation pair.

4.4.3. Error definition

The error is calculated by the difference between the displacement calculated from the voltage equation and the displacement calculated from the force equation.

$$\begin{aligned} \epsilon_{eed}[n] &= x_{d\cdot v}[n] - x_{d\cdot f}[n] \\ &= h_{\int dt}[n] * u_{d\cdot v}[n] - \sigma_x f_{c\cdot p}[n-1] - a_1 x_{d\cdot f}[n-1] - a_2 x_{d\cdot f}[n-2] \end{aligned} \quad (4.76)$$

For the linear case, (4.76) reduces to

$$\epsilon_{eed}[n] = h_{\int dt}[n] * u_{d\cdot v}[n-1] - \sigma_x \phi_0 i_c[n-1] + a_1 x_{d\cdot f}[n-1] + a_2 x_{d\cdot f}[n-2] \quad (4.77)$$

Substituting velocity $u_{d\cdot v}[n]$ with the RHS of (4.72) provides the following explicit difference equation for the error:

$$\epsilon_{eed}[n] = h_{\int dt}[n] * \left(\frac{1}{\phi_0} (v_{c\cdot m}[n-1] - R_{eb} i_{c\cdot m}[n-1]) \right) - \sigma_x \phi_0 i_c[n-1] + a_1 x_{d\cdot f}[n-1] + a_2 x_{d\cdot f}[n-2] \quad (4.78)$$

4.4.4. Parameter updating – linear case

Updating R_{eb}

- $i_{c\cdot m}[n]$ and $v_{c\cdot m}[n]$ are input signals, and thus do not depend on R_{eb}
- $x_{df}[n]$ is calculated from the force equation and thus does not depend on R_{eb}

For the purpose of integration, a discrete-time integrator impulse response in the form of an IIR filter, using a z -domain transfer function determined according to the bilinear transform:

$$h_{\int dt}[n] = Z^{-1} \left\{ \frac{\frac{1}{2F_s}}{1 + z^{-1}} \right\} \quad (4.79)$$

In this case, (4.73) becomes this difference equation:

$$x_{d\cdot v}[n] = b_{\text{int}0} u_{d\cdot v}[n] + b_{\text{int}1} u_{d\cdot v}[n-1] - a_{\text{int}1} x_{d\cdot v}[n] \quad (4.80)$$

The derivative of the error with respect to R_{eb} is therefore

$$\frac{\partial}{\partial R_{eb}} \varepsilon_{eed}[n] = b_{\text{int}0} \frac{\partial}{\partial R_{eb}} u_{d\cdot v}[n] + b_{\text{int}1} \frac{\partial}{\partial R_{eb}} u_{d\cdot v}[n-1] - a_{\text{int}1} \frac{\partial}{\partial R_{eb}} x_{d\cdot v}[n-1] \quad (4.81)$$

With $u_{d\cdot v}[n]$ defined, for the linear case the derivative of the error with respect to R_{eb} will be

$$\frac{\partial}{\partial R_{eb}} \varepsilon_{eed}[n] = -\frac{b_{\text{int}0}}{\phi_0} i_{c\cdot m}[n] - \frac{b_{\text{int}1}}{\phi_0} i_{c\cdot m}[n-1] - a_{\text{int}1} \frac{\partial}{\partial R_{eb}} x_{d\cdot v}[n-1] \quad (4.82)$$

Noting that $\partial x_{d\cdot v}[n]/\partial R_{eb}$ is the same as $\partial \varepsilon_{eed}[n]/\partial R_{eb}$, the partial derivative of the error with respect to R_{eb} is calculated recursively by:

$$\begin{aligned} \varepsilon_{\partial R_{eb}}[n] &\doteq \frac{\partial}{\partial R_{eb}} \varepsilon_{eed}[n] \\ &= -\frac{b_{\text{int}0}}{\phi_0} i_{c\cdot m}[n] - \frac{b_{\text{int}1}}{\phi_0} i_{c\cdot m}[n-1] - a_{\text{int}1} \varepsilon_{\partial R_{eb}}[n-1] \end{aligned} \quad (4.83)$$

From this the instantaneous estimate of the gradient of the error surface along R_{eb} is given by

$$\hat{d}_{R_{eb}}[n] = \varepsilon_{eed}[n] \varepsilon_{\partial R_{eb}}[n] \quad (4.84)$$

Thus the LMS algorithm provides the following parameter-update equation

$$R_{eb}[n+1] = R_{eb}[n] - \mu_{R_{eb}} \varepsilon_{eed}[n] \varepsilon_{\partial R_{eb}}[n] \quad (4.85)$$

It is found that this update method does not lead to proper convergence. Misalignment of R_{eb} accumulates in the estimate of $x_{d\cdot v}[n]$, because its estimation is performed by integration of an equation containing R_{eb} , i.e. Eqs. (4.72) - (4.80). This problem is illustrated by simulation, wherein the input voltage is white noise. The results of this simulation are shown in Figure 4.47.

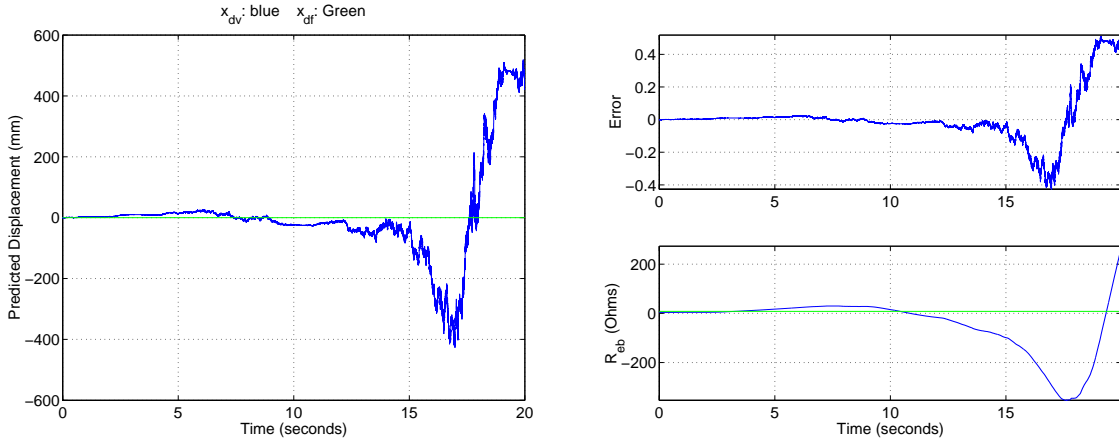


Figure 4.47: LEFT: Displacement predicted from force equation (Green) and from voltage equation (blue); UPPER RIGHT: Error; LOWER RIGHT: Updated R_{eb} (blue) and actual value (8.0, in green).

A filtered-error version of the LMS algorithm was investigated as a potential solution to this problem. By low-pass filtering the error used to update R_{eb} , this problem can be eliminated. Convergence results using this filtered-error approach are shown in Figure 4.48. As can be seen in this figure, this results in convergence of R_{eb} to its correct value. However, error in the displacement predicted from the voltage $x_{dv}[n]$ equation accumulates, and does not fade-away after R_{eb} has converged to its proper value. A different approach is still needed.

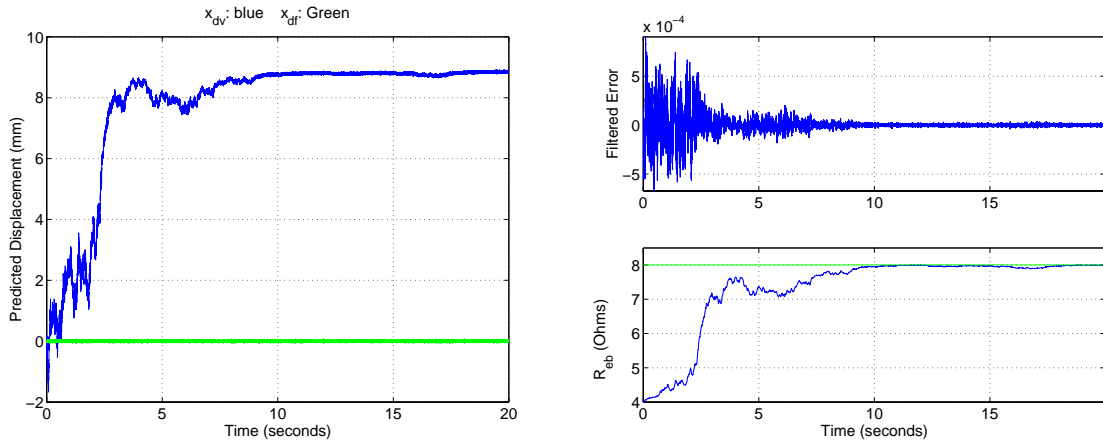


Figure 4.48: Filtered-error approach to adaptive R_{eb} ; LEFT: Displacement predicted from force equation (Green) and from voltage equation (blue); UPPER RIGHT: Error; LOWER RIGHT: Updated R_{eb} (blue) and actual value (8.0, in green).

In order to also eliminate the accumulation of error in $x_{dv}[n]$, a limited-memory integration approximation is used when predicting it from $u_{dv}[n]$. This can be done by creating a modified integration filter whose z -transform is given by the product between the integrator and a first-order high-pass filter, as so:

$$h_{\int dt \cdot lm}[n] = Z^{-1} \left\{ \frac{1}{2F_s} \frac{1+z^{-1}}{1-z^{-1}} H_{HP}(z) \right\} \quad (4.86)$$

In this way, the displacement determined by the voltage equation becomes

$$x_{d \cdot v}[n] = b_{\text{int} \cdot 0} u_{d \cdot v}[n] + b_{\text{int} \cdot 1} u_{d \cdot v}[n-1] + b_{\text{int} \cdot 2} u_{d \cdot v}[n-2] - a_{\text{int} \cdot 1} x_{d \cdot v}[n-1] - a_{\text{int} \cdot 2} x_{d \cdot v}[n-2] \quad (4.87)$$

where the coefficients ($b_{\text{int} \cdot 0} \dots a_{\text{int} \cdot 2}$) are determined from the inverse z -transform in (4.86). Thus the recursive calculation of the partial derivative of the error with respect to R_{eb} becomes:

$$\begin{aligned} \varepsilon_{\partial R_{eb}}[n] &\doteq \frac{\partial}{\partial R_{eb}} \varepsilon_{eed}[n] \\ &= -\frac{b_{\text{int} \cdot 0}}{\phi_0} i_c[n] - \frac{b_{\text{int} \cdot 1}}{\phi_0} i_c[n-1] - \frac{b_{\text{int} \cdot 2}}{\phi_0} i_c[n-2] - a_{\text{int} \cdot 1} \varepsilon_{\partial R_{eb}}[n-1] - a_{\text{int} \cdot 2} \varepsilon_{\partial R_{eb}}[n-2] \end{aligned} \quad (4.88)$$

The LMS algorithm uses this to update the estimate of R_{eb} in the same manner as (4.85).

The convergence performance of R_{eb} using this limited-memory integrator is shown in Figure 4.49. As can be seen, the displacement predicted from the voltage equation does have the accumulated error as it did before. Also, the convergence of R_{eb} is much faster and smoother.

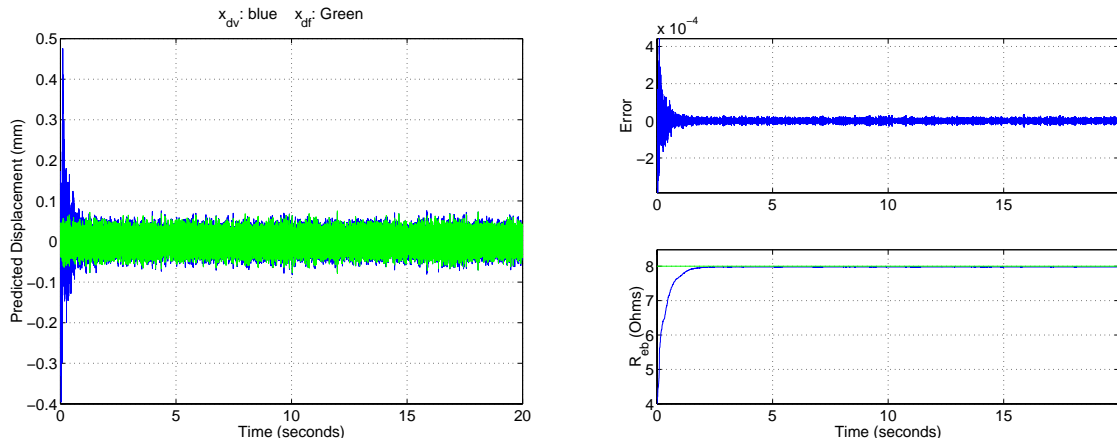


Figure 4.49: Limited-memory integration of $u_{d \cdot v}[n]$; LEFT: Displacement predicted from force equation (Green) and from voltage equation (blue); UPPER RIGHT: Error; LOWER RIGHT: Updated R_{eb} (blue) and actual value (8.0, in green).

Updating a_1, a_2 – linear case

$$\frac{\partial \varepsilon_{eed}[n]}{\partial a_k} = -\frac{\partial x_{d \cdot f}}{\partial a_k} = \frac{\partial}{\partial a_k} \left[-\sigma_x \phi_0 i_{c \cdot m}[n] + a_1 x_{d \cdot f}[n-1] + a_2 x_{d \cdot f}[n-2] \right] \quad (4.89)$$

Given that $i_{c \cdot m}[n]$ is a measured signal, its derivative with respect to a_k is zero. From the definition of σ_x in (2.67), its derivative with respect to a_1 is given by

$$\frac{\partial \sigma_x}{\partial a_1} = \frac{2 + a_2}{k_t} \quad (4.90)$$

and similarly for a_2 . As discussed in §2.4, k_t cannot be known *a-priori*. It is thus written as

$$\frac{\partial \sigma_x}{\partial a_1} = \frac{2 + a_2}{\omega_z^2 F_s^2 m_t} \quad (4.91)$$

where ω_z is determined from a_1 and a_2 as per (2.73). Therefore (4.89) becomes, for a_1 and a_2 :

$$-\frac{\partial x_{d,f}}{\partial a_1} = -\frac{2+a_2}{\omega_z^2 F_s^2 m_t} + x_{d,f}[n-1] + a_1 \frac{\partial}{\partial a_1} x_{d,f}[n-1] + a_2 \frac{\partial}{\partial a_1} x_{d,f}[n-2] \quad (4.92)$$

$$-\frac{\partial x_{d,f}}{\partial a_2} = -\frac{2+a_1}{\omega_z^2 F_s^2 m_t} + x_{d,f}[n-2] + a_1 \frac{\partial}{\partial a_2} x_{d,f}[n-1] + a_2 \frac{\partial}{\partial a_2} x_{d,f}[n-2] \quad (4.93)$$

Using the same principle as the LMS IIR algorithm, the derivative of the error with respect to a_k is defined as α_k ,

$$\begin{aligned} \alpha_k[n] &= \frac{\partial \varepsilon_{eed}[n]}{\partial a_k} \\ &= -\frac{\partial x_{d,f}[n]}{\partial a_k} \end{aligned} \quad (4.94)$$

With this definition, this derivative may be recursively calculated according to (4.92) as so:

$$\alpha_1[n] = \frac{2+a_2}{\omega_z^2 F_s^2 m_t} - x_{d,f}[n-1] - a_1 \alpha_1[n-1] - a_2 \alpha_1[n-2] \quad (4.95)$$

and similarly for $\alpha_2[n]$. The instantaneous estimate of the gradient of the error surface along the parameter a_k is therefore given by

$$\begin{aligned} \hat{d}_{a_k}[n] &= \varepsilon_{eed}[n] \frac{\partial \varepsilon_{eed}[n]}{\partial a_k} \\ &= \varepsilon_{eed}[n] \alpha_k[n] \end{aligned} \quad (4.96)$$

where $\alpha_k[n]$ is calculated iteratively as per (4.95). The a_k parameters are updated according to the LMS algorithm as so:

$$a_k[n+1] = a_k[n] - \mu_{a_k} \hat{d}_{a_k}[n] \quad (4.97)$$

where μ_{a_k} is a convergence parameter specific to a_k . Summing up explicitly, this is

$$a_k[n+1] = a_k[n] - \mu_{a_k} \varepsilon_{eed}[n] \alpha_k[n] \quad (4.98)$$

Updating ϕ_0 – linear case

The derivative of the error with respect to ϕ_0 is complicated by its presence in the voltage equation. Due to the method of integration needed for proper convergence of R_{eb} described in (4.87), the term ϕ_0 appears ‘buried’ in this difference equation. Thus the derivative of ϕ_0 with respect to $x_{d,v}[n]$ is considered separately from $x_{d,f}[n]$, which are defined as so:

$$\begin{aligned} \frac{\partial x_{d,v}[n]}{\partial \phi_0} &\doteq \partial_{\phi,v}[n] \\ \frac{\partial x_{d,f}[n]}{\partial \phi_0} &\doteq \partial_{\phi,f}[n] \end{aligned} \quad (4.99)$$

The derivative of the displacement as determined from the voltage equation, $\partial_{\phi,v}[n]$, is considered first. With $x_{d,v}[n]$ as defined in (4.87), the derivative is given by

$$\partial_{\phi,v}[n] = b_{\text{int},0} \frac{\partial u_{d,v}[n]}{\partial \phi_0} + b_{\text{int},1} \frac{\partial u_{d,v}[n-1]}{\partial \phi_0} + b_{\text{int},2} \frac{\partial u_{d,v}[n-2]}{\partial \phi_0} - a_{\text{int},1} \partial_{\phi,v}[n-1] - a_{\text{int},2} \partial_{\phi,v}[n-2] \quad (4.100)$$

With $u_{d,v}[n]$ as given in (4.72), its derivative with respect to ϕ_0 is given by

$$\frac{\partial u_{d,v}[n]}{\partial \phi_0} = -\frac{1}{\phi_0^2} (v_{c,m}[n] - R_{eb} i_{c,m}[n]) \quad (4.101)$$

Note that the RHS of this is the same as $-u_{d,v}[n]/\phi_0$. The derivative of $x_{d,v}[n]$ with respect to ϕ_0 is therefore given by the following recursive calculation

$$\partial_{\phi,v}[n] = -\frac{1}{\phi_0} (b_{\text{int},0} u_{d,v}[n] + b_{\text{int},1} u_{d,v}[n-1] + b_{\text{int},2} u_{d,v}[n-2]) - a_{\text{int},1} \partial_{\phi,v}[n-1] - a_{\text{int},2} \partial_{\phi,v}[n-2] \quad (4.102)$$

The derivative of ϕ_0 with respect to the displacement determined from the force equation is recursively determined in a manner similar to the a_k coefficients, as so:

$$\partial_{\phi,f}[n] = \sigma_x i_{c,m}[n] - a_1 \partial_{\phi,f}[n-1] - a_2 \partial_{\phi,f}[n-2] \quad (4.103)$$

The derivative of the error is therefore given by

$$\frac{\partial \epsilon_{eed}[n]}{\partial \phi_0} = \partial_{\phi,v}[n] - \partial_{\phi,f}[n] \quad (4.104)$$

resulting in the update equation

$$\phi_0[n+1] = \phi_0[n] - \mu_{\phi_0} \epsilon_{eed}[n] (\partial_{\phi,v}[n] - \partial_{\phi,f}[n]) \quad (4.105)$$

It is noted that the calculation of the derivative of the error with respect to ϕ_0 is considerably more complicated for this displacement equation-error form than it is for either the current or the voltage output error form described above. As this complication will become manifold worse when the nonlinear case is concerned, the displacement equation error form has not been pursued further.

4.5. Conclusions regarding system identification

Three methods are investigated for determination of linear parameters of a loudspeaker. The methods are developed specifically to determine those loudspeaker parameters which are subject to drift, and thus cannot be known *a priori*, as discussed in §2.4. This is made possible because one of the basic parameters of the loudspeaker can the total moving mass be known *a priori* (because it is not subject to drift). This permits system identification of the loudspeaker using a method that only considers its electrical characteristics, without the need for a vibration measurement.

The displacement equation error form investigated in §4.4 is considered too complicated, and is thus not investigated in full detail. The electrical current and voltage output error forms, presented in §4.2 and §4.3 respectively, were both found to be sufficiently simple. Full investigation of these two algorithms is made, including measurements of their convergence performance using signals obtained from an actual loudspeaker. Convergence performance of both algorithms was found to be good for white noise signals. Convergence performance with speech and music signals was found to be similarly accurate, but considerably slower. This slow convergence rate for the speech and music signals may prove problematic in some applications.

It is possible that other common adaptive algorithms, such as the filtered-X or filtered-error LMS, or the recursive-least-squares algorithm, may increase the convergence rate with speech and music signals. This will of course come at the cost of an increase in the algorithm's complexity. This may be a suitable subject for further research.

Little difference in the convergence performance is found between the electrical current and voltage output error forms. The voltage output error form is slightly simpler than the electrical current output error form, and thus seems to have the advantage between the two.

Attempts were made to identify coefficients of a polynomial approximation to the nonuniformity of the transduction coefficient. This is tried with both the electrical current and voltage output error forms. Convergence of the coefficient parameters was found to be erratic. Further research on this subject will be needed if determination of these parameters is deemed necessary.

Parameter determination algorithms have been evaluated only for the case of a loudspeaker mounted in a closed box. More complex acoustic enclosures, such as a vented enclosure, would require a more complicated model of the linear dynamics. For example, in the case of a vented enclosure, an additional second-order IIR section would be needed to model the extra pole pair in the linear dynamics of the vented box system. This may also be a suitable subject for further research.

4.6. References

- Johnson, C. R. Jr., and M. G. Larimore, "Comments on and additions to 'An adaptive recursive LMS filter,'" *Proceedings of the IEEE*, **65**, pp. 1399-1402. (Sept. 1977)
- Klippel, Wolfgang J., "Nonlinear Adaptive Controller for Loudspeakers with a Current Sensor," *presented at the 106th Convention of the AES* (May 8-11, 1999), preprint no. 4864; *J. Audio Eng. Soc. (Abstracts)*, **47**, p. 512 (Jun. 1999)
- Knudsen, M. H., J. Grue Jensen, V. Julskjær, and Per Rubak, "Determination of Loudspeaker Driver Parameters Using a System Identification Technique," *Journal of the Audio Eng. Soc.*, **37**, pp. 700-708. (Sept. 1989)
- Ljung, Lennart, *System Identification: Theory for the User*, Prentice Hall Ptr., Upper Saddle River, NJ, USA. (1999)
- Oppenheim, Alan V., and Ronald W. Schafer, *Discrete-time Signal Processing*, Prentice Hall, Englewood Cliffs, New Jersey, USA. (1989)

5. Applications of active control of a loudspeaker

Applications of active control for a loudspeaker are presented in this chapter. In §5.1, applications of linear control are presented. In §5.2, applications of nonlinear control are presented.

The presentation of these applications assumes the active control system is implemented as an adaptive feedforward controller, as shown in Figure 1.4, and in more detail in Figure 4.1. As per these figures, the feedforward processor is somewhat separate from the system identification processing algorithms. The feedforward processor in this context may be discussed in the same manner as in the non-adaptive feedforward control system, with one important difference. In the adaptive feedforward controller, algorithms for feedforward processing must be designed so that they can be easily updated from the results of system identification algorithms. Particular attention has been given to this requirement in the development and presentation feedforward processing algorithms in this chapter. The algorithms have been designed such that they may be updated with parameters from the system identification algorithms, without the need for any type of transformation on these parameters.

The linear control applications presented in §5.1 are limited to low-order equalisation. This is straightforward equalisation, for extending the low-frequency response and controlling the total Q -value of a loudspeaker mounted in a closed box. The focus of discussion in §5.1 is on the digital implementation of the equaliser, and how this equaliser can be updated using the parameters of the loudspeaker identified by the system identification algorithms presented in Chapter 4.

In §5.2, the use of nonlinear control is considered. Specifically, it is considered how nonlinear control can be used to improve the overall sensitivity of a loudspeaker. The compromise between reduction of coil height and additional amplifier output required for nonlinear distortion compensation is investigated. Results from a series of simulations are presented, showing the net sensitivity of an electroacoustic system for different coil heights, at different vibration displacements, including the additional output required for nonlinear compensation. To test the suggestions from these simulations, loudspeakers were prepared with shortened voice coil heights. The simple algorithm for compensation of nonlinear distortion, developed in §3.3.7, is used to compensate for nonlinear distortion in these shortened-voice-coil-height loudspeakers. Measurements of the linear frequency response of these shortened-voice-coil-height loudspeakers are shown, indicating the small-signal sensitivity increase provided by shortening the voice-coil height. Measurements of nonlinear harmonic distortion, and the compensation of this distortion by the nonlinear compensation algorithm developed in §3.3.7 are presented.

5.1. Linear equalisation

Perhaps the simplest linear equaliser for a loudspeaker is that for controlling the Q-value and cut-off frequency described by Leach (1990). Leach describes an arrangement wherein the input to the power amplifier is processed by a second-order active analogue filter. The filter provides a band-stop characteristic described by the following s -domain transfer function:

$$H_c(s) = \frac{s^2/\omega_0^2 + s/\omega_0 Q_{tc} + 1}{s^2/\omega_d^2 + s/\omega_d Q_d + 1} \quad (5.1)$$

where Q_d and ω_d are the desired Q-value and cut-off frequency, respectively.

A discrete-time version of (5.1) may be derived by mapping the poles and zeros from the s -plane to the z -plane according to the exponential mapping used in §2.3.2, producing

$$H_c(z) = \sigma_c \frac{1 + b_{1,a} z^{-1} + b_{2,a} z^{-2}}{1 + a_{1,d} z^{-1} + a_{2,d} z^{-2}} \quad (5.2)$$

The feedforward coefficients are given by

$$\begin{aligned} b_{1,a} &= a_1 \\ b_{2,a} &= a_2 \end{aligned} \quad (5.3)$$

where a_1 and a_2 are the feedback coefficients of a discrete-time model of the loudspeaker, as described in §2.3.4.

The feedback coefficients are determined by the desired cut-off frequency and damping factor according to

$$\begin{aligned} a_{1,d} &= -2e^{-\omega_d \zeta_d} \cos\left(\omega_d \sqrt{1 - \zeta_d^2}\right) \\ a_{2,d} &= e^{-2\omega_d \zeta_d} \end{aligned} \quad (5.4)$$

The overall system gain σ_c is chosen to provide unity above the cut-off frequency, and is thus given by:

$$\sigma_c = \frac{1 - a_{1,d} + a_{2,d}}{1 - b_{1,a} + b_{2,a}} \quad (5.5)$$

5.1.1. Acoustic response with equalisation

An example of how this filter affects the loudspeaker's frequency response, for three different filter cut-off frequencies, is shown in Figure 5.1. In this figure, the frequency response of the loudspeaker is synthesised from measured small-signal parameters. The overall Q-value of this loudspeaker (Q_{tc}) is about 5.0, typical for a 'microspeaker' placed in a small cavity. Parameters of the equaliser are chosen to produce an equalised Q value of 1.0. The three cut-off frequencies chosen in the equaliser are one half ($\frac{1}{2} \times$) the same ($1 \times$) and twice ($2 \times$) the original resonance frequency of the loudspeaker.

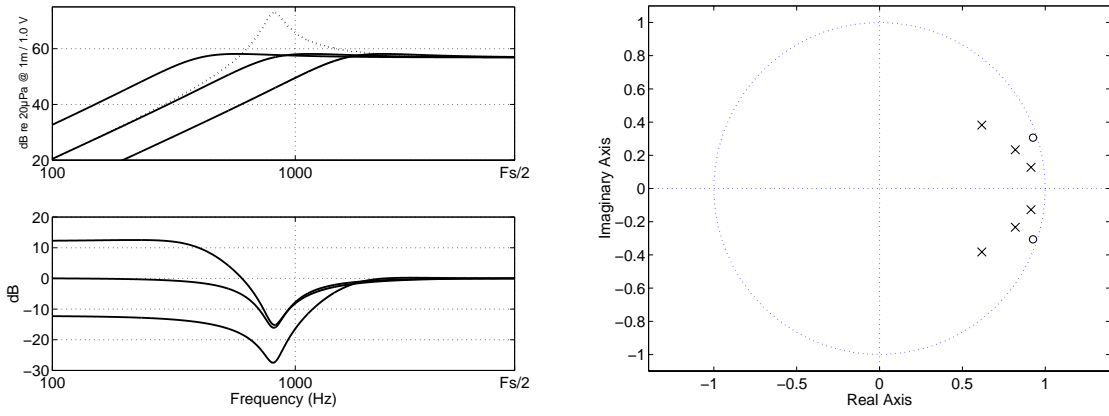


Figure 5.1: Properties of the linear equaliser, for three different cut-off frequencies; UPPER LEFT: equalised loudspeaker response (solid), unequalised (broken); LOWER LEFT: response of equaliser; RIGHT: pole-zero plot in z -plane of equaliser's transfer function. The response is shown for settings of the equaliser where the cut-off frequency is set to $\omega_d = 0.5 \omega_0$ (top curve), $\omega_d = 1.0 \omega_0$ (middle curve), and $\omega_d = 2 \omega_0$ (bottom curve).

This type of equaliser is particularly useful for the microspeaker (Figure 2.1). As can be seen in Figure 5.1, the un-equalised response of the microspeaker has a very high Q -value. This is due to the low magnetic strength of the microspeaker, relative to other, typical loudspeakers. This high Q -value is typically reduced by introducing some type of acoustic resistance, either to rear of the microspeaker, or by a highly damped leak in the rear cavity. As shown Figure 5.1, this high Q -value can be ‘damped’ by the equaliser of (5.2).

One reason the equaliser of (5.2) is not commonly used is that the resonance frequency, ω_0 in (5.2), is subject to manufacturing tolerance and drift, as discussed in §2.4. As shown in (5.3), the loudspeaker-dependent coefficients of the equaliser in (5.2) can be determined from the discrete time model of the loudspeaker presented in §2.3.4. The techniques described in chapter 3 can adaptively identify these parameters. Thus, the loudspeaker system identification techniques presented in chapter 3 can tune the equaliser to the loudspeaker quite in a straightforward manner.

Note that when the filter cut-off frequency is chosen to be below the loudspeaker's cut-off frequency, the filter gain is positive below the cut-off frequency, and *vice versa* when the filter's cut-off frequency is above that of the loudspeaker. This has very important consequences for the variation of the displacement response with respect to filter cut-off frequency, as discussed below.

5.1.2. Displacement response with equalisation

An important property of the equaliser defined by (5.2) is its effect on the displacement frequency response function. This effect is plotted in Figure 5.2, for the same values of the equaliser as plotted in Figure 5.1.

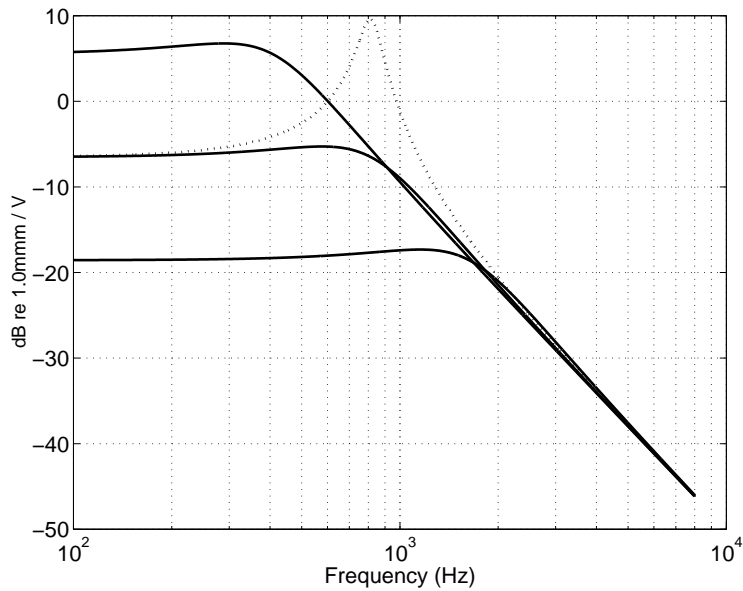


Figure 5.2: Effect on the displacement response on the linear equaliser of (5.2). Broken: response without equaliser; Solid: response with equaliser with $\omega_d = 0.5 \omega_0$ (top curve), $\omega_d = 1.0 \omega_0$ (middle curve), and $\omega_d = 2 \omega_0$ (bottom curve).

For the case where the cut-off frequency of the equaliser is the same as the loudspeaker's resonance, the peak value of the displacement response is reduced by over 10dB. This has an important consequence on the maximum allowable input voltage. As discussed in §2.2.1, part B, the microspeaker under consideration has a hard displacement limit at 0.35 mm (peak). From a system-level standpoint, this represents a limit that cannot be exceeded. As can be seen in the middle curve of Figure 5.2, using the equaliser of (5.2) will increase the headroom by over 10dB.

It may also be possible to adaptively set the cut-off frequency of the equaliser in (5.2). As can be seen for the different cut-off frequencies plotted in Figure 5.2, the peak value of the displacement response reduces by 12dB per doubling of the cut-off frequency. It may be possible to use this effect as a 'dynamic displacement limiter.' Some success has been achieved with similar systems using analogue processing (Bjerre, 1993). A digital implementation using this approach is considered a subject for further research.

5.2. Compensation of nonlinear distortion

As explained in other parts of this thesis, compensation of nonlinear distortion in loudspeakers by electronic means has been a subject of research for several years. To date, it has been reasoned by much of the loudspeaker industry that the added cost and expense of electronic distortion compensation would not be reasonable. It has been considered that the cost of such systems would be much larger than the proper mechanical construction to keep distortion within acceptable limits.

As mentioned in the introduction, it was suggested by Klippel (2000) that a distortion compensation system can offer a net benefit to the loudspeaker's construction. Specifically, it was suggested by Klippel that the distortion caused by non-uniformity in the transduction coefficient ($B \cdot l$ -factor) in an 'equal-hung' voice-coil can be sufficiently compensated over the range of excursions of three-times the coil height, with moderate increased output requirement from the amplifier.

Here an 'equal-hung,' or 'equal-height,' voice-coil, as shown in Figure 5.3, is one which has the same height as the magnet gap. This is in contrast to an over-hung voice-coil, where the voice-coil's height is greater than the magnet gap's height, or an 'under-hung' voice-coil, where the opposite is the case.

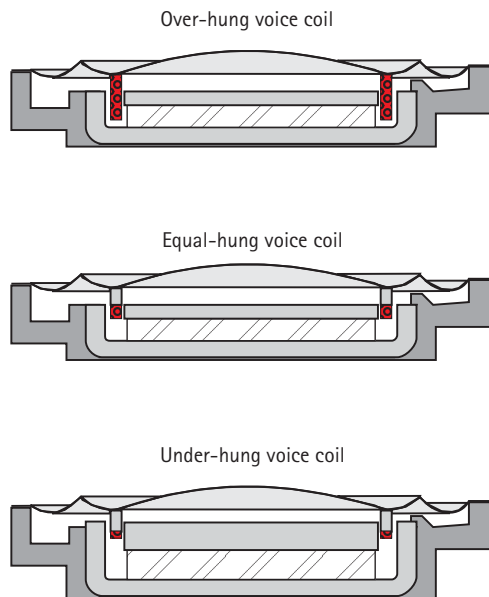


Figure 5.3: Coil shapes for over-hung, equal-hung and under-hung voice-coil, as would be implemented in a microspeaker.

As discussed in §2.1.5, a loudspeaker's acoustic output¹ is directly determined by its volume acceleration. For a given acoustic output, if the effective diameter of a loudspeaker is halved, the axial diaphragm vibration displacement must be increased by a factor of four. As there is typically commercial pressure from product marketing requirements to minimise the overall diameter of a loudspeaker, an important aspect of loudspeaker design is its maximum vibration displacement.

¹ Acoustic output here denotes the pressure-distance product produced by a loudspeaker in free-field (in the absence of any acoustically reflecting surfaces.)

For the microspeaker (Figure 2.1) the coil mass dominates the total moving mass.¹ As explained in §2.1.7, the characteristic sensitivity (or system gain) of a loudspeaker is inversely proportional to the total moving mass. By shortening the height of the voice-coil, the total moving mass may be reduced, thereby increasing the loudspeaker's sensitivity.

However, shortening the coil height has a problem. It will increase nonuniformity in the transduction coefficient, thereby increasing nonlinear distortion. For this reason, loudspeaker designers commonly use over- or under-hung voice-coils in high-displacement loudspeakers to keep nonlinear distortion at acceptably low levels

From the perspective of loudspeaker optimisation, an over-hung voice-coil is sub-optimal, because it requires excess diaphragm mass, reducing its sensitivity. Conversely, an under-hung voice-coil is a sub-optimal design because it requires excess magnet material, which increases the loudspeaker's overall cost and weight. It is, therefore, considered here that the nonlinear distortion created by nonuniformity in the transduction coefficient be compensated electronically.

Electronic compensation of nonlinear distortion does, of course, have its own cost. The cost is measured in this study by the additional amplifier output required for compensation of nonlinear distortion, measured in peak amplitude volts. As mentioned in the introduction, many audio products already employ considerable digital signal processing. It is assumed that the processing needed for distortion compensation is simple relative to existing signal processing algorithms. The cost of the hardware needed for performing the processing for distortion compensation is, therefore, not considered here.

A series of simulations have been made to find the optimal trade-off between increase in sensitivity due to coil height reduction, and increase in amplifier output required for nonlinear distortion compensation. Details of the simulation method are presented in §5.2.1 below, and the results and discussion are presented in §5.2.2.

To test the hypothesis that a net benefit is derived from shortening the coil height and compensating the resulting nonlinear distortion electronically, a set of special microspeakers have been prepared with shortened coil heights. The simple nonlinear distortion compensation algorithm presented in §3.3.7 has been used to compensate for the nonlinear distortion created by the increased nonuniformity in the transduction coefficient caused by shortening the coil height. A set of measurements of harmonic distortion of a narrow-band signal to asses the performance of the distortion compensation algorithm are presented in §5.2.3.

5.2.1. Simulations of effective sensitivity increase vs. coil height

As discussed above, the additional amplifier output required for compensation of nonlinear distortion generated by nonuniformity in the transduction coefficient has been simulated for a range of coil heights, as a function of displacement (excursion) level. The range of voice coil heights considered is from 0.1mm to 2.1mm, as per Figure 5.4.

¹ The total moving mass m_t , defined in (2.34), is the sum of the mass of the diaphragm, voice-coil, and mass-like acoustic loading. The diaphragm of a microspeaker, made of thin polycarbonate plastic, has a mass of about 1mg. Mass-like acoustic loading on the diaphragm, under atmospheric conditions, is about 1mg. Depending on loudspeaker type, the mass of the coil will be 50 – 100 mg.

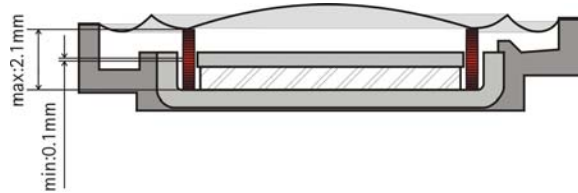


Figure 5.4: Variation of coil height made in simulations.

Lumped parameter quantities vs. coil height

Changing the coil height directly affects several ‘lumped parameters’ of the loudspeaker:

- nonuniformity in the transduction coefficient
- moving mass, m_d
- blocked (DC) electrical resistance R_{eb}

Nonuniformity in the transduction coefficient is determined by variation in the magnetic field along the coil gap $B(x)$, and by the effective coil height in the gap, according to two different formulae presented below. Data on variation in the magnetic field along the coil gap $B(x)$ was derived from a FEM simulation, which is plotted in Figure 5.5.

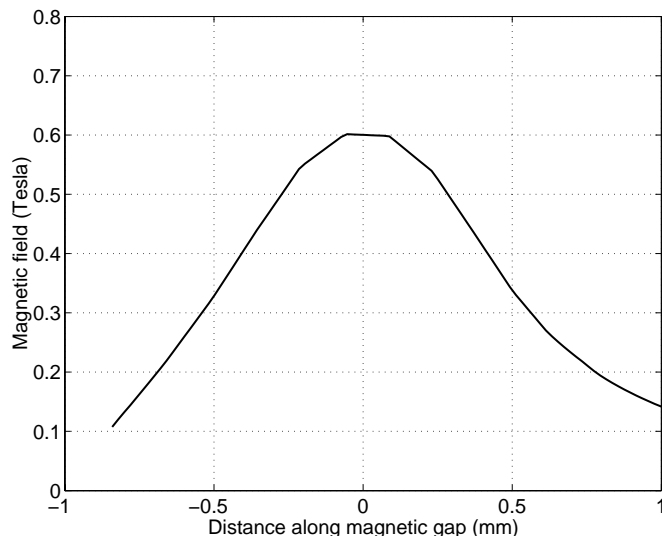


Figure 5.5: Magnetic field strength vs. distance along coil gap, from FEM simulation.

Changes to the force factor profile $\phi(x)$ due to changes in the coil height can be interpreted in two ways. We can consider a coil length that varies directly with the coil height, and thus the force factor profile is determined from

$$\phi(x_d) = l_h \int_{h_l}^{h_u} B(\xi - x_d) d\xi. \quad (5.6)$$

This produces force-factor profiles, for different coil heights, as shown in the upper half of Figure 5.6. Alternatively, we can consider a fixed coil length, l_0 , which is independent of the coil height, and thus determined from

$$\phi(x_d) = \frac{l_0}{h_u - h_l} \int_{h_l}^{h_u} B(\xi - x_d) d\xi. \quad (5.7)$$

For different coil heights, this produces force-factor profiles as shown in the lower half of Figure 5.6.

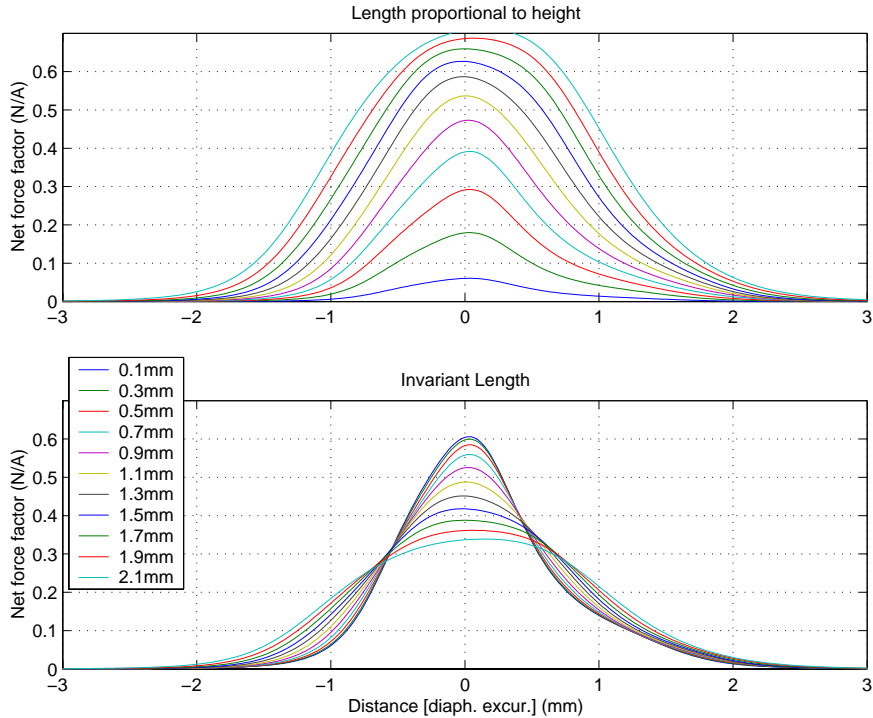


Figure 5.6: Determination of force factor profile, $\phi(x)$. UPPER: Coil wire length proportional to coil height, as per (5.6). LOWER: Coil wire length fixed, as per (5.7).

In order to have a fixed coil length for shorter coil heights, the coil would have to be thicker. A thicker coil would require a wider magnet gap, which would reduce the magnetic field strength, and consequently the sensitivity. Magnet gap widths and coil thicknesses are typically finely optimised. Therefore, it has been chosen to study only the case of (5.6), where the coil length varies linearly with the coil height.

The blocked electrical (DC) resistance is, for the simulation, determined according to the coil height by

$$\begin{aligned} R_{eb} &= R_0 + R_{eff} \frac{h}{h_0} \\ &= 1 + 8 \frac{h}{1.2 \times 10^{-3}} \end{aligned} \quad (5.8)$$

In (5.8), R_0 describes a ‘residual’ resistance, in the output impedance of the amplifier, and the electrical connections between the amplifier and the loudspeaker.

The mass m_d has been determined according to the coil height according to.

$$\begin{aligned} m_d &= m_a + m_{\text{eff}} \frac{h}{h_0} \\ &= 1.78 \times 10^{-6} + 18.5 \times 10^{-6} \frac{h}{1.2 \times 10^{-3}} \end{aligned} \quad (5.9)$$

In (5.9), m_a is the effective mass presented by the acoustic load, which is obviously invariant to the coil height. In the loudspeakers under study, it has been found that the mass of the diaphragm is significantly less than 1mg. Consequently, the total effective moving mass m_d is simply the sum of the coil mass and ‘acoustic’ mass.

For these simulations, it was decided to keep the resonance frequency fixed. The stiffness has therefore been varied along with the mass, so as to have a constant resonance frequency, as so:

$$k_{d,0} = m_d (2\pi f_0)^2 \quad (5.10)$$

The variation in various lumped parameter elements with the coil height used for simulations is shown in Figure 5.7. Attention is drawn to the lower right chart of Figure 5.7, which shows the equivalent rear-cabinet volume, V_{AS} . For the shortest coil heights, and thus the lowest moving mass values, a rather low stiffness (high compliance) is necessary to achieve the same f_0 . This produces significantly higher V_{AS} than would be typical for the loudspeaker under study (4cm³ is typical.)

Attention is also drawn to the lower left chart of Figure 5.7. The shortest coil heights produce a very low DC resistance, and thus low Q_{tc} . The shortest of coil heights produce a Q_{tc} of around 0.3, which is perhaps lower than could be thought ideal. This is shown in the small-signal far-field acoustic-pressure sensitivities, calculated from the lumped parameter quantities for the different coil heights, shown in Figure 5.8.

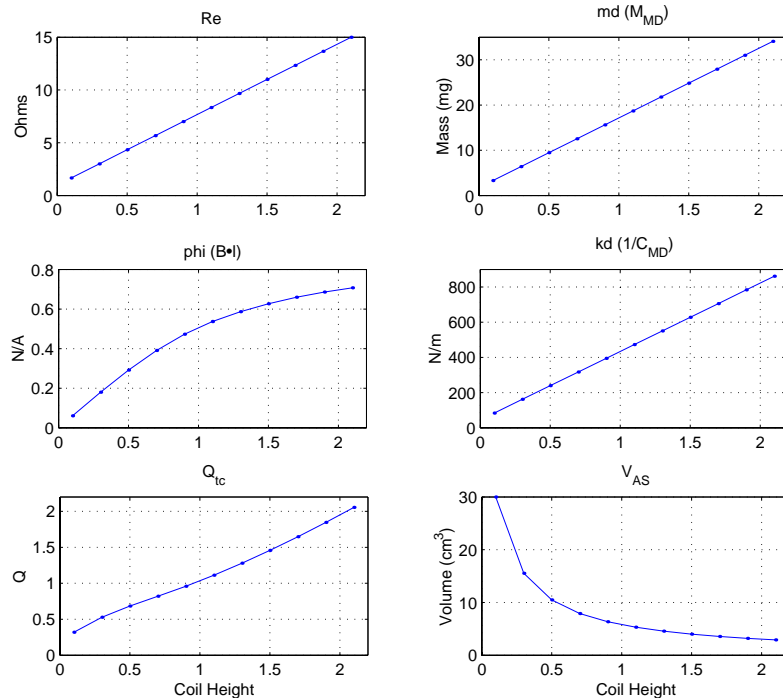


Figure 5.7: Variation in ‘lumped parameter’ quantities with coil height, for purposes of simulation.

The linear pressure/voltage frequency response for the different coil heights was calculated according (2.35) using the parameter value for different coil heights. The frequency response all of these coil heights are plotted in Figure 5.8.

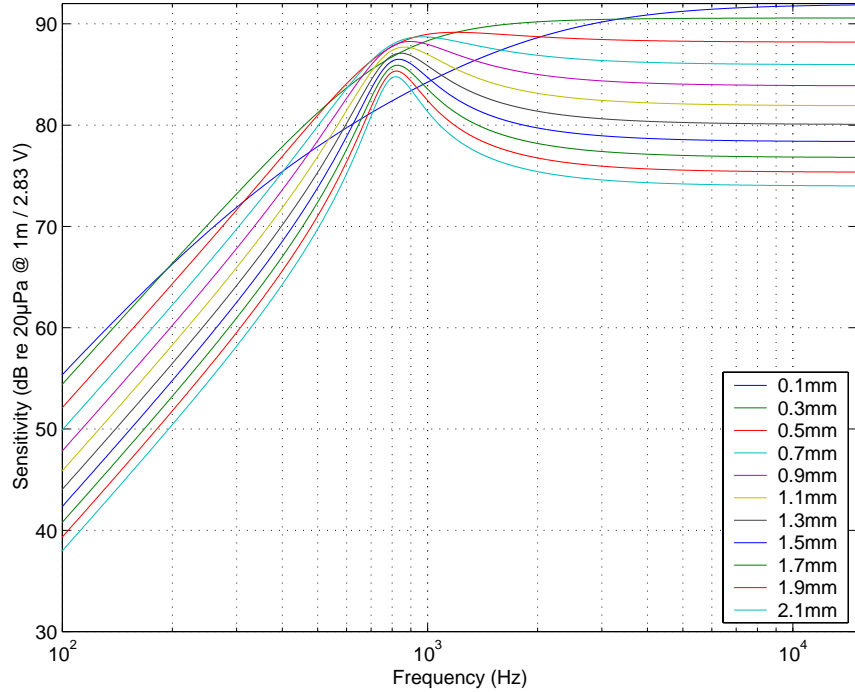


Figure 5.8: Small-signal far-field acoustic pressure sensitivity (referenced to 1m), for LPM quantities calculated for the different coil heights.

Effective sensitivity vs. coil height and excursion

The effective sensitivity, for the combined controller-amplifier-loudspeaker system, has been calculated to evaluate the trade-off between the increased sensitivity provided by a shorter height voice-coil, and the decrease in sensitivity created by the additional amplifier output required for compensation of the distortion generated by shortening the voice coil height. For the simulation herein, the effective sensitivity S_{eff} has been calculated as a function of excursion, based on the small signal sensitivity S_0 , and the ‘correction gain’ at the specified displacement, C_{disp-n} , according to:

$$S_{eff} = \frac{1}{C_c} \left. \frac{p_{lm}(s)}{v_c(s)} \right|_{x \sim 0} \quad (5.11)$$

The correction C_c gain represents the ratio of the peak value of the controller output $u(t)$ to the peak value of the controller input $w(t)$, as per Figure 3.5.

$$C_c = \frac{\text{Pk}\{u(t)\}}{\text{Pk}\{w(t)\}} \quad (5.12)$$

This effective sensitivity has been plotted as a function of peak excursion, for the above mentioned range of coil heights, for several different frequencies. The results of the simulations are plotted in Figure 5.9 - Figure 5.25. The results for each frequency are plotted in a separate figure.

Nonuniformity in the suspension stiffness $k(x_d)$ has not been considered in these simulations, as measurements of its nonuniformity have shown it to be reasonably uniform. Simulations are made for

excursions up to 2.0mm peak, which would cause the diaphragm-coil assembly to contact the magnet or frame, occurring at about 0.35mm, as discussed in §2.2.1, part B. This effect is not considered in the simulations results. As this results in an effective stiffness $k(x_d)$ that is infinite, an infinite correction gain would be required to overcome this problem.

5.2.2. Simulation results

It can be seen in each of Figure 5.9 - Figure 5.25 that, at small displacements (less than 0.1mm Pk), the shortest coil height has the highest effective sensitivity.

There seems to be some ‘critical displacement,’ below which the shorter voice coil heights have a higher effective sensitivity, and above which the larger coil heights have a higher effective sensitivity. The lower effective sensitivity for the shorter coil heights at higher displacement is due to the higher correction gain, defined above (i.e. the additional amplifier output needed to compensate for the resulting nonlinear distortion).

At lower frequencies this ‘critical displacement’ occurs at a single, well defined displacement level of about 0.8mm Pk, for all of the coil heights. This is seen for all frequencies up to 633 Hz (plotted in Figure 5.9 through Figure 5.14). This can be understood as the phenomenon occurring below the main resonance frequency f_0 .

At frequencies around the main resonance frequency, this ‘critical displacement’ is not so well defined. From about 825 Hz (plotted in Figure 5.15) through 1816 Hz (plotted in Figure 5.18), the peak displacement level above which the larger voice-coil heights have a higher effective sensitivity is different for different coil heights.

At higher frequencies, 2000Hz and above (plotted in Figure 5.19 through Figure 5.25), this critical displacement is again well defined, occurring at a higher level of about 1.1mm.

From these simulations, it is concluded that a significant increase in sensitivity can be obtained by shortening the voice-coil height. For the motor structure under consideration (i.e. the magnetic field variation shown in Figure 5.5), it is concluded that shortening the coil height from 1.2mm to 0.3mm should provide a sensitivity increase of about 8dB, when used over the specified displacement range of 0.35mm Pk. Furthermore, the additional amplifier output required for compensating the distortion resulting from a reduction of the coil height from 1.2mm to 0.3mm should be marginal, i.e. less than 1dB.

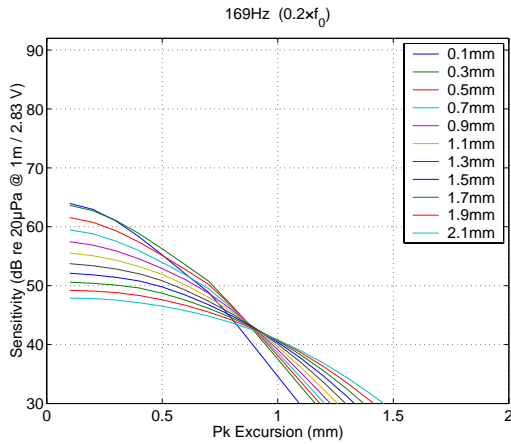


Figure 5.9: 168 Hz

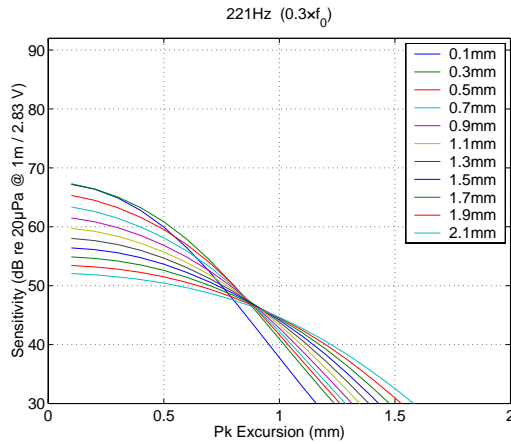


Figure 5.10: 221 Hz

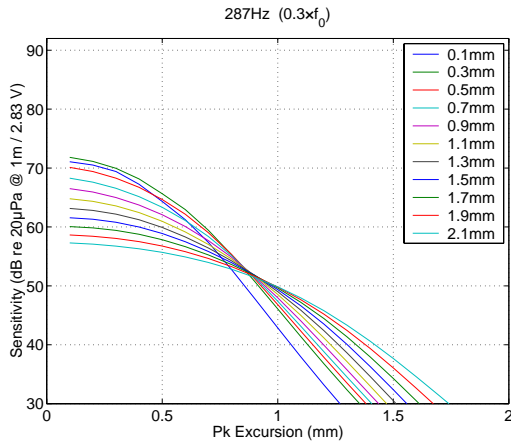


Figure 5.11: 287 Hz

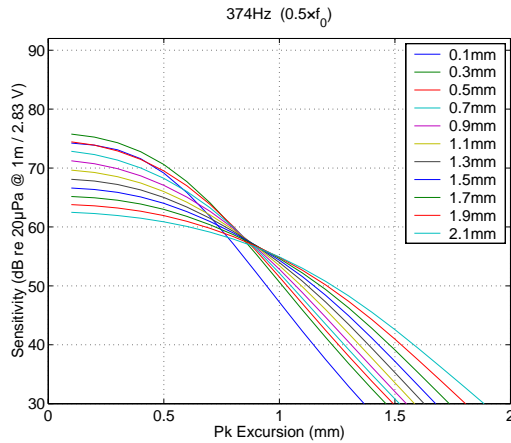


Figure 5.12: 374 Hz

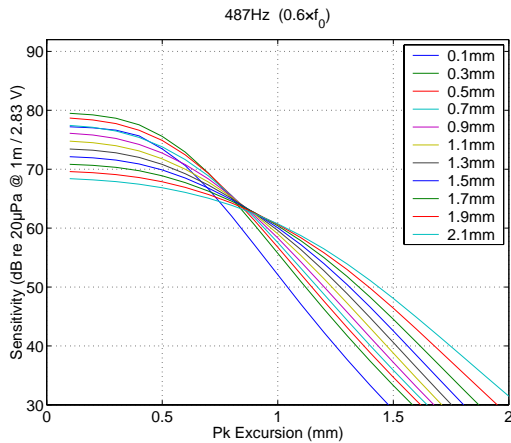


Figure 5.13: 487 Hz

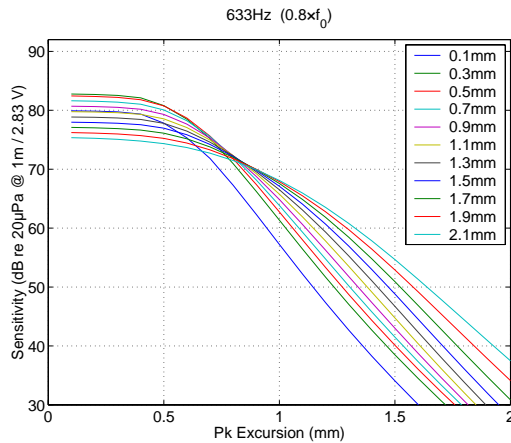


Figure 5.14: 633 Hz

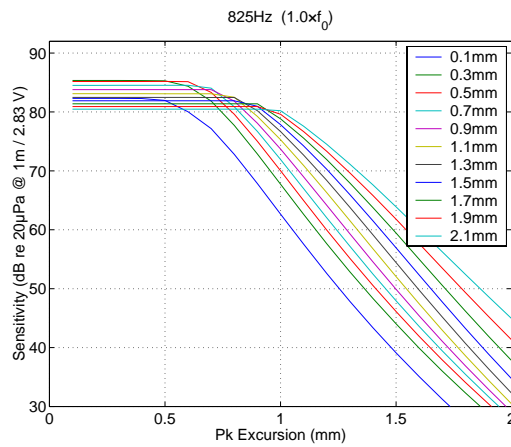


Figure 5.15: 825 Hz

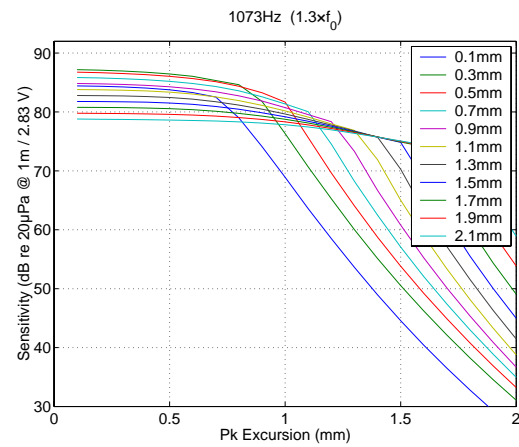


Figure 5.16: 1073 Hz

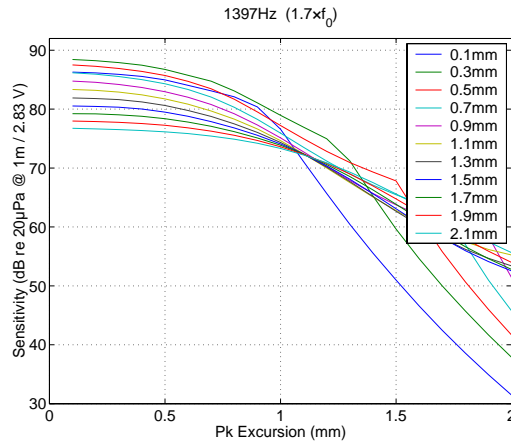


Figure 5.17: 1397 Hz

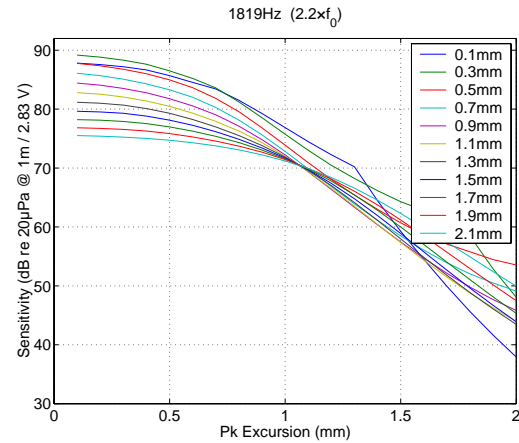


Figure 5.18: 1819 Hz

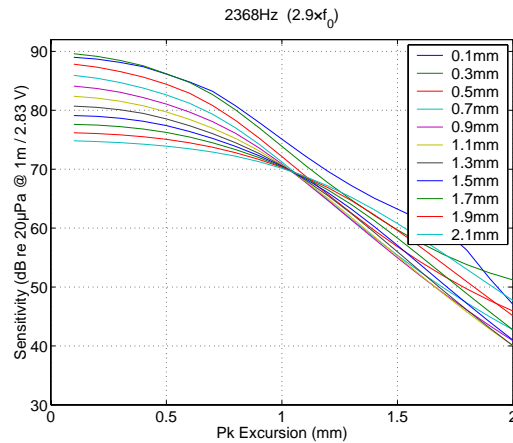


Figure 5.19: 2368 Hz

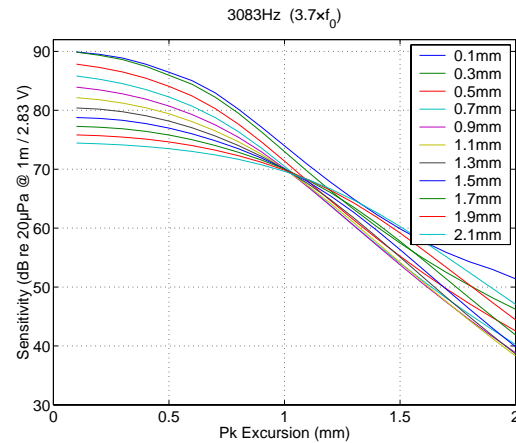


Figure 5.20: 3083 Hz

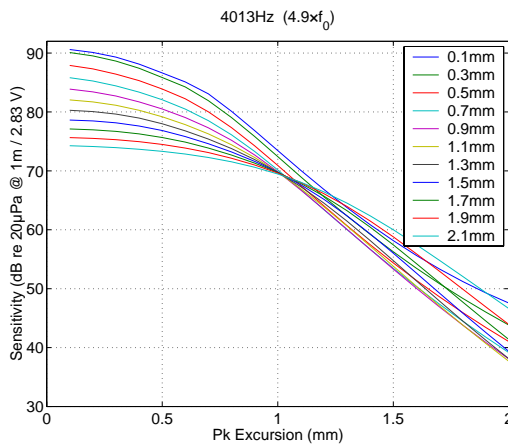


Figure 5.21: 4013 Hz

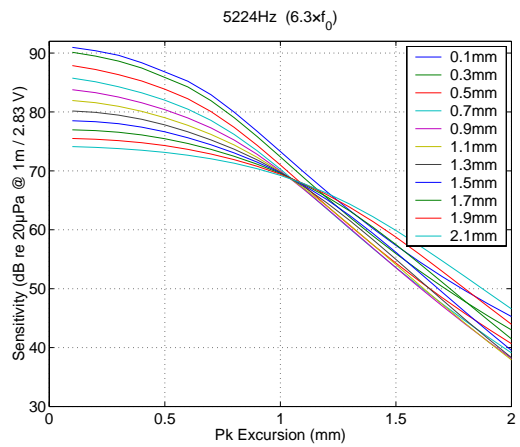


Figure 5.22: 5224 Hz

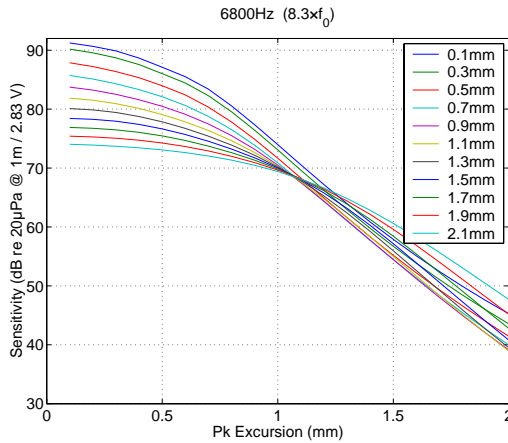


Figure 5.23: 6800 Hz

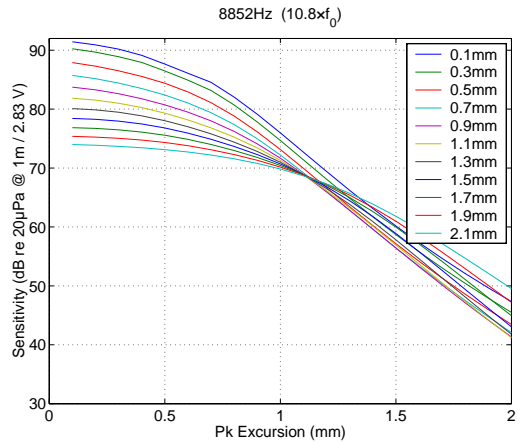


Figure 5.24: 8852 Hz

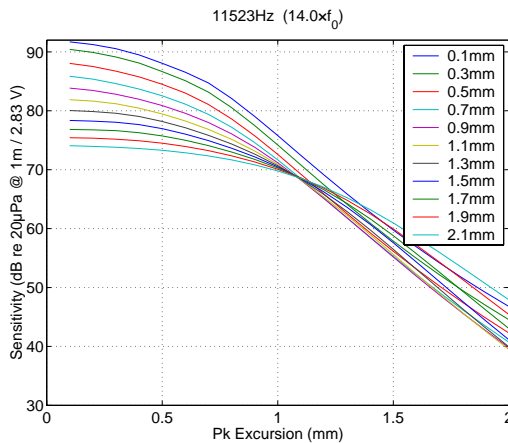


Figure 5.25: 11523 Hz

5.2.3. Distortion compensation on shortened- height voice-coil loudspeakers

In order to verify the simulation results presented in §5.2.2 above, a set of modified coil-height loudspeakers was prepared on which measurements were made. The modified coil-height speakers were made according to the specification shown in Figure 5.26. These modified coil-height loudspeakers were prepared by Philips Speaker Solutions for the purpose of this research.

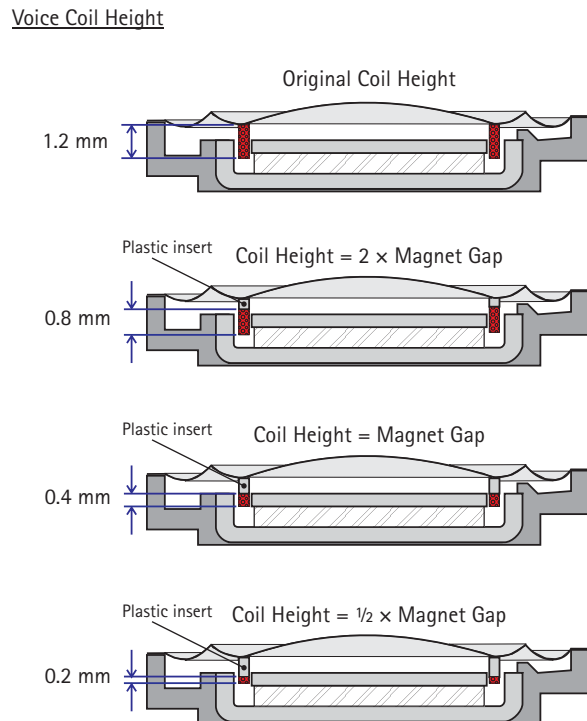


Figure 5.26: Specially prepared microspeakers with shortened coil heights.

Measurements of the linear response

Measurements of the linear frequency response of these modified coil height loudspeakers are shown in Figure 5.27. Measurements were made according to the set-up described in §A.4 in Appendix A (see p. 177.) The loudspeakers were placed in an acoustically free field. The loudspeakers were mounted in a closed-box, with a rear cavity volume of approximately 2.0cc. In this way, the acoustic environment corresponded as closely as possible to that assumed by (2.36).

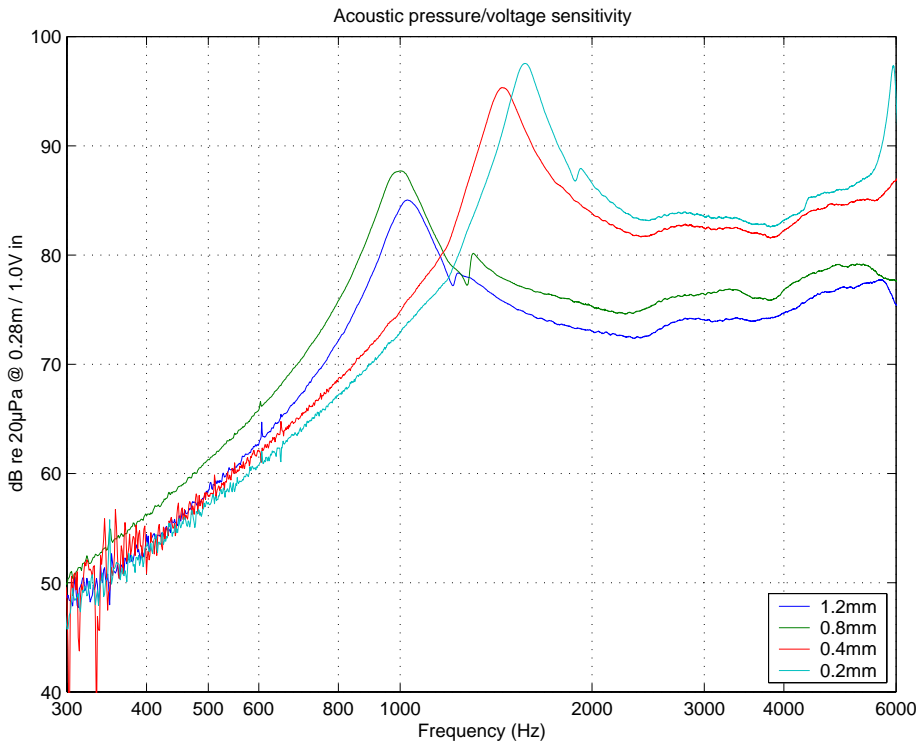


Figure 5.27: Linear pressure/voltage frequency response of specially prepared shortened-voice coil height loudspeakers. The original specification voice coil height, 1.2mm, is shown in blue for reference.

The acoustic frequency response measurements in Figure 5.27 show that the shorter coil height loudspeakers have a higher characteristic sensitivity. Recall that the characteristic sensitivity, S_0 defines the sensitivity above the resonance frequency, as per (2.36). As can be seen in Figure 5.27, the characteristic sensitivity of the shortest-height voice coil (0.2mm) is approximately 10dB above the original-specification voice coil height (1.2mm).

The higher resonance frequency of the shorter-height voice-coil speakers is indicative of the lighter mass produced by shortening the voice coil. As can be seen below the resonance frequency, all speakers have roughly the same sensitivity. As, below resonance, the response is dominated by the suspension stiffness, it can be said that the stiffness of all of the samples is roughly the same. The one exception is the 0.8mm voice-coil height sample. By comparison to the response of the original specification 1.2mm height voice coil, the 0.8mm high voice-coil sample has the same resonance frequency, but has approximately 3dB higher voltage sensitivity throughout the measured frequency range. This can be attributed to a slightly lower suspension stiffness in the 0.8mm high voice-coil sample. Small deviations in the suspension stiffness from one sample to another are known to occur due to manufacturing tolerances, as discussed in §2.4.

The nominal power sensitivity, calculated from the voltage sensitivity, is plotted in Figure 5.28. This nominal power sensitivity has been calculated from the voltage sensitivity according to:

$$p_{1W}(s) = p_{1V}(s)\sqrt{R_{eb\cdot n}} \quad (5.13)$$

where $p_{1W}(s)$ is the nominal power sensitivity, $p_{1V}(s)$ is the voltage sensitivity, and $R_{eb\cdot n}$ is the DC-resistance of the sample concerned.

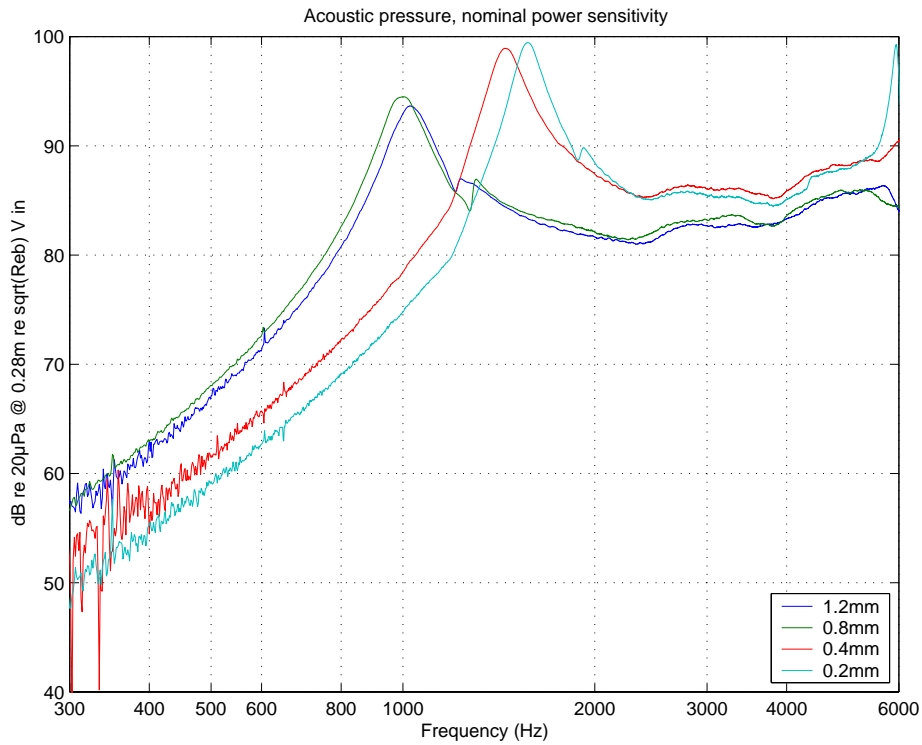


Figure 5.28: Nominal pressure / power sensitivity for the same loudspeakers for which measurements are plotted in Figure 5.27. This represents the theoretical 1W sensitivity.

The increase in nominal power sensitivity for the 0.2mm high coil is only about 4dB over the original 1.2mm coil height. This is due to the lower DC resistance of the 0.2mm high coil (approx. 1.5Ω) compared to the 1.2mm high coil (7.2Ω). The nominal power sensitivity below the resonance frequency is somewhat lower for the shorter-height voice coils. It is expected that this is due to a higher effective stiffness in the shorter-height voice coil speakers - an accidental result not caused by shortening the voice coil height, but due to manufacturing tolerances. This can be seen in the lower voltage sensitivity that the shorter voice-coil height speakers have below the resonance frequency shown in Figure 5.27. With the below-resonance power sensitivity given by

$$p_{1W}(s)|_{f \ll f_0} = s^2 \frac{S_d \phi_0}{\sqrt{R_{eb}}} \quad (5.14)$$

It is expected that if the effective stiffness were to have been the same for all for loudspeakers, the below-resonance power sensitivity would be more similar between them.

In the simulations presented in §5.2.2 above, the suspension stiffness was changed for different coil heights, so as to keep the resonance frequency constant. This was not done in the physically prepared samples. Although it is generally possible to freely adjust the suspension stiffness, by adjusting the thickness of the plastic making up the suspension material, this was not done, in order to simplify the sample preparation process.

Set-up and parameter tuning

The distortion compensation algorithm developed in §3.3.7 is used to compensate for nonlinear distortion created in the modified coil-height loudspeakers. Harmonic distortion is assessed with a

specially synthesised narrow-band signal. This signal is synthesised by band-pass filtering white noise with 10th-order Chebyshev filters, providing a 30Hz pass-band with high out-of-band cut-off slope. This signal was chosen to assess the harmonic distortion created by the loudspeaker with a simple measurement of the autopower spectrum of the acoustic pressure field. This narrow-band noise signal was chosen over sinusoidal signals to demonstrate the proper operation of the distortion compensation algorithm. It was considered that this narrow-band noise signal would be a more effective assessment of the operation of the distortion compensation algorithm than more commonly used sinusoidal signals, as the harmonic distortion created by sinusoidal signals could be compensated for by simple harmonic superposition.

For all measurements of the compensation of nonlinear distortion, the input level to the loudspeaker was set so that the maximum allowable diaphragm-coil displacement was achieved. For the loudspeakers under investigation here, this was 0.35mm Pk. This limit is set by the mechanical construction of this particular loudspeaker type.¹

Parameters of the loudspeaker model were obtained in the following manner. The effective moving mass of the loudspeaker was determined using the method described in Appendix B. The remaining parameters describing the linear characteristics were determined using the system identification algorithms presented in chapter 4, above. Specifically, the electrical current output error form described in §4.2 was used. Parameters were allowed to converge to their final values using a white noise signal.

Parameters describing nonlinear characteristics were determined by trial-and-error, tuning ϕ_k (the coefficients of a polynomial representation of $\phi(x_d)$) by hand. Values of ϕ_k were chosen which minimised the harmonic distortion over a range of frequencies of the narrow-band signal.

The commercial instrument discussed in §2.2.1, part A, which can determine ϕ_k , though available at the time measurements were made, could not be used. This is due to the fact that at that time the commercial system could not analyse loudspeakers with a resonance frequency higher than 800Hz. As can be seen from Figure 5.27, the resonance frequency of these loudspeakers is above this limit. The values of ϕ_k determined by hand compared favourably with those determined by this commercial instrument on similar loudspeakers with a resonance frequency lower than 800Hz.

The set-up of the loudspeakers under test was otherwise the same as that for which the linear response of the shortened-voice-coil-height loudspeakers was measured, as described above.

Measurement results

Harmonic distortion of the narrow-band signal can be seen in measurements of the autopower spectrum of the acoustic pressure, shown on the left side of Figures 5.29 through 5.32. The reduction in the harmonic distortion provided by the nonlinear control algorithm in (3.28) is plotted in the same figures. In each of these figures, the solid line shows the spectra with the compensation on, and the broken line shows the spectra with the compensation off.

The autopower spectrum of the voltage from the controller to the speaker is shown on the right side of Figures 5.29 through 5.32. Again, in these figures, the solid line shows the spectra with the compensation on, and the broken line shows the spectra with the compensation off. As can be seen in these figures, there is an increase in the ‘harmonics’ of the narrowband signal when the compensation

¹ As discussed in §2.2.1, part B, higher displacements than 0.35mm peak cause contact between its diaphragm-coil assembly and magnet-frame. Therefore this hard limit could not be exceeded in these measurements.

is on. This represents the ‘anti-distortion’ generated by the nonlinear control algorithm needed to compensate for the distortion generated in the loudspeaker.

The harmonic distortion of the narrow band signal generated by each of the different coil-height loudspeakers is summarised in Table 5.1. The percentage-values shown in this table are sum of the level of 2nd-4th harmonics relative to the fundamental. The percentage harmonic distortion, calculated in this way, is shown in Table 5.1 for both the compensation on and off.

Coil height	Fig. No.	BP sig. Cen. Freq.	Max % Harm. Dist.	
			Comp. Off	Comp. On
0.8mm	Figure 5.29	800 Hz	5.4 %	1.2 %
0.4mm	Figure 5.30	800 Hz	12.9 %	3.2 %
0.2mm	Figure 5.31	800 Hz	17.8 %	3.2%
0.2mm	Figure 5.32	1200 Hz	3.1%	2.3%

Table 5.1: Reduction of harmonic distortion for each coil-height.

As can be seen in Table 5.1, the shorter coil-height loudspeakers generate more harmonic distortion; the 0.8mm height coil (the highest) shows the least distortion, and the 0.2mm height coil (the shortest) shows the most increase in harmonic distortion. This is as expected, due to the increase in nonuniformity of the transduction coefficient caused by decreasing the coil height.

The nonlinear control algorithm was found to reduce the maximum harmonic distortion from at most 17.8% (in the 0.2mm height coil) to about 3%. The highest amount of harmonic distortion measured with the compensation on was 3.2% (for the same 0.2mm height coil).

The harmonic distortion present in the original-specification height coil (1.2mm) was about 5% for the same signal, at the same displacement. It is concluded, therefore, that the nonlinear control algorithm of (3.28) is capable of compensating the distortion caused by the reduction in coil height, at least for this narrow-band signal used for these measurements.

The additional voltage needed for compensation of the resulting distortion was at most 10% above the voltage level with the compensation off. This translates to an increase of about 0.85dB. These measurements thus seem to confirm the conclusions drawn from the simulations presented in §5.2.2. Specifically, these measurement results seem to confirm the conclusion that reducing the coil height from 1.2mm to 0.3mm would result in an 8dB voltage sensitivity increase, and require at most 1dB of additional amplifier output for compensation of the resulting distortion. In measurements, the coil height was reduced to 0.2mm, the voltage sensitivity increase was found to be 10dB, and the additional amplifier output required for compensation was at most 0.85dB.

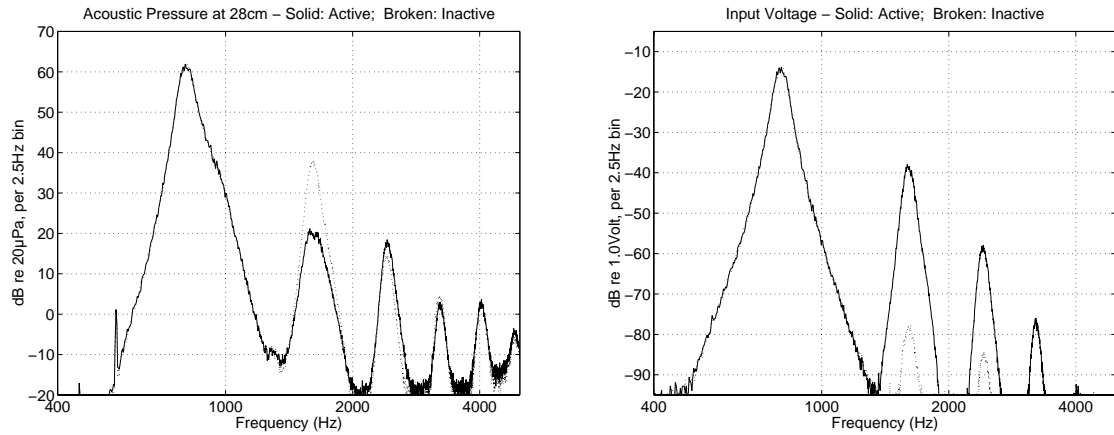


Figure 5.29: 0.8mm coil height, distortion analysis for NB signal centred on 800Hz. LEFT: Acoustic pressure; RIGHT: Output voltage from amplifier.

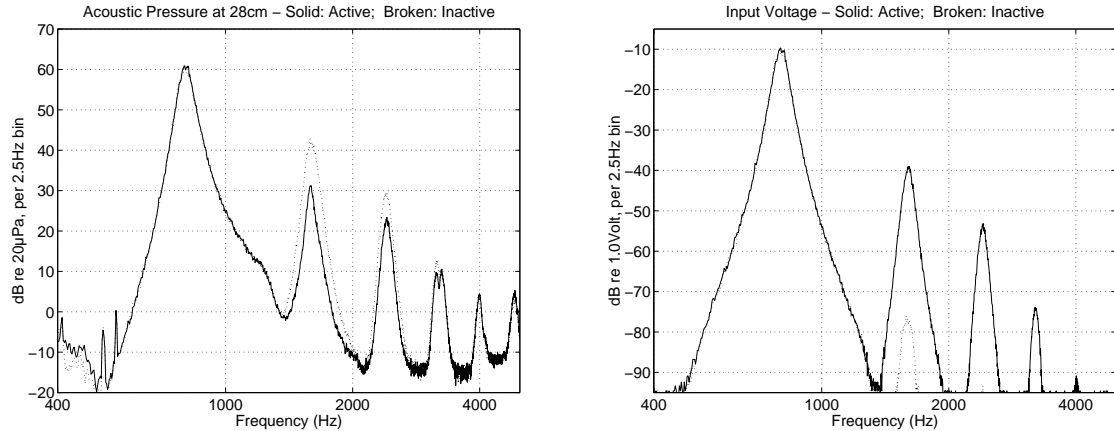


Figure 5.30: 0.4mm coil height, distortion analysis for NB signal centred on 800Hz. LEFT: Acoustic pressure; RIGHT: Output voltage from amplifier.

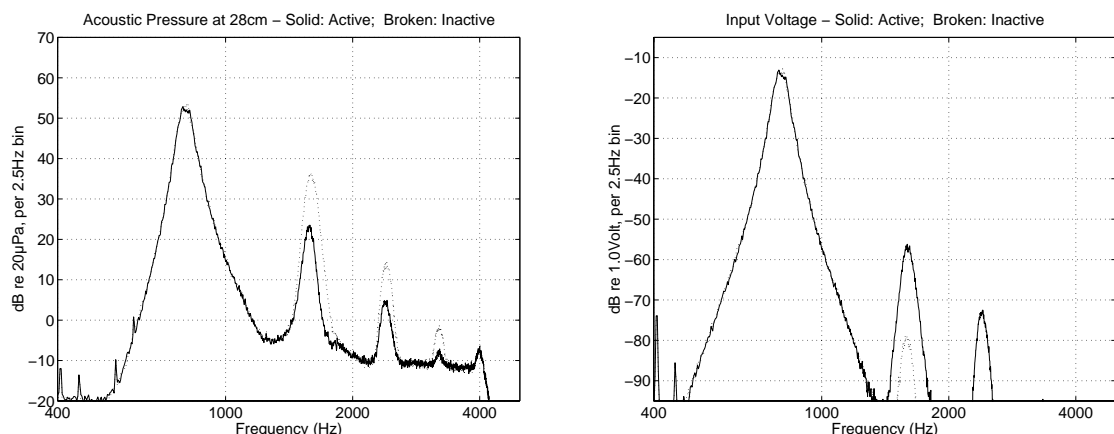


Figure 5.31: 0.2mm coil height, distortion analysis for NB signal centred on 800Hz. LEFT: Acoustic pressure; RIGHT: Output voltage from amplifier.

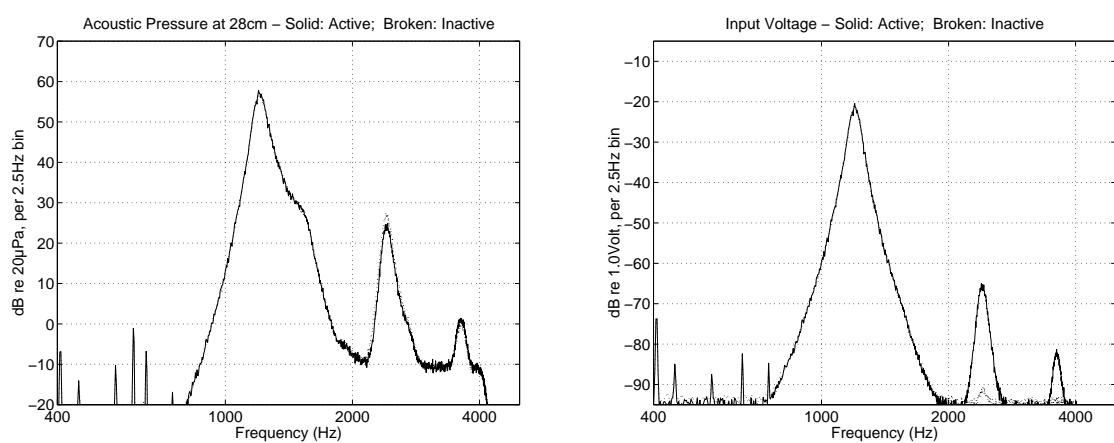


Figure 5.32: 0.2mm coil height, distortion analysis for NB signal centred on 1200Hz. LEFT: Acoustic pressure; RIGHT: Output voltage from amplifier.

5.3. References

- Bjerre, Egon, "Loudspeaker Arrangement with Frequency Dependent Amplitude Regulation," U. S. Patent 5,481,617. Filed: Mar. 1, 1993. Granted: Jan. 2, 1996. Assignee: Bang & Olufsen A/S, Struer, Denmark.
- Klippel, Wolfgang, "Direct Feedback Linearisation of Nonlinear Loudspeaker Systems," *J. Audio Eng. Soc.*, **46**, pp. 499-507. (Jun. 1998)
- Klippel, Wolfgang J., "Adaptive Nonlinear Control of Loudspeaker Systems," *J. Audio Eng. Soc.* **26**, pp. 939-954. (Nov. 1998)
- Klippel, Wolfgang J., Personal, unwritten correspondence, Paris, France. (February 22, 2000)
- Leach, W. Marshall , Jr., "A Generalised Active Equaliser for Closed-Box Loudspeaker," *J. Audio Eng. Soc.*, **38**, pp. 142-146. (Mar. 1990)
- Schurer, Hans, *Linearisation of Electroacoustic Transducers*, Ph.D. Thesis, University of Twente Enschede, ISBN 90-365-1032-5. (1997)
- Schurer, Hans, Cornelis H. Slump, and Otto E. Herrmann, "Theoretical and Experimental Comparison of Three Methods for Compensation of Electrodynamic Transducer Nonlinearity," *J. Audio Eng. Soc.*, **46**, pp. 723 – 740. (Sept. 1998)

6. Conclusions

This thesis studies practical implications of applying active control to a loudspeaker. By developing a discrete-time model of the continuous-time loudspeaker dynamics, digital processing for active control is made sufficiently simple so that it may be cost-effective to introduce active control to existing products. The adaptive feedforward architecture is found to be the most practical implementation of active control. It is shown that active control can provide a net benefit to the loudspeaker, using both linear and nonlinear processing.

A discrete-time model of a loudspeaker is developed in this thesis. This discrete-time model simplifies the digital signal processing algorithms for active control. The key simplification is derived from digital filters designed to have the same response characteristics as dynamics of the loudspeaker. Simplicity is enabled by keeping the order of the digital filters the same as the order of dynamics of the loudspeaker. This achieves simplification over previously published algorithms for active control, which simulated continuous-time dynamics by numerical integration, or by high-order non-recursive filters.

The adaptive feedforward architecture, using digital signal processing, is found to be the most practical method for implementing active control of loudspeakers. Two alternative architectures, feedback processing and non-adaptive feedforward processing, are considered impractical. The feedback architecture is discarded due to its need for a direct feedback signal from the loudspeaker, which is impractical or expensive to obtain. The pure feedforward (non-adaptive) architecture is discarded due to its sensitivity to misalignment to the loudspeaker. The adaptive feedforward architecture is chosen due to its ability to tune itself to changes in the loudspeaker caused by temperature fluctuations and ageing. Furthermore, it is shown that the adaptive process, performed by system identification, can operate effectively using a voice-coil current signal, which is simple and inexpensive to obtain from the loudspeaker.

Active control is shown to provide a net benefit to a loudspeaker system. Standard linear active control, or equalisation, enables certain parts of a loudspeaker's response to be controlled electronically. It is specifically shown that the highly undamped nature of small loudspeakers can be controlled by simple equalisation. The adaptive feedforward architecture for active control, described above, ensures the equaliser is properly tuned to the loudspeaker.

Active control is also shown to provide a net benefit through nonlinear processing. Nonlinear active control can correct small nonlinearities introduced by relaxing certain standard loudspeaker design requirements. Specifically, shortening the height of a loudspeaker's voice-coil increases its sensitivity, though introduces a certain amount of weak nonlinearity. Simulations and measurement show that this weak nonlinearity can be compensated by active control. Furthermore, it is shown that the additional amplifier voltage output required for compensation of this nonlinearity is less than the increase in sensitivity provided by shortening the voice-coil height. Simulations and measurements show this method can provide a net increase in voltage sensitivity up to 9dB, and a power sensitivity increase up to 4dB, over existing loudspeaker designs.

Nonlinear active control is assessed in this thesis by its ability to control harmonic distortion. Intermodulation distortion – generally considered more important in regard to subjective loudspeaker quality – has not been studied. Subjective tests assessing the performance of the nonlinear distortion compensation algorithm have not been carried out either. It is expected that by reducing harmonic distortion at the frequencies concerned, the algorithm would reduce intermodulation distortion by consequence. This has not, however, been verified, and would be a suitable subject of further investigation. Furthermore, it is recommended that some degree of formal subjective evaluation of the

nonlinear distortion compensation algorithm be performed before this algorithm is used in a commercial product.

Results from all algorithms are from implementations using double-precision floating point processing. Implementation of any of these algorithms in actual commercial products would be done using fixed-point arithmetic. No investigations have been made on the impact of using fixed-point arithmetic on these algorithms. Experience with other algorithms suggests that the most likely problem in fixed-point implementation is the proximity of poles in various systems' transfer functions to the unit circle. This most likely will require 16 bit data input-output streams to be computed with 32 bit or 40 bit arithmetic. This kind of architecture has been successfully used in many audio DSP applications. Thus fixed-point considerations for these algorithms are currently thought to be more a matter of engineering implementation than further academic research.

Appendix A. Experimental set-up and tuning

The various experimental set-ups and hardware used through this thesis are presented in this appendix. This includes set-ups for primary experiments presented in the thesis, as well as those used in ‘background research.’

A.1. Hardware implementation of algorithms

The algorithms for system identification of the loudspeaker presented in Chapter 4 and the distortion compensation algorithm presented in §3.3.7 were written and implemented on a standard desktop PC. The algorithms were written in ANSI C, using double-precision floating point arithmetic. Analogue input-output was handled by a standard sound card.

The system identification algorithm developed in §4.2, i.e. the electrical current output error plant model form, was used to identify those parameters of the loudspeaker which were known to change. These identified parameters were then used in the linear dynamics and inverse dynamics blocks of the nonlinear feedforward processor. A block diagram of the complete system architecture is shown in A as mentioned in §4.1.2.

A.2. Electrical impedance measurement

A.2.1. Differential vs. single-ended considerations

The simplest conceptualisation of the arrangement for using a shunt resistor to measure the electrical current is shown in Figure A.1.

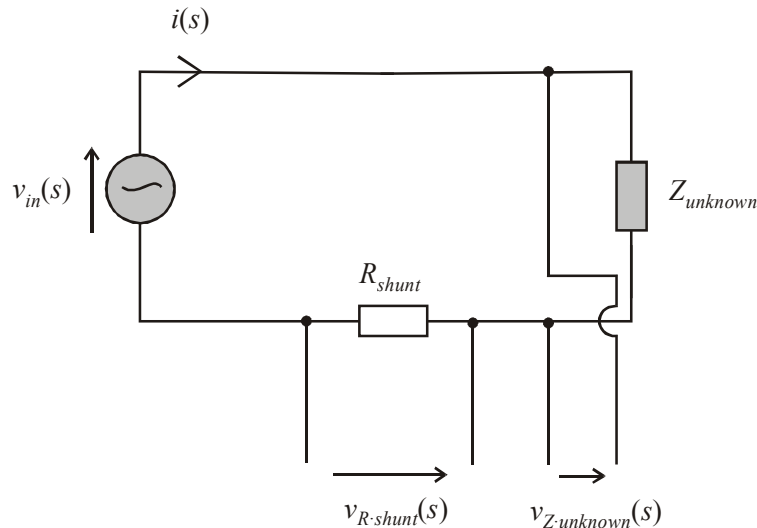


Figure A.1: Circuit arrangement for measurement of electrical current and voltage. Note this arrangement is suitable only for differential inputs and outputs.

With this arrangement, the electrical current can be determined from the measured voltage $v_{R\cdot shunt}(s)$ according to

$$i(s) = \frac{v_{R\cdot shunt}(s)}{R_{shunt}} \quad (A.1)$$

The electrical impedance may, therefore, be determined by

$$Z_{e\text{-meas}}(s) = R_{shunt} \frac{v_{Z\text{-unknown}}(s)}{v_{R\text{-shunt}}(s)} \quad (\text{A.2})$$

Note that in this arrangement, the ground of the two measured signals, $v_{R\text{-shunt}}(s)$ and $v_{Z\text{-unknown}}(s)$ are different. Simultaneous measurement of current and voltage in this way will, therefore, require differential analogue inputs on the analyser.

If only single-ended inputs are available, it will be necessary to reverse the polarity of the measurement of the shunt resistance voltage. The negative value of R_{shunt} should consequently be used as a calibration value to $v_{R\text{-shunt}}(s)$.

In some applications, all output as well as input will be single ended. This is generally the case if both analogue input and output are handled by a standard PC computer sound card. In this case, the arrangement shown in Figure A.2 must be used.

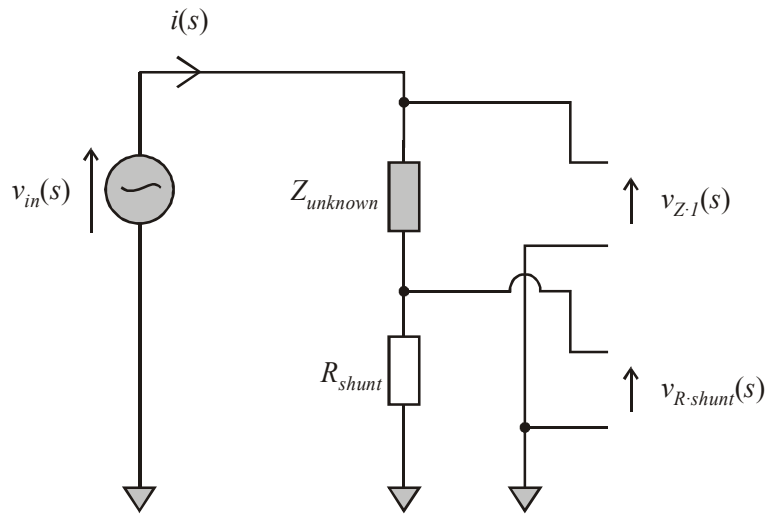


Figure A.2: Arrangement for measurement of electrical current and voltage with single-ended circuit inputs and outputs.

The signals obtained from the arrangement in Figure A.2 must be interpreted somewhat differently from those measured according to Figure A.1. The signal $v_{R\text{-shunt}}$ will still give a signal directly proportional to the electrical current $i(s)$. However, the signal $v_{Z\text{-}I}(s)$ will provide the voltage drop across the unknown load *and* the shunt resistor. In this case, the electrical impedance of the unknown load may be obtained from the measured signals as so:

$$Z_{e\text{-meas}}(s) = R_{shunt} \frac{v_{Z\text{-}I}(s)}{v_{R\text{-shunt}}(s)} - R_{shunt} \quad (\text{A.3})$$

A.2.2. Extraneous resistances

The arrangements for measuring electrical impedance shown in Figure A.1 and Figure A.2 assume ideal, zero-resistance contacts and interconnect cables. In practice, contacts and interconnect cables will have some finite resistance. It was found that, to ensure the accuracy of the displacement predicted by the linear dynamics block in Figure 4.1, it was necessary to include the effect of the output resistance of the power amplifier, and the resistance of the wires connecting the power amplifier to the loudspeaker. This is due to the generally low impedance of electrodynamic

loudspeakers. A technique for determining these resistances and the values determined are described in this section.

Extraneous resistance in the circuit may be considered in two parts:

- The output resistance from the power amplifier
- The contact and interconnect resistance between the voltage drop measurement point and that point for which the impedance of the device-under-test is defined

These two resistances are represented as R_{out} and R_{lead} , respectively, in the circuit in Figure A.3.

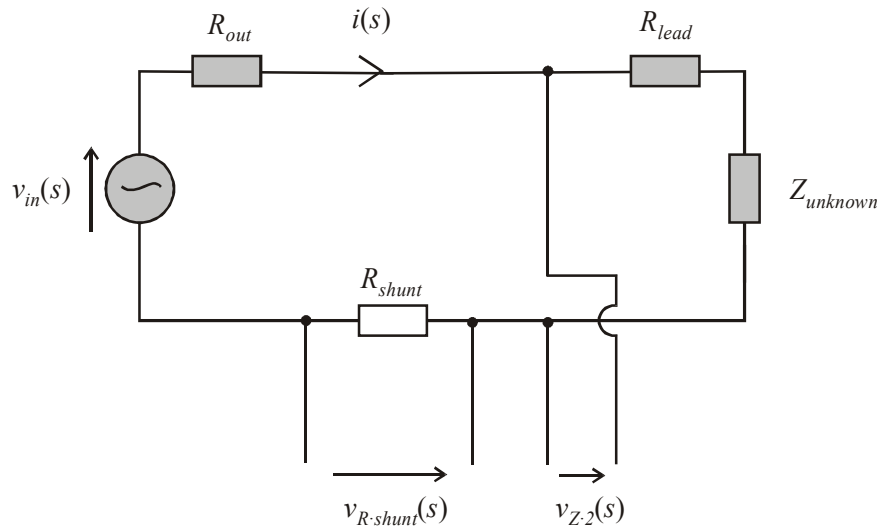


Figure A.3: Arrangement for measuring electrical impedance, with consideration of amplifier output resistance and contact and interconnect resistance. This arrangement is only suitable for differential inputs.

The first of these, the output resistance from the power amplifier R_{out} , need not be considered in ordinary measurement of the electrical impedance. It need be known only when it is necessary to predict the voltage drop across the device under test directly from the *input* to the power amplifier, as is the case in the applications of feedforward control described in the main body of this thesis.

The second of these, the contact and interconnect resistance R_{lead} , does sometimes need to be considered when measuring the electrical impedance. Typical values of R_{lead} are between 0.005 and 0.3 Ω , depending on the interconnect lead wire and the contact type. As the typical impedance of loudspeakers is between 4 and 32 Ω , this resistance needs to be accounted for if the electrical of the loudspeaker needs to be measured with high absolute accuracy. If this is the case, this resistance should be determined separately, by e.g. shorting the terminals on the loudspeakers. With R_{lead} then known, the measured impedance can be corrected according to

$$Z_{e\text{-meas}}(s) = R_{shunt} \frac{v_{Z-2}(s)}{v_{R\text{-shunt}}(s)} - R_{lead} \quad (\text{A.4})$$

The correction according to (A.4) is generally applicable, as the capacitive and inductive components of the interconnect cable and contacts will be multiple orders of magnitude below those of an electrodynamic loudspeaker.

A.2.3. Determination of extraneous resistances with single-ended I/O

For single-ended input-output systems, it is necessary to determine both the lead and the amplifier output resistance. A circuit showing the elements under consideration is shown in Figure A.4. Notice that in this figure the unknown impedance has been replaced with a known resistance R_{load} .

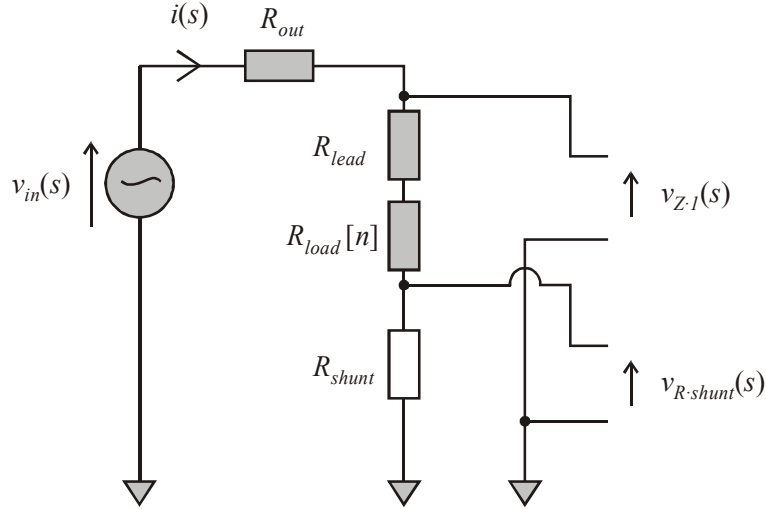


Figure A.4: Arrangement for measurement of electrical current and voltage with single-ended circuit inputs and outputs, with lead and amplifier output resistance considered.

A set of different load impedances, $R_{load}[n]$ for $n = 1$ to N , are inserted into the circuit where the unknown impedance would be located. For each $R_{load}[n]$, the voltage across the shunt resistor $v_{R\cdot shunt}$ and the voltage across all components $v_{Z\cdot I}$ are measured.

The relationship between these voltages and resistances is given by

$$R_{shunt} v_{Z\cdot I}[n] = v_{R\cdot shunt}[n] (R_{lead} + R_{load}[n] + R_{shunt}) \quad (\text{A.5})$$

An error function may be determined from this

$$\chi^2(R_{lead}, R_{shunt}) = \sum_{n=1}^N \left[v_{R\cdot shunt}[n] (R_{lead} + R_{load}[n] + R_{shunt}) - v_{Z\cdot I}[n] R_{shunt} \right]^2 \quad (\text{A.6})$$

The partial derivatives of the error function with respect to R_{lead} and R_{shunt} lead to two equations. The terms R_{lead} and R_{shunt} may be determined by setting these equations to zero, and solving the resulting system. This may be expressed in the following matrix form:

$$\begin{bmatrix} R_{lead} \\ R_{shunt} \end{bmatrix} = \begin{bmatrix} \sum_n v_i[n] (v_i[n] - v_t[n]) & \sum_n (v_i[n] - v_t[n])^2 \\ \sum_n v_i^2[n] & \sum_n v_i[n] (v_i[n] - v_t[n]) \end{bmatrix}^{-1} \begin{bmatrix} -\sum_n R_{load}[n] v_i[n] (v_i[n] - v_t[n]) \\ -\sum_n R_{load}[n] v_i^2[n] \end{bmatrix} \quad (\text{A.7})$$

Now consider

$$v_{in} = i_c[n] (R_{out} + R_t[n]) \quad (\text{A.8})$$

where $i_c[n]$ is the current through the circuit $i(s)$ for the n^{th} value of R_{load} , and $R_t[n]$ is the sum of R_{lead} , R_{shunt} , and $R_{load}[n]$. Using the results above, the current for the n^{th} value of R_{load} is given by

$$i_m[n] = \frac{v_{R\cdot shunt}[n]}{R_{shunt}} \quad (\text{A.9})$$

An error function is defined from (A.8) as so:

$$\chi^2(R_{out}, v_{gen}) = \sum_{n=1}^N (i_c[n](R_{out} + R_t[n]) - v_{in})^2 \quad (\text{A.10})$$

As above, the partial derivatives of this error function are taken with respect to R_{out} and v_{in} . This produces a set of two equations, which in matrix form are

$$\begin{bmatrix} R_{out} \\ v_{gen} \end{bmatrix} = \begin{bmatrix} \sum_n i_{cm}^2[n] & -\sum_n i_{cm}[n] \\ -\sum_n i_{cm}[n] & N \end{bmatrix}^{-1} \begin{bmatrix} -\sum_n i_{cm}^2[n]R_t \\ \sum_n i_{cm}[n]R_t \end{bmatrix} \quad (\text{A.11})$$

Use of appropriate different values of R_{load} and the use of (A.11) with measured data permit calculation of the output impedance of the amplifier (including cabling) as well as the ‘original’ output voltage. The values shown in Table A.1 have been determined with this method for the experimental equipment shown in Figure A.6 - Figure A.9.

Parameter	Determined value
R_{lead}	0.11981 Ω
R_{shunt}	1.0339 Ω
R_{out}	0.09493 Ω
v_{gen}	0.951 Vrms

Table A.1: Typical values of the interconnect cable and contact resistance (R_{lead}), the shunt resistance (R_{shunt}), and the amplifier output resistance (R_{out})

A.3. Experimental set-up for diaphragm for vibration measurement

The measurement set-up for measurement of parameters of a single-degree-of-freedom model of an electrodynamic loudspeaker is shown in a block diagram in Figure A.5. Photographs of the test-bench are shown in Figure A.6 and Figure A.7. These photographs are taken from the same equipment as shown in Figure 4.1.

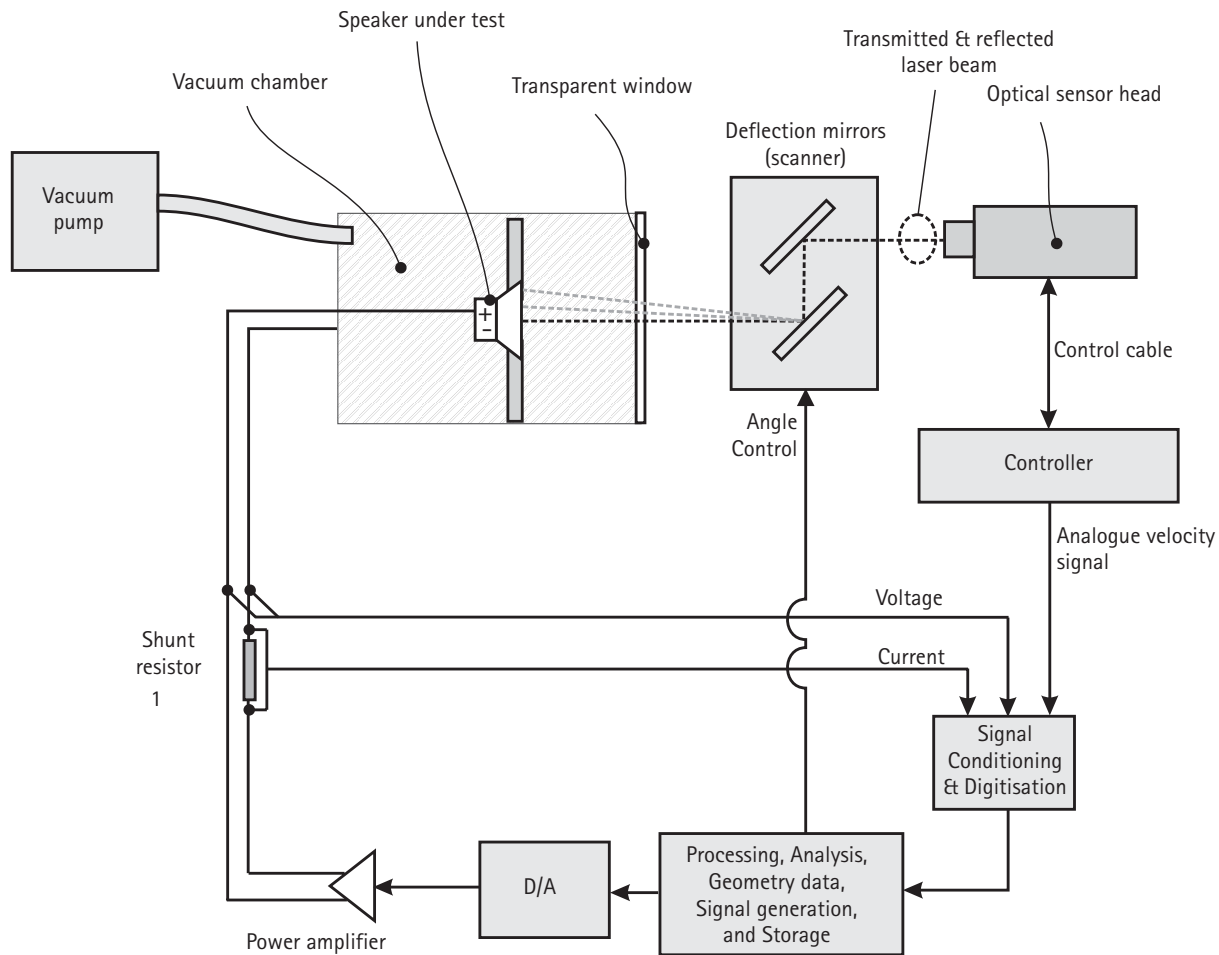


Figure A.5: Experimental set-up for measurement of parameters of a single-degree-of-freedom model for a loudspeaker.

The laser vibrometer used was a commercially available device from Polytec, model OFV 303 sensor head with companion OFV 3001 controller. Signal conditioning and digitisation of the analogue signals was performed by an HP E1433A data acquisition card. Signals were analysed and stored using the Cada-x Fourier Monitor software from LMS. A standard audio constant output-voltage power amplifier was used to drive the loudspeaker. No other special equipment was used.

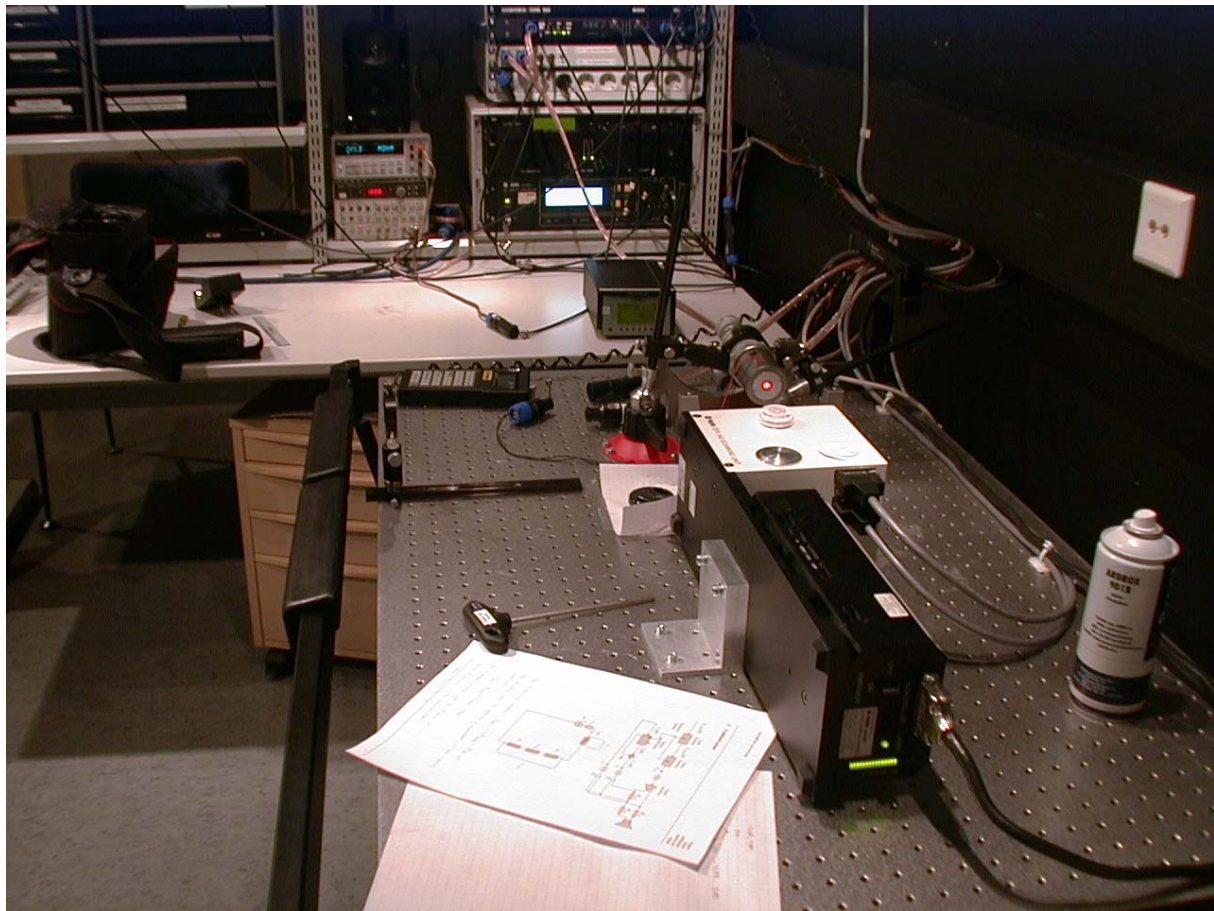


Figure A.6: Photograph of test-bench for the experimental set-up shown in Figure A.5, showing optical sensor head, with scanning mirrors, for direct measurement of a loudspeaker. The measurement is being made in-air, and thus the vacuum chamber is not present.

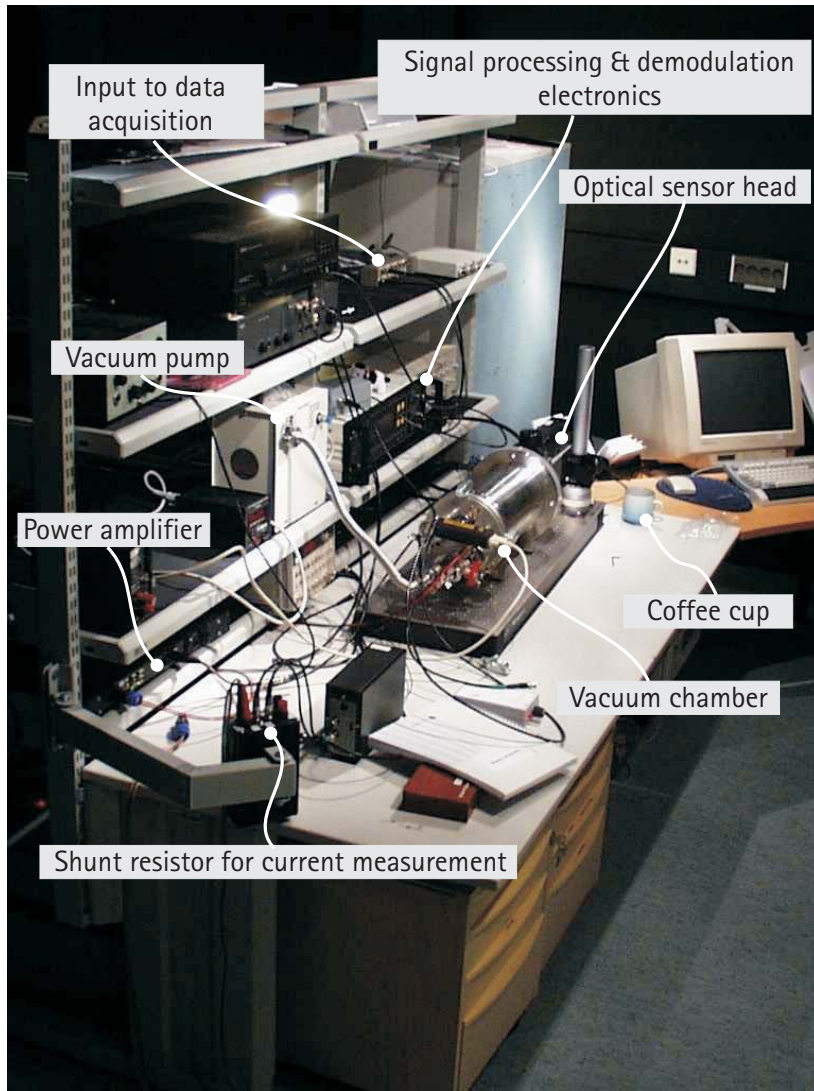


Figure A.7: Photograph of the test bench for a variant of the set-up shown in Figure A.5, showing the vacuum chamber & pump, used to remove the effects of acoustic loading from the loudspeaker. The vibration of the loudspeaker can be measured in a vacuum by the laser vibrometer by virtue of a transparent window in the vacuum chamber.

A.4. Experimental set-up for acoustic measurement

The experimental set-up for measurement of various aspects of the acoustic response of loudspeakers described in different parts was as described in this section.

All acoustic measurements were performed in an anechoic chamber. The loudspeaker was mounted in a variable back-volume test jig, and its acoustic response was measured with a standard laboratory microphone. The distance from the loudspeaker to the microphone was 28cm, as in Figure A.8.

A photograph of equipment for signal generation, active control, and signal analysis in a control room adjacent to the anechoic room is shown in Figure A.9

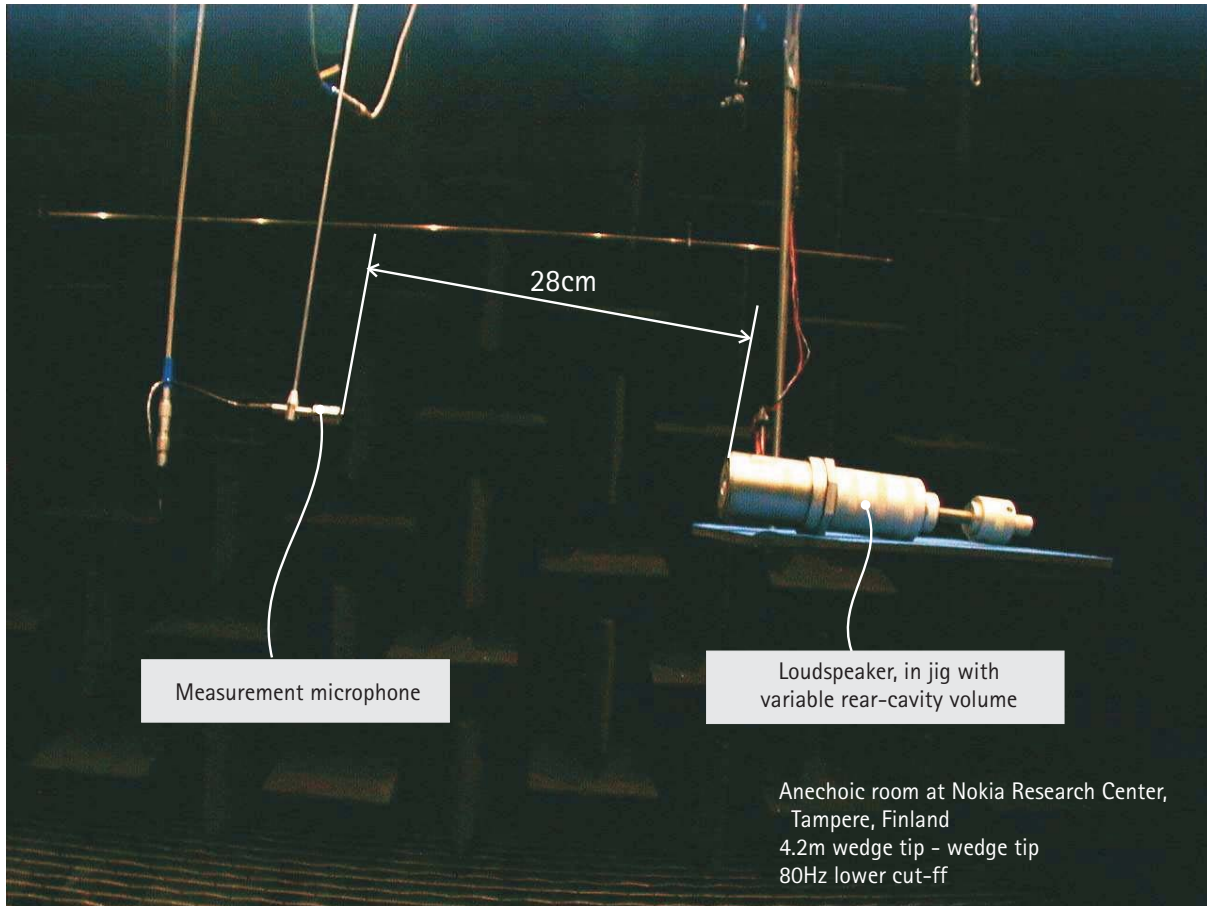


Figure A.8: Photograph of measurement set-up in anechoic chamber for acoustic measurements.

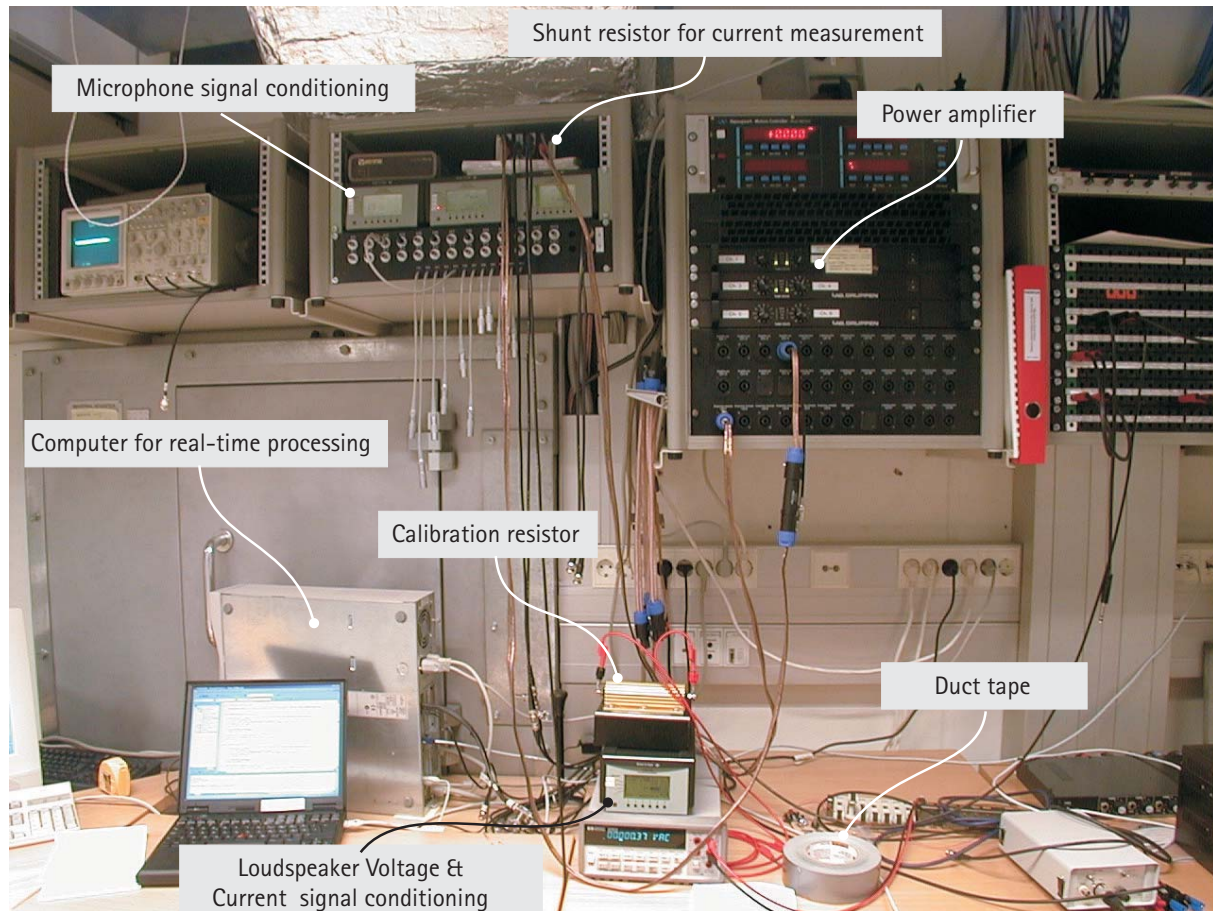


Figure A.9: Photograph of experimental equipment used for acoustic measurement (located in room adjacent to anechoic chamber.)

Appendix B. Experimental determination loudspeaker parameters

Classical theory for determination of parameters for loudspeakers is developed from the 1930's, when RMS voltmeters were the most sophisticated instrument available for analysing dynamic systems. This technique, well-known to most electroacousticians, is described in Beranek's *Acoustics* (1957) and the well-known paper by Thiele (1961). The essence of the technique is to work out the loudspeaker's parameters from changes in its electrical impedance caused by known changes applied to its mechanical load impedance. In Beranek's case this is done by applying a known mass to the diaphragm, and in Thiele's case this is done by changing the volume of a sealed enclosure onto which the loudspeaker is mounted.

In this dissertation, an unpublished method using an FFT analyser and laser Doppler vibrometer has been used. Several methods using an FFT analyser have been published (Struck, 1987.) One method using an FFT analyser and a laser vibration sensor has also been published (Monero, 1991). As the technique used in this thesis is different from these previous techniques, and as it has not been published elsewhere, it is presented in this appendix.

B.1. Parameters to be determined

The six basic parameters governing the loudspeaker's electrical and mechanical behaviour can be determined in two separate stages:

1. Determination of the electrical parameters: R_{eb} , L_{eb} , and ϕ_0 .
2. Determination of the mechanical parameters: m_d , c_d , and k_d .

The fitting of curves can be weighted according the standard deviation of the measured FRF functions. The standard deviation can be estimated from the coherence.

B.2. Electrical parameter determination (R_{eb} , L_{eb} , and ϕ_0)

An appropriate equation for determining the electrical parameters R_{eb} , L_{eb} , and ϕ_0 comes from the coil voltage equation. Dividing by the current $i_c(s)$ and subtracting the left-hand-side, we have

$$R_{eb} + sL_{eb} + \phi_0 \frac{u_d(s)}{i_c(s)} - \frac{v_c(s)}{i_c(s)} = 0. \quad (\text{B.1})$$

The parameters R_{eb} , L_{eb} , and ϕ_0 can be determined by measuring the two frequency response functions (FRF's) $u(s)/i(s)$ and $v(s)/i(s)$, then minimising the left hand side of (B.1) by a least-mean-square method. To ease in notation, recalling that $s = -i\omega$, we define:

$$Y_i(f_n) = \frac{u_d(-i\omega_n)}{i_c(-i\omega_n)} \quad (\text{B.2})$$

$$Z_e(f_n) = \frac{v_c(-i\omega_n)}{i_c(-i\omega_n)} \quad (\text{B.3})$$

With this notation, $Y_i(f_n)$ is the complex-valued FRF of velocity / current at the frequency f_n . Similarly, $Z_e(f_n)$ is the complex-valued electrical impedance at frequency f_n . Substituting these expressions into (B.1), one may define an error function to be minimised is as so:

$$\chi^2(R_{eb}, L_{eb}, \phi_0) = \sum_{n=N_{start}}^{N_{stop}} |R_{eb} - i\omega_n L_{eb} + \phi_0 Y_i(f_n) - Z_e(f_n)|^2 \quad (\text{B.4})$$

where N_{start} and N_{stop} are the indices to f_n giving the beginning and end of the frequency range over which the parameters R_{eb} , L_{eb} and ϕ_0 are to be fit. By taking the partial derivatives of $\chi^2(R_{eb}, L_{eb}, \phi_0)$ with respect to R_{eb} , L_{eb} , and ϕ_0 and setting each to zero, a linear set of three equations is created as so:

$$\frac{\partial \chi^2}{\partial R} = \sum_{n=N_{start}}^{N_{stop}} 2R_{eb} + 2\phi_0 \operatorname{Re}\{Y_i(f_n)\} - 2 \operatorname{Re}\{Z_e(f_n)\} \quad (\text{B.5})$$

$$\frac{\partial \chi^2}{\partial L_{eb}} = \sum_{n=N_{start}}^{N_{stop}} 2\omega_n^2 L_{eb} - 2\omega_n \phi_0 \operatorname{Im}\{Y_i(f_n)\} + 2\omega_n \operatorname{Im}\{Z_e(f_n)\} \quad (\text{B.6})$$

$$\frac{\partial \chi^2}{\partial \phi_0} = \sum_{n=N_{start}}^{N_{stop}} 2R_{eb} \operatorname{Re}\{Y_i(f_n)\} - 2\omega_n L_{eb} \operatorname{Im}\{Y_i(f_n)\} + 2\phi_0 |Y_i(f_n)|^2 - 2[\operatorname{Re}\{Y_i(f_n)\} \operatorname{Re}\{Z_e(f_n)\} - \operatorname{Im}\{Y_i(f_n)\} \operatorname{Im}\{Z_e(f_n)\}] \quad (\text{B.7})$$

Rewriting Eqs. (B.5)-(B.7) into matrix form provides:

$$\begin{bmatrix} N & 0 & \Sigma \operatorname{Re}\{Y_i(f_n)\} \\ 0 & \Sigma \omega_n^2 & -\Sigma \omega_n \operatorname{Im}\{Y_i(f_n)\} \\ \Sigma \operatorname{Re}\{Y_i(f_n)\} & -\Sigma \omega_n \operatorname{Im}\{Y_i(f_n)\} & \Sigma |Y_i(f_n)|^2 \end{bmatrix} \begin{bmatrix} R_{eb} \\ L_{eb} \\ \phi_0 \end{bmatrix} = \begin{bmatrix} \Sigma \operatorname{Re}\{Z_e(f_n)\} \\ -\Sigma \omega_n \operatorname{Im}\{Z_e(f_n)\} \\ \Sigma [\operatorname{Re}\{Y_i(f_n)\} \operatorname{Re}\{Z_e(f_n)\} + \operatorname{Im}\{Y_i(f_n)\} \operatorname{Im}\{Z_e(f_n)\}] \end{bmatrix} \quad (\text{B.8})$$

where N is the total number of points over which the summation is made, given by $N_{stop} - N_{start} + 1$. The parameters R_{eb} , L_{eb} , and ϕ_0 are determined by multiplying the vector on the right-hand-side of Eq (B.8) with the inverse of the matrix on the left-hand-side of (B.8).

The determined parameters are verified by plotting the terms in (B.1) against each other. The determined electrical resistance R_{eb} is verified by comparing

$$R_{eb} \stackrel{?}{=} \operatorname{Re} \left\{ \frac{v_c(s)}{i_c(s)} - \phi_0 \frac{u_d(s)}{i_c(s)} \right\} \quad (\text{B.9})$$

Although the comparison requires a value for ϕ_0 , an incorrect value thereof would not mislead one when making a comparison of plots of the right and left-hand side of (B.9). The determined value of L_{eb} is verified by comparing

$$-\omega L_{eb} \stackrel{?}{=} \operatorname{Im} \left\{ \frac{v_c(s)}{i_c(s)} - \phi_0 \frac{u_d(s)}{i_c(s)} \right\} \quad (\text{B.10})$$

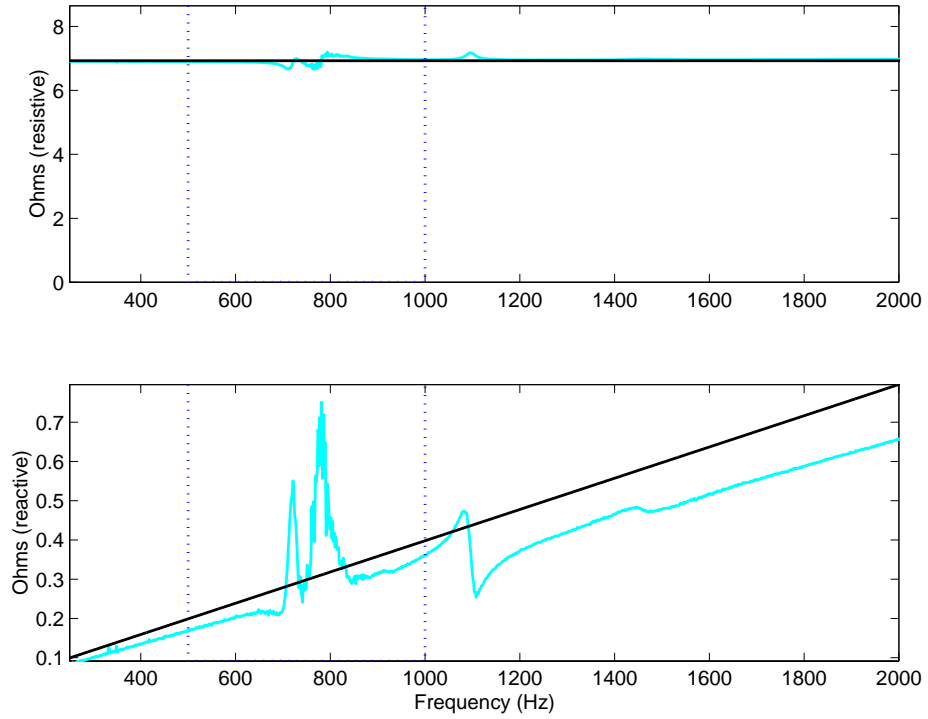


Figure B.1: Verification of R_{eb} (upper) and L_{eb} (lower); in the upper frame, the grey¹ trace shows the RHS of (B.9), and the solid black trace shows the value R_{eb} fit from this data; in the lower frame, the grey trace shows the RHS of (B.10), and the solid black trace shows the value L_{eb} fit from this data

The value of ϕ_0 may be verified by comparing

$$\phi_0 \frac{u_d(s)}{i_c(s)} = \frac{v_c(s)}{i_c(s)} - R_{eb} - sL_{eb}. \quad (\text{B.11})$$

An example of a comparison of the LHS and RHS of this equation is shown in Figure B.2. The real part of this equation is shown in the upper frame of Figure B.2, and the imaginary part in the lower frame.

¹ On colour print and electronic media, this will appear as a ‘cyan’ or ‘sky-blue’ trace in these figures.

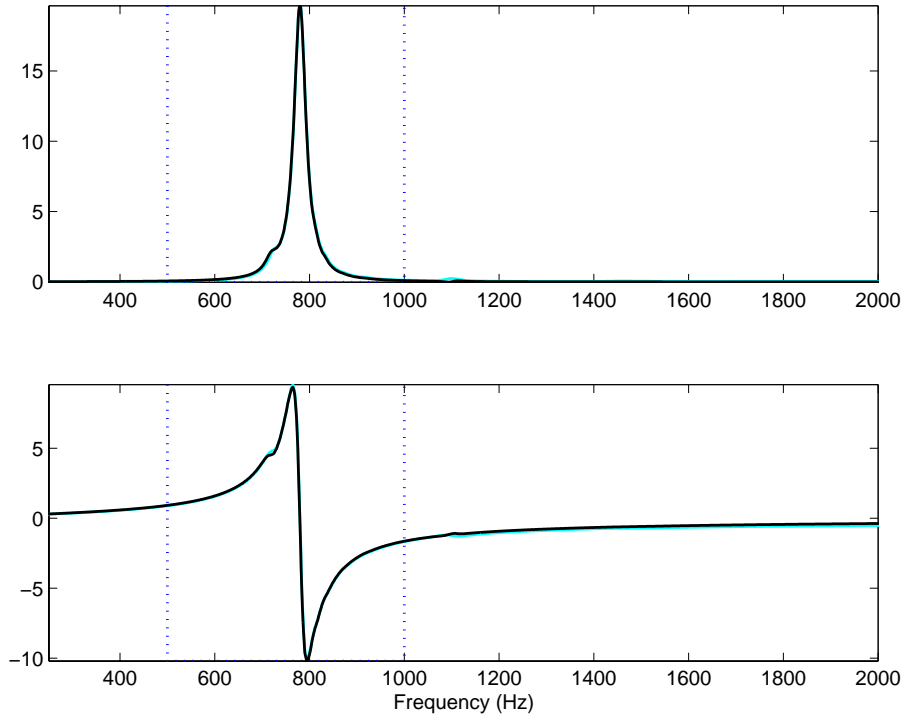


Figure B.2: Verification of ϕ_0 ; the upper frame shows the real part of (B.11), the LHS of which is plotted as a solid black trace, and the RHS of which is plotted as a grey¹ trace ; the lower frame shows the imaginary part of (B.11), again the LHS of which is plotted as a solid black trace, and the RHS of which is plotted as a grey trace.

B.3. Mechanical parameter determination (m_d , c_d , and k_d)

Once the parameter ϕ_0 is determined, the force on the diaphragm can be deduced from the electrical current as per (2.12). The open-circuit mechanical impedance of the loudspeaker can then be known from:

$$Z_{mo}(s) = \phi_0 \frac{i_c(s)}{u_d(s)} - Z_{rm}(s) \quad (\text{B.12})$$

where $Z_{rm}(s)$ is the mechanical-equivalent acoustic radiation impedance. The function $i_c(s)/u_d(s)$ can be measured directly. There are various methods for estimating $Z_{rm}(s)$. Typically, it is estimated by analytical models. It may also be removed, by placing the loudspeaker-under-test in a vacuum. This is what is typically done with microspeakers, as per Figure A.5 and Figure A.7. The following assumes this is the case, i.e. that $Z_{rm}(s) = 0$. Thus the error function for the mechanical parameters m_d , c_d , and k_d is therefore

$$\chi^2(m_d, c_d, k_d) = \sum_{n=N_{\text{start}}}^{N_{\text{stop}}} | -i\omega_n m_d + c_d + ik_d/\omega_n - Z_{mo}(f_n) |^2 \quad (\text{B.13})$$

The partial derivatives of χ^2 with respect to m_d , c_d , and k_d are thus:

¹ On colour print and electronic media, this will appear as a ‘cyan’ or ‘sky-blue’ trace.

$$\frac{\partial \chi^2}{\partial m_d} = \sum_{n=N_{start}}^{N_{stop}} 2\omega_n^2 m_d - 2k_d + 2\omega_n \operatorname{Im}\{Z_{mo}(f_n)\} \quad (\text{B.14})$$

$$\frac{\partial \chi^2}{\partial c_d} = \sum_{n=N_{start}}^{N_{stop}} 2c_d - 2\operatorname{Re}\{Z_{mo}(f_n)\} \quad (\text{B.15})$$

$$\frac{\partial \chi^2}{\partial k_d} = \sum_{n=N_{start}}^{N_{stop}} -2m_d + 2\frac{k_d}{\omega_n^2} - 2\frac{1}{\omega_n} \operatorname{Im}\{Z_{mo}(f_n)\} \quad (\text{B.16})$$

Re-writing these into matrix form gives

$$\begin{bmatrix} \Sigma\omega_n^2 & 0 & -N \\ 0 & N & 0 \\ -N & 0 & \Sigma/\omega_n^2 \end{bmatrix} \begin{bmatrix} m_d \\ c_d \\ k_d \end{bmatrix} = \begin{bmatrix} -\Sigma\omega_n \operatorname{Im}\{Z_{mo}(f_n)\} \\ \Sigma\operatorname{Re}\{Z_{mo}(f_n)\} \\ \Sigma/\omega_n \operatorname{Im}\{Z_{mo}(f_n)\} \end{bmatrix} \quad (\text{B.17})$$

The validity of the determined parameters may be verified by comparing

$$sm_d + c_d + k_d/s \stackrel{?}{=} Z_{mo}(s) \quad (\text{B.18})$$

where $Z_{mo}(s)$ is derived from the measured FRF's as per (B.12).

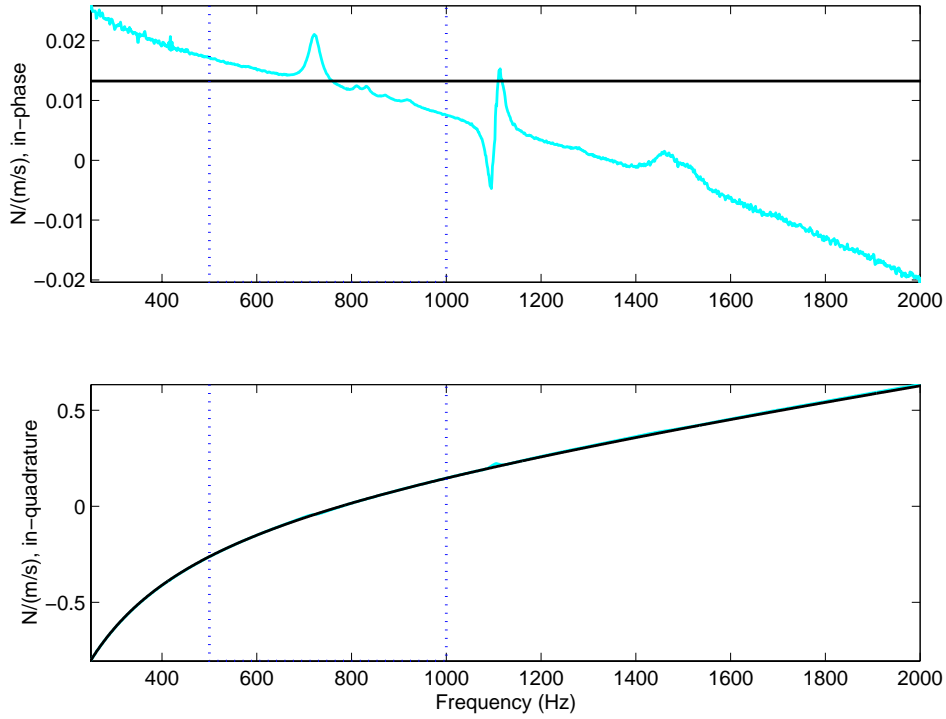


Figure B.3: Open-circuit mechanical impedance estimation; upper frame: real part; lower frame: imaginary part. In both the upper and the lower frames, the solid black trace represents the parameter fit (the LHS of (B.18)), and the grey¹ trace the measured estimate (the RHS of (B.18)). Large frequency dependence in the measured estimate is due to phase errors in the measurement, and additional modes in the system.

Complete assessment of the accuracy of fit also requires comparison also of the multiplicative inverse of these quantities, i.e. the mobility. An example of such an assessment is shown in Figure B.4.

¹ On colour print and electronic media, this will appear as a ‘cyan’ or ‘sky-blue’ trace.

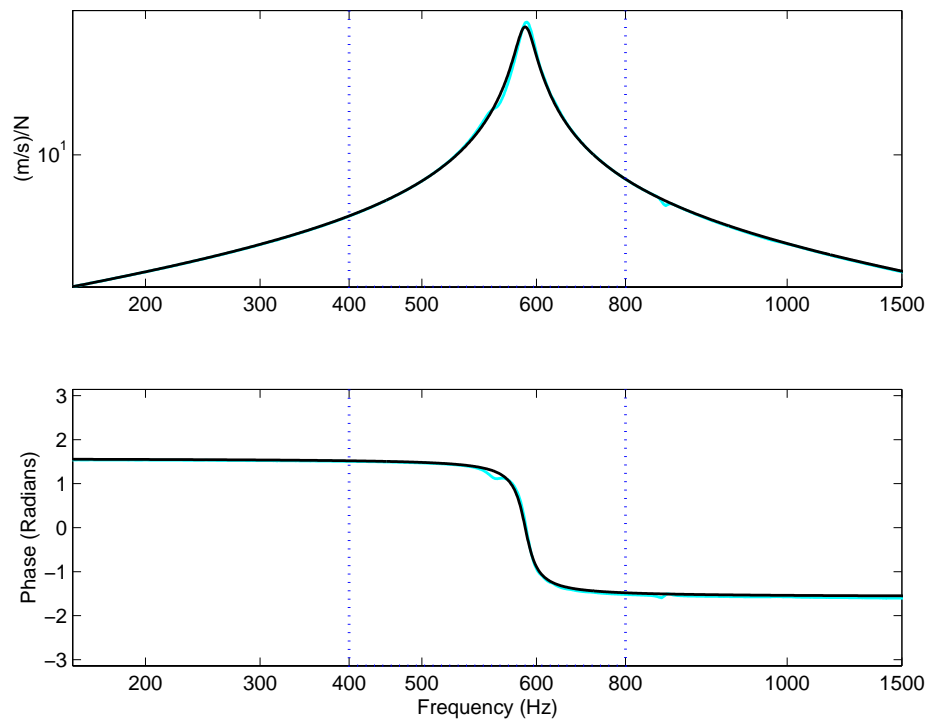


Figure B.4: Mechanical mobility (open-circuit); upper frame: magnitude (log-log plot); lower frame: phase (log-frequency plot). In both the upper and the lower frames, the solid black trace represents the parameter fit, and the grey¹ trace the measured estimate.

¹ On colour print and electronic media, this will appear as a ‘cyan’ or ‘sky-blue’ trace.

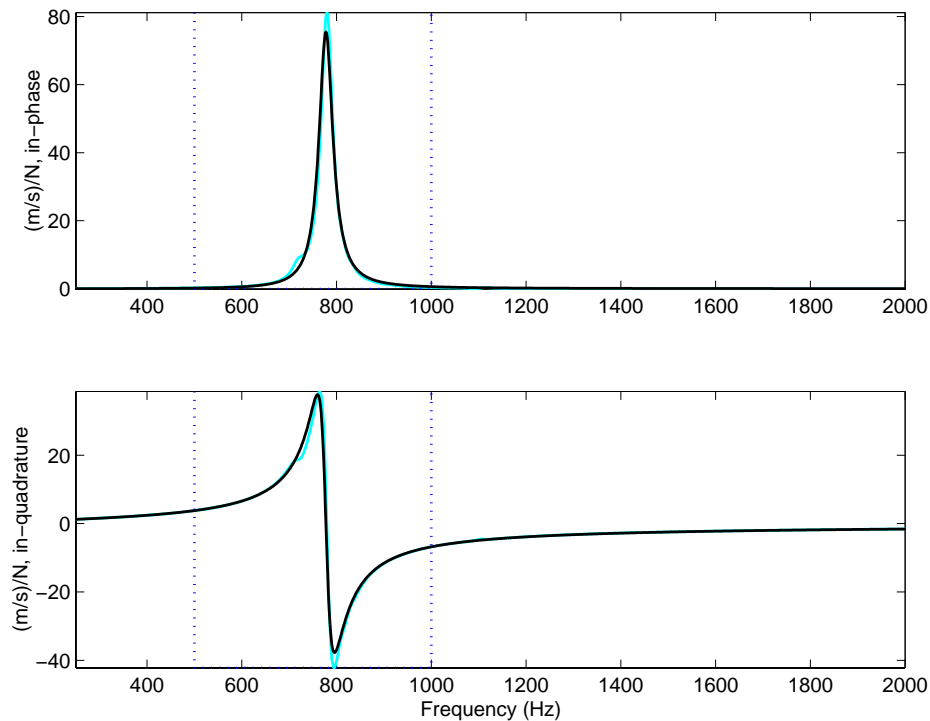


Figure B.5: Mechanical mobility (open-circuit); real part (upper) and imaginary part (lower). In both the upper and the lower frames, the solid black trace represents the parameter fit and the grey trace the measured estimate.

B.4. References

- Beranek, Leo L., *Acoustics*. The Acoustical Society of America, Woodbury, New York, USA (1954, 1993 ed.)
- Moreno, Jorge N., "Measurement of Loudspeaker Parameters Using a Laser Velocity Transducer and Two-Channel FFT Analysis," *Journal of the Audio Eng. Soc*, Vol. 39, No. 4, pp. 243-249 (Apr. 1991)
- Struck, C. J., "Determination of the Thiele-Small Parameters Using Two-Channel FFT Analysis," presented at the 82nd Convention of the Audio Eng. Soc., *Journal of the Audio Eng. Soc.*, (*Abstracts*), Vol. 35 p. 386, preprint no. 2446 (May 1987)
- Thiele, A. Neville, "Loudspeakers in Vented Boxes," *Proceedings of the IRE Australia*, Vol. 22, pp.487-508 (Aug. 1961). Reprinted in *Journal of the Audio Eng. Soc*, Vol. 19, pp. 382-392. (May 1971)

Appendix C. Modal analysis of loudspeaker diaphragms

C.1. Introduction

The models of loudspeakers presented in chapter 2 consider only single-degree-of-freedom dynamics of the loudspeaker diaphragm. This assumes the diaphragm vibrates as a single rigid structure - a valid assumption up to a certain frequency. Above some frequency, the diaphragm will vibrate in a more complex manner. Just above this frequency up to which the diaphragm may be treated as a single rigid structure, the vibration may be efficiently modelled by a collection of vibration modes. These are commonly referred to as ‘break-up’ modes of a loudspeaker diaphragm. These modes may be understood as standing waves in the diaphragm structure. Assuming an equation of motion for the diaphragm’s structure can be defined, these modes will be given by the eigenvalues and functions of that equation of motion. If the structure is only considered at discrete points, as is the case in FEM modelling and experimental modal analysis, the modes will be eigenvectors. Each eigenvalue and eigenvector will add one pole-pair and possibly one zero-pair to an s -domain representation of any vibration frequency response function. Experimental modal analysis is the process of determining these pole- and zero-pairs from measured frequency response functions, and subsequently deducing properties of an appropriate equation of motion based upon the eigenvalues and eigenfunctions defined by these pole- and zero-pairs. Experimental modal analysis may be used in this way to study loudspeaker rocking and ‘break-up’ modes.

There are several practical problems in measuring suitable frequency response functions (FRF’s) on loudspeakers for experimental modal analysis. Standard instruments and techniques for measurement of these FRF’s have existed for several decades, as described by Serridge and Licht (1987), Ewins (1988), and Bendat and Piersol (1993). These standard methods have been developed for the study of large structures, such as automotive and aerospace frames, buildings, and bridges. Two problems are incurred in trying to scale these standard methods down to the comparatively small loudspeaker diaphragm: measurement of the vibration response without excessive mass-loading, and excitation of the diaphragm by a point-force.

The first of these problems has been solved by the recently available scanning laser Doppler vibrometer (Polytec GmbH, 2002). The standard instrument for vibration measurement – the inertial piezoelectric accelerometer – was too large and heavy for use on loudspeaker diaphragms. This instrument permits point-vibration-velocity measurement on loudspeaker diaphragms with sufficiently fine spatial resolution, and without mass-loading the diaphragm.

Vibration excitation of the loudspeaker diaphragm has also remained a problem. The process for determination of eigenvectors (mode shapes) from measured response functions assumes the vibration response measurements are referenced to a point excitation force. On large structures, this can be achieved with traditional shaker and referencing the response to a signal from a force transducer connected between the shaker and the structure. Such equipment is suitable only for relatively large loudspeaker diaphragms. For small diaphragms, there is no practical means for attaching the force transducer to the diaphragm. In other cases, bending moments are likely to corrupt the signal generated by the force transducer due to its large mass relative to the diaphragm.

The obvious alternative is to use the loudspeaker’s own motor structure to excite vibration in the diaphragm. The problem with this is that it does not provide a point-force excitation. This complicates the process of determining the loudspeaker diaphragm’s eigenvectors from the measured response functions. Using the loudspeaker’s own motor structure requires the excitation force to be

considered as a distributed force. Details of this consideration and how it affects the process for determining the diaphragm's eigenvectors are presented in this appendix.

Experimental modal analysis of loudspeaker diaphragms has been studied by other authors. Bank and Hathaway (1981) describe an early laser-based measurement system which avoids the mass-loading problem of accelerometers, mentioned above. Bank and Hathaway used his system to measure operational deflection shapes of a typical electrodynamic loudspeaker diaphragm. They did not consider their measurement results in the context of experimental modal analysis. This was considered to some extent by Struck (1990). Struck used a laser-measurement system that provided a direct dynamic analogue signal proportional to velocity, suitable for frequency-response measurement with an FFT analyser. Struck also seems to be the first to subsequently perform curve-fitting on the complex frequency-response data, and showed how perturbation analysis was possible by modifying the resulting modal mass and stiffness values. However, the above mentioned problem of a non-point force excitation was not addressed. Skrodzka and Sek (1998) mention this problem in their study of the vibration behaviour of a three-way loudspeaker. In their analysis, the centre point of the low-frequency driver is taken as the point force input. Skrodzka and Sek correctly note that the error caused by the single-point excitation can be estimated by making a [coherent] multi-point excitation in the simulation. This was not done, however, as the damping factor was the only modal parameter of interest to the authors, which can be obtained without knowledge of the driving point (i.e. the geometric nature of the excitation force). The vibration shapes shown by Skrodzka and Sek are in fact the operational deflection shapes, as referenced to the input voltage, and not the modal shapes of the mechanical systems in the loudspeaker. A generally similar method was used by Døssing et al. (1989) to analyse the vibration characteristics of a loudspeaker enclosure.

C.2. Modal analysis of structural vibration

An equation of motion for a structure considered at M discrete-points can be written as

$$\left[s^2 \mathbf{M} + s \mathbf{C} + \mathbf{K} \right] \mathbf{x}(s) = \mathbf{f}(s) \quad (\text{C.1})$$

where the terms in (C.1) are as follows:

$\mathbf{M} \in \Re^{M \times M}$	Mass matrix
$\mathbf{C} \in \Re^{M \times M}$	Damping (viscous) matrix
$\mathbf{K} \in \Re^{M \times M}$	Stiffness matrix
$\mathbf{x}(s) : \mathcal{C} \rightarrow \mathcal{C}^M$	Displacement response vector – note each element of this vector is a function of the Laplace variable s
$\mathbf{f}(s) : \mathcal{C} \rightarrow \mathcal{C}^M$	Forcing vector – note each element of this vector is a function of the Laplace variable s

Note that if a continuous-space model of the structure is considered, then a continuous displacement response function $\xi(\bar{\mathbf{x}}_R, s)$ is used instead of the vector $\mathbf{x}(s)$, and the mass, damping, and stiffness matrices become differential operators. The forcing vector must, in this case, also be considered as a continuously distributed forcing function. In all discussions below, it is assumed that the structure is only considered at discrete-points, and thus the displacement response and forcing term are considered as vectors.

Generally, the problem to be solved is the prediction of the displacement response vector $\mathbf{x}(s)$ given a specification of the forcing vector $\mathbf{f}(s)$. The solution can be considered as $\mathbf{H}(s)$, a set of $M \times M$ transfer functions, where the j^{th} , k^{th} such transfer function defines the displacement response at point- j due to a point-force at point- k , i.e.

$$H_{jk}(s) = \frac{x_j(s)}{f_k(s)} \quad (C.2)$$

where $x_j(s)$ is the j^{th} element of $\mathbf{x}(s)$, and $f_k(s)$ is the k^{th} element of $\mathbf{f}(s)$. These transfer functions can be determined from (C.1) according to

$$\mathbf{x}(s) = [s^2\mathbf{M} + s\mathbf{C} + \mathbf{K}]^{-1} \mathbf{f}(s) \quad (C.3)$$

Determination of the transfer function matrix as per (C.3) is complicated by the fact that there is no general solution for the inverse of a matrix larger than 4×4 . Analysis of models with larger than four degrees of freedom will, therefore require numerical evaluation at a specific frequency (value of s), and re-inversion of this matrix for each such frequency. This problem can be overcome by determining eigensolutions to this matrix. The process for doing this is illustrated here for the case where the viscous-damping matrix \mathbf{C} may be ignored. With the damping matrix \mathbf{C} removed, the homogeneous form of (C.1) may be expressed as this M^{th} -order eigenvalue problem:

$$[\mathbf{M}^{-1}\mathbf{K}] \mathbf{x}(s) = -s^2 \mathbf{x}(s) \quad (C.4)$$

This eigenvalue problem, given certain conditions, will have M different solutions, each comprising an eigenvalue ω_m^2 and an eigenvector $\boldsymbol{\varphi}_m$ which are referred to as the m^{th} solution, m^{th} mode, or m^{th} eigenvalue and eigenvector. These are solutions to (C.4) as so

$$[\mathbf{M}^{-1}\mathbf{K}] \boldsymbol{\varphi}_m = \omega_m^2 \boldsymbol{\varphi}_m \quad (C.5)$$

As per standard modal analysis theory (Ewins, 1988), the transfer function $H_{jk}(s)$ may be determined from the eigensolutions of (C.5) according to

$$H_{jk}(s) = \sum_{m=1}^M \frac{\phi_{m,j} \phi_{m,k}}{\omega_m^2 - s^2} \quad (C.6)$$

where $\phi_{m,j}$ is the j^{th} element of the m^{th} eigenvector, i.e. the j^{th} element of $\boldsymbol{\varphi}_m$.

In simulation modal analysis, the eigensolutions (ω_m^2 and $\boldsymbol{\varphi}_m$) are determined from appropriate descriptions of the mass and stiffness matrices, \mathbf{M} and \mathbf{K} . In experimental modal analysis, the eigensolutions are determined by curve-fitting measured frequency response functions (FRF), i.e. measurements of the FRF of the transfer function $H_{jk}(s)$ in (C.2) and (C.6). The curve-fitting process for determining these modal values from measured FRF's is described in the next section.

C.3. Experimental modal analysis

As discussed above, in experimental modal analysis, the eigenvalues and eigenvectors are determined from measured frequency response functions (FRF's). A set of parameters are determined from the FRF's by a curve-fitting process. Details of various possible curve-fitting techniques are well described by Ewins (1988). Given certain conditions, the original eigenvalues and eigenvectors can be determined from the parameters determined from the measured FRF's. These parameters are:

$\alpha_{jk,m}$	'Modal constant'
ω_m^2	Eigenvalue, or 'undamped natural frequency'
ζ_m	Damping ratio ¹

These parameters are used to obtain estimates of the measured FRF's according to:

$$\hat{H}_{jk}(s) = \sum_{m=1}^M \frac{\alpha_{jk,m}}{\omega_m^2 - s^2} \quad (\text{C.7})$$

The parameters are chosen so as to minimise the error between the measured FRF's and the estimate calculated according to the RHS of (C.7). Notice that in the estimate of the FRF from experimentally determined parameters in (C.7) differs from that determined directly from the eigenvectors in (C.6). Specifically, the numerator in the fraction on the RHS is determined by the product between two elements of the eigenvector in (C.6), and by the modal constant $\alpha_{jk,m}$ in (C.7). In order to work out elements of the eigenvector from the results from the curve-fitting process on the measured FRF's it is necessary to have measured the response at the same point at which the force was applied. If this has been done, then one may interpret the modal constant for all modes this FRF as follows:

$$\alpha_{kk,m} = \phi_{k,m}^2 \quad (\text{C.8})$$

With this parameter available, it is possible to calculate the elements of the eigenvector from the modal constant according to

$$\phi_{j,m} = \frac{\alpha_{jk,m}}{\sqrt{\alpha_{kk,m}}} \quad (\text{C.9})$$

C.4. Interpretation of modal analysis on loudspeakers

As mentioned in the introduction to this appendix, the only practical method for vibration excitation in small loudspeakers is to use the loudspeaker's own motor structure. This changes the interpretation of the results from the curve-fit parameters and the process for working out the original the eigenvectors. Details and theoretical aspects of measuring FRF' on a loudspeaker diaphragm are presented first.

C.4.1. Measuring structural FRF's on loudspeakers

By using the loudspeaker's own motor structure to excite the diaphragm, a distributed force, instead of a point force, is applied to the diaphragm. It is generally not possible to measure this distributed force directly, as there is no practical method of inserting a force transducer between the voice coil and the diaphragm. Instead, the force must be indirectly deduced by measurement of the voice coil current. As per (2.12), the force on the voice coil is given by the electrical current according to

$$f_c(s) = \phi_0 i_c(t) \quad (\text{C.10})$$

The voltage drop across a shunt resistor can be used to measure the electrical current, as per Figure A.1.

The vibration response of the loudspeaker diaphragm can be measured with a scanning laser Doppler vibrometer, as shown in Figure A.5 and Figure A.6, presented in §A.3. As described in that section, this instrument provides a signal proportional to the velocity of the diaphragm.

¹ The damping ratio ζ_m assumes a viscous damping mechanism in the model. This was not considered in the theoretical presentation of eigensolutions in § C.2.

Receptance (displacement/force) FRF's are needed for determination of the modal parameters as per (C.7). These may be calculated from the FRF's measured with the system shown in Figure A.5 according to

$$H_{jc}(s) = \frac{Y_{ji}(s)}{s \phi_0} \quad (C.11)$$

where:

$H_{jc}(s)$	receptance FRF; displacement at point j due to force from voice-coil.
$Y_{ji}(s)$	FRF of velocity at point j due to voice-coil current $i_c(s)$.
ϕ_0	transduction coefficient of loudspeaker motor ($B \cdot l$ product, 'force factor')
s	Laplace variable

The reasoning for the choice of notation H_{jc} for the receptance FRF is explained below.

C.4.2. Interpretation of curve-fit parameters

The distributed force presented by the voice-coil requires measured FRFs to be interpreted differently from how they are in traditional modal analysis.

Measured structural FRFs are usually noted as H_{jk} where j indicates the point at which the response has been measured, and k indicates the point at which the structure was excited. When the loudspeaker diaphragm is excited by the loudspeaker's own motor structure, the response must be considered as that not due to force at a single point k , but a force distributed over a set of points. This set of points is the circle forming the junction between the voice-coil and the diaphragm. These points are given the notation \mathbf{c} , a vector with N_c elements, and defined described as 'the set of points on the coil,' as so:

$$\mathbf{c} \doteq [p_1, p_2, \dots, p_{N_c}] \quad (C.12)$$

where p_n is the n^{th} point on the coil. The FRFs measured on the loudspeaker diaphragm are therefore given the notation:

$$H_{jc}(s) = \sum_{n=1}^{N_c} \frac{x_j(s)}{f_{p_n}(s)} \quad (C.13)$$

where $f_{p_n}(s)$ is the point-force at the point p_n . According to (C.10), this force can be determined from the measured voice-coil current according to:

$$f_{p_n}(s) = \frac{\phi_0}{N_c} i_c(s) \quad (C.14)$$

The modal parameters extracted from the measured receptance functions $H_{jc}(\omega)$ have a different interpretation than in traditional modal analysis. The notation convention for the modal constant $\alpha_{jk,m}$ uses the first sub-script to indicate the response point (j) and the second sub-script to indicate the excitation point (k). Thus for the loudspeaker case we write the modal constants as $\alpha_{jc,m}$, where the second sub-script c indicates an average over the set of coil points given in (C.12). The natural frequency, ω_m , and the damping ratio, ζ_m , are not affected by the circular distribution of force, and therefore in this case have the same interpretation as traditional modal analysis. Thus the estimated FRFs are given by

$$\hat{H}_{jc}(s) = \sum_{m=1}^M \frac{\alpha_{jc,m}}{\omega_m^2 - \omega^2 + 2i\zeta_m\omega_m\omega} \quad (C.15)$$

As the FRFs are derived from the product between the eigenvector (or eigenfunction for continuous systems) evaluated at the excitation point and the response point, according to the discussion above, it is necessary to create an average of the eigenvector over the coil points. Such an eigenvector is defined in a manner similar to (C.13),

$$\phi_{\mathbf{c},m} = \frac{\Psi_{\mathbf{c},m}}{\sqrt{m_m}} = \frac{1}{N_{\mathbf{c}}} \sum_{n=1}^{N_{\mathbf{c}}} \phi_{p_n,m} \quad (\text{C.16})$$

The mode vector $\phi_{\mathbf{c},m}$ is simply the average of the mode shape vector for mode m at the coil points, defined in set \mathbf{c} in (C.12). This is the coil-force contribution factor for mode number m .

With the definition of $\phi_{\mathbf{c},m}$ in (C.16), the modal interpretation of the measured functions $H_{j\mathbf{c}}(\omega)$ is

$$H_{j\mathbf{c}} = \sum_{m=1}^M \frac{\phi_{j,m} \phi_{\mathbf{c},m}}{\omega_m^2 - \omega^2 + 2i\zeta_m \omega_m \omega} \quad (\text{C.17})$$

The driving point measurement for a loudspeaker is affected by the distributed excitation force in a manner similar to the modal parameter extraction. A driving point measurement is that for which the response is measured at the same point as the excitation. This enables recovery of the structures mode shape functions from the curve-fit parameters. For the loudspeaker case, given that the force is distributed, a distributed response is evaluated for the driving point measurement.

Summing the modal parameters at the coil points \mathbf{c} defined in (C.12) and dividing by the number of number of coil points provides:

$$\alpha_{\mathbf{c}\mathbf{c},m} = \frac{1}{N_{\mathbf{c}}} \sum_{n=1}^{N_{\mathbf{c}}} \alpha_{p_n\mathbf{c},m} \quad (\text{C.18})$$

According to the modal model, the eigenvectors (mass- and unity-normalised) are related to the modal constant defined in (C.18) by:

$$\alpha_{\mathbf{c}\mathbf{c},m} = \frac{1}{N_{\mathbf{c}}} \sum_{n=1}^{N_{\mathbf{c}}} \phi_{p_n,m} \phi_{\mathbf{c},m} = \phi_{\mathbf{c},m}^2 \quad (\text{C.19})$$

(C.19) permits determination of the system's eigenvectors according to both normalisation schemes. With determination of the unity-normalised eigenvectors and adoption of a well-defined unity normalisation convention, specification of generalised modal mass, damping and stiffness is possible. The mass-normalised eigenvectors $\phi_{n,m}$ are determined by

$$\phi_{n,m} = \frac{\alpha_{n\mathbf{c},m}}{\sqrt{\alpha_{\mathbf{c}\mathbf{c},m}}} \quad (\text{C.20})$$

Determination of the unity-normalised eigenvectors $\psi_{n,m}$ requires adoption of a convention regarding what 'unity' is. The *mean-axial coil motion* is adopted in this work. This normalisation has been adopted for these two reasons:

- Compatibility with lumped-parameter modelling conventions.
- Simplicity in coupling to the electrical domain.

The *mean-axial coil motion* unity normalisation convention requires that the unity-normalised eigenvectors $\psi_{n,m}$ be unity when averaged over the set of points on the coil, \mathbf{c} . This is defined by:

$$\psi_{\mathbf{c},m} = \frac{1}{N_{\mathbf{c}}} \sum_{n=1}^{N_{\mathbf{c}}} \psi_{p_n,m} = 1 \quad (\text{C.21})$$

With this definition, the modal mass may be determined from the drive-point modal parameter α_{cc} according to (C.19).

$$m_m = \frac{1}{\alpha_{cc,m}} \quad (C.22)$$

With the modal-mass definition in (C.22), the unity-normalised eigenvectors can be determined from the modal parameters according to

$$\Psi_{n,m} = \frac{\alpha_{nc,m}}{\alpha_{cc,m}} \quad (C.23)$$

C.4.3. Differential vs. single-ended considerations

A lumped parameter mechanical model which is equivalent to the modal model, when driven by the voice-coil, can be derived. The lumped parameter modal treats the voice-coil as a lumped mass. With such a definition, it becomes identical to the drive point measurement, which is given by the generalised modal mass, damping, and stiffness:

$$H_{cc} = \sum_{m=1}^M \frac{1}{s^2 m_m + sc_m + k_m} \quad (C.24)$$

The modal mass m_m is given by (C.22). The modal damping c_m is given by

$$c_m = \zeta_m \omega_m / \alpha_{cc,m} \quad (C.25)$$

The modal stiffness k_m is given by

$$k_m = \omega_m^2 / \alpha_{cc,m} \quad (C.26)$$

An electrical circuit can be constructed which is equivalent to the modal model of the diaphragm. An example showing an electrical analogy of a modal model with three modes is shown in Figure C.1. This analogous electrical circuit illustrates how the mechanical modes couple to the electrical and acoustical domains.

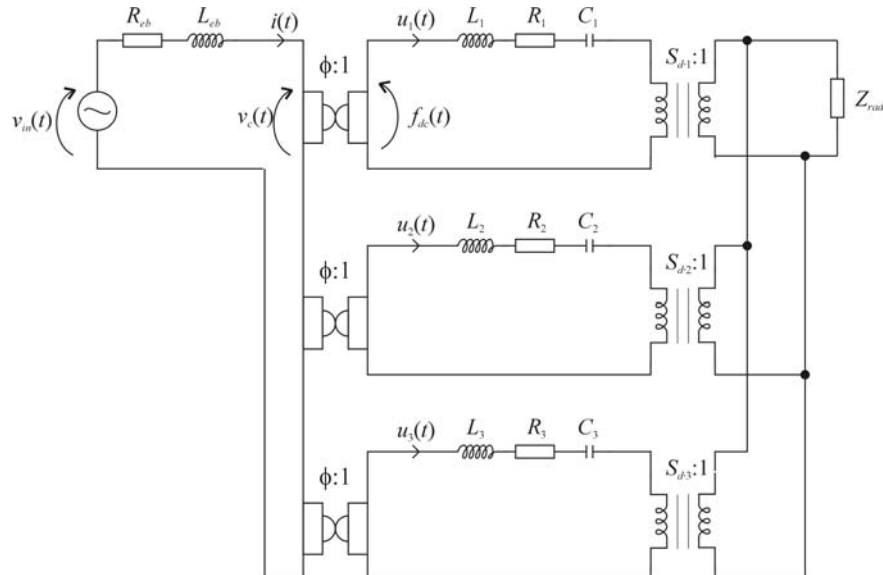


Figure C.1: Equivalent circuit representation of a modal model of a loudspeaker diaphragm. This circuit is equivalent to a modal model which contains three (3) modes.

For each mode in the mechanical modal model, there is an analogous current loop in the electrical circuit. Each current loop corresponds to one mode in the modal model. For each current loop m , there is an inductor L_m , resistor R_m , and capacitor (condenser) C_m , and an effective acoustic radiating area S_m .

The inductor L_m simulates the behaviour of the modal mass m_m , and is thus given by

$$L_m = 1/\alpha_{cc,m} \quad (C.27)$$

The resistor R_m simulates the modal damping for each mode m , and is thus given by

$$R_m = c_m = \zeta_m \omega_m / \alpha_{cc,m} \quad (C.28)$$

The capacitor (condenser) C_m simulates the modal stiffness for each mode m , which is

$$C_m = (k_m)^{-1} = \alpha_{cc,m} / \omega_m^2 \quad (C.29)$$

The effective acoustic radiating area S_m is given by the product of mean-value of the unity-normalised eigenvector for mode m and the total area which is covered by the eigenvector, S_0 .

$$S_m = \frac{S_0}{N} \sum_{n=1}^N \psi_{n,m} \quad (C.30)$$

In (C.30), N is the total number of elements of the eigenvector $\psi_{n,m}$. Determination of the total area covered by the eigenvector S_0 requires analysis of the geometry corresponding to the eigenvector.

C.5. Summary

Experimental techniques for obtaining FRF's from loudspeaker diaphragms suitable for modal analysis are reviewed. A method for interpreting modal analysis results when the loudspeaker's own motor structure is used for force excitation is presented. Methods for interpreting these results in terms of traditional lumped-parameter (equivalent electrical circuit) models are presented.

C.6. References

- Bendat, Julius S., and Allan G. Piersol, *Engineering Applications of Correlation and Spectral Analysis*, 2nd Ed., John Wiley & Sons., Inc., NY, NY, USA. (1993)
- Bank, G., and G. T. Hathaway, "A Three Dimensional Interferometer Vibrational Mode Display," *J. Audio Eng. Soc.*, **29**, pp. 314-319. (1981)
- Døssing, Ole, Christian Hoffman, Lars Mattiesen, and Ole Jacob Veiergang, "Measurement of Operating Modes on a Loudspeaker Cabinet", *presented at the 87th Convention of the Audio Engineering Society*, preprint no. 2848. (18-21 Oct. 1989)
- Ewins, D. J., *Modal Testing: Theory and Practice*, Research Studies Press Ltd., Letchworth, Hertfordshire, England. (1988)
- Hewlett Packard Inc. *The Fundamentals of Modal Testing*, Application Note 243-3. (1991)
- Heylen, W., S. Lammens, and P. Sas (eds.), "Modal Analysis Theory and Testing," ISBN 90-73802-61-X, K. U. Leuven. (1997)
- Larsson, Daniel, "Using Modal Analysis for Estimation of Anisotropic Material Constants." *Journal of Engineering Mechanics*, 123, No. 3. (March 1997)
- Polytec GmbH, "Laser Doppler Vibrometer," Polytec GmbH, Polytec-Platz 1-7, 76337 Waldbronn, Germany. (2002)

- Serridge, Mark, and Torben R. Licht, *Piezoelectric Accelerometer and Vibration Preamplifier Handbook*, Brüel & Kjær A/S (printed by K. Larsen & Søn A/S · DK 2600 Glostrup) (Nov. 1987)
- Skrodzka, E. Eb., and A. P. Sek “Vibration Patterns of the front panel of the loudspeaker system: Measurement conditions and results.” *Journal of the Acoustical Society of Japan*, **19**, pp. 249-257. (July 1998)
- Struck, Christopher J., “Investigation of the Nonrigid Behaviour of a Loudspeaker Diaphragm Using Modal Analysis,” *Journal of the Audio Eng. Soc.*, **8**, pp. 667-675. (Sept. 1990)

Appendix D. Rocking modes in single-suspension loudspeakers

D.1. Introduction

This appendix discusses the problem of rocking modes in single suspension loudspeakers, develops a theoretical model of rocking modes, and describes a method for measuring rocking modes experimentally. Rocking modes are problematic in single-suspension loudspeakers because their rotational vibration is not impeded by a spider, as in traditional loudspeakers. The basic construction principle of a single-suspension loudspeaker is contrasted with a traditional electrodynamic direct-radiating loudspeaker in Figure D.1.

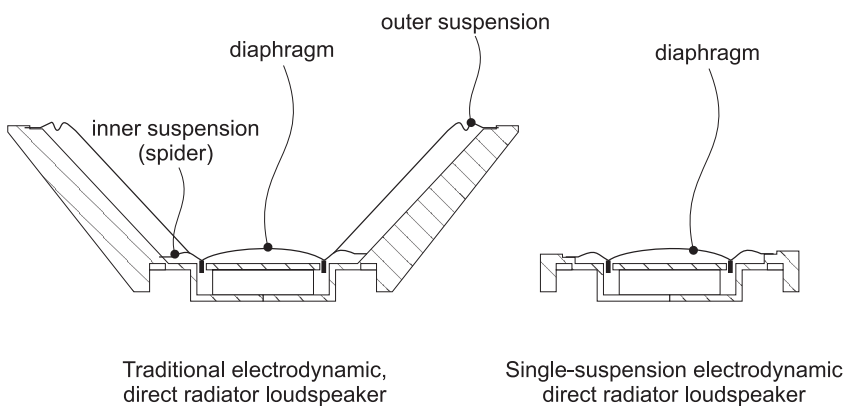


Figure D.1: Single-suspension loudspeaker vs. traditional electrodynamic direct radiator loudspeaker.

The current work is motivated by a study of loudspeakers used in hand-held mobile phones. However, single-suspension loudspeakers are found in other incarnations of electrodynamic loudspeakers, such as horn compression drivers and dome tweeters.

In Chapter 4, Section 7, of McLachlan's book 'Loud Speakers,' the subject of the various rigid-body modes of vibration are considered. McLachlan studies the rigid body modes by analogy to a two-dimensional mechanical system of a lumped mass supported by two membranes. Using this model, McLachlan predicts the natural frequency of the rocking mode ('wobble' in MacLachlan's text) to occur at a frequency relative to the fundamental mode of vibration of $\sqrt{3 m_s / m_d}$ or 'about twice' as written by McLachlan (1934). In the preceding section of MacLachlan's book, the construction of 'centring devices' is introduced. The 'centring device,' nowadays referred to as a 'spider,' is explained by McLachlan to 'preserve axial motion of the coil, thereby eliminating wobble...'

It is interesting to notice the absence of a discussion on spiders (or 'centring devices') in other classic texts on Loudspeakers e.g. Beranek (1954), Hunt (1954), and Olson (1957). The actual author's deduction from this absence is that during the 20 years between MacLachlan's and the other classic texts, the necessity of a spider to the operation of loudspeaker became widely accepted. To imagine a direct radiator loudspeaker without a spider would be as unthinkable as an automobile without brakes.

One may view, therefore, the renewed popularity of loudspeakers without spiders as at worst a step backwards in technology, and at best a venture into known dangerous waters.

D.2. Low frequency modes of vibration of a single suspension loudspeaker

As stated in the introduction, in a single-suspension loudspeaker, diaphragm rocking, or 'wobble,' will occur at approximately $1.5 \sim 2$ times the fundamental resonance frequency. A theoretical model of the rocking modes can be developed using rigid body mechanics. The first step in this process is to

establish the interaction between translational and rotational modes of vibration. The second step is to describe this interaction in terms of the physical characteristics of a loudspeaker.

D.2.1. Translational vs. rotational modes of vibration

To understand the behaviour of rocking modes, it is necessary to be familiar with the difference between rotational and transitional motion. We may describe the in-plane motion of a lumped mass-spring damper system as shown in Figure D.2 with a linear, translational component of motion $x(t)$, and a rotational component motion $\theta(t)$.

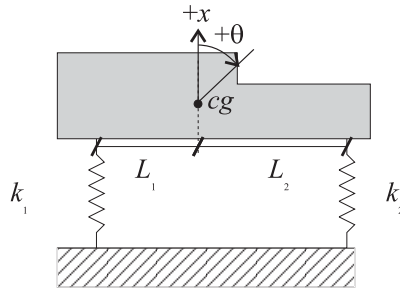


Figure D.2: Linear (translational) and rotational in-plane modes of vibration.

From Tse et al. (1978), the equations of motion of this system in matrix form are

$$s^2 \begin{bmatrix} m & 0 \\ 0 & J \end{bmatrix} \begin{bmatrix} x \\ \theta \end{bmatrix} + \begin{bmatrix} k_1 + k_2 & -(L_1 k_1 - L_2 k_2) \\ -(L_1 k_1 - L_2 k_2) & k_1 L_1^2 + k_2 L_2^2 \end{bmatrix} \begin{bmatrix} x \\ \theta \end{bmatrix} = \begin{bmatrix} 0 \\ 0 \end{bmatrix}. \quad (\text{D.1})$$

Attention here is drawn to the off-diagonal coupling terms in the stiffness matrix in (D.1), which are both $-(L_1 k_1 - L_2 k_2)$. The distances L_1 and L_2 are the those between the mass' centre of gravity and the springs k_1 and k_2 respectively. If $L_1 k_1 = L_2 k_2$, then a force applied in the $+x$ direction will produce only a linear, translational deflection. Conversely, if a torque, or moment, is applied at exactly the centre of gravity, it will produce only a rotational deflection. However, if $L_1 k_1 \neq L_2 k_2$, force applied to the centre of gravity will produce rotational in addition to linear deflection and vice versa for a torque, or moment, applied at the centre of gravity.

Herein lies a key to understanding the problem of rocking modes in loudspeakers. Although the motor unit of a loudspeaker produces no torque or direct moment on the diaphragm, an asymmetric diaphragm stiffness or an off-balance drive position will cause a moment to be imposed on mass of the diaphragm.

It should be noted that the coupling terms between the equations of motion are characteristic of the choice of co-ordinate system, chosen here for convenience. The diaphragm will vibrate in its own natural manner, independent of the co-ordinate system. Note also that coupling between the equations of motion is not equivalent to coupling between the natural modes of vibration, which is a different property of the diaphragm. A good discussion of this technique is available in Tse et al.

D.2.2. ‘Rocking’ modes of diaphragm vibration

By extending the model developed above to two dimension, we can develop a model for the rocking of a diaphragm coil on its suspension. We consider the linear, translational, or ‘axial’ mode of vibration along the z -axis and two rotational modes of vibration, one about the x -axis and the other about the y -axis. This is shown diagrammatically in Figure D.3

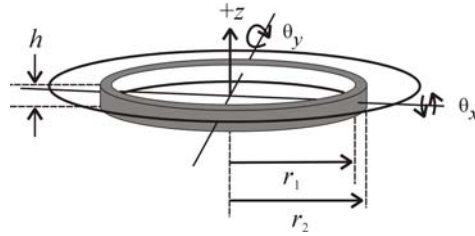


Figure D.3: Diagram of rocking modes in a single-suspension loudspeaker diaphragm.

For the speakers under investigation in this paper, the diaphragm is constructed of very thin plastic. This makes the diaphragm mass much smaller than that of the coil. Therefore only the inertial component of the coil mass is considered in the mechanical dynamics. The effective mass moment of inertia of the coil about the x - and y -axes is assumed to be that of a hollow cylinder

$$J = \frac{1}{12} m(3r_1^2 + 3r_2^2 + h^2) \quad (\text{D.2})$$

This assumption does not limit other aspects of the current study of single-suspension loudspeakers, as they are valid for other distributions of the mass moment of inertia.

Ideally, the two rocking modes about θ_x and θ_y are degenerate. That is, they occur at the same frequency, and their mode-shapes are identical, except for a right-angle difference between them. In experimental modal analysis, they will appear as one mode; it is not possible to distinguish between them unless the structure is excited in more than one location. This is generally not possible to do on small loudspeaker diaphragms. In some cases, however, if the material stiffness is not completely isotropic, these normally degenerate modes will ‘split,’ i.e. occur at different frequencies. This property can be used to determine anisotropy the membrane stiffness (Larsson, 1997).

In general, rocking modes are more problematic in telecom-type speakers than most incarnations of single-suspension speakers for consumer or commercial music reproduction or public address such as dome-tweeters. This is due to the use of ferro-fluids in the air gap, which provide a high degree of damping for the rocking modes.

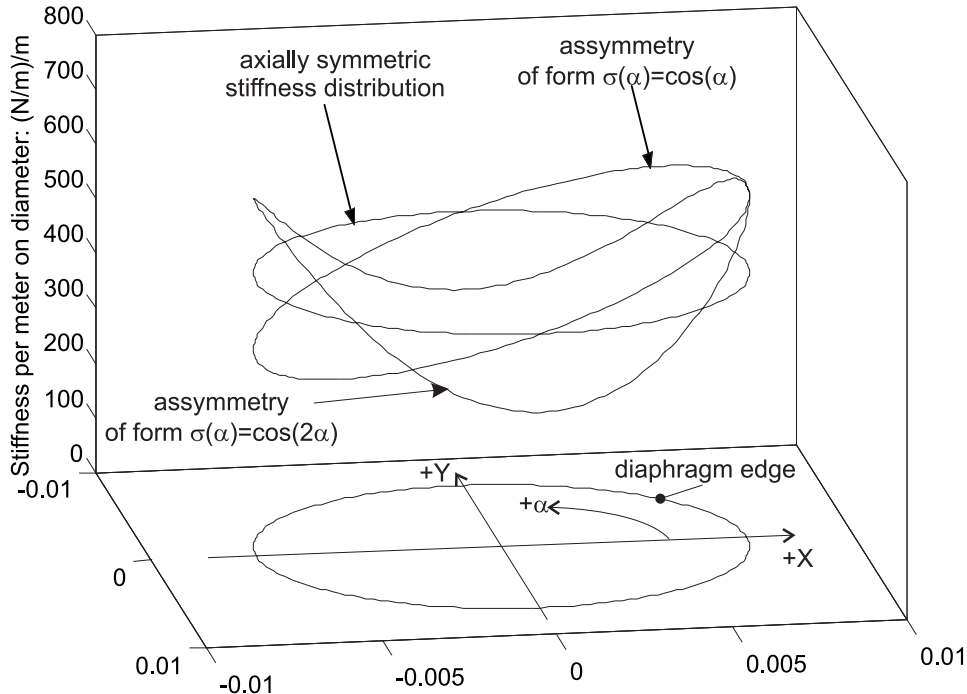
We consider the suspension between the coil and mounting edge to have a stiffness distribution dependent upon the angle around the coil, α . This dependence of the suspension on this angle is represented as a stiffness distribution function $\sigma(\alpha)$. Any stiffness distribution around the coil can be represented by a Fourier series of sinusoidal functions around the angle α :

$$\sigma(\alpha) = \sum_{n=0}^{\infty} \sigma_n \cos(n\alpha + \phi_n) \quad (\text{D.3})$$

It will be shown that the dominant features of rocking modes can be described with only the first three terms of the series in (D.3), so that

$$\sigma(\alpha) = \sigma_0 + \sigma_1 \cos(\alpha + \phi_1) + \sigma_2 \cos(2\alpha + \phi_2) \quad (\text{D.4})$$

For example, the stiffness distributions for $\sigma_0=500\text{N/m}^2$, $\sigma_1=\sigma_2=150\text{N/m}^2$, $\phi_1=\phi_2=0$ are shown in Figure D.4. The dimension of the distribution functions are N/m^2 , for stiffness per unit length along the diameter path.

Figure D.4: Stiffness distributions for given values of σ .

The equations of motion for the three degrees of freedom may be represented in matrix form as

$$s^2 \mathbf{Mx} + \mathbf{Kx} = \mathbf{f} \Rightarrow s^2 \begin{bmatrix} m & 0 & 0 \\ 0 & J_x & 0 \\ 0 & 0 & J_y \end{bmatrix} \begin{bmatrix} z \\ \theta_x \\ \theta_y \end{bmatrix} + \begin{bmatrix} k_z & k_{z\theta_x} & k_{z\theta_y} \\ k_{z\theta_x} & k_{\theta_x} & k_{\theta_x\theta_y} \\ k_{z\theta_y} & k_{\theta_x\theta_y} & k_{\theta_y} \end{bmatrix} \begin{bmatrix} z \\ \theta_x \\ \theta_y \end{bmatrix} = \begin{bmatrix} \phi_0 \\ 0 \\ 0 \end{bmatrix} \quad (D.5)$$

where the notation has the following definitions:

- s The Laplace variable. $s = i\omega$, $i = \sqrt{-1}$, $\omega = 2\pi f$, f = frequency in Hz.
- ϕ_0 Transduction coefficient.
- m The lumped mass of the diaphragm, excluding the effects of any air loading.
- J_x The mass moment of inertia of the diaphragm about the x -axis.
- J_y The mass moment of inertia of the diaphragm about the y -axis.
- k_z Stiffness of the membrane ($= 1/\text{compliance}$), excluding any ‘air cushion’ on which the loudspeaker is mounted,
- opposing linear (axial) motion of the diaphragm.
- k_{θ_x} Rotational stiffness of the membrane about the x -axis.
- k_{θ_y} Rotational stiffness of the membrane about the y -axis.
- $k_{z\theta_x}$ Coupling stiffness between translational motion along the z -axis, and rotational motion about the x -axis.
- $k_{z\theta_y}$ Coupling stiffness between translational motion along the z -axis, and rotational motion about the y -axis.
- $k_{\theta_x\theta_y}$ Coupling stiffness between rotational motion about the x -axis and rotational motion about the y -axis.

All of the terms in the stiffness matrix in (D.5) and described above can be derived from the stiffness distribution function in (D.4). The terms are derived using the same strategy as the stiffness terms for the simple mass-and-spring system described in (D.1). However, because the stiffness is continuously distributed along the diaphragm's edge, the stiffness terms must be determined by integrals instead of sums.

The first stiffness term to be defined is that opposing linear (axial) motion of the diaphragm. This term is equal to the inverse of the mechanical compliance of the diaphragm:

$$k_z = \int_0^{2\pi} \sigma(\alpha) d\alpha = 2\pi\sigma_0 = 1/C_{MD} \quad (\text{D.6})$$

Rotational stiffness is in general defined as the integral of the product between a stiffness distribution and the square of a distance function, giving the distance between the stiffness and the axis of rotation.

$$k_\theta = \int_x (\text{axis to stiffness distance})^2 (\text{stiffness distribution}) dx \quad (\text{D.7})$$

For the loudspeaker, we want to integrate around the path of the diaphragm edge, where the stiffness is defined by the stiffness distribution function in (D.4). The distance between the x -axis and the stiffness may be defined in terms of the angle α , as shown in Figure D.4, according to $r \cdot \sin(\alpha)$. Therefore the rotational stiffness is defined as

$$k_{\theta_x} = r^2 \int_0^{2\pi} \sin^2 \alpha \sigma(\alpha) d\alpha = \pi r^2 \sigma_0 + \frac{\pi}{2} r^2 \sigma_2 \cos \phi_2 \quad (\text{D.8})$$

The same technique can be applied to determine the rotational stiffness about the y -axis

$$k_{\theta_y} = r^2 \int_0^{2\pi} \cos^2 \alpha \sigma(\alpha) d\alpha = \pi r^2 \sigma_0 - \frac{\pi}{2} r^2 \sigma_2 \cos \phi_2 \quad (\text{D.9})$$

The coupling terms are defined in the same manner as a (D.1), except again using integrals.

$$k_{z\theta_x} = -r \int_0^{2\pi} \sin \alpha \sigma(\alpha) d\alpha = \pi r \sigma_1 \sin \phi_1 \quad (\text{D.10})$$

$$k_{z\theta_y} = -r \int_0^{2\pi} \cos \alpha \sigma(\alpha) d\alpha = \pi r \sigma_1 \cos \phi_1 \quad (\text{D.11})$$

The coupling term between the two rotational modes is similarly defined:

$$k_{\theta_x \theta_y} = -r^2 \int_0^{2\pi} \sin \alpha \cos \alpha \sigma(\alpha) d\alpha = -\frac{\pi}{2} r^2 \sigma_2 \sin \phi_2 \quad (\text{D.12})$$

From the foregoing analysis, the impact of the terms in the stiffness distribution of (D.4) can be qualitatively described.

σ_0 Fundamental resonance frequencies

σ_1 Coupling between translational (axial) and rotational modes.

σ_2 Splitting of frequencies of x -axis and y -axis rotational modes; coupling between rotational modes

D.3. Eigenvalue analysis

Traditional eigenvalue analysis of equations in (D.5) is straightforward. This system has three eigenvalues, ω_m^2 (for $m = 1$ to 3), and a 3×3 eigenvector matrix Ψ , for which the m^{th} column of Ψ corresponds to eigenvalue ω_m^2 .

If the off-diagonal terms of \mathbf{K} in (D.5) are zero, there will be no coupling between translational and rotational degrees of freedom. This will be reflected in Ψ ; which will also be diagonal. If off-diagonal terms are introduced to \mathbf{K} ,

We may look at Ψ by analysing linear motion on the $+z$ direction caused by small angular oscillations. Thus we analyse modified eigenvectors

$$_{\text{lin}}\Psi = \begin{bmatrix} 1 & 0 & 0 \\ 0 & r_2 & 0 \\ 0 & 0 & r_2 \end{bmatrix} \Psi$$

D.4. Problems with rocking modes

D.4.1. Mechanical tolerances

The magnitude of coil rocking can be sufficiently large to cause contact between the coil and/or diaphragm and the magnet assembly, as shown in Figure D.5. Contact between the coil and/or diaphragm and the magnet assembly will produce unacceptably high distortion. It may also cause damage to the coil or diaphragm, which can result in failure of the loudspeaker. This may necessitate a widening of the coil gap, which is significantly disadvantageous, as this will reduce the magnetic field strength in the coil gap.

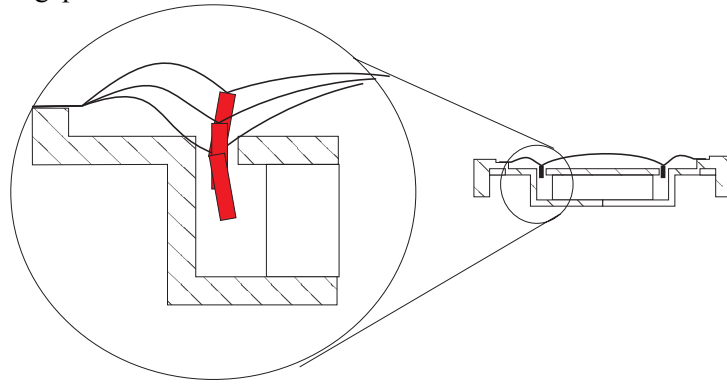


Figure D.5: Deflection in severe rocking mode may cause contact between coil and magnet assembly.

D.4.2. Acoustic radiation

A rocking mode can create acoustic radiation either by monopole or dipole radiation. Monopole radiation is only possible when the shape of natural rocking mode is not completely symmetric. This tends to occur when there is a large $\cos(\alpha)$ asymmetry in the suspension stiffness distribution.

D.5. References

- Beranek, Leo L., *Acoustics*, The Acoustical Society of America (1954).
- Ewins, D. J., *Modal Testing: Theory and Practice* Research Studies Press Ltd., Letchworth, Hertfordshire, England (1988).
- Hunt, Frederick V., *Electroacoustics: The Analysis of Transduction, and Its Historical Background*. Harvard University Press, Cambridge, Mass., USA. (1954)
- Larsson, Daniel, "Using Modal Analysis for Estimation of Anisotropic Material Constants." *Journal of Engineering Mechanics*, **123** (3). (March 1997)
- McLachlan, N. W., *Loud Speakers, Theory, Performance, Testing, and Design*. pp. 69 – 72. Oxford University Press, London, U. K. (1934).
- Olson, Harry F., *Acoustical Engineering*. D. Van Nostrand Company, Inc. (1957)
- Tse, Francis S. et al. *Mechanical Vibrations* p. 156. Prentice-Hall Inc., Englewood Cliffs, New Jersey (1978).